

Propositions

1. The way to model is more important than the exact model results.
(this thesis)
2. Non-ideal membrane processes can give better separation than ideal membrane processes.
(this thesis)
3. Generalizing a model means simplifying it.
4. The best order of ingredient addition in the preparation of 'nastar' can only be understood by full consideration of multicomponent mass transfer effects.
5. There is no scientific progress without a model.
6. The PhD journey is like a Lutz jump; preparing for one direction while executing another one.
7. Success can only be achieved via iterations that are not repetitions; an improvement with every attempt.

Propositions belonging to the thesis entitled

“Rational Design of Cascaded Nanofiltration Systems”

Zulhaj Rizki

Wageningen, 3 November 2020

Rational Design of Cascaded Nanofiltration Systems

Zulhaj Rizki

Thesis committee

Promotors

Prof. Dr Ir Remko M. Boom
Professor of Food Process Engineering
Wageningen University and Research

Prof. Dr Ir Albert van der Padt
Special Professor of Sustainable Production of Food
Wageningen University and Research

Co-promotor

Dr Ir Anja E. M. Janssen
Associate professor at the laboratory of Food Process Engineering
Wageningen University and Research

Other members

Prof. Dr J. H. Bitter, Wageningen University and Research
Prof. Dr M. H. M. Eppink, Wageningen University and Research
Prof. Dr D. C. Nijmeier, Eindhoven University of Technology
Dr M Verschueren, Friesland Campina

This research was conducted under the auspices of the Graduate School VLAG
(Advanced studies in Food Technology, Agrobiotechnology, Nutrition and Health
Sciences)

Rational Design of Cascaded Nanofiltration Systems

Zulhaj Rizki

Thesis

submitted in fulfillment of the requirements for the degree of doctor

at Wageningen University

by the authority of the Rector Magnificus,

Prof. Dr. A.P.J. Mol,

in the presence of the

Thesis Committee appointed by the Academic Board

to be defended in public

on Tuesday 3 November 2020

at 1.30 p.m. in the Aula

Zulhaj Rizki

Rational design of cascaded nanofiltration systems

235 pages

PhD thesis, Wageningen University, Wageningen, The Netherlands (2020)

with references, with summary

ISBN : 978-94-6395-536-2

DOI : <https://doi.org/10.18174/530907>

Content

Chapter 1	1
Introduction	
Chapter 2	13
Modelling temperature effects in a membrane cascade system for oligosaccharides	
Chapter 3	45
Separation of fructose and glucose via nanofiltration in presence of fructooligosaccharides	
Chapter 4	61
Oligosaccharides fractionation cascades with 3 outlet streams	
Chapter 5	91
Multi-criteria design of membrane cascades: Selection of configurations and process parameters	
Chapter 6	125
Design optimization of a 3-stage membrane cascade for oligosaccharides purification using mixed integer non-linear programming	
Chapter 7	151
Design of nanofiltration cascades for fructooligosaccharides using the McCabe-Thiele approach	
Chapter 8	185
General discussion	
References	199
Summary	217
Appendices	221



1

Chapter 1

Introduction



1.1 Rational design of process systems

In industry, processes are generally arranged in process systems rather than single processes. A process system consists of several process units that need to be designed carefully so that they work in synergy to achieve a global target. Process systems are conventionally designed in an unsystematic fashion. The designs are either developed through a trial-and-error procedure or generated subjectively using heuristic knowledge. For some widely known processes (e.g. heat exchangers, reactors), the use of rules of thumb is common practice [1]. Some design procedures might have been applied to structure the design process. These procedures often consist of a brainstorming of alternative designs, evaluating them and selecting the most promising alternative [2]. The brainstorming and the following decision process are often subjective. This limits the possible alternatives because the generated ideas depend on the experience. Moreover, the selected system may not be the globally optimal system. This raises a need for a systematic design procedure to ensure optimum conditions.

The major challenges in designing a process system are setting a target and selecting a process layout. The process layout of a process system consists of functional units. Each unit can be selected from a set of options that have their own purpose and target. This individual purpose and target contributes to the global performance. In a hierarchical procedure for process design, it is common to achieve most of the global target in the first steps with smaller refining contributions in the later steps [3]. The process is then selected to have an optimum target. However, this is an assumption based on heuristic knowledge and does not always guarantee the global optimum.

The units within a process system can be divided into 3 categories: reactions, separations or mass exchanges and energy or heat exchanges. The process system itself can be a network of units within one category or a combination of two or more categories. Even within one category, combinations of different type of units can be made, such as the combination of plug flow and stirred reactors, or a combination of different separation units. Strategies to develop efficient designs have been developed, mostly specific for each category [4,5]. These strategies often simplify the system by considering the units to be uniform [6], working towards a single target performance (e.g. product purity, conversion, cost) or by setting a specific process layout, as explained in the previous paragraph.

For a more global approach to process system design, a more systematic procedure is needed. This procedure should eliminate the subjective presumption of the units so that more options are considered and a global optimum can be achieved. In this thesis, a rational design procedure is developed for a membrane cascade for a separation in the food industry.

1.1 Membrane processes for food materials

Membrane processes are commonly used in food processing to concentrate or isolate specific components from a fluid stream. The processes are operated at a relatively mild temperature and do not require dissolution or precipitation of solutes and therefore avoid the degradation of the solutes and do not require much energy or chemicals [7,8].

Membrane separation uses a membrane as a barrier that is selective for some components, allowing other components to pass through the membrane. The driving forces can be diverse, but a pressure difference is perhaps most used in food applications. In pressure driven membrane processes, the membrane mostly acts as a sieve, with pressure driving the feed fluid through the membrane, while some components are retained due to size exclusion [9–11].

Membrane (pore) sizes vary from 100 nm to several μm in microfiltration, from 2 to 100 nm in ultrafiltration, from 0.5 - 2 nm for nanofiltration, and are even smaller for reverse osmosis [10,12] (Figure 1.1). The required transmembrane pressure (TMP) also varies. In nanofiltration, which is suitable to separate molecules that have a molecular weight of hundreds to a few thousand Daltons, typical pressures need to compensate the difference in osmotic pressure, and need to drive the permeation of the solvent (which is water in aqueous nanofiltration) and the other components that pass the membrane [13,14]. In addition, a crossflow is required that can take up and carry away the components that were retained by the membrane, and would otherwise accumulate and block the membrane.

The degree of separation of the retained components is generally expressed with the retention coefficient, which is the reduction of the concentration in the permeate c_p , compare to the retained concentration on the retentate side c_r :

$$R = 1 - \frac{c_p}{c_r} \quad (1.1)$$

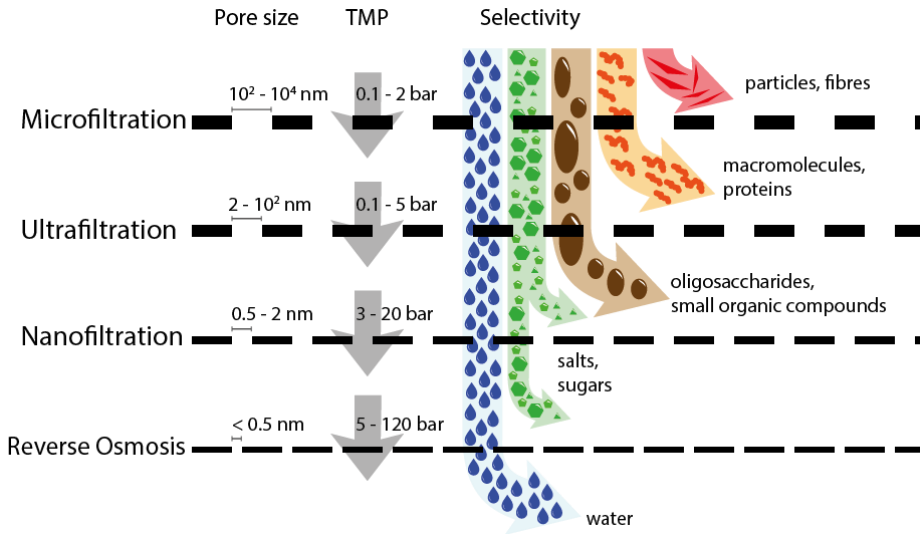


Figure 1.1. Illustration of separation spectrum for pressure-driven membrane processes for food applications. Adopted from van der Bruggen, et.al. [10]

The retention is not a constant, but depends strongly on the process conditions (e.g. TMP and temperature), the molecular size of the components to be retained and the membrane pore size.

1.2 A single step is often not enough

More challenging separations appear between components that are similar in properties and molecular weight. These components may have retentions that are quite close. Strategies to overcome this can be based on 2 approaches: (1) improving the membrane or (2) the application of multiple membranes in a cascade. The first approach may give better retentions, but may not give much better selectivity between the components that need to be separated. One possible way to improve a membrane example is to modifying the membrane materials or surface [15–17]. However, this will influence both components, and higher retention for both components may not lead to better selectivity or resolution between those that should be retained, and those that should pass the membrane.

The second approach is a more generic approach to increase the resolution in a separation process. In this approach, the exiting flows of a first stage are fed to next stages, until sufficient separation is attained [18–20]. This approach is common in separations using distillation, extraction and crystallization in which the separation per stage is also

limited, but by combining stages, one can attain quite high separations [21,22]. This principle of cascading can be applied to any processes, and is thus a common aspect in the design of process systems. The optimal design of such process systems has been established for distillation and to some degree for extraction and crystallization, but is quite new in the field of membrane processes.

Separation processes by definition produce (at least) two outlet streams. Applying a consecutive multi-stage process on just one of the outlet streams will leave the other stream untreated. Therefore, material will get lost in every stage, so that the more stages are involved, the higher the loss coming from the process. Overcoming this issue, a design with counter-current recycling is developed. The stream that is not fed to the consecutive stage is recycled and mixed with the feed stream of the previous stage. This design is known as a counter-current recycle cascade, or just a cascade [19,23–25]. Such a cascade design is not only developed for membrane processes but for other processes as well.

Figure 1.2 shows schematic representations of counter-current cascades for (A) a heat exchanger network, (B) a refrigeration cycle, (C) an extraction process, and (D) membrane separation. The cascade configuration in a heat exchanger network is meant to re-use heat in a plant, ultimately leading to a much lower energy use. The heating or cooling streams can come from other streams within a plant that still have a heating or cooling potential. Doing so will greatly reduce the energy requirement [5,26]. Applying cascaded refrigeration units, as shown in example B, is applied to reduce the energy requirement for achieving a given refrigeration temperature [27]. The purpose of applying a cascaded system in both extraction and membrane process is similar: the separation target cannot be reached in a single step [28]. As an added benefit, the cascade configuration will also reduce the amount of solvent needed in an extraction process. Similarly in membrane separation, a cascade will reduce or even eliminate the requirement for water for diafiltration [19,23].

Having similarities with various processes, the membrane cascade becomes a good model for a general process system. The insight that comes out of the study in a membrane cascade should be applicable for other process systems.

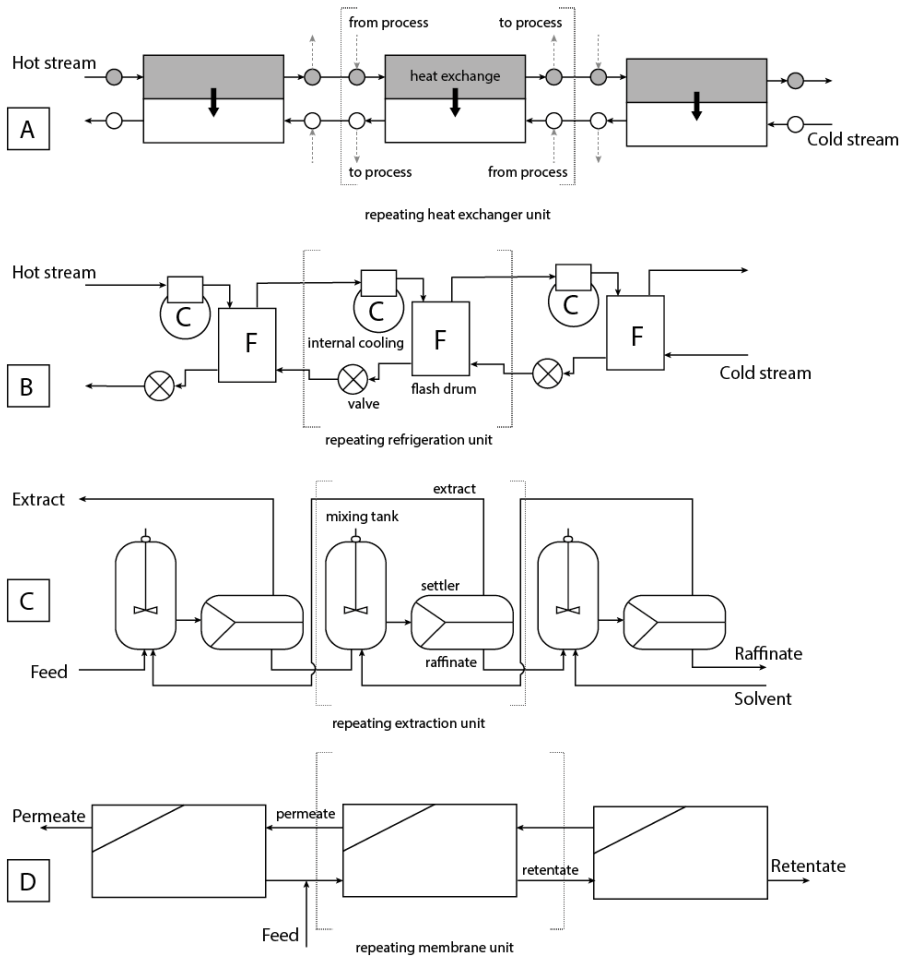


Figure 1.2. Illustration of counter current cascades for various processes (adapted from references): (A) heat exchanger network [26], (B) refrigeration [27], (C) extraction [28] and (D) membrane separation [19].

1.3 Options, freedom of operation and multiple objectives

In general, the performance of a multi-stage process can be characterized by a performance indicator, PI , which is often expressed as the ratio of a certain parameter at the outlet and the feed. Since the feed of the consecutive stage is the outlet of the previous stage, the overall performance indicator, PI_{total} , can be obtained by multiplying the performances in every stage. In terms of the utilization, U , of resources, every stage is added to the total amount of resources used. This resource utilization may be the area of a heat exchanger or the surface area of membranes, total process volume of the equipment or the overall energy requirement.

$$PI_{total} = \prod_{stage=1}^n PI_{stage}(v), \quad v \in \{p, t, c, \dots\} \quad (1.2)$$

$$U_{total} = \sum_{stage=1}^n U_{stage}(v), \quad v \in \{p, t, c, \dots\} \quad (1.3)$$

The performance and utility for each stage are dependent on the process variables, v , which can be the operating pressure, p , temperature, t , concentration, c , or other parameters. Even within a single unit, a combination of those operating variables needs to be found. In non-ideal process systems, the combination of the overall system design (cascade setup) and combination of process variables for each stage, quickly make the design of these systems very complex. While in a few cases, attempts have been made for a thorough procedure to rationally select the combination of system design and setpoints for operating variables [29,30], in general the design is done intuitively and subjectively. This results in sub-optimal system design and operation.

Even though most existing approaches for cascade design are simplified towards the 'ideal' systems, in practice we have more freedom to, for example, combine stages and units that are different from each other. This opens a much wider window of design, and should lead to processes that inherently are more effective and efficient [20,25]. Such a system is known as an inhomogeneous cascade. The drawback for this design however, is that its design is much more complex, as the number of design decisions and operating parameters to optimize is much larger.

An efficient process is mostly assessed by evaluating what use of resources (U_{total}) it needs to attain a certain target (PI_{total}). In many cases, attaining a difficult target (e.g., high purity) may be unrealistically demanding in resources. A reconsideration of the target into a trade-off between these two parameters may then yield a more realistic design. In many practical situations, a process is actually assessed using multiple PI s (e.g. purity and yield) while using multiple resources (e.g. membrane surface area and energy requirement). The design then becomes more challenging due to the multiple objectives. This problem appears in inhomogeneous membrane cascades and is even more common in more complex process system that involve more types of unit operations. The design certainly needs a rational procedure to address this issue.

1.4 Nanofiltration of Fructooligosaccharides

Commercially available fructo-oligosaccharides (FOS) generally consist of a mixture of oligosaccharides, with a range of degrees of polymerization (DP). This DP is important for the functional properties. The larger the DP, the longer our gastro-intestinal tract needs to hydrolyze the oligosaccharide and thus the higher is the prebiotic effect [31,32]. In addition, oligosaccharides with longer DP give a higher viscosity and are less sweet in taste [33–35]. Generally, mono- and disaccharides are not desired as they are readily digestible, thus contribute to the caloric value of the mixture, and have a strongly sweet taste. However, for some other applications, short chain oligosaccharides can be a good solution to have a product with certain degree of prebiotic activity, not viscous and somewhat sweet. Monosaccharides have no prebiotic effect but are natural sweeteners: fructose is even sweeter than glucose and is a very common sweetener [36]. In short, all components in a FOS mixture are useful, and a correct a fractionation of FOS components into valuable fractions is relevant.

FOS molecules are around 0.4 nm (DP1) to 4 nm (DP10) in size [37], which is in the range of nanofiltration membranes. In practice, one can select the membrane with the best possible average pore size. However, while the largest oligosaccharides will always have a high rejection, and the smallest will be able to pass the membrane, the membrane will only have intermediate rejection for the components with intermediate molecular weights. To have better resolution between similar FOS components, a membrane cascade can be used. The fact that FOS nanofiltration therefore requires multiple stages and can be separated using a certain range of nanofiltration membranes makes this process a good model to study the design of inhomogeneous cascaded processes. The outcome can then be applied, with modifications, to other cascaded process systems.

1.5 Aim and scope of this thesis

The main goal of this thesis is to develop rational design methods to design complex process systems; instantiated on the design of inhomogeneous nanofiltration systems, for the fractionation of FOS mixtures. The performance of the process system is evaluated with the purity of the fractions obtained, in combination with the yield for each fraction. Within the multistage separation, several membranes that can be operated in a range of operating conditions are considered. This makes our model process as an inhomogeneous nanofiltration cascade. The inhomogeneous cascade is a perfect model for a complex

process system that may contain a mixed of unit operations that have various targets and are able to be operated with various combinations of operating conditions.

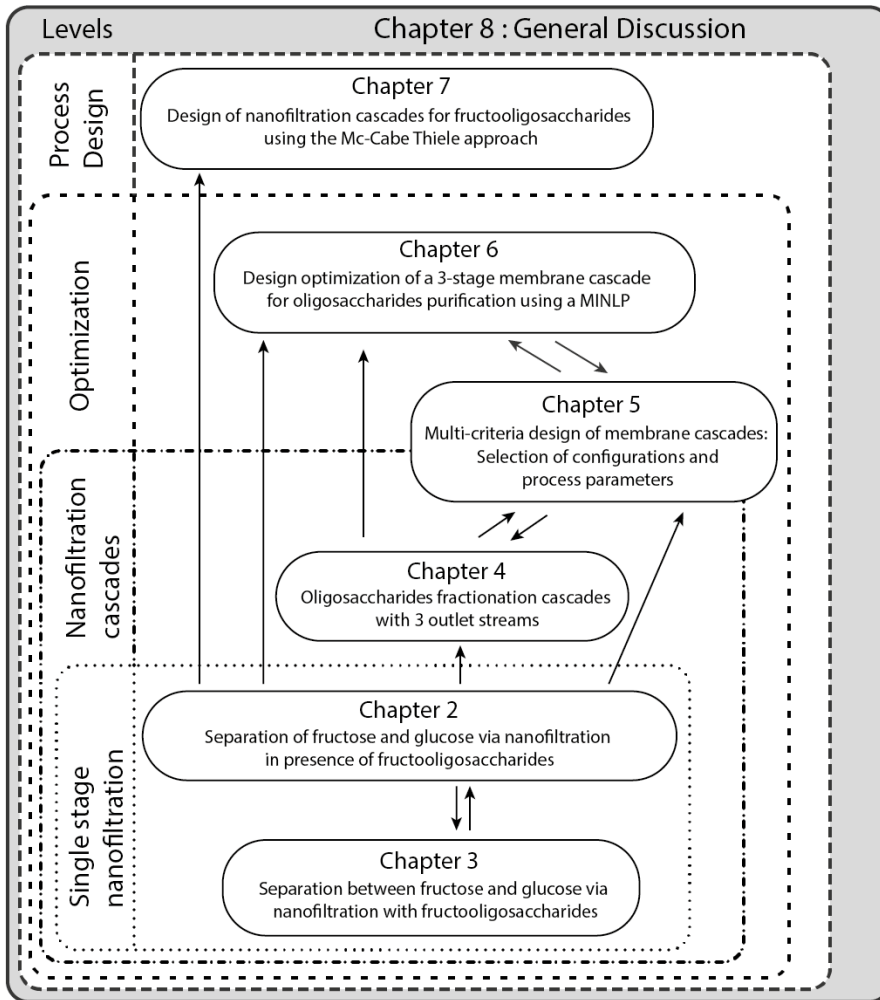


Figure 1.3. Scope of chapters and connections between chapters in this thesis

This thesis consists of 4 levels in designing the nanofiltration cascades : (1) single stage nanofiltration, (2) nanofiltration cascades, (3) optimization and (4) process design. For complete guidelines on the rational design, the process is quantified on the smallest level, which is the single stage. This is then used to devise models for the next level. One typically observes that the complexity increases at each level, and the larger the complexity on lower level, the much larger the complexity is at higher design levels. Therefore, the lower-level models are often simplified to limit the overall complexity.

Here, the outcomes of the lower-level outcomes are summarized into a relatively simple empirical model, which is then used as input for the higher system level modelling. In this way, it is possible to keep the overall complexity in check, but still have access to the full design freedom that is the characteristic of inhomogeneous cascaded systems.

This thesis is broken down into 6 research chapters within the 4 levels of modelling. The thesis is then concluded with a general discussion in chapter 8, in which the findings are extrapolated towards the design of process systems in general. The scope of each chapter related to its level of modelling and the connection between chapters in this thesis is shown in Figure 1.3. The details of each chapter are explained in the following paragraphs.

A single stage nanofiltration model for oligosaccharides was developed in **Chapter 2**. The model was derived based on the steric pore model giving specific attention to the effect of temperature. This model elaborates the sieving mechanism in a nanofiltration system considering the physical properties of the oligosaccharides as solutes, the solution and membrane properties. Using this model, three membranes are characterized for their hydrodynamic resistance and rejection, which are then related to their pore size, within ranges of TMP and temperatures obtained via experiments. This is used for modelling in the next levels, which are elaborated in the next chapters.

Chapter 3 discusses an experimental observation of separation between fructose and glucose during nanofiltration of fructooligosaccharides. Both sugars have different functionalities that makes their separation desirable. However, their separation is difficult to perform since they have the same molecular weight. According to conventional sieving theory, separation of two molecules with the same size will not take place. Nevertheless, separation was observed in presence of FOS components. This phenomenon enriches the fractionation spectrum of nanofiltration for FOS that was described in Chapter 2, which only considers separation based on the molecular weights.

In **Chapter 4**, a model for an inhomogeneous membrane cascade is discussed. In this model, an empirical relation for a single stage model was used to limit the complexity. The extraction of a middle product via a side stream taken from one of the recycle streams was evaluated. Improved design was reported by the addition of stages. In this chapter, the best combination of operating variables was chosen by simulating a set of limited combinations and selecting the best outcome out of those.

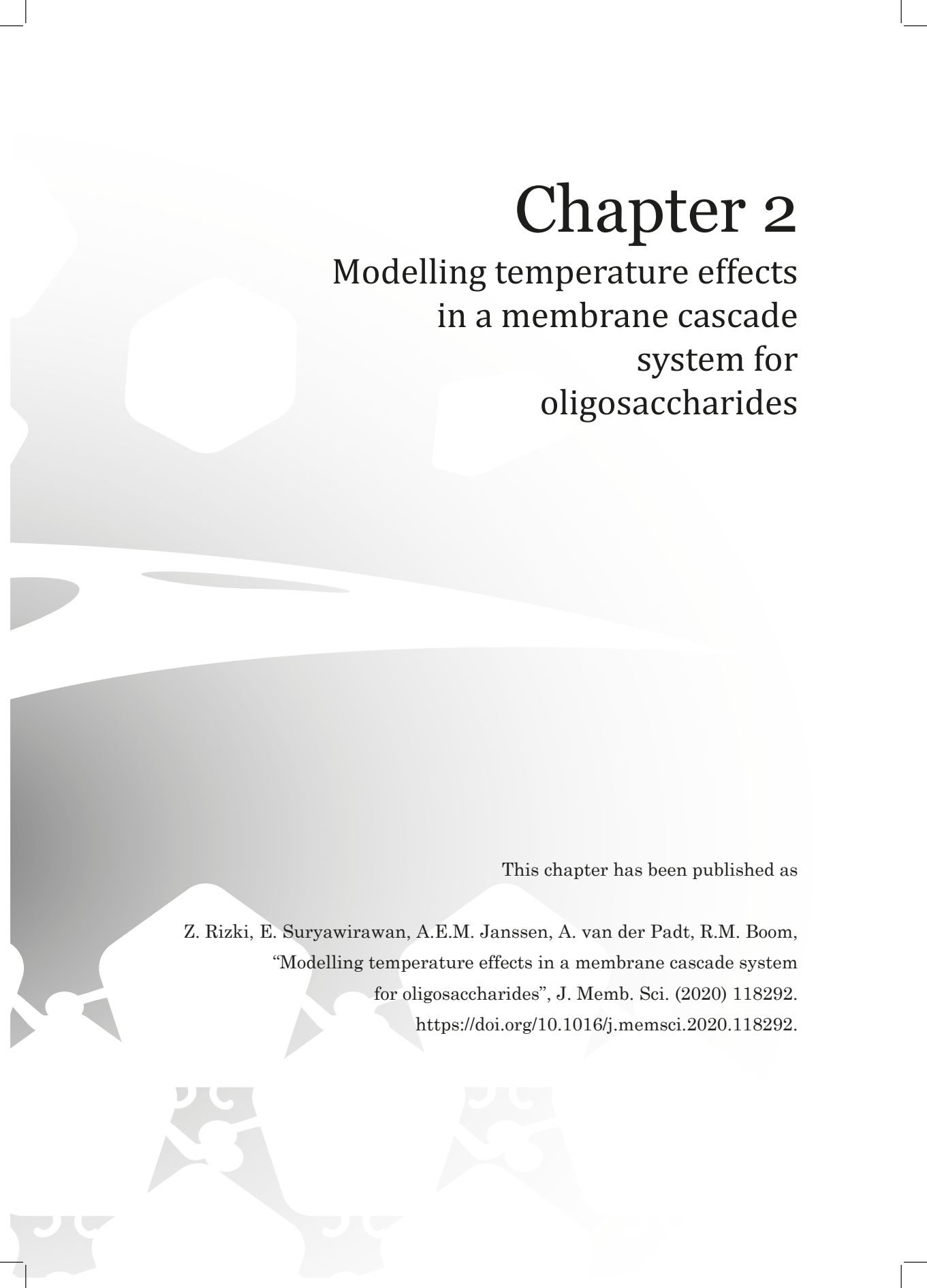
Another approach to improve the cascade is considered in **Chapter 5**. By keeping the number of stages at 3, different stream configurations were evaluated on their separation performance. Eight new configurations of 3-stage cascades with 3 outlet streams were proposed. A procedure to use multiple separation objectives was developed. This multiple objective problem appears in most separation cases and escalates with the increase number of products. Based on the decision making procedure, a sensitivity analysis was performed to find the critical operating parameters.

The process to select a combination of process variables in chapter 4 and 5 did not explore the whole design parameter space and was performed manually. A limited set of possible combinations was generated and the combination with the best simulated outcomes was chosen. This method does not guarantee that the best combination is within this limited set. Therefore, in **Chapter 6**, an optimization method was used based on mixed integer - non-linear programming (MINLP). Using this model, a selection of process variables could be generated computationally given certain constraints. A map of operating variables along a pareto curve was made to visualize the window of operation with maximum performance.

With the methods discussed in chapter 2 to chapter 6, a cascaded membrane system with a given set up can be designed. However, any given setup has its limits, even at its optimum configuration. Chapter 4 showed that increasing the stage number can indeed improve the separation performance. However, this model cannot yet predict how many stages would be needed to achieve certain target purities. In **Chapter 7**, a design method based on the classical McCabe-Thiele approach for distillation was developed for designing inhomogeneous membrane cascades. Using this method, we can estimate the number of stages and membrane areas required to achieve specific purity targets at both product streams.

Chapter 8 concludes this thesis with a general discussion from the results in the previous chapters. The main findings from the previous chapters are highlighted. The guidelines that were developed are extrapolated towards the general design of process systems.



The background features a stylized illustration of a membrane cascade system. It shows a series of membrane proteins, represented as white structures with various shapes and sizes, embedded in a grey membrane. The proteins are arranged in a line, with some having multiple subunits. The overall style is clean and scientific, with a focus on the structural components of the system.

Chapter 2

Modelling temperature effects in a membrane cascade system for oligosaccharides

This chapter has been published as

Z. Rizki, E. Suryawirawan, A.E.M. Janssen, A. van der Padt, R.M. Boom,
“Modelling temperature effects in a membrane cascade system
for oligosaccharides”, *J. Memb. Sci.* (2020) 118292.
<https://doi.org/10.1016/j.memsci.2020.118292>.

Abstract

2

Open nanofiltration of mixtures of fructo-oligosaccharides was assessed by experiment and by modelling the overall permeation behaviour of 3 different membranes. The temperature effect was modelled using the steric pore model, incorporating the molecular volumetric expansion of fructo-oligosaccharides as solutes, the decrease in the solution viscosity and the volumetric expansion of the membrane with increasing temperature. The thermal expansion of the solute was described as a linear increase in the bare molecular volume plus a non-linear decrease in its hydration number. The viscosity reduction was modelled by incorporating the temperature as a variable into an existing exponential relation derived by Chirife and Buera. The thermal expansion of membranes was described with a linear increase in the pore size and a linear decrease in its hydrodynamic resistance. Although the purity of the oligosaccharide product was hardly affected by the temperature, the yield was much lower at higher temperatures. The yield can therefore be improved by decreasing the temperature while maintaining the product purity. This behaviour was also observed in a 3-stage filtration cascade. The temperature effect is closely related to the increase in fluxes with temperature, leading to a different split of the feed into permeate and retentate. In a membrane cascade, the lower yield with higher temperatures was seen most strongly at the top stage, and much less at the middle and lower stages, which can be explained by the configuration of the cascade.

2.1 Introduction

Membrane separation has become popular to fractionate food components, due to its simplicity, mild operating conditions and relative cost effectiveness compared with other separation processes. Its implementation varies from ultrafiltration for protein separation [38] and nanofiltration for separation of sugars and carbohydrates [39–42] to reverse osmosis for removing salts [43]. Each application needs a particular membrane and an appropriate process design for optimum performance. Designing a membrane process can be time consuming, but a proper model aids the designer to determine which process parameters should be applied and which properties of the membrane are required [44–46].

Here, we concentrate on the interface of nanofiltration and ultrafiltration, open nanofiltration, for the fractionation of oligosaccharides. The Donnan Steric Pore Model (DSPM) has been used extensively for this. This approach combines the diffusive, convective and electrical transport inside the membrane [47]. Apart from the electrical interactions, this model also explains the sieving mechanism for neutral solutes [48,49]. Coupled with a mass transfer model that describes the transport phenomena outside the membrane, this DSPM model has been modified and applied to various applications [37,50–52].

Oligosaccharide fractionation has become an important application for membrane separation. Some oligosaccharides have prebiotic properties [31,32,53,54] and improve the rheological behaviour [33,35,55] of food products; however, mono- and disaccharides are sweet and increase the caloric density of a product. Oligosaccharide fractionation with membrane processes has been explored using an experimental approach [41,56] that was then extended to models [40,57,58]. Multistage membrane processes have also been investigated to improve the fractionation of oligosaccharides, both as a consecutive configuration without recycle [56,59] and as a cascaded configuration with recycle [24,25,60].

Most experiments and models have been explored using specific operating conditions, typically at one particular operating temperature. The operating temperature is known to have a strong effect, for example, on the transmembrane fluxes and is believed to have an effect on other aspects as well [52,61,62]. However, it has not yet been explicitly included in the models. A change in temperature often requires reformulating the models

or carrying out more experiments to determine the values of the parameters at the new temperature. Therefore, it is important to develop a model that explicitly considers the effect of temperature as a process variable.

In cascades of membranes, it is possible to use different conditions at each stage to achieve better overall performance [20,25,60,63]. So far, inhomogeneous cascades have been operated using the same temperature at each stage while various membranes and pressure were used; however, we foresee that a cascade that operates at different temperatures in each stage may perform better.

In this paper, we develop an integrated model that includes the influence of the temperature in the nanofiltration of oligosaccharides for a single-stage membrane. This model is expanded later towards a cascade system to explore the benefit of having different temperatures in the cascade setup.

2.2 Model development

We use the steric pore model (SPM, which is a simplification of the DSPM, valid for neutral solutes) for the transport inside the membrane. According to this model, the separation mechanism for a neutral solute is pure sieving via convective and diffusive transfer. In this model, the molecular dimensions of solutes and the membrane pore size determine the separation as well as the solution properties, such as the viscosity and the solute diffusivities. By combining this theory with an appropriate concentration polarization model, we can predict the overall performance of the membrane.

2.2.1 Temperature effect on the molecular volume of fructo-oligosaccharides

Most derivatives of the SPM consider the solutes to be spherical. The dimension of these solutes is characterized using the Stokes radius ($r_{s,i}$), which can be estimated from its diffusivity (equation. (2.1)). This diffusivity can be estimated using a relation derived by Sano and Yamamoto [64] that depends on its molecular weight (equation. (2.2)).

$$r_{s,i} = \frac{k_B T}{6 \pi D_i} \quad (2.1)$$

$$D_i = \frac{T}{9.5 \times 10^{13} MW^{1/3} \eta} \quad (2.2)$$

Fructo-oligosaccharides (FOS) are oligomers of fructose with glucose; they have a chain-like structure and are therefore definitely not spherical. This is typically not considered in most models. Recently, Aguirre et al. [37] modelled the filtration of FOS by considering them as elongated capsules with 2 dimensions: diameter ($L_{0,i}$) and length ($L_{1,i}$). They compared 3 ways to include these dimensions: (1) considering them as completely spherical using their Stokes radii, (2) considering them as completely capsular using both the capsule diameter and length, and (3) using a semi-capsular approach with the so-called Giddings radius [65] as an average of both the capsule radius and the half-capsule length (equation (2.3)). Both the complete capsular and the semi-capsular approaches predicted the filtration performance better than the spherical approach. Since the full capsular model is complex and requires significant computation time, the semi-capsular approach was adopted for further use. In this approach, each oligosaccharide is characterized by its own diameter and length, and then its Giddings radius, $r_{G,i}$, is used for further calculations.

$$r_{G,i}(T) = \frac{1}{4}(L_{0,i}(T) + L_{1,i}(T)) \quad (2.3)$$

The FOS capsules are constructed using spheres of hydrated glucose and fructose as building blocks (Figure 2.1). The capsule half-length is estimated from the sum of the radius of each sphere. The sphere radius is calculated using the hydrated molar volume and assuming the monosaccharide to be a perfect sphere. Unlike glucose, the dimension of a hydrated fructose in a chain may differ from its free form. To construct the FOS capsules, the dimension of hydrated fructose in a chain is used, which is estimated by subtracting the molar volume of glucose from that of sucrose.

In general, the molar volume of hydrated sugars, $V_{m,h}$, can be expressed as the total volume of the non-hydrated sugar, $V_{m,b}$, plus the water that is bound to it. The amount of bound water can be estimated by the hydration number of a particular sugar, n_h , multiplied by the volume of the individual bound water molecules, $V_{m,bw}$.

$$V_{m,h}(T) = V_{m,b}(T) + V_{m,bw}n_h(T) \quad (2.4)$$

The parameters in equation (2.4) were investigated by Gharsallaoui et al. [66] using sugar density data. They proposed different values for the non-hydrated volumes, bound water volumes and hydration numbers for mono- and disaccharides at several chosen

temperatures. However, they did not propose a clear relation between the temperature and these parameters.

2

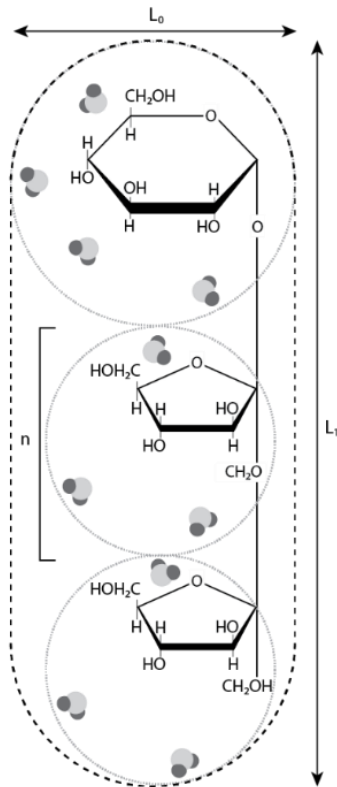


Figure 2.1. Graphical representation of a FOS capsule. The capsule is composed of spherical hydrated monosaccharides as its building blocks. The capsule is characterized by the capsule diameter L_0 and capsule length, L_1 . Adapted from Aguirre et al. [37].

Gharsallaoui et al. [66] proposed values for the individual bound water volume between 16.4 and 17.2 mL/mol for sucrose in a temperature range of 0°C to 100°C, and 16.2 mL/mol for glucose at 20°C. The bound water volume is somewhat dependent on the type of sugars it binds to as a monomer, and its dependence on temperature is not clear. Therefore, we used a constant value of 16.5 mL/mol for the bound water volume of both sucrose and glucose, which we can assume to be accurate in between 25°C and 45°C.

Using density data, Gharsalloui et al. [66] then estimated the molar volume of non-hydrated sucrose, $V_{m,b}$, at several temperature points between 20°C and 80°C. Those

Modelling temperature effects in a membrane cascade system for oligosaccharides estimates showed a linear relationship with the temperature (equation (2.5)). Unlike sucrose, the data for glucose density at various temperature is not widely available. However, it is possible to estimate the molar volume of non-hydrated glucose with the partial molar volume of glucose at infinite dilution, as was derived by Fucaloro et al. [67]. Both approaches gave more or less the same estimates for the molar volume of sucrose at 20°C. Therefore, we can use Fucaloro et al.'s data for the temperature dependency of $V_{m,b}$ for glucose as well. As found with sucrose, the molar volume of non-hydrated glucose is also linear with the temperature (equation (2.6)). Both molar volumes in equations (2.5) and (2.6) are presented in mL/mol and temperatures in °C (Figure. 2.2).

$$V_{m,b}(T)_{sucrose} = 219.55 + 0.07T \quad (2.5)$$

$$V_{m,b}(T)_{glucose} = 109.41 + 0.09T \quad (2.6)$$

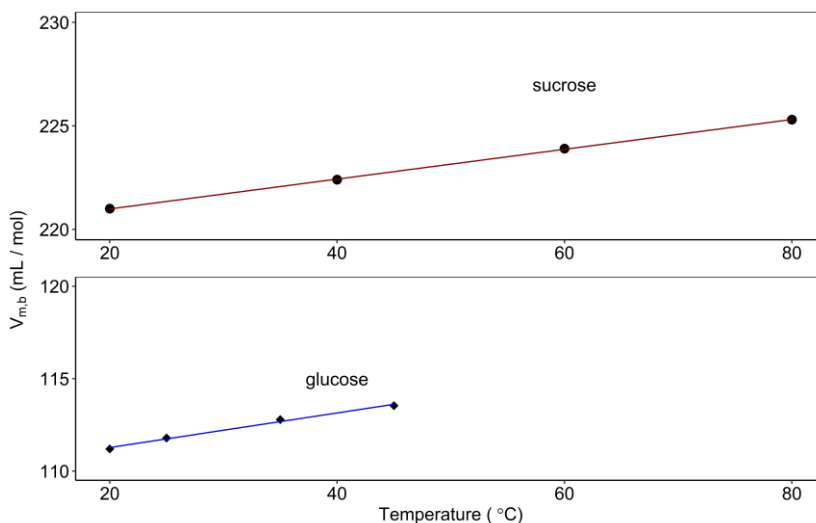


Figure. 2.2. Linear relationship between the temperature and bare volume of sucrose derived from density data [66] and fructose derived from infinite dilution [67].

The hydration numbers of both sucrose and glucose are not linear with the temperature. Gharsalloui et al. [66] fitted a quadratic equation to the hydration number of sucrose and temperature (in °C), as shown in equation (2.7). A similar approach can be taken for glucose using the data from Shiio [68]; a quadratic relationship (equation (2.8)) was also found here. The hydration number is plotted versus the temperature in Figure. 2.3.

$$n_H(T)_{sucrose} = 7.1 - 0.06 T + 3.69 \times 10^{-4} T^2 \quad (2.7)$$

$$n_H(T)_{glucose} = 7.22 - 0.19 T + 1.70 \times 10^{-3} T^2 \quad (2.8)$$

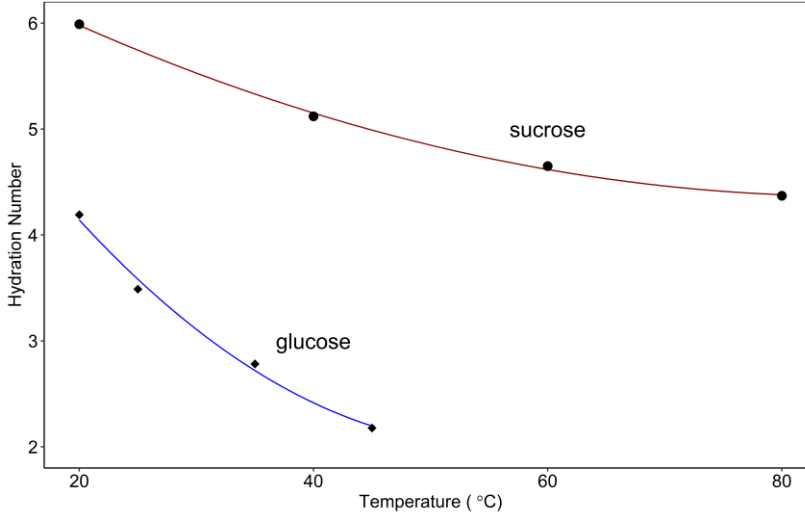


Figure 2.3. Quadratic fitting of the hydration number as a function of temperature for sucrose based on the work of Gharsallaoui et al. [66] and glucose based on the work of Shiio [68].

The combination of the molar volumes of the unhydrated molecules and the hydration numbers of sucrose and glucose enables us to estimate their hydrated molar volumes and with that, the dimension of FOS with any degree of polymerization (DP). At a given temperature, the molar volume of glucose and sucrose can be estimated using equations (2.4) - (2.8). With these values, we can calculate the molar volume of fructose in a chain. Assuming that the hydrated monosaccharides have a spherical shape, the length, $L_{0,i}$, of the glucose and fructose monomers in the chain can be calculated. Assuming that all FOS chains have only one glucose monomer (see Figure 2.1), the capsule length of FOS at a certain DP can be estimated using equation (2.9). The capsule diameter is equal to the largest diameter of the monomers, glucose.

$$L_{1,i} = L_{0,glucose} + (DP_i - 1) L_{0,fructose} \quad (2.9)$$

2.2.2 Temperature effect on viscosity

Chirife and Buera [69] have derived a model to predict the viscosity of sugar mixtures, η_s , with an exponential relation to sugar concentration relative to the viscosity of water, η_w , (equation (2.10)).

$$\frac{\eta_s}{\eta_w} = a \exp(EX) \quad (2.10)$$

Both a and E are fitting parameters. To predict the sugar viscosity, these parameters need to be estimated. In most cases, a is close to unity.

The value of E differs for every mixture and shows a linear relationship with the average molecular weight (equation (2.11)).

$$E = b\overline{MW} + c \quad (2.11)$$

Using equation (2.10), the viscosities of any sugar solutions with known average molecular weight can be estimated. This is not limited to simple sugars, because this model has been validated for oligosaccharides by knowing their average molecular weight.

Aguirre et al. [25] and Rizki et al. [60] reported estimates of the parameters in equations (2.10) and (2.11) for FOS at 45°C. To use these equations for other operating temperatures, we need to either estimate the parameters at each temperature point or define the temperature dependency of these estimates. Chirife et al. [70] reported a temperature dependency of E as in equation (2.12),

$$E = \frac{\Delta G}{R_g T} \quad (2.12)$$

in which ΔG represents the free energy of activation for viscous flow per mole of solute. Combining this with equations (2.10) and (2.11) yields equation (2.13).

$$\frac{\eta_s}{\eta_w} = a \exp \left[\left(\frac{b^* \overline{MW} + c^*}{R_g T} \right) X \right] \quad (2.13)$$

In this equation, parameters b^* and c^* represent the activation energy and its dependency on molecular weight. Therefore, this modified equation is applicable for mixtures with any average molecular weight and different operating temperatures.

2.2.3 Mass transfer model

In the absence of a cake or fouling layer on the membrane, the volumetric flux, J_v , can be calculated using Darcy's law and the effective pressure difference across the membrane, the solution viscosity and the membrane resistance, R_m . The effective pressure is defined as the transmembrane pressure, TMP , corrected for the osmotic pressure difference across

the membrane that results from the concentration gradient between 2 sides of the membrane after considering the extent of the polarization concentration (equation (2.14)). The osmotic pressure can be estimated using Van't Hoff's equation (equation (2.15)).

$$J_v = \frac{TMP - \Delta\pi_o}{\eta R_m} \quad (2.14)$$

$$\Delta\pi_o = \sum_{i=1}^n (C_{m,i} - C_{p,i}) R_g T \quad (2.15)$$

The concentration at the membrane surface, $C_{m,i}$, has a higher value than that in the bulk as a consequence of concentration polarization, which can be calculated once we know the mass transfer coefficient, k_i . We can estimate the mass transfer coefficient, k_i , using a Sherwood relation. For spiral wound modules, the relationship proposed by Schock and Miquel [71] is widely used. In addition to k_i , Stewart [72] proposed a correction on the mass transfer coefficient that corrects for flow stabilizing effects due to the suction of the solvent into the membrane (equation (2.16)). Some models neglect this correction, which is presumably acceptable for low fluxes. At low flux, the corrected mass transfer coefficient is close to its original estimate, whereas its value deviates more at higher flux.

$$\frac{k_i^*}{k_i} = \frac{J_v/k_i}{[1 - \exp(-J_v/k_i)]} \quad (2.16)$$

Recently, Aguirre et al. [37] applied a modified SPM to the transport of FOS inside a membrane based on the work of Bowen and Welfoot [11,73]. In their approach, the solute flux of a neutral component is expressed as the sum of convective and diffusive transport resulting from the concentration and pressure gradients across the membrane (equation (2.17)). In equation (2.17), C_i represents the local concentration as a function of the axial position, z .

$$J_i = K_{c,i} C_i V - D_{p,i} \frac{dC_i}{dz} - \frac{C_i D_{p,i}}{R_g T} V_m \frac{dP}{dz} \quad (2.17)$$

The convective part of the flux equation depends on the local concentration C_i , the solvent velocity inside the pore V , and a convective hindrance coefficient $K_{c,i}$. Assuming a cylindrical pore, the average solvent velocity may be approached using the Hagen-Poiseuille equation (equation (2.18)). This equation was developed for a single cylinder.

Modelling temperature effects in a membrane cascade system for oligosaccharides
 Assuming the membrane consists of parallel pores, this relation is also valid for a porous membrane. The porosity itself is considered in the effective membrane surface.

The hindrance coefficient for a solute through a cylinder can be expressed as a function of the ratio of the solute size to the pore width, λ_i , referring to the work of Dechadilok and Deen [74]. This relation was adapted by Aguirre et al. [37] by substituting the solute radius with the average Giddings radius (equation (2.19)).

$$V = -\frac{r_p^2 \Delta P}{8 \eta \Delta x} \quad (2.18)$$

$$K_{c,i} = \frac{1 + 3.867 \lambda_i - 1.907 \lambda_i^2 - 0.834 \lambda_i^3}{1 + 1.867 \lambda_i - 0.741 \lambda_i^2} \text{ with } \lambda_i = \frac{r_{G,i}}{r_p} \quad (2.19)$$

Inside the pore, the diffusivity of a solute $D_{p,i}$, is corrected with a hindrance coefficient, K_d , and a relative viscosity increase, η_r (equation (2.21)). This increase in viscosity is explained by many authors as a consequence of a thin, stagnant water layer that is attached to the pore wall, leaving less volume for diffusion of a solute. In this equation, d_w represents the thickness of this stagnant water layer, which is estimated to be 0.28 nm, the typical size of a water molecule.

$$D_{p,i} = \frac{K_d D_i}{\eta_r} \quad (2.20)$$

$$\eta_r = 1 + 18 \frac{d_w}{r_p} - 9 \left(\frac{d_w}{r_p} \right)^2 \quad (2.21)$$

$$K_d = \frac{9}{4} \pi^2 \sqrt{2} (1 - \lambda)^{-5/2} \left[1 - \frac{73}{60} (1 - \lambda) + \frac{77293}{50400} (1 - \lambda)^2 - 22.5083 - 5.6117 \lambda - 0.3363 \lambda^2 - 1.216 \lambda^3 + 1.647 \lambda^4 \right] \quad (2.22)$$

Solving equation (2.17) with boundary conditions, $C_i = \phi_i C_{m,i}$ at $z = 0$ and $C_i = \phi_i C_{p,i}$ at $z = \Delta z$, allows us to predict the solute real rejection coefficient, $R_{r,i}$ (equation (2.23)). The real rejection coefficient relates to the solute concentration at the membrane surface, which is estimated by taking into account the concentration polarization phenomenon (equation (2.26)). The partition coefficient, ϕ_i , is estimated as a function of the solute to pore ratio, λ_i , following the work of Dechadilok and Deen [74] for a cylindrical pore.

$$R_{r,i} = 1 - \frac{(K_{c,i} - K_{y,i})\phi_i}{1 - [1 - (K_c - K_y)\phi_i]\exp(-Pe)} \quad (2.23)$$

$$Pe = -\frac{(K_{c,i} - K_{y,i})r_p^2}{8\eta D_{p,i}} \Delta P \quad (2.24)$$

$$K_y = -\frac{D_{p,i}}{R_g T} V_m \frac{8\eta}{r_p^2} \quad (2.25)$$

$$R_{r,i} = 1 - \frac{C_{p,i}}{C_{m,i}} \quad (2.26)$$

$$\phi_i = 1 - \lambda_i^2 \quad (2.27)$$

2.2.4 Pore size distribution

In the model described in Section 2.2.3, the solute rejection is dependent only on the size of the individual pore. However, estimating the pore size by fitting the experimental rejection with the SPM for a mixture of FOS results in a different estimated pore size for each oligosaccharide. This is somewhat overlooked in the literature, because most publications using the SPM report on studies for single solutes. However, it is very important when dealing with mixtures.

The different pore sizes obtained with different solutes can be explained by the pore size distribution in the membrane. Even though the SPM can predict the rejection of a single cylindrical pore, not all pores are equally accessible to all solutes; larger solutes may not enter a smaller pore at all. All practical membranes have pore size distributions.

Bowen and Welfoot [73] incorporated the pore size distribution into the SPM, but only for a single solute. Based on their work, Aguirre et al. [37] predicted the rejection of FOS for a mixture by expanding equation (2.23) to all pores in the membrane, assuming a normal distribution. As a consequence, the membrane is characterized by 2 intrinsic parameters: the average pore size and the standard deviation in the pore size. This has the drawback that estimating 2 parameters in a complex, non-linear model is not trivial.

Another approach to incorporate a pore size distribution related to multicomponent mixture permeation was proposed by Kuhn et al. [40]. They assumed that some pores retain some solutes, whereas other pores let these pass freely, which they called non-rejecting pores. Further, they calculated the ratio between the flux via the non-rejecting pores for each solute and the pure water flux, i.e. the solvent flux through all pores. A

Modelling temperature effects in a membrane cascade system for oligosaccharides pore size distribution can be derived by differentiating this ratio to the pore size fitted from the SPM. In this way, a mean pore size and a standard deviation can be estimated, assuming a normal distribution of pore sizes. This yields the 2 similar parameters as in Aguirre et al.'s [37] approach.

2.2.5 Temperature effect on membrane properties

The expansion of a material is in general relatively linear over the temperature interval of interest here. If the membrane expands with temperature, it is logical that the membrane pores expand at the same rate. Therefore, we can describe the temperature effect on the membrane pore size using a one-dimensional thermal expansion of the membrane material [75]. In equation (2.28), $r_{p,0}$ is the pore size estimated at a reference temperature, T_0 . α_{rp} is the temperature coefficient of the membrane pore size.

$$r_p = r_{p,0}[1 + \alpha_{rp}(T - T_0)] \quad (2.28)$$

This relationship does not lead to a linear dependency of the hydrodynamic membrane resistance with the temperature. Combined with the effects of the temperature on the viscosity and the diffusion rates, the flux through the membrane increases strongly with the temperature. Within a limited temperature range, the flux increase can still be approximated by a linear decrease in the hydrodynamic resistance (equation (2.29)).

$$R_m = R_{m,0}[1 + \alpha_{Rm}(T - T_0)] \quad (2.29)$$

2.2.6 Membrane cascade setup

A membrane cascade consists of multiple stages of membranes arranged consecutively. A consecutive stage produces a more refined or more concentrated outlet stream and may recycle other streams to the previous stage. This way, the purity and yield of a single-stage membrane process can be improved. A schematic drawing of a 3-stage membrane cascade based on the ideal design proposed by Lightfoot [23] is shown in Figure. 2.4.

Within a 3-stage design, the streams follow the mass balance relationship. The total and component mass balances for the whole system are expressed in equation (2.30) and (2.31). These equations relate the flow rates (Fl) and concentration (C_i) in any position of the design. Subscripts F , $T1$ and $B1$ indicate the stages that the stream comes from.

$$Fl_F = Fl_{P_{T1}} + Fl_{R_{B1}} \quad (2.30)$$

$$C_{f,i} Fl_F = C_{p,i} Fl_{P_{T1}} + C_{r,i} Fl_{R_{B1}} \quad (2.31)$$

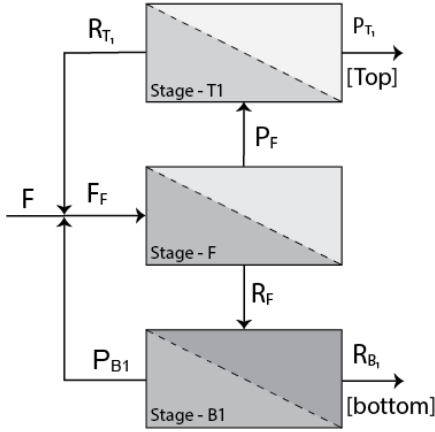


Figure. 2.4. Schematic drawing of a 3-stage membrane cascade configuration based on the ideal design proposed by Lightfoot [23].

At the mixing point, the streams follow the mass balances as expressed in equation (2.32) and (2.33). Equations (2.34) and (2.35) give the mass balances over the membrane stages. The permeate from the feed stage is also the feed for stage T1, and the retentate acts as the feed for stage B1.

$$Fl_{F_F} = Fl_F + Fl_{R_{T1}} + Fl_{P_{B1}} \quad (2.32)$$

$$C_{f,i} Fl_{F_F} = C_{f,i} Fl_F + C_{r,i} Fl_{R_{T1}} + C_{p,i} Fl_{P_{B1}} \quad (2.33)$$

$$Fl_{F_{stage}} = Fl_{P_{stage}} + Fl_{R_{stage}} \quad (2.34)$$

$$C_{f,i} Fl_{F_{stage}} = C_{p,i} Fl_{P_{stage}} + C_{r,i} Fl_{R_{stage}} \quad (2.35)$$

2.3 Materials and methods

2.3.1 Materials

All experiments were performed using Fructose L85® provided by Sensus (Roosendaal, the Netherlands). Fructose is a FOS syrup with 75% dry matter. In this research, we use 0.5 wt% of this syrup for characterization experiments and 5 wt% for validation experiments. All dilutions were with demineralized water.

Modelling temperature effects in a membrane cascade system for oligosaccharides

Fructose is a mixture of FOS with a DP ranging from 3 to 10, as well as mono- and disaccharides. In our study, oligosaccharides with a DP of 5 and higher are treated as one lumped component. We ascribe average physical properties to this lumped component, based on its overall weight fraction. The feed concentration of FOS solution used in this research is shown in Table 2.1.

Table 2.1. Feed concentration for characterization and validation experiments diluted in demineralized water.

Component	Concentration for characterization (g/L) ^a	Concentration for validation (g/L) ^a
Glucose	0.307 ± 0.019	3.126 ± 0.082
Fructose	0.073 ± 0.012	1.254 ± 0.030
DP2	0.396 ± 0.024	4.660 ± 0.120
DP3	0.706 ± 0.049	7.906 ± 0.196
DP4	0.769 ± 0.050	8.611 ± 0.214
DP ≥ 5	1.329 ± 0.089	14.973 ± 0.369

^aUncertainties are calculated based on the 95% confidence interval for all experiments.

2.3.2 Filtration experiment setup

All experiments were performed using a pilot-scale membrane unit with a process volume of 10 L. The experiments were divided into 2 groups: characterization experiments and validation experiments. The characterization experiments were performed to estimate the membrane resistance R_m and the pore size r_p using 0.5% FOS syrup diluted in demineralized water. The characterization experiments were performed at 5 temperatures between 25°C and 45°C with an interval of 5°C, and using transmembrane pressures (TMP) between 4 and 16 bar. The model that was developed using the characterized membrane properties was then validated using 5% FOS syrup in demineralized water. These validation experiments were performed at 3 temperatures (25°C, 35°C, and 45°C) and 3 TMPs (8, 12 and 16 bar).

We used 3 different membranes which vary in molecular weight cut-off: GE (MWCO 1kDa), GH (MWCO 2.5 kDa) and GK (MWCO 3.5 kDa). All membranes are model 1812C-34D from General Electric (GE Osmonics, Sterlitech, Kent, WA, USA) with an effective

membrane area of 0.38 m². The validation experiments were performed later using these same membranes. All experiments were carried out using a crossflow velocity of 0.10 m/s until steady state conditions were reached. The steady state condition was indicated by a constant refractive index at both permeate and retentate streams, which were measured inline. In practice, this was reached within 25 min.

2.3.3 Analyses

The FOS samples were analysed for their concentrations at all DPs. Components with a DP higher than 5 were analysed as 1 lumped component. The analyses were performed using high-performance liquid chromatography. A Shodex column (KS-802 8.0 × 300 mm) integrated with a refractive index detector (Shodex RI-501) was used. The chromatography system was operated at 50°C using deionized water (Milli-Q®) as eluent at a flow rate of 1 mL/min. The retention times of all FOS components in the chromatography system are presented in Table 2.2.

Table 2.2. Retention time of carbohydrate components in HPLC analysis

Component	Retention time (min) a
Glucose	10.00 ± 0.15
Fructose	9.40 ± 0.10
DP2	8.40 ± 0.10
DP3	8.00 ± 0.15
DP4	7.50 ± 0.15
DP ≥ 5	7.20 ± 0.20

^aThe interval represents the window of detection for particular components

2.3.4 Computational approach

The membrane resistance, R_m , was estimated using the experimental clean water flux. Using only water in the experiments eliminates the osmotic pressure effect in equation (2.14). The membrane resistance can then be calculated using the viscosity of water and establishing a linear regression between the TMP and the volumetric flux.

The membrane pore size, $r_{p,i}$, was estimated using very diluted FOS syrup (Table 2.1, second column). Under this condition, the effect of osmotic pressure in equation (2.14) was assumed to be small and thus negligible. The same assumption was made by Aguirre et

Modelling temperature effects in a membrane cascade system for oligosaccharides al. [37] to characterize their membrane using a modified SPM. The pore size estimation was performed by minimizing the sum of the squared errors between the predicted and the experimental rejection values (equation (2.36)). The experimental solute rejection was calculated with equation (2.26) using the measured concentrations at the permeate and retentate. The predicted solute rejection was calculated using equation (2.23) by solving the other relations in Section 2.2.3. The fitting procedure to estimate $r_{p,i}$ was performed by minimizing the residual SR_R (with the *optimize* function in R [76]) as defined in equation (2.36).

$$SR_R = \left(R_{r,i_{experiment}} - R_{r,i_{predicted}} \right)^2 \quad (2.36)$$

We did not estimate the pore size distribution; instead, different pore sizes were estimated for every solute, membrane and temperature point as mentioned in Section 2.3.2

The estimated membrane resistance and the pore size were then fitted in temperature-dependent models (equation (2.28) and (2.29)) to estimate the standard values ($r_{p,0}$ and $R_{m,0}$) and the temperature coefficients (α_{Rm} and α_{rp}) through linear regression. These linear regressions were computed using the *lm* function in R [76]. The same function was also used to estimate the parameters in quadratic models in equation (2.7) and (2.8) from literature data.

Using the standard values of the membrane resistance, pore size and their temperature coefficients, we can predict the outcome of a single-stage membrane. This model was validated using a higher concentration than the characterization experiments (Table 2.1, third column). In this case, the osmotic pressure was taken into account. To estimate the osmotic pressure, the permeate concentration is required, creating a circular calculation. In this study, we used the iterative approach developed by Yun and Petkovic [77] to solve this circular calculation. The model was then extended to predict the outcome of a cascaded system (Figure. 2.4) by solving the mass balances (equations (2.30) – (2.35)).

The separation performance for both single and cascaded membrane was evaluated according to the product purity and yield. For FOS, all oligosaccharides with DP higher than 3 are considered valuable. In a single-stage separation, the retentate stream was considered as being the most valuable product, whereas in a cascaded system, stream R_{B1} was considered to be the target product. Based on those considerations, equations (2.37) and (2.38) were formulated to describe the product purity and yield.

$$\text{Purity} = \frac{\sum_{i=3}^5 C_{r,i}}{\sum_{i=1}^5 C_{r,i}} \times 100\% \quad (2.37)$$

$$\text{Yield} = \frac{\sum_{i=3}^5 C_{r,i} Fl_R}{\sum_{i=1}^5 C_{r,i} Fl_F} \times 100\% \quad (2.38)$$

2

2.3.5 Viscosity analysis

To estimate the parameters in the temperature-dependent viscosity model (equation (2.13)), the viscosity of FOS at various concentrations and temperatures was measured using an Anton Paar MCR 502 rheometer (Graz, Austria) in a temperature range of 25°C–45°C with a 5°C interval. Dilutions of FOS syrup in demineralized water at concentrations of 1.5–8.5 wt% were used.

The parameters in equation (2.13) were estimated using a non-linear solver (*nls* function) in R [76]. This function minimized the square of residuals between the predicted and measured viscosity (equation (2.39)).

$$SR_\eta = (\eta_{measured} - \eta_{predicted})^2 \quad (2.39)$$

2.4 Results and discussion

2.4.1 Viscosity model

Our extension of the model by Chirife and Buera [69], shown in equation (2.13), showed good agreement with experiments using FOS at various concentrations (mole fraction) as shown in Figure. 2.5. The fitted parameters were estimated and expressed in equation (2.40). In this equation, fitted parameter b^* is presented in J/g and c^* in J/mol. Using this equation, the viscosity of oligosaccharide mixtures at any temperature and concentration can be predicted. In addition to the temperature effect, the ability to predict the viscosities at any concentration is also important for further application in a cascaded design. In a cascade system, each stage has different concentrations as the streams are getting more concentrated at the bottom stage and less concentrated at the top stage.

$$\frac{\eta_s}{\eta_w} = (1.043 \pm 0.011) \exp \left\{ \frac{(228.2 \pm 24.91) \overline{MW} + (27,620 \pm 10,400) X}{R_g T} \right\} \quad (2.40)$$

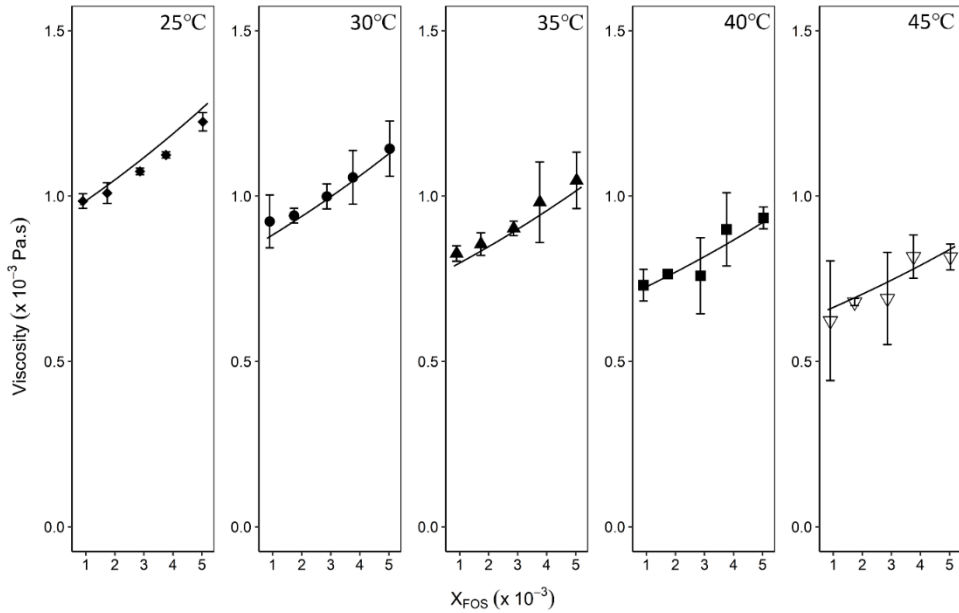


Figure 2.5. Validation of the temperature-dependent viscosity model (equation (2.13)) using various FOS concentrations (as mole fractions) at a temperature range of 25°C–45°C.

2.4.2 Membrane resistance and flux prediction

In this section, we discuss the effect of the temperature on the membrane resistance and the flux in total, as a combination of both the viscosity and the membrane resistance. The resistance and the clean water flux are discussed first, and later extended to systems with solutes.

Figure 2.6 confirms the linearity of the relationship between the temperature and the membrane resistance. The estimated parameters from Darcy's law are summarized in Table 2.3. Both the figure and the table show that the GH and GK membranes had a lower resistance at higher temperatures, while the GE membrane showed the opposite. The behaviour of the GH and GK membranes was expected, because the membrane material expands at higher temperatures, which also enlarges the pores. The opposite behaviour of the GE membrane might come from the fabrication of the membrane itself. Whereas the GH and GK were both polysulfone/polyamide composites, the GE membrane was a composite polyamide.

Figure 2.6 also depicts that the estimated inaccuracies were much larger in the GE membrane, and they were smaller in the GH membrane and even smaller in the GK membrane. This could be related to measurement inaccuracies. The measured permeate flow rate was used to calculate the flux, which was later used to estimate the membrane resistance. The GE membrane exhibited low permeate flows, which resulted in larger inaccuracies than with the higher flow rates that were measured with the GH and GK membranes. Regardless, the inaccuracy in the temperature constant, α_{Rm} , did not show this relationship; all errors were in the same order of magnitude with the estimates. This may result from error propagation in the calculation.

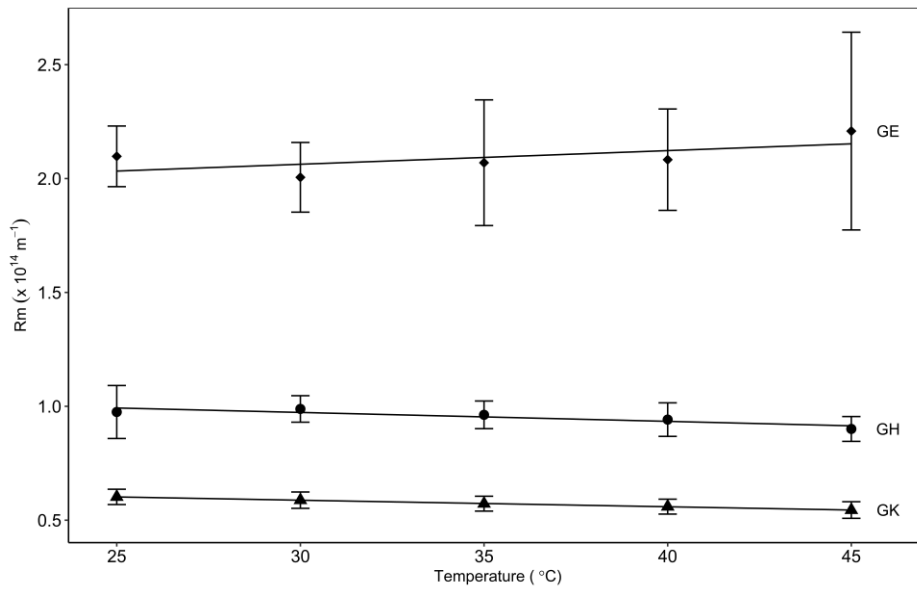


Figure 2.6. Linear relationship between temperature and membrane resistance for 3 different membranes. Membrane resistances were estimated using clean water flux at various pressures.

Table 2.3. Estimated parameters for the temperature dependency model of membrane resistance (equation (2.34)).

Membrane	R_{m_0} ($\times 10^{13} m^{-1}$)	α_{Rm} ($\times 10^{-3} m^{-1} K^{-1}$)
GE	20.33 ± 0.99	2.94 ± 3.98
GH	9.93 ± 0.79	-3.94 ± 6.53
GK	6.02 ± 0.27	-4.77 ± 3.68

Because both the viscosity and the membrane resistance depend on the temperature, the clean water flux through the membrane also depends on the temperature. Figure. 2.7 shows the temperature effect on the flux for 3 different membranes. All membranes showed strong increases in the clean water flux with temperature, despite the opposite behaviour of the membrane resistance of the GE membrane. The viscosity is therefore the dominant factor in the temperature dependence of the clean water flux for the GE membrane.

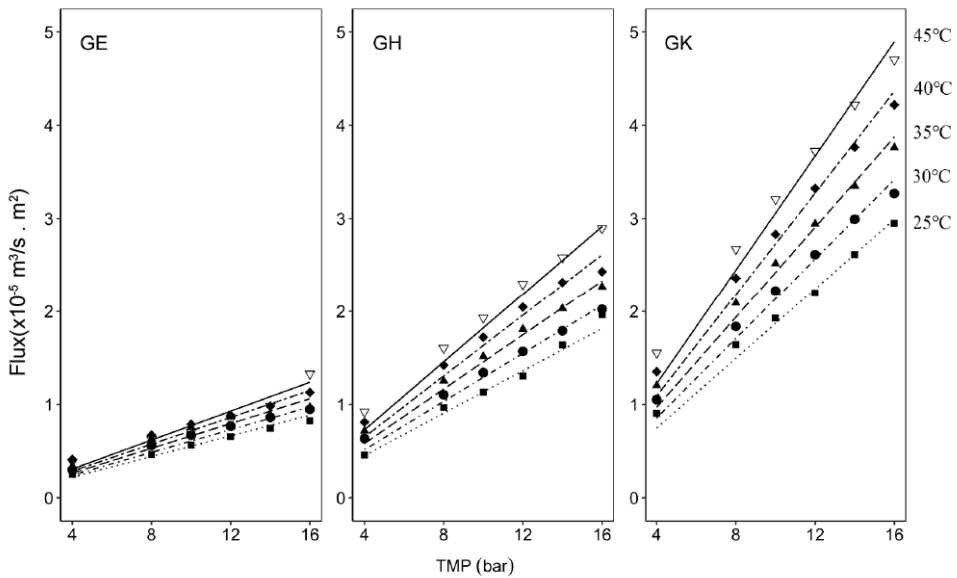


Figure. 2.7. Temperature effect of clean water flux for 3 different membranes.

The 3 membranes used in this study, being polymeric membranes, might show an irreversible response to heating, as commonly observed in many polymers as they cross their glass transition temperature (T_g). We observed a hysteresis upon immediate cooling in the GE membrane. The membrane resistance at lower temperatures showed higher values than its initial resistance after being operated at 45°C, resulting in lower fluxes. This implied that the T_g for the GE membrane lies within 25°C–45°C. Further detail about the glass transition was not studied in this research. However, from Figure. 2.6, we guess that this point existed between 30°C and 35°C for the GE membrane. The resistance initially decreased from 25°C to 30°C, as expected from the other membranes, and then increased from 30°C to 45°C. Membranes that operate above the glass transition

temperature might experience a compaction resulting in a non-linear relationship between TMP and the flux. We indeed observed this behaviour in the GE membrane as shown in Figure. 2.7.

This effect was only observed in the GE membrane upon immediate cooling. We did observe that the resistance of the GE membrane returned to its original value, as reported in Figure. 2.6, after storage. This implies that the membrane was able to slowly restructure during storage. For the other membranes, the resistance returned to its initial value upon immediate cooling after being operated at 45°C. This better explained the linear relationships for both temperature–resistance and TMP–flux for GH and GK membranes.

2.4.3 Temperature effect on membrane pore size

The membrane pore size was estimated by fitting the pore size to the data using the modified SPM (Section 2.2.3). Figure. 2.8 shows the rejections from the fitted model and the experimental data at 45°C. The same estimation procedure was repeated for every temperature point in duplicate; figures similar to Figure. 2.8 can be constructed for every repetition (see supplementary material). Using the estimates at all repetitions, a linear relationship between the pore size and the temperature was then determined by estimating the standard pore size, $r_{p,i,0}$, and the temperature coefficient, α_{rp} .

This was done for every solute, resulting in 5 values of pore sizes corresponding to 5 solutes. These values could be compiled into a mean pore size and a standard distribution, as explained in the work of Kuhn et al. [40]. However, in this work, we directly used the different pore size values that correspond to the 5 solutes. The translation towards a normal distribution would not have added predictive value to the model, and the direct use avoids the assumption of having a normal pore size distribution, which is an approximation at best.

Figure. 2.9 shows linear relationships between the temperature and the membrane pore sizes for DP4. Other solutes give similar relations (see supplementary material), which are summarized for the pore size $r_{p,i,0}$ and temperature increment α_{rp} in Table 2.4 Using both $r_{p,i,0}$ and α_{rp} values, the pore sizes at any temperature can be calculated using equation (2.28). The estimated pore sizes are in the range of those commonly reported for nanofiltration membranes (0.7–2 nm). The pore sizes for the GK membrane were the largest while the GH membrane had a similar pore size compared with the GE membrane.

However, it was not clear what the operating temperature was for these specifications, which might have been higher than 25°C; despite the similar pore size at 25°C, the GH membrane had a higher temperature increment of the pore size. Therefore, the pore size of this membrane could be higher and different from that of a GE membrane at higher temperatures.

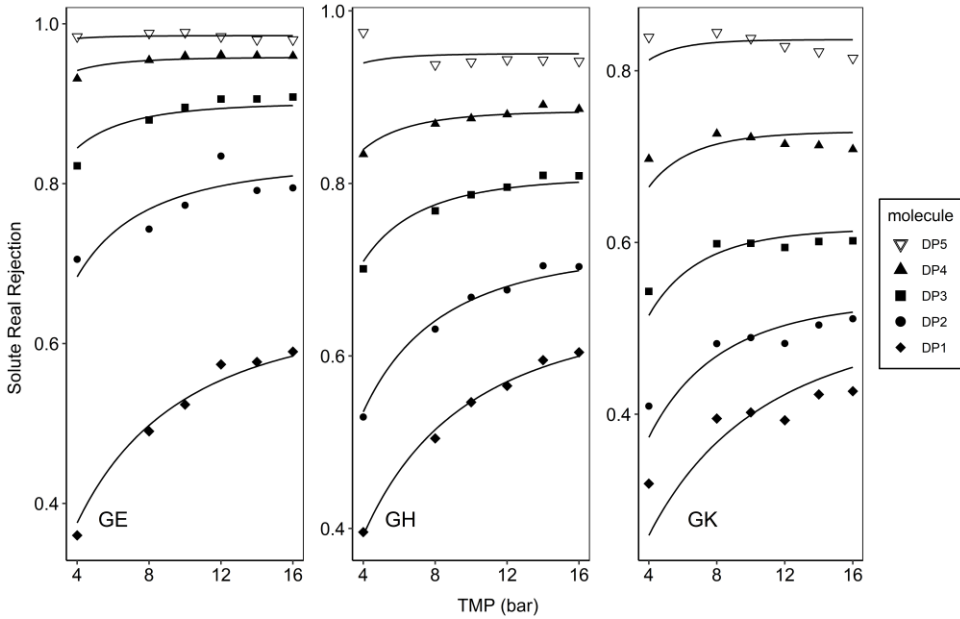


Figure. 2.8. The real rejection as function of pressure for 3 different membranes at 45°C using 0.5% FOS syrup. The symbols represent the experiments. The lines are the fitted models with the estimated pore sizes.

In addition, for all solutes, we observed larger temperature increments with a GK membrane compared with the other membranes, as shown in Figure. 2.9 and Table 2.4. The difference in these properties for different membranes might relate to the different materials and structure of the membrane. Table 2.4 tells us that the thermal increments of the pore sizes (α_{rp}) over the temperature range considered were far lower than the absolute pore size ($r_{p,i,0}$). These values varied by a maximum of 2% for GK membrane. That gave us an increase of a maximum of 0.4 nm with a temperature increase of 20°C, as used in this study.

As the temperature increases, both the solute and the membrane expand. Both changes affect the solute rejection. According to the modified SPM, the solute rejection was dependent on the solute to pore size ratio. When both change, a change in rejection would

occur depending on the sizes of the 2 changes. Here, we report that the temperature expansions of the pore size and the hydrated volume of sugar are in the same order of magnitude. Despite the similar orders of magnitude, higher values were observed for the solute dimension, which results in a small increase in the solute to pore size ratio. Thus, we predict a small increase in the rejection.

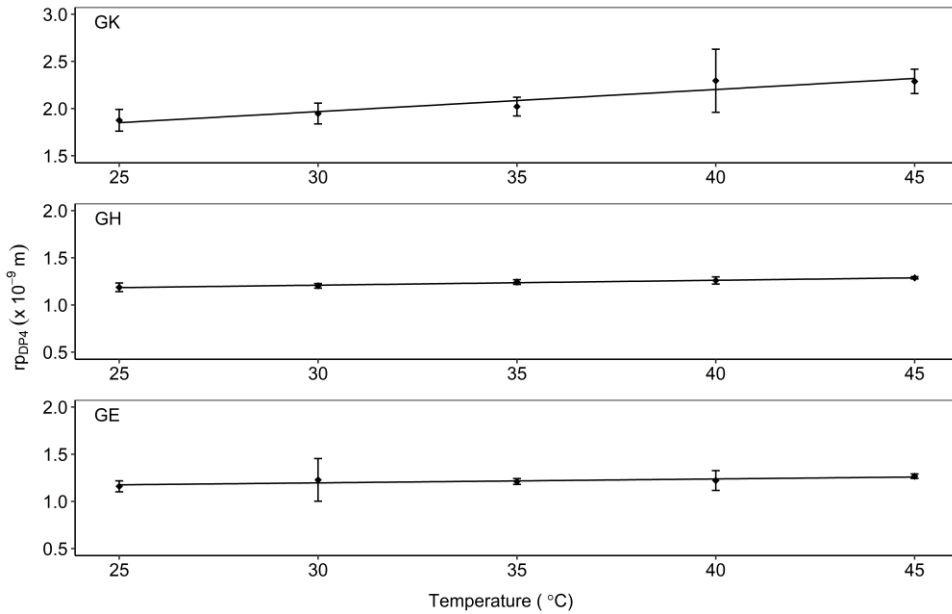


Figure 2.9. Linear relationship of temperature and pore size corresponding to DP4 for different membranes.

2.4.4 Prediction of single-stage separations

With all parameters estimated using low concentrations, we can now predict the single-stage performance at realistic concentrations.

At higher solute concentrations, the concentration polarization effect is more prominent. This leads to a larger osmotic pressure difference over the membrane and hence a lower effective driving force. At the same time, the larger concentration of solutes at the membrane also implies more transmission of the solutes through the membrane and hence a lower effective rejection than the real rejection would indicate. The concentration polarization depends on the transmembrane flux, which depends on the membrane resistance and on the viscosity. In general, the membrane resistance decreases with

Modelling temperature effects in a membrane cascade system for oligosaccharides temperature, and the solution viscosity decreases strongly. This together leads to a strong increase in the transmembrane flux with temperature.

Table 2.4. Estimate parameters (standard pore size and thermal increment) for the temperature dependency model of pore size with respect to each solute.

Membrane	Solute	$r_{G,i} (\times 10^{-9} m)$		
		at 25°C	$r_{p,i,0} (\times 10^{-9} m)$	$\alpha_{rp} (\times 10^{-10} m/K)$
GE	DP1	0.407	0.746 ± 0.014	0.011 ± 0.016
	DP2	0.601	0.950 ± 0.015	0.039 ± 0.013
	DP3	0.794	1.070 ± 0.016	0.045 ± 0.013
	DP4	0.987	1.176 ± 0.018	0.035 ± 0.013
	DP≥5	1.330	1.461 ± 0.015	0.023 ± 0.009
GH	DP1	0.407	0.703 ± 0.007	0.013 ± 0.008
	DP2	0.601	0.921 ± 0.004	0.059 ± 0.004
	DP3	0.794	1.058 ± 0.006	0.054 ± 0.004
	DP4	0.987	1.184 ± 0.005	0.044 ± 0.003
	DP≥5	1.330	1.486 ± 0.006	0.026 ± 0.003
GK	DP1	0.407	0.948 ± 0.062	0.070 ± 0.054
	DP2	0.601	1.598 ± 0.151	0.195 ± 0.079
	DP3	0.794	1.783 ± 0.096	0.168 ± 0.045
	DP4	0.987	1.851 ± 0.054	0.127 ± 0.024
	DP≥5	1.330	2.101 ± 0.024	0.089 ± 0.009

The strong increase in the water flux with temperature is not followed by the solute flux. Even though the membrane expands with temperature, the solute itself also expands. This limits the solute transport, resulting in only a slight increase in the solute flux. A rapid increase in the water flux that is not followed by the solute flux results in only a slight increase in the solute rejection. Figure. 2.10 shows that the product purity indeed increases slightly with temperature. This was expected because the solute rejection only increased slightly. Among the 3 membranes, the GK membrane was the most sensitive to

temperature change, because it had the highest temperature coefficient. Therefore, a higher FOS purity was obtained at higher temperatures.

2

The increase in flux at higher temperature resulted in a declining yield. As the temperature increases, the transmembrane flux increases strongly, and therefore, more of the feed ends up as permeate. As a consequence, less liquid is obtained as retentate. Most of the product stayed at the retentate side, but as the rejection was not 100%, a part of it also ended up in the permeate. Hence, if the permeate forms a larger part of the total volume, more of the product is lost into the permeate and hence the yield is lower. At the same time, producing more permeate also means that more of the “impurities” (smaller DPs) end up in the permeate. This effect was stronger for the smaller DPs than for the \geq DP5 product, because their rejections were smaller, and the purity was therefore slightly increased. The strongest decline in yield was observed with the GK membrane because it exhibited the largest flux increase with temperature (Section 2.4.2).

Figure. 2.10 shows a classic trade-off between purity and yield, but this trade-off was not the same for every membrane. In addition, the temperature effect in the product yield is strong. Based on these phenomena, we conclude that we can improve the separation performance by decreasing the temperature, resulting in a higher yield without losing product purity; however, this is at the cost of a lower throughput.

2.4.5 Performance of a 3-stage filtration cascade

The predictive model that was validated for single-stage membranes was extended to a cascaded system (Figure. 2.4). We selected 1 combination of process parameters as a standard, which was chosen based on the work of Aguirre et al. [25]. A membrane with double area at the feed stage was chosen. To achieve this in practice, two GK membranes were used at the feed stage and operated at a TMP of 8 bar. After the feed stage, a GH membrane was used at the top stage using a TMP of 16 bar and a GK membrane operated at a TMP of 12 bar at the bottom. The feed stream entered the feed stage at 50 kg/h.

One of the advantages of using a cascade is that each stage can be run at a different temperature. To simplify the investigation, we simulated the separation process for 2 scenarios: a homogeneous and an inhomogeneous temperature configuration. In the homogeneous configuration, the temperature was equal at all stages and was varied as a whole. In the inhomogeneous configuration, the temperature at 1 stage differed from the others. Here, 3 different cases were assessed: the feed, top and bottom cases. In these

Modelling temperature effects in a membrane cascade system for oligosaccharides cases, the temperature in 1 stage was varied from 25°C to 45°C, and the temperatures of the other stages were constant at 45°C.

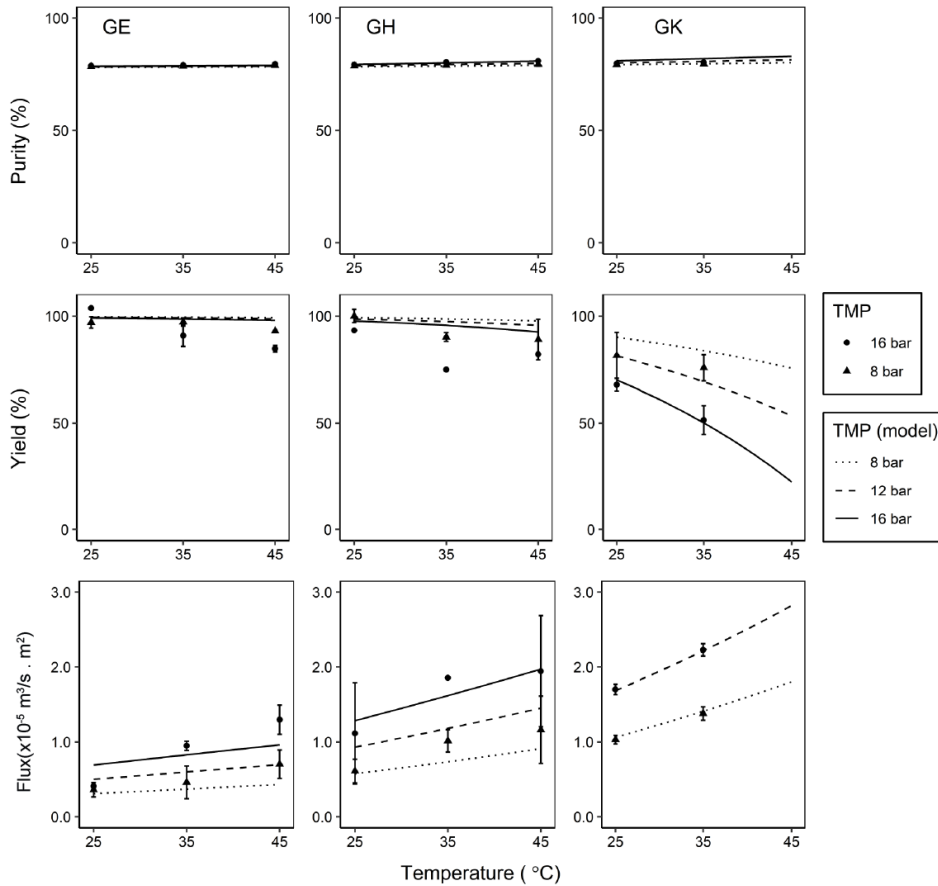


Figure. 2.10. Prediction of the temperature effect on the performance of single-stage membranes validated with 5% FOS syrup (experimentally) using a feed flow rate of 50 kg/h. The discontinued line for the GK membrane at 16 bar was due to insufficient flow rate at the retentate.

Figure. 2.11 shows the effect of the temperature on the purities and yields obtained with the membrane cascade as a function of the temperature, with the homogeneous (a) and inhomogeneous (b) temperature configurations. For all systems, qualitatively similar behaviour as in a single-stage separation was observed. The yield could be increased by lowering the temperature while the purity remained essentially the same (around 80%). The purity achieved using a cascade system (see Figure. 2.11) was higher than using a single-stage separation (see Figure. 2.10), which of course was the main purpose of using a cascaded system.

In an inhomogeneous configuration, the temperature effect on the product yield varies depending on which stage is varied in temperature. The effect of temperature was more substantial for the top stage, whereas it had hardly any effect at the bottom stage. This was related to the destination of the permeate flow at each stage. The permeate of the bottom stage was recycled to the feed stage, and the permeate of the feed stage forms the feed of the top stage. Therefore, the permeate streams of these 2 stages were processed again. On the other hand, the permeate of the top stage was directly extracted from the system. In the case of FOS (\geq DP3), the oligosaccharides in the permeate of the top stage are considered as a loss, lowering the yield of the oligosaccharides in the bottom retentate. Although the purity of the stream remained more or less the same, the increase in the permeate flow rate at the top stage directly reduced the yield. Using this treatment, the separation can achieve 97% yield.

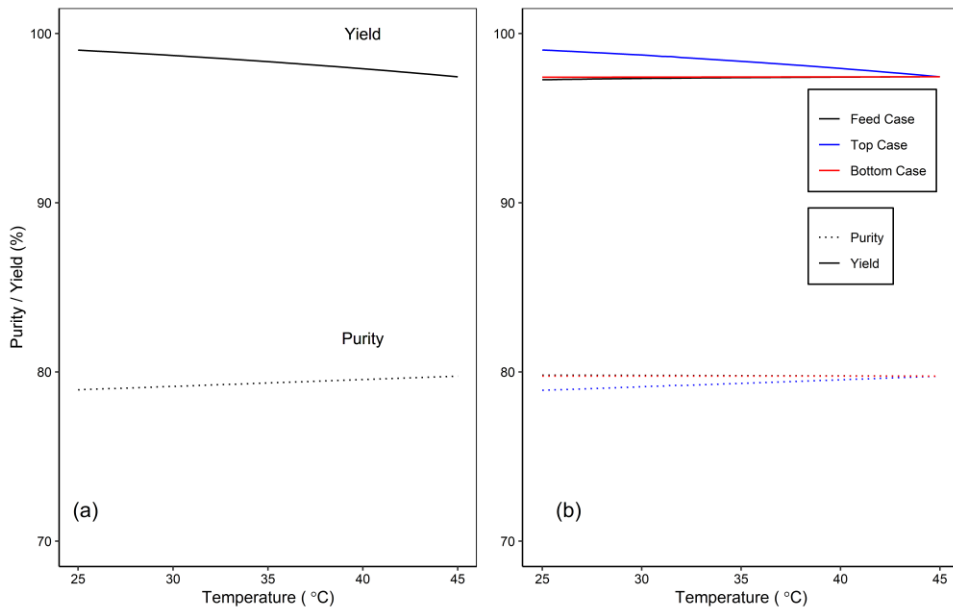


Figure 2.11. Temperature effect in the cascaded filtration system using the homogeneous (a) and inhomogeneous (b) temperature setup. In the inhomogeneous setup, the temperature at 2 other stages were set at 45°C, and 1 was varied according to the case. All simulations were done using a feed flow rate of 50 kg/h.

2.5 Conclusions

The effect of the temperature on the nanofiltration of a mixture of fructo-oligosaccharides was investigated through experiment and through modelling. An increase in the temperature affects the process in 3 ways: (1) it expands the solute, (2) it reduces the solution viscosity, and (3) it expands the membrane pore size while at the same time reducing its hydraulic resistance. All these factors contribute to the overall performance of a filtration process, which was assessed by measuring and modelling its purity and yield.

Although the fluxes become much larger with increasing temperature, the temperature hardly affects the product rejection and purity. However, the yield is strongly affected by the temperature, with higher yields at lower temperatures. This is related to the larger fluxes at higher temperature, leading to a larger split of the feed into the permeate, and more of the product ending up in the permeate flow. Similar behaviour was observed in a 3-stage cascaded system. The temperature effect was more prominent at the top stage, due to the permeate stream that is directly extracted off the system.

Acknowledgements

The authors would like to acknowledge Lembaga Pengelola Dana Pendidikan (LPDP), and Kementerian Keuangan Indonesia for financial support.

Nomenclature

C	solute concentration [g L^{-1}]
D	diffusion coefficient [$\text{m}^2 \text{s}^{-1}$]
d_h	hydraulic diameter [m]
D_p	diffusion coefficient inside the pore [$\text{m}^2 \text{s}^{-1}$]
E	dimensionless parameter in the viscosity model [dimensionless]
Fl	flow rate [kg h^{-1}]
J_v	volumetric flux [$\text{m}^3 \text{s}^{-1} \text{m}^{-2}$]
k	mass transfer coefficient [m s^{-1}]

k^*	corrected mass transfer coefficient [m s^{-1}]
k_B	Boltzmann constant [$1.38 \times 10^{-23} \text{ m}^2 \text{ kg s}^{-2} \text{ K}^{-1}$]
K_c	convective hindrance coefficient [dimensionless]
K_D	diffusive hindrance coefficient [dimensionless]
K_Y	lumped parameter in the modified SPM [dimensionless]
L_0	capsule diameter [m]
L_1	capsule length [m]
MW	molecular weight [kg mol^{-1}]
n_h	hydration number [dimensionless]
P	product purity [wt%]
Pe	Peclet number [dimensionless]
R_g	gas constant [$\text{J mol}^{-1} \text{ K}^{-1}$]
r_G	Giddings radius [m]
R_m	membrane resistance [m^{-1}]
r_p	pore radius [m]
R_r	real rejection coefficient [dimensionless]
r_S	Stokes radius [m]
T	process temperature [K]
T_0	reference temperature [25°C]
TMP	transmembrane pressure [Pa]
u	crossflow velocity [m s^{-1}]
V	solvent velocity [m s^{-1}]
$V_{m,b}$	bare molar volume of non-hydrated components [m^3]
$V_{m,bw}$	molar volume of bound water [m^3]
$V_{m,h}$	molar volume of hydrated components [m^3]
X	total sugar molar fraction [dimensionless]
Y	product yield [%]

Greek letters

α_{Rm}	temperature coefficient for membrane resistance [K ⁻¹]
α_{rp}	temperature coefficient for membrane pore radius [K ⁻¹]
η_s	solution viscosity [Pa s]
η_w	water viscosity [Pa s]
λ	solute to pore ratio [dimensionless]
π_o	osmotic pressure [Pa]
ρ	density [kg m ⁻³]
ϕ	partition coefficient [dimensionless]

Subscripts

$F, T1, B1$	stage
i	solute, degree of polymerization
m	membrane wall
p	permeate side
P, R	permeate and retentate streams
r	retentate side



Chapter 3

Separation of fructose and glucose via nanofiltration in presence of fructooligosaccharides

This chapter is based on

Z. Rizki, A.E.M. Janssen, A. van der Padt, R.M. Boom,
“Separation of fructose and glucose via nanofiltration
in presence of fructooligosaccharides”,
submitted for publication

Abstract

Fructose and glucose are commonly present together in mixtures and may need to be separated. Current separation methods for these isomers are complex and costly. Nanofiltration is a cost-effective method that has been widely used for separating carbohydrates of different sizes; however, it is not commonly used for such similar molecules. Here, we report the separation of fructose and glucose in a nanofiltration system in the presence of fructooligosaccharides (FOS). Experiments were performed using a pilot-scale filtration setup using a spiral wound nanofiltration membrane with molecular weight cutoff of 1 kDa. We observed 3 important factors that affected the separation: (1) separation of monosaccharides only occurred in the presence of FOS and became more effective when FOS dominated the solution; (2) better separation was achieved when the monosaccharides were mainly fructose; and (3) the presence of salt improved the separation only moderately.

3.1 Introduction

Fructose and glucose are sugar isomers with different properties. Fructose is sweeter than glucose [36], thus less is needed for the same sweetness. Moreover, fructose follows a different metabolic path in humans that makes it less prone to cause diabetes [78]. Therefore, fructose consumption in our diet is preferred to glucose [79]. Fructose is commonly produced by enzymatic isomerization of glucose obtained from starch [80]. After the conversion, fructose needs to be separated from the mixture, which still contains glucose.

The fact that glucose and fructose are isomers implies that they have somewhat similar chemical and physical properties [81]. Thus, they are difficult to separate by conventional means. Separation of monosaccharides has been attempted via crystallization [82], chromatography [83–85] and liquid membranes [86]. However, these methods are costly and difficult to operate and maintain.

Nanofiltration is a more cost-effective and flexible separation process. It has been widely used to separate or purify sugars [48,87] and oligosaccharides [37,40,41,56,60,88] from mixtures of carbohydrates. However, the separation is generally based primarily on a difference in size, and therefore cannot be used to separate sugars or isomers that have similar properties and are of similar size [11,25,52].

Nanofiltration is already used for the purification of fructooligosaccharides (FOS) to remove small sugars from long-chain oligosaccharides [56,57,88]. FOS in its native form is a mixture of oligofructoses with various degrees of polymerization (DP). The DP determines the health benefits and functional properties of the FOS products [31,34]. Monosaccharides add to the caloric content of the mixture and add sweetness, which is not always desired.

FOS purification using nanofiltration aims to achieve a higher content of long oligosaccharides in the product. Separation of the monosaccharides is not expected and therefore often ignored or not reported. Based on the similar molecular sizes of glucose and fructose, it was expected that both molecules would be rejected more or less equally. However, this is not observed. In some studies, the rejection of fructose is much lower than that of glucose [25,60,88]; in other studies the opposite is observed [40,56]. The ratio of the rejection of fructose and glucose from these studies is shown in Figure 3.1. Various types of membranes and feed sources were used that may relate to their difference in

selectivity. Unfortunately, to date, this phenomenon has not been explored and explained. We therefore investigate this separation of monosaccharides and the influence of the presence of larger sugars on this separation.

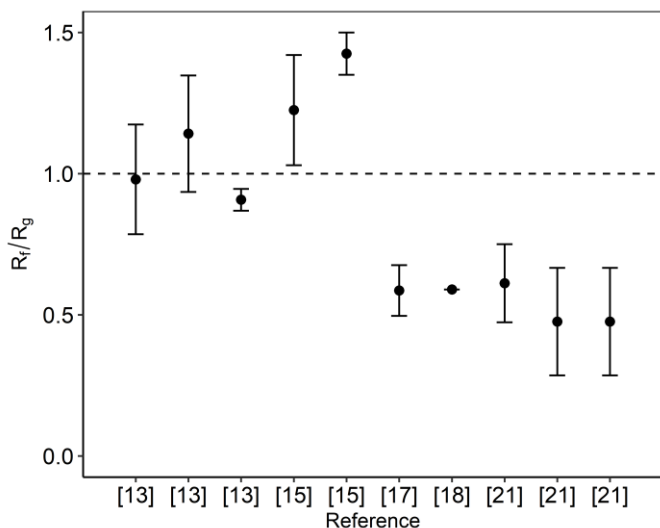


Figure 3.1. Rejection ratio of fructose over glucose (R_f/R_g) from various references [25,40,56,60,88] under different set-ups and feeds.

Both glucose and fructose show polymorphic behaviour in solution; several configurations of the sugars are present simultaneously. Apart from their open chain form, glucose has the pyranose form, whereas fructose has both the pyranose and the furanose forms [89,90]. Since it has fewer carbon atoms in its main ring, the furanose form is smaller than the pyranose form. In equilibrium, around 25% fructose is in its furanose form, which makes its average size smaller than that of glucose [91]. Therefore, a smaller rejection is often observed for fructose compared with glucose.

Both glucose and fructose are reported to have affinity with cations such as sodium and calcium. This is used in affinity separations such as chromatography [83]. Both sugars show different affinity towards specific ions, and therefore one sugar migrates faster than the other in a chromatographic column containing a specific sequestered ion. If the ion is not sequestered to the column, a sugar-ion complex that is larger than a free sugar is formed [92–94]. In addition, this complexation transforms a neutral sugar into a charged complex, which may also affect the sieving mechanism in nanofiltration. Separating sugars with the aid of cations was previously reported with a cellulose acetate membrane

— Separation of fructose and glucose via nanofiltration in presence of fructooligosaccharides [95]; residual trace cations in the industrial FOS mixture may have been responsible for this.

In this research, we study the separation of fructose and glucose using nanofiltration in the presence of FOS. The feed composition is varied to find the key factor for this separation and its mechanism. Further development of this separation will be useful for finding alternative methods to separate sugar isomers, which currently requires more costly processes.

3.2 Experimental

3.2.1 Materials

The experiments in this research were performed using mixtures of FOS syrup (Frutalose L85), glucose (D-(+)-glucose monohydrate) and fructose (D-(-)-fructose) in various compositions. The Frutalose syrup was kindly provided by Sensus (Roosendaal, the Netherlands) and the monosaccharides were purchased from Merck KGaA (Darmstadt, Germany). The FOS syrup contained 75 wt% of dry matter, consisting of carbohydrates with a degree of polymerization (DP) ranging from 1 to 10. Monosaccharides were added to this mixture taking into account the monosaccharides that were already present in the FOS syrup. The carbohydrate composition (dry basis) of the FOS syrup is presented in Table 3.1. In this table, the oligosaccharides with DP 5 and higher are shown as a single lumped component.

Table 3.1. Carbohydrate composition (on a dry weight basis) of FOS syrup used in this research.

Component	Concentration (%-wt) ^a
Glucose	6.9 ± 0.5
Fructose	2.0 ± 0.2
DP2	10.0 ± 1.1
DP3	23.6 ± 1.5
DP4	23.9 ± 1.4
DP 5 and higher	33.6 ± 2.3

^aUncertainties were calculated based on a 95% confidence interval.

Salts were added to the mixtures in the form of NaCl (purity $\geq 99.5\%$) and CaCl₂ (purity $\geq 93\%$). Both salts were purchased from Sigma-Aldrich (Merck KGaA, Darmstadt, Germany).

3.2.2 Filtration experiment setup

All experiments were performed using a pilot-scale membrane unit with a total process volume of 7.5L, which included a volume of 2.5L inside the equipment. A spiral wound nanofiltration membrane (GE type, 1812 model) from General Electric (GE Osmonics, Sterlitech, Kent, WA, USA) was used. The experiments were carried out at a fixed temperature of 45°C, a transmembrane pressure (TMP) of 16 bar and a cross flow velocity of 0.10 m/s. Each experiment was operated until a steady state condition was achieved. This was indicated by stable refractive indices in both permeate and retentate streams. After steady state conditions had been achieved, samples were taken from the feed, permeate and retentate streams to be analysed for their carbohydrate composition.

We carried out filtration experiments with various concentrations and compositions of carbohydrates with and without addition of salts. Mixtures of carbohydrates were prepared by combining the FOS syrup with glucose and fructose powder and diluting with demineralized water. All experiments that involved FOS were prepared by diluting to 5% of the FOS syrup resulting in 35 g/L total oligosaccharides (DP \geq 3). Except the experiments that investigated the effects of the ratio of mono- to oligosaccharides, all experiments had the same overall monosaccharide concentration of 16 g/L but with various ratios of fructose to glucose. In the experiments that involved salts, the salts were added to have a cation concentration of 0.25 – 2 g/L. The experiments performed in this study are summarized in Table 3.2.

Table 3.2. Variation of carbohydrates and salts concentration in all experiments

Experiments	C_{DP1}	$C_{DP\geq 3}$	$C_{DP1}/C_{DP\geq 3}$	C_{fru}/C_{glu}	C_{Na^+} or $C_{Ca^{2+}}$
	[g/L]	[g/L]			[g/L]
Experiment A	9 – 140	35	0.25 – 4	1	–
Experiment B	16	35	0.45	0.25 – 4	–
Experiment C	16	–	–	0.25 – 4	–
Experiment D	16	35	– and 0.45	0.25 – 4	0.25 – 2

3.2.3 Analyses

The carbohydrate concentrations of all samples were analysed using high-performance liquid chromatography on a Shodex column (KS-802 8.0 × 300 mm) that was integrated with a refractive index detector (Shodex RI-501). The separation in the column was carried out at 50°C with demineralized water (Milli-Q) as eluent at a flow rate of 1 mL/min. Apart from the monosaccharides, the other carbohydrates were quantified regarding their DPs. Oligosaccharides with DP5 or higher were quantified as one grouped component. The monosaccharides, on the other hand, were quantified as fructose and glucose separately.

3.3 Results and discussion

This work was inspired by a finding while studying the separation of FOS with nanofiltration, with the composition shown in Table 3.1. We use this solution as a benchmark, because it gave a surprising selectivity between fructose and glucose during nanofiltration. The selectivity is presented as a rejection ratio, R_f/R_g . Its value during nanofiltration of the FOS solution was found to be 0.59 and this is presented as a dot-dashed line in the figures. We compared this solution with a mixture containing the same concentrations of fructose and glucose without the oligosaccharides, which did not show good separation, with $R_f/R_g = 0.92$. This value is presented as a dotted line. We found 3 essential differences in the FOS solution that may cause the separation: (1) oligosaccharides were present; (2) fructose and glucose were present in non-equimolar concentrations; (3) as a natural mixture, the FOS solution may contain some trace ions. We investigate these 3 factors in the following sections.

3.3.1 The effect of oligosaccharides

We varied the ratio of mono- to oligosaccharides in the FOS mixture by adding fructose and glucose. The oligosaccharides concentration was kept constant at 35 g/L. The total monosaccharides concentration was varied (Table 3.2, experiment A) while keeping the final concentration of fructose similar to that of glucose. The effect on their selectivity, R_f/R_g , is shown in Figure 3.2. The horizontal axis in Figure 3.2 can be divided into 2 zones: the positive side of the axis where the monosaccharides are dominant and the negative axis where the oligosaccharides are dominant. Extending this axis towards

infinity represents systems with only monosaccharides (right-hand side) and only oligosaccharides (left-hand side).

A selectivity < 1 represents higher retention of glucose. This selectivity is independent of the ratio of mono- to oligosaccharides with higher concentrations of monosaccharides but tending towards lower values with lower ratios, indicating a better separation between fructose and glucose if the oligosaccharide concentration is high. All results were between the 2 reference values (indicated by the dotted line and dot-dashed line; see previous section). This implies that the presence of oligosaccharides (or other dissolved and retained components) indeed influences and promotes the separation of fructose and glucose. The FOS reference naturally has an excess of oligosaccharides compared with the monosaccharides, with $\ln(C_{DP1}/C_{DP\geq 3}) = -2.2$, which positions further left (Figure 3.2). The result shows a tendency towards this reference value.

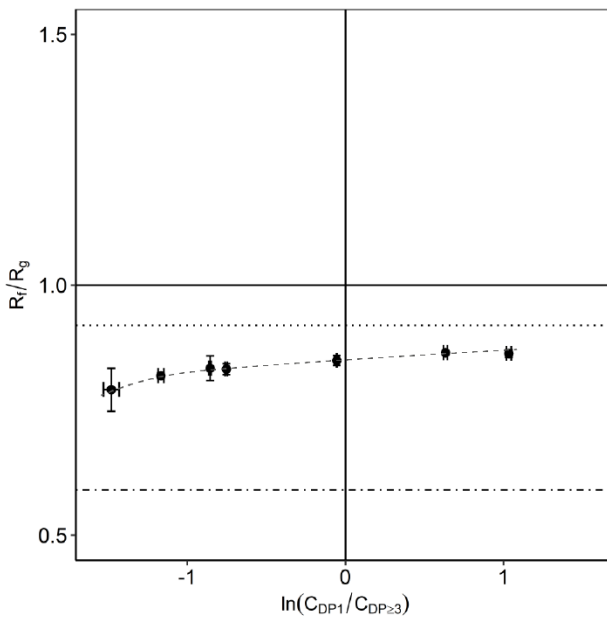


Figure 3.2. Effect of oligosaccharides concentration on selectivity in a nanofiltration system. The dotted line is the reference rejection ratio for a mixture with only fructose and glucose. The dot-dashed line is the reference rejection ratio for the FOS mixture. The dashed line is shown to guide the eye.

3.3.2 Effect of monosaccharides composition

Keeping the oligosaccharide and total monosaccharide concentrations constant (Table 3.2, experiment B), we varied the ratio between fructose and glucose, and show the results in

— Separation of fructose and glucose via nanofiltration in presence of fructooligosaccharides

Figure 3.3. The separation was enhanced with an excess of fructose. This was mainly due to a lower retention of fructose, whereas the retention of glucose did not really change. With an excess of glucose, the separation factors tended to 1, which is even higher than without any FOS present.

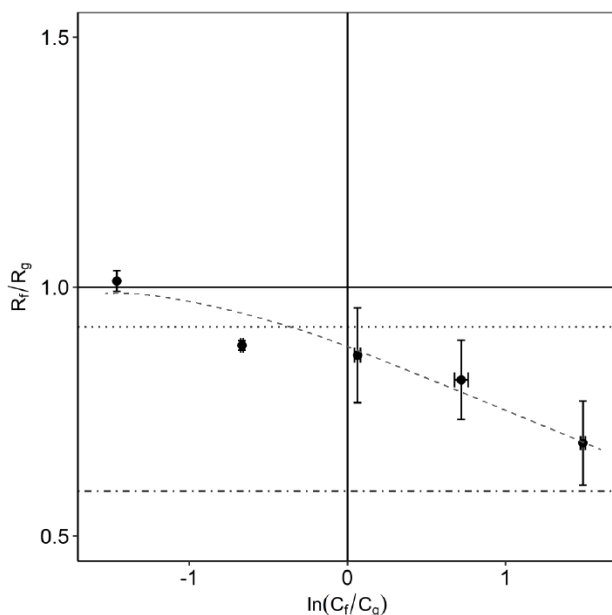


Figure 3.3. Effect of the monosaccharide composition on selectivity in a nanofiltration system. The total oligosaccharide concentration was 35 g/L, and the total monosaccharide concentration was 16 g/L. The dotted line is the reference rejection ratio for a mixture with only fructose and glucose. The dot-dashed line is the reference rejection ratio for the FOS mixture. The dashed line is shown to guide the eye.

The better separation with an excess of fructose was only observed when FOS was present. When the oligosaccharides were absent, the rejection ratio of fructose and glucose was almost constant at various ratios of fructose to glucose (Figure 3.4). The reason that this value is slightly below 1 is caused by fructose being partly in the furanose form, which is slightly smaller than fructose in the pyranose form.

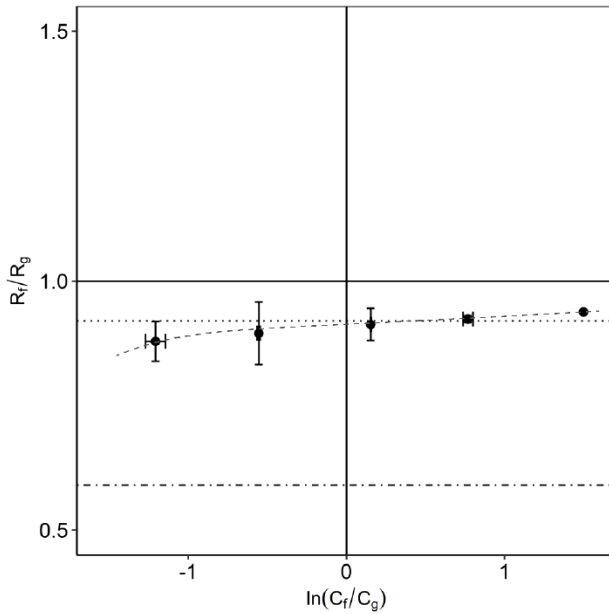


Figure 3.4. The rejection ratio of fructose and glucose in a nanofiltration system with only monosaccharides. The total monosaccharide concentration was 16 g/L. The dotted line is the reference rejection ratio for a mixture with only fructose and glucose. The dot-dashed line is the reference rejection ratio for FOS mixture. The dashed line is shown to guide the eye.

3.3.3 Effect of electrolytes

The addition of small amounts of salts increased the separation somewhat as indicated by a decrease in the rejection ratio of fructose and glucose. However, at some point, adding more salts did not change the separation further (Figure 3.5). Both sugars interact with the cations, albeit at different levels. Depending on the ion, one sugar may have stronger affinity than the others. In a mixture with only monosaccharides, the addition of NaCl improved the separation by lowering the rejection ratio. This implies that the retention of glucose increased more strongly than that of fructose, based on the stronger interaction of glucose with sodium ions. At some point, the addition of salt did not improve the separation any further. We again saw that the effect was mostly present with an excess of fructose; with equimolar concentrations or an excess of glucose, we saw little influence of the metal ions.

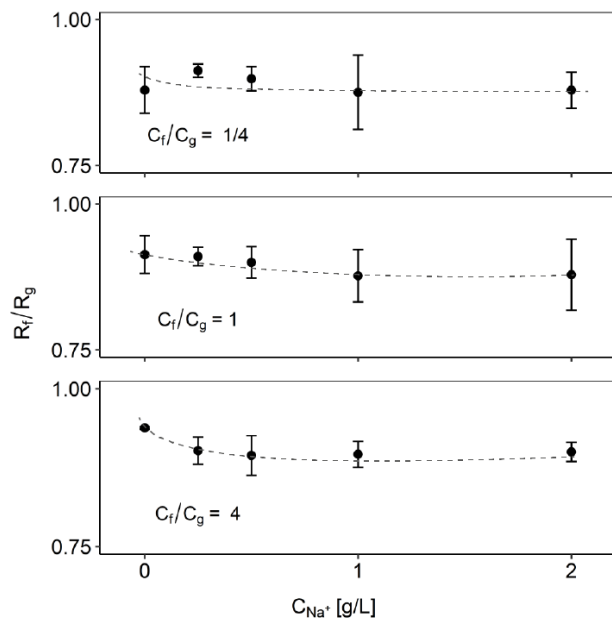


Figure 3.5. Effect of addition of salt on the separation of fructose and glucose in nanofiltration with only monosaccharides. The total monosaccharide concentration was 16 g/L. The dashed lines are shown to guide the eye.

In solutions with FOS (Figure 3.6), we observed similar trends, but with much larger selectivity. An equimolar concentration of glucose and fructose gave a slight increase in the separation (reduction in the selectivity factor), but only with small amounts of salt. Both sodium and calcium affected the separation similarly. With an excess of glucose present ($C_f/C_g = 1/4$), there was no significant effect of either Ca or Na on the separation. However, with an excess of fructose, the separation was larger (lower separation factor), and Na had a stronger effect than Ca ($C_f/C_g = 4$).

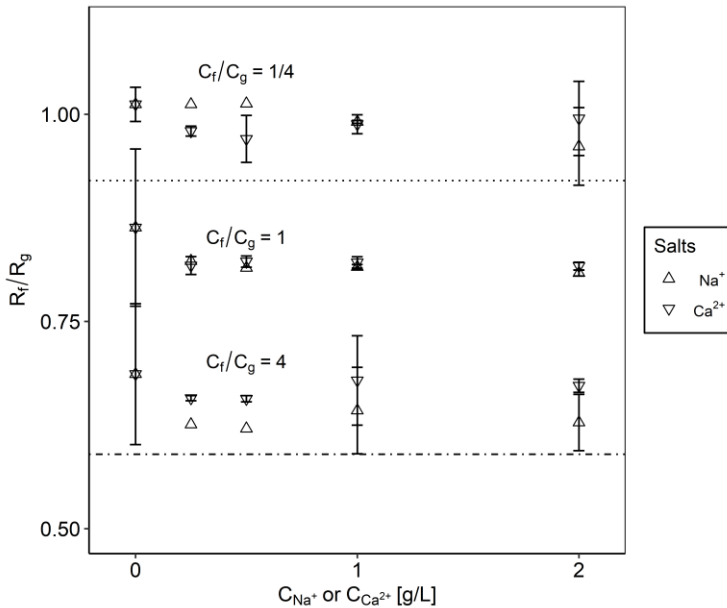


Figure 3.6. Effects of addition of salt on the separation of fructose and glucose in the FOS system. The oligosaccharide concentration was 35 g/L, and the monosaccharide concentration was 16 g/L.

3.3.4 General discussion

Separation between fructose and glucose during nanofiltration only occurred at a significant level in the presence of oligosaccharides, and this separation was stronger with low concentrations of monosaccharides relative to the oligosaccharides. The separation was much more pronounced with an excess of fructose relative to glucose. There was some influence of the presence of small concentrations of metal ions (Ca or Na), but the addition of salt had a much smaller effect than the composition of the monosaccharides.

We expect that a concentration polarization layer is present near the membrane. In this layer, the FOS concentration gradually increases from the bulk to the surface of the membrane. This polarization layer acts as an additional barrier for the transport of components towards the permeate. We expect that the selectivity between the monosaccharides is due to different transport in the polarization layer.

This sugar transport across the polarization layer can be affected by the interaction between FOS and the monosaccharides, e.g. by hydrogen bonding. FOS molecules contain free hydroxyl groups that can form hydrogen bonds. Also fructose and glucose have free hydroxyl groups that allow them to form hydrogen bonds with FOS. Topographically, the

— Separation of fructose and glucose via nanofiltration in presence of fructooligosaccharides hydroxyl groups in fructose are positioned differently compared with glucose. Fructose is reported to form stronger hydrogen bonds [96,97]. Therefore fructose may have more affinity towards FOS than glucose. However, these fructose molecules will take up space between the FOS molecules, which will exclude the glucose molecules, leading to a net selectivity.

The presence of the polarization layer explains the results described in Sections 3.3.1 and 3.3.2. Without FOS in the polarization layer, the only selectivity is through sieving by the membrane. As the difference in the size of the monosaccharides is small, a low and constant selectivity was observed. As soon as FOS are present in the solution, selective transport through the polarization layer results in lower fructose rejection. When the concentration of oligosaccharides is low, the polarization layer features low concentrations. Therefore, there may still be some residual selectivity. With higher concentrations of FOS in the mixture, the polarization layer is more concentrated, the selective transport is more effective and the separation is enhanced.

We therefore hypothesize that the selective transport occurs due to hydrogen bonding between mono- and oligosaccharides, leading to preferential binding of fructose, and thus exclusion of glucose from the concentration polarization layer. Therefore, the presence of salts does not significantly affect this mechanism. The small effects that were observed with ions may have been because of weak complexation, but may also have been because of different ionic strengths. However, these effects were small.

3.4 Conclusions

Separation of fructose and glucose was observed using nanofiltration in the presence of FOS. The FOS formed a polarization layer on the membrane surface, which acted as a selective barrier for the monosaccharides. Fructose has stronger interaction with FOS, therefore glucose is excluded from the concentration polarization layer; hence, fructose permeates faster than glucose. This separation occurs only when the FOS is present at sufficient concentration relative to the monosaccharides.

The separation is strongest with an excess of fructose relative to glucose. The presence of low concentrations of metal ions (sodium or calcium) enhanced the selectivity somewhat, but higher concentrations had no additional effect. This may be due to charge interaction with the membrane itself. We did not observe any clear indication of complexation between monosaccharides and metal ions.

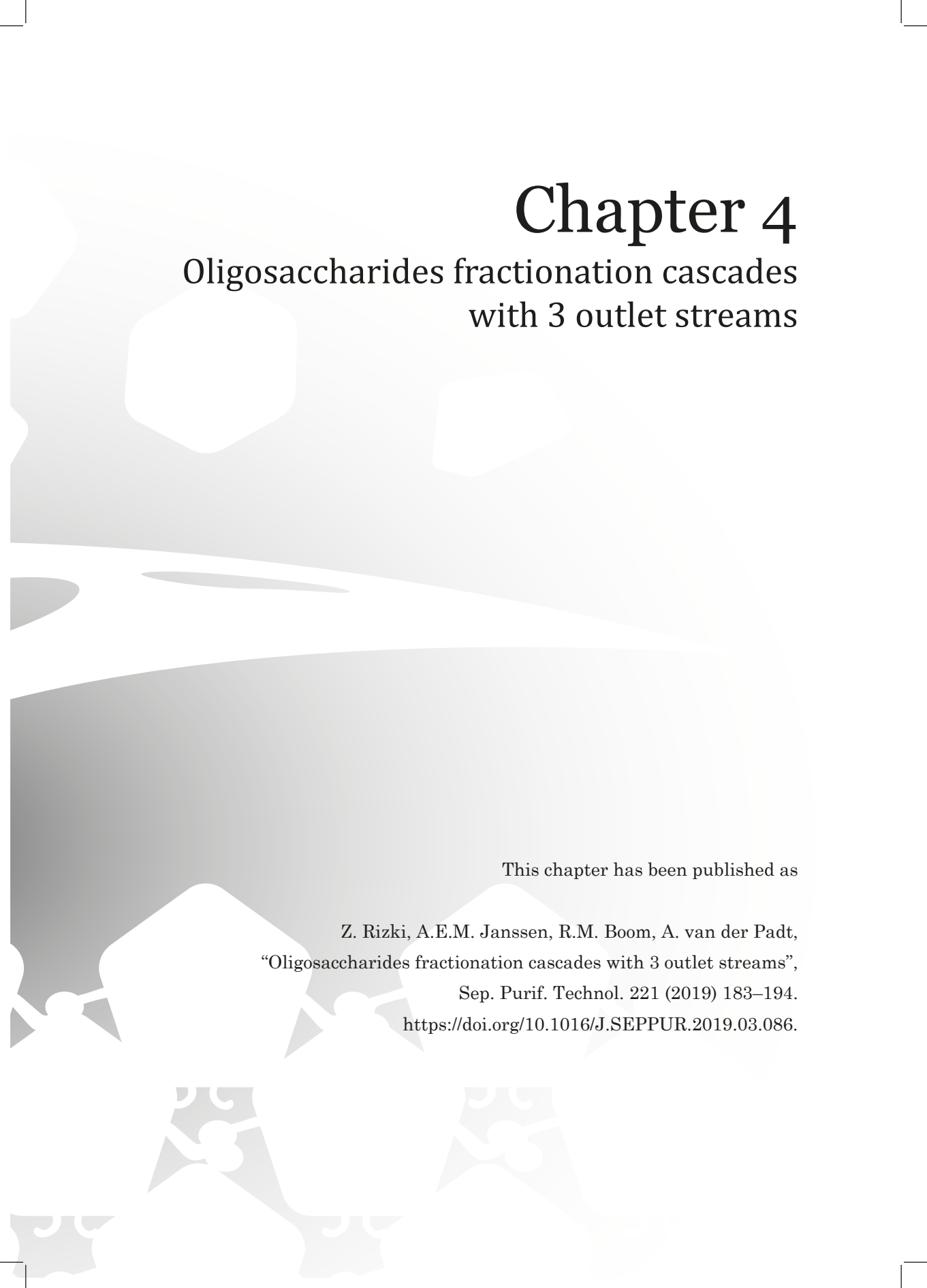
Acknowledgements

The authors would like to acknowledge Lembaga Pengelola Dana Pendidikan (LPDP), and Kementerian Keuangan Indonesia for financial support.

— Separation of fructose and glucose via nanofiltration in presence of fructooligosaccharides

3





Chapter 4

Oligosaccharides fractionation cascades with 3 outlet streams

This chapter has been published as

Z. Rizki, A.E.M. Janssen, R.M. Boom, A. van der Padt,
“Oligosaccharides fractionation cascades with 3 outlet streams”,
Sep. Purif. Technol. 221 (2019) 183–194.
<https://doi.org/10.1016/J.SEPPUR.2019.03.086>.

Abstract

Fructooligosaccharides (FOS) were fractionated using nanofiltration cascades. Instead of creating one product and a residual stream, we report on configurations that create 3 separate product streams rich in: (1) monosaccharides (DP1), (2) DP3 and (3) DP \geq 5. We developed a modular system allowing different operating pressures and membrane types at each stage. Two possible alternative configurations were assessed for a 3-stage cascade both experimentally and via simulation. The simulation was performed using a steady state model and was in a good agreement with the experimental data. Using the simulation model, the system was optimized towards 4 and 5 stage cascades. All designs were evaluated based on the purities and yields of 3 components of interest in the corresponding product streams. Selecting the correct set up, the cascade was able to reach maximum purity of monosaccharides to 66 wt% (from 9 wt%), DP3 to 33 wt% (from 24 wt%) and DP \geq 5 to 54 wt% (from 34wt%). Increasing the number of stages improved the maximum purities of the 3 fractions. However, a fifth stage did not increase the purification and the best purities were found using 4-stage rather than 5-stage cascades.

4.1 Introduction

Membrane separation processes are often used to purify certain food components or ingredients; reported applications include proteins [38], fruit juices [98], sugars and oligosaccharides [39–42] and salt removal [99]. Corresponding to the molecular size of the main products, the membranes used vary from ultra- and nanofiltration to reverse osmosis.

To increase the purity of the target components, these membrane processes require dilution, which is commonly known as diafiltration. This makes the process inefficient with regard to water usage and requires subsequent concentration of the permeate. Li et al. [57] and Foley [100] investigated varying the volume of diafiltration to reduce the water requirement during separation, but a single-stage membrane process has limits regarding product yield and purity. Cordova [59] used 3-stage nanofiltration to improve oligosaccharide purification. Patil et.al. [20,24] and Aguirre et. al. [25] investigated multi-stage membrane processes using a cascaded configuration, both experimentally and by modelling. Such configuration increased the product purity and did not require continuous diafiltration.

The membrane cascade concept is based on further processing both the permeate and retentate streams while recycling the secondary streams to the former stages (Figure 4.1.a). The systems used by Patil and Aguirre differ from the “ideal cascade” concept proposed by Lighfoot [23] in which the streams enter the mixing point at the same composition; both recycle streams and the feed stream in Figure 4.1.a should have similar compositions. Unlike the ideal cascade, Aguirre’s cascade system may contain various types of membranes and operating conditions at each stage. This system raises an optimization issue in designing the best conditions: selecting the best membrane type for each stage as well as the operating conditions becomes a challenge due to the large number of possible combinations. By solving this challenge, better separation performance can be achieved.

So far, research on membrane cascades has focused on purification of valuable products with 2 outlet streams [20,24,25,101]: one stream containing the “light” fraction with smaller molecular weight components that is isolated from a “heavy” stream with larger molecular weight components. This article investigates the potential to extract a third stream that contains a middle fraction. A side stream can be extracted from the recycled

stream in a certain ratio such that the middle fraction can be obtained as a product (Figure 4.1b and c). This approach maintains the system as close as possible to the ideal configuration, however the concentration entering the mixing point must differ to ensure the separation of the middle size component.

Fructooligosaccharides (FOS) are naturally occurring multicomponent mixtures that have gained interest as a prebiotic ingredient. FOS are oligomers of fructose and glucose, with a degree of polymerization (DP) ranging from one to several tens [32]. These oligomers have different properties depending on their chain length. Long- and short-chain FOS show different rheological behaviour and have different sweetness and nutritional value [31,33–35,54]. The small sugars are undesired because of their sweet taste and high calorie content. Considering the mild conditions during membrane processing and the molecular size of the oligomers in the FOS mixtures, a nanofiltration cascade is a highly promising option for removing the mono- and disaccharides, and at the same time fractionating into short- (SC-) and long-chain FOS (LC-FOS).

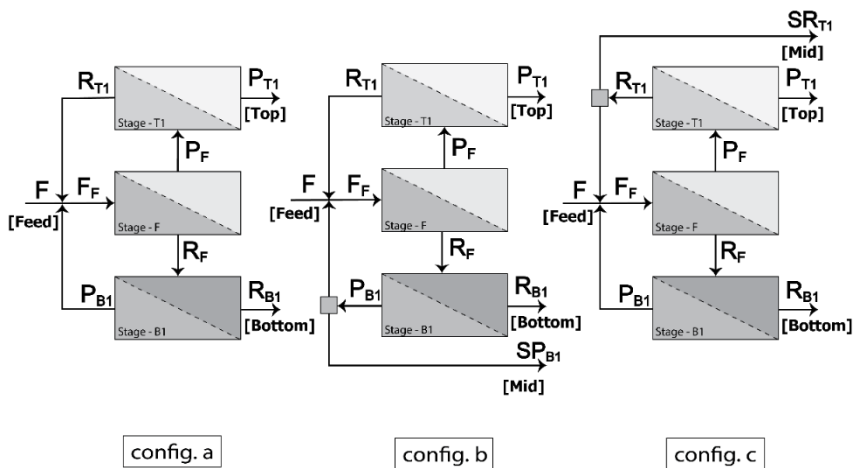


Figure 4.1. Configuration of an ideal membrane cascade (a) and fractionation using a membrane cascade with different side stream positions: SP_{B1} from stage-B1 (b) and SR_{T1} from stage-T1 (c). Mono- and disaccharides are expected in the top product stream. Oligosaccharides rich in DP3 and DP \geq 5 are expected in the mid and bottom product streams.

4.2 Model development

4.2.1 Mass transfer model

The model used in this study is derived from a previous model used for membrane cascade systems [25]. This model includes the behaviour in the concentration polarization layer (Eq. (4.1)), which causes the concentration at the membrane surface ($c_{w,i}$) to be larger than the retentate bulk concentration ($c_{r,i}$); $c_{p,i}$ is the solute concentration at permeate.

$$\frac{c_{w,i} - c_{p,i}}{c_{r,i} - c_{p,i}} = \exp\left(\frac{J}{k_i}\right) \quad (4.1)$$

The permeate flux, J , is a function of the driving force and the hydraulic membrane resistance. The driving force in the system consists of the imposed transmembrane pressure (TMP) corrected with the osmotic pressure difference ($\Delta\pi$) over the membrane (Eq. (4.2)). The osmotic pressure difference depends on the concentration of each component at the permeate side and the membrane surface (Eq. (4.3)). Furthermore, the hydraulic membrane resistance, R_m , can be determined experimentally using pure water, which eliminates the effect of the osmotic pressure in equation. (4.2).

$$J = \frac{\Delta P_{\text{eff}}}{\mu R_m} = \frac{\text{TMP} - \Delta\pi}{\mu R_m} \quad (4.2)$$

$$\Delta\pi = \sum_{i=1}^n \frac{RT}{MW_i} (c_{w,i} - c_{p,i}) \quad (4.3)$$

The viscosity of the sugar mixture is calculated using an empirical relation introduced by Chirife and Buera [69] (Eq. (4.4)); the relative viscosity (μ_r) is the ratio of the viscosities of the mixture and of water and depends on the total sugar molar fraction (X). This relationship uses a parameter E , which is linearly dependent on the molecular weight, MW , of the sugars (Eq. (4.5)). This relationship was validated by Aguirre and co-workers [25] for a mixture of oligosaccharides, but a fixed value for E using the average FOS concentration was used.

$$\mu_r = a \exp(EX) \quad (4.4)$$

$$E = b MW + c \quad (4.5)$$

In our cascade system, the concentration in each stream varies as well as the average molecular weight. Therefore, the viscosity model should consider the variation of the

molecular weight in each stream instead of using a fixed value for E . Combining Eqs. (4.4) and (4.5), a viscosity model dependent on concentration and molecular weight is constructed (Eq. (4.6)). This relation has 3 parameters, which can be estimated via experiments.

$$\mu_r = a \exp[(bMW + c)X] \quad (4.6)$$

The mass transfer coefficients for each species, k_i , are determined using a Sherwood equation (Eqs. (4.7) – (4.10)) derived by Schock and Miquel [71] and the values for the diffusion coefficients are determined from the literature (mono- and disaccharides) or estimated (degree of polymerization $[DP] \geq 3$) using a relationship developed by Sano and Yamamoto [64].

$$k_i = \frac{Sh_i D_i}{d_h} \quad (4.7)$$

$$Sh_i = 0.065 Re^{0.875} Sc^{0.25} \quad (4.8)$$

$$Sc_i = \frac{\mu}{\rho D_i} \quad (4.9)$$

$$Re = \frac{\rho u_v d_h}{\mu} \quad (4.10)$$

Our model utilizes the real rejection coefficient, $R_{r,i}$, which was calculated using experimental data for concentrations and the concentration polarization equation (Eq. (4.1)).

$$R_{r,i} = 1 - \frac{c_{p,i}}{c_{w,i}} \quad (4.11)$$

4.2.2 Performance parameters

We evaluate the performance of the system based on the purities and yield for the desired fractions. Three fractions rich in (1) monosaccharides, (2) SC-FOS and (3) LC-FOS are extracted from the top, middle and bottom products, respectively. The long-chain oligosaccharides with a DP more than 5 are considered as one lumped component with average properties based on the weight composition of the individual components. This simplifies the system into a mixture of 5 components with various DPs split into 3 products. The purity evaluation is referred to the purity of monosaccharides (P_1), DP3 (P_3)

and $DP \geq 5$ (P_5) at their corresponding outlet streams. These purities are compared with the purities of the respective components at the feed mixture and are represented as purification factors (PF_i) showing a relative purity increase for a particular component. In the case of oligosaccharides, all carbohydrates with $DP \geq 3$ are considered valuable; the yield for mid- ($Y_{FOS, Mid}$) and bottom ($Y_{FOS, Bottom}$) products are calculated based on these carbohydrates. The cumulative value of both yields ($Y_{FOS, Total}$) expresses the total amount of oligosaccharides collected from both mid and bottom products.

Besides the purities and yields, the separation factor is also used to evaluate the process. The separation factor is defined as the ratio of the concentration of 2 components in the outlet stream normalized with their concentrations in the feed stream. Pairwise combinations can be generated for all components considered in the system. However, the key separation occurs in between 2 adjacent components in the order of size. This implies that the separation of $DP1/DP \geq 5$ is guaranteed to be good if the separation $DP3/DP \geq 5$ is also good. For that reason, only the separation of $DP3$ and $DP \geq 5$ ($SF_{3,5}$) considered in our fractionation cascade system. In addition, a high $SF_{3,5}$ implies that the mid product is richer in $DP3$ and thus has different properties than the bottom product, despite the contamination of monosaccharides in the product.

Calculations of the aforementioned parameters are summarized in Eqs. (4.12) – (4.20). The purities and concentrations are calculated based on mass.

$$P_1 = \frac{c_{1, Top}}{\sum_{i=1}^5 c_{i, Top}} \quad (4.12)$$

$$P_3 = \frac{c_{3, Mid}}{\sum_{i=1}^5 c_{i, Mid}} \quad (4.13)$$

$$P_5 = \frac{c_{5, Bottom}}{\sum_{i=1}^5 c_{i, Bottom}} \quad (4.14)$$

$$PF_i = \frac{\frac{c_{i, Product}}{\sum_{i=1}^5 c_{i, Product}}}{\frac{c_{i, Feed}}{\sum_{i=1}^5 c_{i, Feed}}} \quad (4.15)$$

$$Y_1 = \frac{\sum_{i=1}^2 c_{i, Top} \cdot F_{Top}}{\sum_{i=1}^2 c_{i, Feed} \cdot F_{Feed}} \quad (4.16)$$

$$Y_{\text{FOS.Mid}} = \frac{\sum_{i=3}^5 c_{i,\text{Mid}} \cdot F_{\text{Mid}}}{\sum_{i=3}^5 c_{i,\text{Feed}} \cdot F_{\text{Feed}}} \quad (4.17)$$

$$Y_{\text{FOS.Bottom}} = \frac{\sum_{i=3}^5 c_{i,\text{Bottom}} \cdot F_{\text{Bottom}}}{\sum_{i=3}^5 c_{i,\text{Feed}} \cdot F_{\text{Feed}}} \quad (4.18)$$

$$Y_{\text{FOS.Total}} = Y_{\text{FOS.Mid}} + Y_{\text{FOS.Bottom}} \quad (4.19)$$

$$SF_{3,5} = \frac{c_{3,\text{Mid}}/c_{5,\text{Mid}}}{c_{3,\text{Feed}}/c_{5,\text{Feed}}} \quad (4.20)$$

4.3 Materials and methods

4.3.1 Materials

The separation experiments were performed using a 5 wt% solution of FOS syrup (Frutalose L85[®]) kindly provided by Sensus (Roosendaal, the Netherlands). This syrup contains FOS oligomers ranging from DP3 to DP10 as well as smaller sugars (mono- and disaccharides). The syrup itself has 75% dry matter content. The feed solutions were analysed via high performance liquid chromatography (HPLC) and are summarized in Table 4.1.

Table 4.1. Feed components and concentration for all experiments using 5%-wt of FOS syrup.

Annotation, <i>i</i>	Component	Concentration (mg/mL) ^a	Composition (wt %)
1a	Fructose	3.02 ± 0.18	6.9
1b	Glucose	0.88 ± 0.10	2.0
2	Sucrose	4.41 ± 0.46	10.0
3	DP3	10.37 ± 0.58	23.6
4	DP4	10.52 ± 0.53	23.9
5	≥ DP5	14.76 ± 0.89	33.6

^aUncertainties were calculated based on the 95% confidence interval from all experiments.

4.3.2 Experimental setup

A pilot-scale 3-stage cascade with spiral wound membranes was used. Each stage was connected with flexible tubes allowing the creation of different configurations. Each membrane stage had a process volume of approximately 2.5 L.

The membranes used were GE, GH and GK (model 1812C-34D) from GE (GE Osmonic, Sterlitech, Kent, WA, USA). Each membrane had a surface area of 0.32 m² and a spacer thickness of 0.86 mm. Following previous research [25], the feed stage used 2 membrane modules (total area 0.64 m²) and the other 2 stages used a single module. Despite the different membranes and pressures used in the experiments, the setup and areas of the membranes in all stages were not changed.

Each membrane has a different molecular weight cut-off (MWCO) and hydraulic resistance. The hydraulic resistance of the membrane is determined via a preliminary experiment using clean water. The use of several batches of membranes cannot be avoided when measuring a wide range of possible combinations in the setups. Therefore, there is some variation in the membrane properties due to the variations in the membrane preparation process. The clean water flux for each membrane type is presented in Figure. 4.2 with hydraulic resistance values of 22.17, 9.58 and 7.87 × 10¹³ m⁻¹ for GE, GH and GK membranes, respectively. The confidence interval shown is calculated based on 3 different membranes selected randomly for each type of membrane.

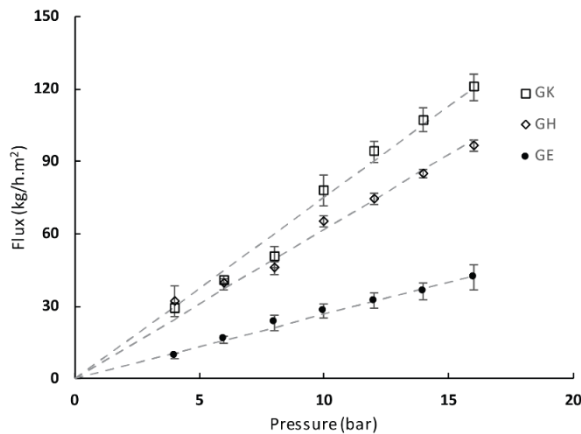


Figure. 4.2. Clean water flux of GE, GH, and GK membranes at 45°C. Error bars show 95% confidence intervals calculated from 3 different batches of membranes.

The cascade stage units are equipped with mass flow and refractometers and are logged automatically. Each experiment was performed until steady state was achieved, which was identified as a constant value of the refractive indices of all streams. Typically, steady state was achieved within 25 minutes. All experiments were performed at $45 \pm 1^\circ\text{C}$, which was 5°C lower than the maximum allowable temperature of the membranes. A cross-flow velocity of 0.08 ms^{-1} was used in all experiments

The combinations used in the experiments with configuration a were developed based on the optimized parameters reported in a previous study [25]; the pressures over the top and bottom stage were set at maximum and the pressure over the membrane of the first stage was lower. A larger area at the first stage is important to have sufficient flow to further process at the top stage. However, such a combination was found to be not feasible in some other configurations. Therefore, a lower pressure at the top and bottom stage was chosen.

The combinations used in the experiments using configuration b and c were pre-screened via simulation. The combinations that had maximum purities and yields for each component of interest (monosaccharides, DP3 and DP \geq 5) were chosen. An overview of the validation experiments is given in Table 4.2.

4.3.3 Analyses

The analyses of the sugars were performed with HPLC using a Shodex KS-802 8.0×300 (mm) column. The column is operated at 50°C and connected to a refractive index (RI) detector (Shodex RI-501). Milli-Q water was used as eluent with a flow rate of 1.5 mL/min .

The concentration-dependent viscosity was measured using a rheometer (Physica MCR 301, Anton Paar, Germany). A set of solutions was made with various compositions of FOS, sucrose, fructose, and glucose representing the variation of all streams inside the cascade system, yielding different combinations of concentration and average molecular weight. All measurements were performed at 45°C . The 3 parameters in Eq. (4.6) were estimated by fitting the relation to the experimental data following the Levenberg-Marquardt algorithm.

Table 4.2. List of experiments and their operating conditions using 3 different configurations (Figure 4.1). The feed stage used doubled membrane ($A=0.64 \text{ m}^2$) while the other stages used a single membrane ($A=0.32 \text{ m}^2$).

Experiment	Membrane at stage T1/F/B1	Pressure at stage T1/F/B1 (bar)	Feed flow rate (kg/h)	Configuration
a-1	GH/GK/GK	16/8/16	50	Configuration a
a-2	GH/GK/GK	8/8/8	50	
a-3	GK/GK/GE	16/12/16	50	
b	GH/GK/GK	8/8/8	50	Configuration b, $r=0.5^a$
b-1	GE/GE/GE	8/8/8	50	
b-2	GH/GH/GK	16/8/16	60	
b-3	GK/GK/GE	16/12/16	50	
c	GH/GK/GK	8/8/8	50	Configuration c, $r=0.5^a$
c-1	GE/GE/GE	8/8/8	50	
c-2	GE/GE/GK	12/8/12	60	
c-3	GE/GK/GK	8/16/12	50	
c-4	GK/GK/GE	16/12/16	50	

^aThe ratio between the side stream (SP_{B1} or SR_{T1}) and the recycle stream.

4.3.4 Modelling and prediction

We focused on the steady state and thus use a steady state model instead of the previously proposed dynamic model [25]. By simplifying the dynamic model into a steady state one, the use of differential equations can be avoided, and a simpler algorithm is developed via iteration. Furthermore, the current model does not have an implicit derivative, which is required in most iteration procedures (e.g. Newton-Raphson). To avoid this, an iteration procedure developed by Yun [102] was used. The solution of the steady state model is explained in Figure. 4.3. The numeric calculation was performed using MATLAB.

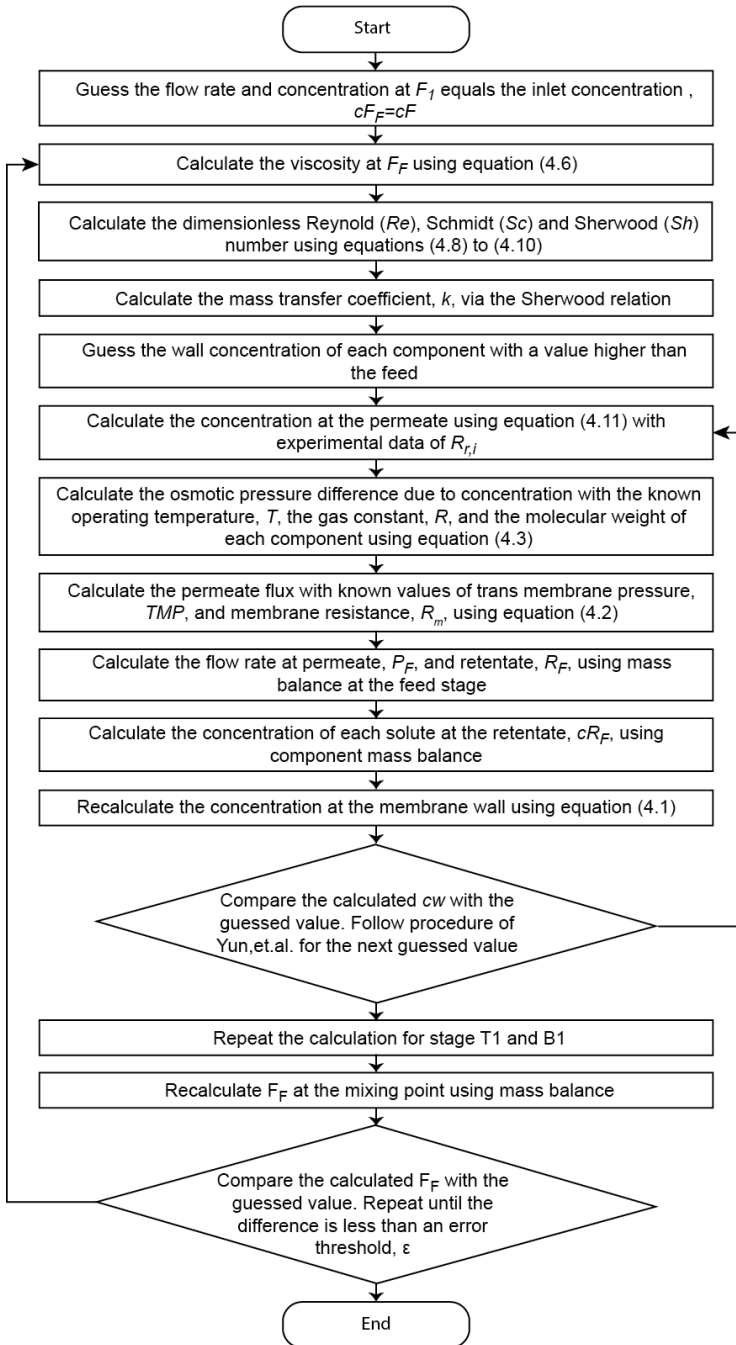


Figure. 4.3. Algorithm to solve the steady state model.

The algorithm first solves the iteration for each stage and then repeats the same procedure for the other stages. Finally, the iteration is performed over the whole system by constructing a mass balance that is dependent on the configuration. This stepwise iteration approach allows for easier adjustment of the configuration, which is part of the objective of this study. The mass balance calculation can be easily altered when the configuration changes.

The simulation is used to calculate the purities and yields (eq. (4.12) - (4.19)). To see the correlation between each purity and yield (x and y), the (Pearson) correlation coefficient, CC, is calculated (eq.(4.21)). This parameter shows whether a change of one purity affects the other purities or yields.

$$CC_{x,y} = \frac{\sum_{k=1}^n (x_k - \bar{x})(y_k - \bar{y})}{\sqrt{\sum_{k=1}^n (x_k - \bar{x})^2} \sqrt{\sum_{k=1}^n (y_k - \bar{y})^2}} \quad (4.21)$$

4.4 Results and discussion

4.4.1 Concentration-dependent viscosity

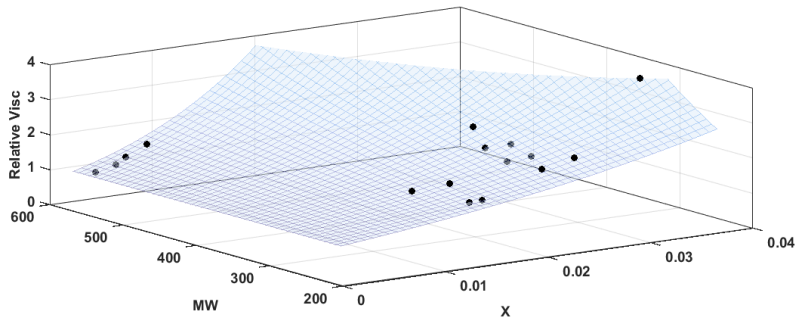


Figure 4.4. Curve fitting of the concentration-dependent viscosity model for mixtures of sucrose, glucose, fructose and FOS with various concentrations at 45°C.

As shown in Figure 4.4, Eq. (4.6) fit well with the experimental data with an R^2 value of 0.995, so the viscosities of mixtures of mono- and oligosaccharides were predicted well inside this range of concentrations. This implied that the viscosity model was suitable for use in a comprehensive model to predict the system behaviour in the cascaded system. The values of the 3 estimated parameters in the viscosity equation are shown in Eq. (4.22). The value of c (1.45 ± 5.22) was much bigger than the value of b (0.12 ± 0.04); c is a coefficient for the molar fraction, X , which was quite small in the range of this study.

Therefore, a significant change in c still gave a comparable viscosity when multiplied by the molar fraction.

$$\mu_r = (1.13 \pm 0.04) \exp \{[(0.12 \pm 0.02)MW + (1.45 \pm 5.22)]X\} \quad (4.22)$$

4.4.2 Rejection coefficient of single-stage membranes

The performance of single-stage membrane processes is important in this study to predict the behaviour of a cascaded system. The confidence interval was due to the variation of the membrane resistance (Figure. 4.2), and also due to the variation of the rejection coefficient over different batches of membranes. Three experiments using different batches of membrane were performed to find the rejection coefficient, including the variation for each type. The summary of the rejection coefficients for each membrane is shown in Figure. 4.5.

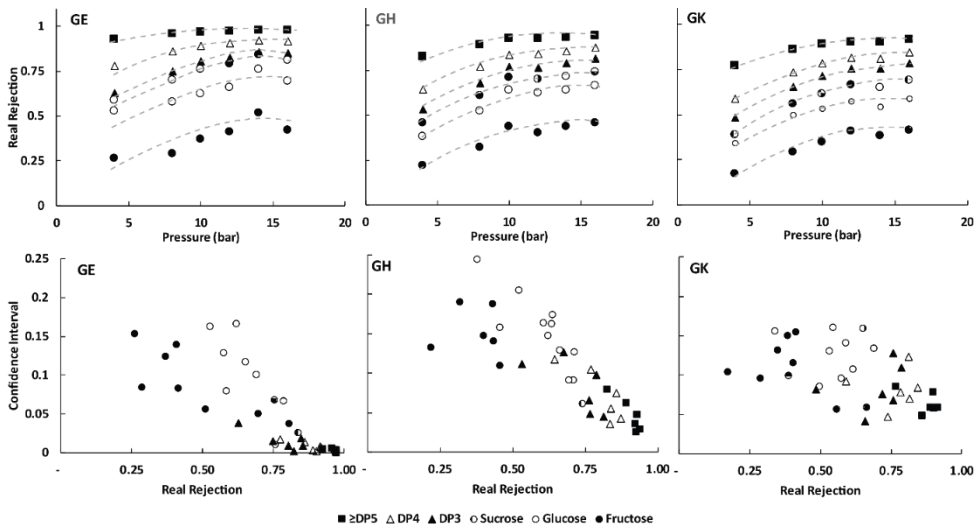


Figure. 4.5. Average (top) real rejection ($R_{r,i}$) values of GE, GH and GK membranes at 45°C and their 95% confidence interval (bottom) measured from 3 different batches of membranes. The dashed lines are guides for the eye.

The rejection coefficients found in this study were of the same magnitude as those previously reported [25], however, our values showed a significant variance. This variance depended on the value of the rejection coefficient itself; a low rejection had bigger variance and the deviation was much smaller at high rejections. This phenomenon was closely related to the definition of the rejection (Eq. (4.11)) and the error accumulation was higher

at a low value; in practice, the concentration was measured instead of the rejection. Comparing 2 values that were almost equal results in a higher error than for values that were largely apart. Although the detailed mechanism of rejection was not studied in this project, this phenomenon was important in the use of a cascade, because the usage of various batches of membrane cannot be avoided either in this study or in later applications.

4.4.3 Validation for the cascaded system

We used a comprehensive approach to investigate all streams inside the cascaded system. A good prediction for all streams in the system ensured that the model was versatile and robust enough for various conditions and configurations. Figure 4.6 shows that a good prediction was achieved for both (a) flow rate and (b) concentration in all streams in the cascade configurations (Table 4.2, experiments a–c). Despite the various membrane types and operating pressures chosen, the model successfully predicted both the flow rate and the concentrations of all component in all streams. However, the prediction of the concentration of large oligomers (\geq DP5) deviated in certain conditions. At stage T1, the permeate was diluted; in contrast, the retentate at stage B1 was concentrated. In the diluted regime, the prediction of concentrations was good, but in the concentrated regime (indicated at the upper right side of the chart), the deviation from the model was most prominent. This might be caused by the non-idealities related to the viscous materials, especially in the concentration polarization layers.

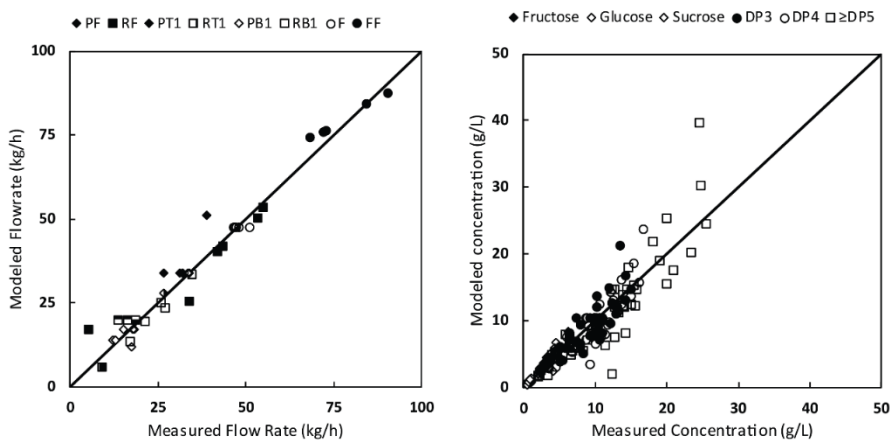


Figure 4.6. Measured versus modelled (a) flow rate and (b) concentration for each stream in the membrane cascade set up at 45°C for all experiments listed in Table 4.2.

The over-prediction for the larger oligomers was even higher in experiment a-3. In this experiment, a GE membrane was used at a high pressure. This membrane had a high rejection for large molecules, and this was even higher at high pressures. Considering this and the concentration polarization phenomena, the concentration of LC-FOS at the membrane surface could be high, and the solution might not behave ideally anymore. Furthermore, the empirical viscosity correlation tended to be less accurate for mixtures with high average molecular weight.

4.4.4 Configuration b and c

Extracting a side stream from the system as shown in Figure 4.1b and c allowed us to obtain a third stream that was richer in DP3. Configuration b used the permeate of the bottom stage as the third stream; configuration c used the retentate of the top stage. In this study, a side-to-recycle stream ratio r equal to 0.5 was used. In the case of configuration b, the flow rate of SP_{B1} was half the flow rate of P_{B1} and the same for SR_{T2} in configuration c.

There were many possible parameter combinations for the fractionation cascade system. Considering the 3 types of membrane used in this research and the range of operating pressure allowed, there were numerous possible combinations. Furthermore, the flow rate also needed to be optimized in order to widen the feasible combinations and have good purity and yield. To acquire the optimum combination, we generated 27 combinations (Table 4.A.1) based on a 3-level fractional factorial design with 7 variables [103]. These combinations were used as variables in the simulation. The outcome of the simulation is summarized in Table 4.3. In addition, Table 4.3 shows the optimal parameter combinations when specific performance indicators are chosen, plus the values of other indicators that are not optimized. The parameter combination number refers to the matrix in Table 4.A.1.

The fractionation cascade system showed results for purifying monosaccharides: a maximum purity of 41.3wt% is achieved starting from 8.9 wt% at the feed, giving a purification factor of 4.6. Even though the purity increase for DP3 and DP \geq 5 were not as large as for the monosaccharides, both showed a significant increase. Table 4.3 also shows that maximizing one parameter results in a trade-off of other parameters. A very high purification factor for monosaccharides was achieved by sacrificing the other purities, especially DP \geq 5 with a purification factor of 1. The opposite was shown for the maximum purity of DP \geq 5, giving a very low purity for the monosaccharides. However, despite the

compromises, the purification factors never went below 1 for any component. This implies that whichever combination was chosen, products with increased purities were still acquired. In addition, the design was able to recover practically all the FOS in the desired product streams (middle and bottom), giving a very high overall yield. However, this yield was greatly sacrificed when aiming at a maximum purity of $DP \geq 5$.

Table 4.3. Maximum (calculated) performance parameters (purities and purification factor of monosaccharides, DP_3 and $DP \geq 5$, separation factor of $DP_3/DP \geq 5$ and total FOS yield) in the fractionation cascade system using a side-to-recycle stream ratio, $r = 0.5$.

Condition	Combination number	P_1	P_3	P_5	PF_1	PF_3	PF_5	$SF_{3,5}$	$Y_{FOS.Total}$
Configuration b									
Max{ P_1 }	1	41.2	31.8	34.5	4.6	1.3	1.0	5.0	99.2
Max{ P_3 }	13	20.5	32.0	37.3	2.3	1.4	1.1	4.3	90.3
Max{ P_5 }	25	13.4	31.5	42.5	1.5	1.3	1.3	3.3	64.9
Max{ $Y_{FOS.Total}$ }	1	41.2	31.8	34.5	4.6	1.3	1.0	5.0	99.2
Max{ $SF_{3,5}$ }	1	41.2	31.8	34.5	4.6	1.3	1.0	5.0	99.2
Configuration c									
Max{ P_1 }	1	41.3	32.2	34.6	4.6	1.4	1.0	4.1	99.2
Max{ P_3 }	1	41.3	32.2	34.6	4.6	1.4	1.0	4.1	99.2
Max{ P_5 }	25	13.8	24.8	43.3	1.5	1.0	1.3	1.1	66.1
Max{ $Y_{FOS.Total}$ }	1	41.3	32.2	34.6	4.6	1.4	1.0	4.1	99.2
Max{ $SF_{3,5}$ }	1	41.3	32.2	34.6	4.6	1.4	1.0	4.1	99.2

Purities and yields are weight percentages.

The configuration selection depends on the objective of the separation. Combination number 1 was the optimal parameter combination for maximum purity of the monosaccharides in both configurations. This parameter combination used 3 GE membranes with the lowest MWCO and low pressures. Maximizing the purity of $DP \geq 5$ required a more open membrane, which was used in parameter combination 25. A lower rejection coefficient was beneficial to improve the purity of the targeted component. The rejection of monosaccharides was low with any of the 3 membranes, and its purification was easier regardless of the membrane type that is chosen.

The simulation showed that choosing a more open membrane with lower rejection of $DP \geq 5$ allowed more components to be recycled and removed from the $DP \geq 5$ fraction, and therefore a higher purity was achieved. However, in this case, the bottom product was extracted from the retentate side; and a higher permeation would also give a higher loss of the $DP \geq 5$ fraction. Thus, a compromise had to be made between purity and yield. Increasing the permeation of $DP \geq 5$ would also increase the permeation of other smaller components, and therefore the purity of those components was more difficult to achieve.

4

In term of purities and yields, configuration b gave a similar performance to configuration c. However, configuration b gave a significantly higher separation factor. This implied that configuration b was better to produce a middle stream that was richer in DP3. Although the monosaccharides still contaminate this stream, the ratio of DP3 to $DP \geq 5$ was higher than both the feed and bottom products; a product with different functionalities was expected.

It was obvious that trade-offs between indicators have to be made; improving one parameter could only be achieved by sacrificing others. However, the severity of the compromise varied among pairs of indicators. Table 4.4 shows the correlation coefficients between each pair of indicators for both configurations. There were large negative correlations between purity and its corresponding yield. This implied that improving purity in one can be done by greatly sacrificing its yield. A large negative correlation was also found between P1 and P5. Besides the trade-off behaviour depicted by large negative correlations, some indicators showed a positive correlation, implying that maximizing one parameter also maximizes the other; this phenomenon was observed between P1 and YFOS total and between P5 and Y1.

Some correlations between indicators were configuration dependent. P1 had no correlation with P3 in configuration b; however, it had a large positive correlation with P3 in configuration c. This is also expressed in Table 4.3 where the combination chosen to maximize P1 is the same as the one to maximize P3. Some negative correlations were also reduced by choosing configuration c.

The combinations achieved by maximizing certain parameters were tested experimentally and are presented in Figure. 4.7. In general, the models were able to predict the purity and yield in the combinations. In some combinations, the model deviated from the experimental data, probably due to non-ideality of concentrated solutions, which was discussed in Section 4.4.3 . The results showed that the model

developed in this research was useful to find an optimum combination for fractionation cascade. Despite some deviations under certain conditions, the prediction for extreme combinations was quite good.

Table 4.4. (Pearson) correlation coefficient matrix of performance indicators simulated using configuration b (top diagonal) and configuration c (bottom diagonal, italic). The correlation coefficient were calculated using all feasible combinations explained in table 4.A.1.

	P1	Y1	P3	YFOS.Mid	P5	YFOS.Bot	YFOS Total
P1	1	- 0.824	0.007	- 0.059	- 0.762	0.652	0.792
Y1	- 0.806	1	0.211	- 0.020	0.927	- 0.744	- 0.980
P3	0.724	- 0.545	1	-0.889	- 0.110	0.432	- 0.219
YFOS.Mid	- 0.028	- 0.080	- 0.565	1	0.322	- 0.636	0.052
P5	- 0.555	0.662	- 0.720	0.654	1	- 0.924	- 0.913
YFOS.Bot	0.484	- 0.509	0.813	- 0.811	- 0.942	1	0.738
YFOS.Total	0.786	- 0.985	0.573	0.058	- 0.666	0.537	1

The upper diagonal represents configuration b; the bottom diagonal (italics) represents configuration c.

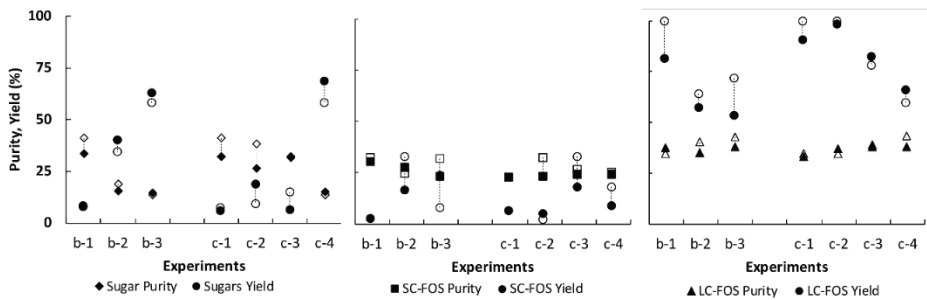


Figure. 4.7. Validation experiments for purity and yield at selected combinations that give maximum values (Table 4.3) using configuration b and configuration c with a side stream ratio $r=0.5$. The dashed lines connect the experimental values (closed bullets) and their corresponding predictions (open bullets).

4.4.5 Process improvement using more stages

Extension of the ideal cascade configuration in several ways was simulated to improve the fractionation performance (Figure. 4.8). Configuration d had an extra top stage and configuration e was expanded towards the bottom section. The 5-stage configuration (f) was a combination of both proposed 4-stage configurations. We used the same optimization procedure to evaluate these new proposed configurations. Matrices with 81 runs developed from the same table [104] were used in the simulation. Introducing more stages gave more possible positions to extract the middle stream; depending on the configuration; in total, there were 4 possible alternative side streams: namely, SR_{T2} , SR_{T1} , SP_{B1} and SP_{B2} .

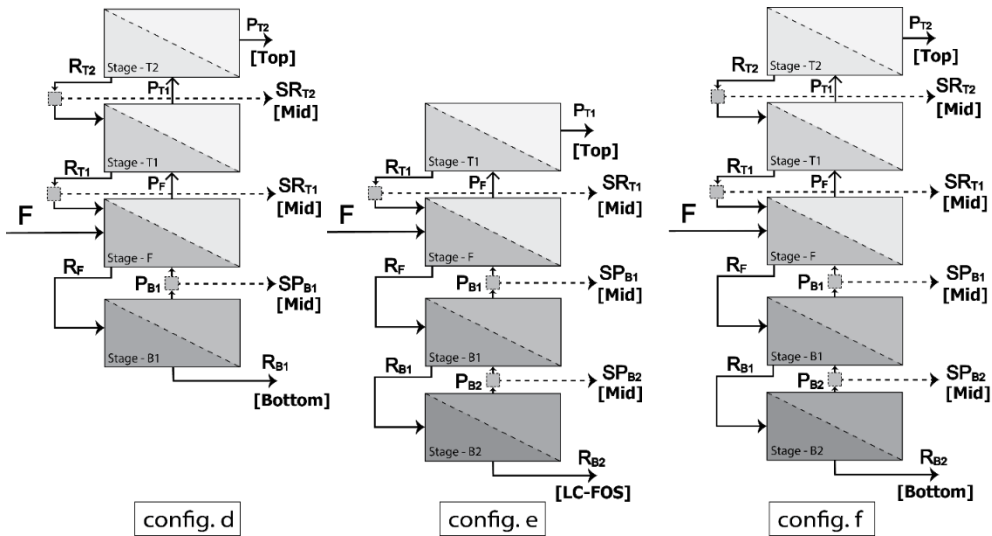


Figure. 4.8. The 4-stage configuration with extra (d) top stage, (e) bottom stage and (f) 5-stage membrane cascades. The dashed lines show the alternative extraction points of the mid product.

In general, increasing the number of stages improved the fractionation performance as depicted in Figure. 4.9. The purification factor of monosaccharides was already quite high with the 3-stage fractionation cascade, but this parameter increased even further with the addition of stages. An extra stage at the top section gave a more significant increase than an extra stage at the bottom. The opposite effect was found for $DP \geq 5$. For this fraction, configuration e gave a better result. However, expanding the design towards 5 stages with symmetric top/bottom stages reduced the separation performance; the maximum purities were achieved using the 4-stage cascade rather than the 5-stage cascade.

The maximum purity of the $DP \geq 5$ fraction differentiated with the location of the middle stream. There was a clear difference between having it at the SR_{T2} or the SP_{B2} location: the further the side stream was from the bottom, the lower was the purity of the $DP \geq 5$ fraction. Having the side stream close to the feed (SP_{B1} and SR_{T1}) did not make any significant difference, as was also observed in the 3-stage design.

Unlike the other 2 purities, the purity of the middle size $DP3$ was not really improved much by the addition of extra stages. As an intermediate stage, we saw that most optimization procedures lead to an increase in the purities of the monosaccharides ($DP1$) and oligosaccharide ($DP \geq 5$) fractions, and only a slight improvement in the purity of the intermediate fraction.

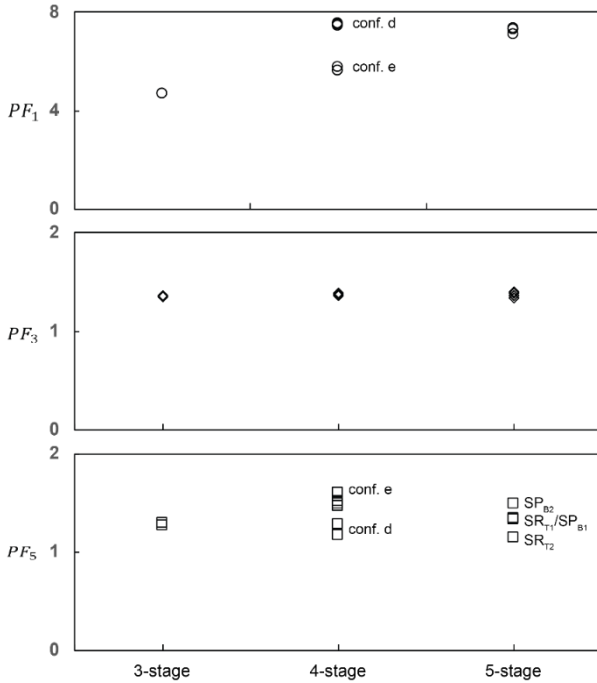


Figure. 4.9. Maximized purification factor for different configurations using a side stream ratio $r=0.5$. Each point represents each configuration using each position of the side stream.

We could evaluate the performance with respect to the isolation of the FOS in 2 ways: (1) the overall recovery of the FOS, which include $DP3$ and $DP \geq 5$, and (2) the separation between $DP3$ and $DP \geq 5$.

We first evaluated the first aspect, which in fact was equivalent to the separation of these components from the $DP1$ components. The systems could recover basically all $DP3$ and

higher in the combination of the mid and bottom streams. Figure. 4.10 shows the distribution of the $DP \geq 3$ components over these 2 fractions. Since 100% yield implied that all $DP \geq 3$ end in that particular stream, the possible window was that below the diagonal in the graphs. The points on the diagonal represent those systems in which all $DP \geq 3$ end up in these 2 streams, and hence not in the monosaccharide stream.

We saw that in the 3-stage system (configuration b), most of the $DP \geq 3$ ended up in the bottom stream; the contribution of the middle stream was relatively small. Adding more stages (1) moved many systems closer to the diagonal and hence increases the overall yield, and (2) showed a stronger contribution to the overall yield by the middle stream. Configuration e showed a wider scattering than configurations d and f. However, a stronger contribution from the middle stream was achieved compared with configuration b.

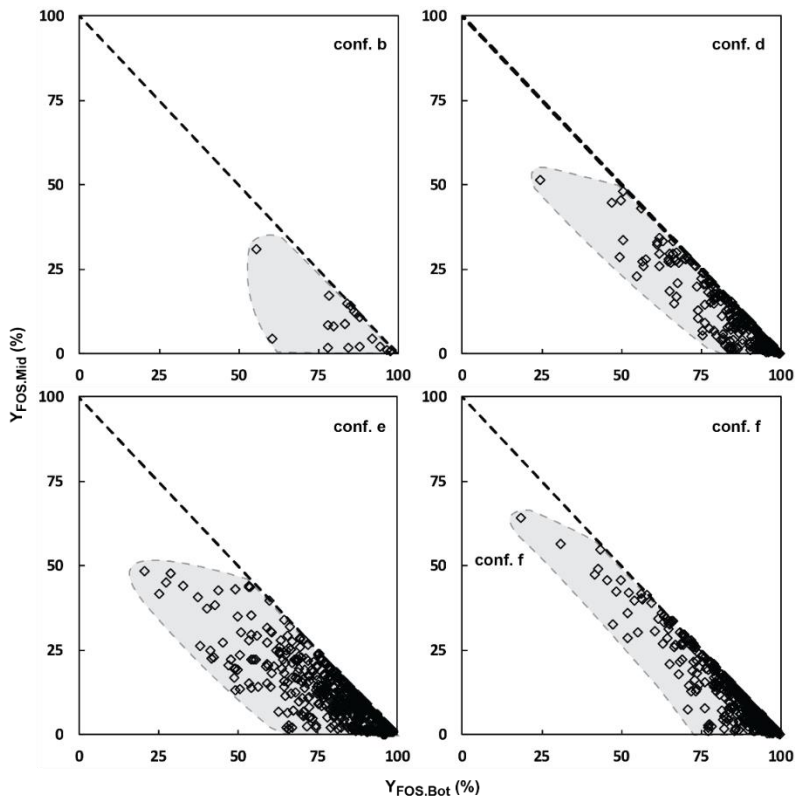


Figure. 4.10. Simulated yield of FOS ($DP \geq 3$) obtained in the bottom versus middle stream using the 3-stage (configuration b), 4-stage (configurations d and e) and 5-stage (configuration f) membrane cascade. Each point represents each feasible combination.

To evaluate the separation between DP_3 and $DP \geq 5$ at the middle size product, we used the separation factor as defined in Eq. (4.20). Interestingly, the separation factor increased as the total yield increases. Furthermore, Figure. 4.11 also shows that the points are more concentrated on the right side, implying a higher yield was more likely to be achieved. However, the points that were located on the right side in Figure. 4.11 were also located on the right side in Figure. 4.10; the contribution of the high yield mostly came from the bottom product.

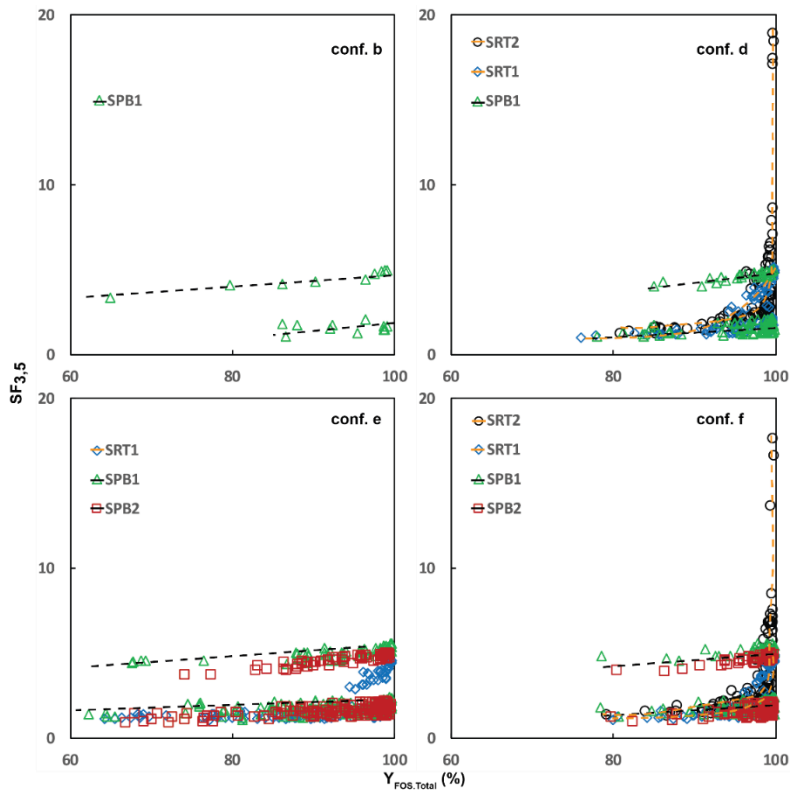


Figure. 4.11. Simulated separation factor of DP_3 and $DP \geq 5$ versus total yield using 3-, 4- and 5-stage membrane cascades at various side stream positions (Figure. 4.8). Each point represents a feasible combination. Lines are drawn as a guide for the eye.

Regardless of the stage number, the overall yield depended on the side stream position. Both positions extracted from the bottom section (SP_{B1} and SP_{B2}) showed bifurcated values: a separation factor of 1, implying no separation between DP_3 and $DP \geq 5$, and a separation factor of 5. We saw the latter behaviour in systems that used the “tight” (GE)

membrane at the stage at which the intermediate stream was taken out. The exact conditions at this and other stages were not very important.

Extracting the intermediate stream at the SR_{T2} position broke the value limit of 5. By selecting the correct combination, the system reached a maximum separation factor of 18. Apparently, these high values could only be achieved by using specific combinations; we could see less frequent points in the charts. These combinations appeared to use GE membranes at the feed and all top stages. However, using GE membrane at the feed stage limited the flow that went to the top stages. This explained why only a few combinations were applicable under this condition.

4

The simulation and optimization for the fractionation cascade were performed based on data obtained of single membrane experiments. These calculations can be applied to separation of other feed streams provided that the performance of a single membrane separation has been measured. Two major properties are needed to characterize a single membrane: the membrane resistance and the solute real rejections. These two properties are assumed to be independent of the feed concentration, which was proven to be acceptable within the scope of this study. Using the characterized values, a prediction of flow rate and concentration for both permeate and retentate in a single stream can be performed. Applying the same procedure as is used in this study, we can predict the outcome of a cascaded system. Noting that the concentration independency was valid for diluted solutions, a concentration dependent model is needed as the stream becomes more concentrated.

4.5 Conclusions

A steady state model was used to optimize multi-stage cascades, taking into account the configuration of the cascade, the choice of membrane and the operating pressures at each stage, simultaneously. Optimization could be done on a range of objective functions, which may have relevance depending on the aim of the operator of the system.

It was possible to separate FOS in 3 streams with a 3-stage cascade, in which the bottom ($DP \geq 5$) streams and the middle (DP 3-4) stream might recover almost all oligosaccharides ($DP \geq 3$). The streams could not all reach high purity; a compromise needed to be found here. The purity of the middle stream was hard to improve. Selecting an optimized combination, purities of 41wt%, 32 wt% and 43 wt% were achieved starting from a feed

————— Oligosaccharides fractionation cascades with 3 outlet streams mixture of 9 wt%, 24 wt% and 34 wt% for monosaccharides, DP3 and DP \geq 5, respectively, using 3-stage fractionation cascades.

Extension of a 3-stage cascade to 4 and 5 stages improved the purity of the monosaccharides (top) fraction and the long-chain oligosaccharides (DP \geq 5) fraction, but not significantly improved the middle (DP3) fraction. By optimizing the overall system, the purities of the 3 fractions that could be reached were 66 wt% in the top fraction for DP1-2, 33 wt% in the middle fraction for DP3-4 and 54 wt% in the bottom fraction for DP \geq 5. Expansion of stages on the top led to a better purity of the top fraction; expansion of the bottom conversely led to a better purity of the bottom fraction. The middle fraction was relatively unaffected, even in a symmetric 5-stage system. The additional fifth stage reduced the purity achieved in the 4-stage system; the best purities were found in the 4-stage cascades.

Acknowledgements

The authors would like to acknowledge Lembaga Pengelola Dana Pendidikan (LPDP), and Kementerian Keuangan Indonesia for financial support.

Appendix

Table 4.A.1. Combination matrix of the 3-stage fractionation design.

Combination number	Membrane type			Pressure (bar)		Feed flow rate (kg/h)	
	Stage 1	Stage 2	Stage 3	Stage 1	Stage 2	Stage 3	
1	GE	GE	GE	8	8	8	50
2	GE	GE	GH	8	16	16	70
3	GE	GE	GK	8	12	12	60
4	GE	GH	GE	12	8	12	70
5	GE	GH	GH	12	16	8	60
6	GE	GH	GK	12	12	16	50
7	GE	GK	GE	16	8	16	60
8	GE	GK	GH	16	16	12	50
9	GE	GK	GK	16	12	8	70
10	GH	GE	GE	12	12	8	60
11	GH	GE	GH	12	8	16	50
12	GH	GE	GK	12	16	12	70
13	GH	GH	GE	16	12	12	50
14	GH	GH	GH	16	8	8	70
15	GH	GH	GK	16	16	16	60
16	GH	GK	GE	8	12	16	70
17	GH	GK	GH	8	8	12	60
18	GH	GK	GK	8	16	8	50
19	GK	GE	GE	16	16	8	70
20	GK	GE	GH	16	12	16	60
21	GK	GE	GK	16	8	12	50
22	GK	GH	GE	8	16	12	60
23	GK	GH	GH	8	12	8	50
24	GK	GH	GK	8	8	16	70
25	GK	GK	GE	12	16	16	50
26	GK	GK	GH	12	12	12	70
27	GK	GK	GK	12	8	8	60

Nomenclature

c	solute concentration [g L^{-1}]
D	diffusion coefficient [$\text{m}^2 \text{s}^{-1}$]
d_h	hydraulic diameter [m]
E	dimensionless parameter in viscosity model [dimensionless]
F	flow rate [kg h^{-1}]
J	mass flux [$\text{kg m}^{-2} \text{s}^{-1}$]
k	mass transfer coefficient [m s^{-1}]
MW	molecular weight [kg mol^{-1}]
P	product purity [%-w]
PF	purification factor [dimensionless]
R	gas constant [$\text{J mol}^{-1} \text{K}^{-1}$]
R_r	real rejection [dimensionless]
Re	Reynold number [dimensionless]
Rm	membrane resistance [$\text{m}^2 \text{kg}^{-1}$]
Sc	Scmidt number [dimensionless]
SF	separation factor [dimensionless]
Sh	Sherwood number [dimensionless]
T	process temperature [K]
TMP	trans membrane pressure [Pa]

u_v cross-flow velocity [m s^{-1}]

X total sugar molar fraction [dimensionless]

Y product yield [%]

Greek letters

μ dynamic viscosity [Pa s]

μ_r relative viscosity [dimensionless]

π osmotic pressure [Pa]

ρ density [kg m^{-3}]

Subscripts

Product, Top, Mid, Bottom product streams

i solute, degree of polymerization

p permeate side

r retentate side

w membrane wall

5



Chapter 5

Multi-criteria design of membrane cascades: Selection of configurations and process parameters

This chapter has been published as

Z. Rizki, A.E.M. Janssen, G.D.H. Claassen, R.M. Boom, A. van der Padt,
“Multi-criteria design of membrane cascades: Selection of configurations
and process parameters”, Sep. Purif. Technol. (2019).
<https://doi.org/10.1016/j.seppur.2019.116349>.

Abstract

5

Membrane cascades can fractionate fructooligosaccharides into 3 different fractions with varying degrees of polymerization (DP). In contrast to the traditional membrane system, membrane cascades have flexibility in configuration and setup for each stage. Apart from the improvement flexibility of the cascades provides, it raises problems related to multiple performance indicators and multiple process parameters. Therefore, new design criteria are required. We have designed an optimization approach for this multi-criteria problem. Eight configurations of cascaded membranes were built, measured and simulated to develop a design strategy. The performance of the separation process was evaluated by 10 different indicators: purities and yields for 3 different fractions and 4 separation factors between molecules with an adjacent DP. We found that the proposed configurations exceeded the performance of the previously reported 3-stage membrane cascade. Within those configurations, the cascade designs were able to increase the purity of (1) monosaccharides to 47% from 9%, (2) DP3 to 34% from 24% and (3) $DP \geq 5$ to 77% from 34%. We also report a procedure to select a single optimum combination that compromises all performance indicators. This procedure systematically calculated the weights, which were then used to rank all feasible combinations and select the best one. In addition, a backward analysis using sensitivity coefficients was performed to pinpoint critical process parameters. Knowing these parameters, more targeted and more efficient improvements could be made. This approach is applicable for most integrated systems with multi-process variables and multi-performance indicators combining process modelling and multi-criteria decision making.

5.1 Introduction

Research on membrane processes is increasing with broader applications and improvements. Various applications have been reported to include food components, e.g. sugars and oligosaccharides [39,42,57]. Membrane processes have been improved using various approaches: searching for more selective materials [105], modifying membrane surface properties [106], tailoring the fabrication [15] and improving the process design [107]. An improved process design includes the incorporation of additional stages [18,19,108].

The additional membrane stages can be configured either sequentially or in a cascaded manner with recycles. In a sequenced configuration, either the permeate or retentate is further processed until desirable product purity is achieved [59]. The cascaded configuration works similarly with the addition of recycle streams, which makes the system more efficient. The streams create a counter-current configuration [19,108] analogous to vapour–liquid streams between plates in a distillation column. This concept, introduced by Lightfoot et al. [23], is known as an ideal cascade. This concept was later investigated in a system of oligosaccharides via simulation by Patil et al. [101].

The ideal membrane cascade has a substantial constraint that makes it difficult in practice: the design only allows incoming streams with similar compositions at the mixing point. These streams come as recycle streams from other stages. Considering the modular characteristic of a membrane system, every stage can be operated under different conditions (inhomogeneous setup). These conditions are most likely to produce different outlet compositions. The idea of non-ideal inhomogeneous membrane cascades was previously studied [24,25] and was reported to have a better separation performance. In addition to the various setups among stages, the membrane cascade design allows flexible configurations. Several modified configurations were investigated by Patil et al. [20]. With this flexibility, the membrane cascade system shows further improvement.

The flexibility of the cascade system opens a window for further improvement but raises an optimization problem: which setup combination should be used? Each operating condition for each stage can be operated independently, therefore there are a factorial number of combinations. The more variable operating conditions (e.g. type of membrane and pressure) and stage numbers, the more combinations exist. The optimized setup must be chosen within these combinations. The simplest way to find the optimized combination

is by simulating the performance of each combination and selecting the best performance among those combinations. The decision must be made based on a particular criterion. To do that, a model that is representative of the system is required.

Despite the improvements that membrane cascades provide, they are mostly studied in the context of a purification system in which a main product and a waste stream are extracted from the system. Another context of fractionation using a membrane cascade has been introduced to obtain 3 fractions simultaneously [60]. The membrane cascade setup was used to fractionate fructooligosaccharides (FOS) into 3 different fractions that varied in size in relation to their degree of polymerization (DP): a small fraction rich in monosaccharides (DP1), a middle fraction rich in DP3 and a large fraction rich in $DP \geq 5$.

5

FOS is a mixture of oligofructoses that has a prebiotic effect. The prebiotic effect depends on the chain length of the carbohydrates in the mixture [31,33–35,54]. In addition to the prebiotic properties, the chain length also affects the mixture's physical properties. Therefore, fractionating FOS into different fractions varying in chain length becomes an interesting process to produce multiple oligosaccharide products with different functionalities.

FOS fractionation into 3 different products using membrane cascades was previously improved by increasing the stage number from 3 up to 5 while keeping the configuration close to the ideal (Figure 5.1). Considering the flexibility in configuring the design, the performance may still be improved while keeping the stage number at a minimum. Being able to improve the performance using a minimum stage number can also save investment and operational cost, considering that every additional unit means an addition of pumps, membrane module, heat exchangers and other instrumentation units.

Having 3 different products, the system faces another problem related to the objective that should be chosen for optimization. Sacrificing the quality of 2 streams may be needed to achieve good quality of 1 selected stream. However, previous knowledge is needed to decide which streams should be sacrificed. Moreover, 1 single product may also have conflicting performance indicators, e.g. purity and yield. Our previous study on fractionation cascades [17] considered this issue and analysed the correlation between each pair of performance indicators. However, a single decision could not be made.

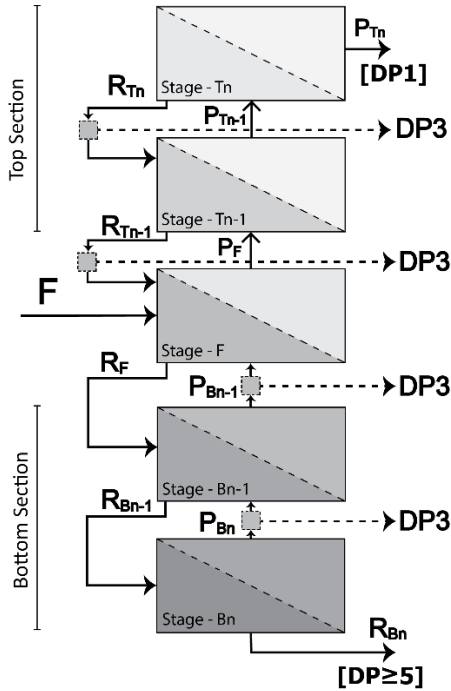


Figure 5.1. Generalized configuration of n stages at the top region and n stages at the bottom section of the ideal cascade with a side stream. The dotted lines are the possible positions to extract the side stream with mid-products.

This chapter aims to optimize the design of a membrane cascade to produce 3 product fractions. Maintaining the stage number at 3, we propose 8 new configurations to produce 3 FOS fractions. Within those configurations, we use the multi-criteria decision-making (MCDM) approach to select the best alternative combination that compromises all performance indicators. This approach helps us to select the best alternative that accommodates all performance indicators. We develop a mathematical model to rank all available alternatives without involving subjective opinions. This model was developed and assessed using 1 of the 8 proposed configurations and later used for all configurations. The developed model can be used not only to support the decision-making process but also to pinpoint the critical process parameters. We performed a backward analysis from the rank that comes out of the MCDM model to distinguish the critical process parameters.

5.2 Development of the model

5.2.1 Prediction of membrane performance

Membranes can be characterized based on the resistance (Res) and solute real rejection ($R_{r,i}$). The membrane resistance can be estimated using clear water fluxes at different pressures (Eq. (5.1)), eliminating the osmotic pressure effect.

$$J = \frac{\Delta \text{Press}_{\text{eff}}}{\mu \cdot \text{Res}} = \frac{\text{TMP} - \Delta \pi}{\mu \cdot \text{Res}} \quad (5.1)$$

The osmotic pressure difference in the system with solutes is expressed by the van't Hoff relation (Eq. (5.2)) considering the concentrations on both sides of the membrane.

$$\Delta \pi = \sum_{i=1}^n \frac{R_g \cdot T}{\text{MW}_i} (C_{w,i} - C_{p,i}) \quad (5.2)$$

The real rejections of each solute can be characterized by measuring concentrations at both membrane product streams while also taking into account the concentration polarization phenomena (Eq. (5.3)).

$$R_{r,i} = 1 - \frac{C_{p,i}}{C_{w,i}} \quad (5.3)$$

The predicted value of a single membrane can be used to further predict the flow rate and concentration of a cascaded system. The outlet stream of one particular stage with known flow rate and concentration values becomes the feed stream of the consecutive stage. The outcome of this consecutive stage is predictable by applying the same procedure.

5.2.2 Performance indicators

The performance of a filtration process can be assessed using several indicators. Common indicators used to assess a separation process are the purities, Py_i , and yields, Y_i , associated with the component of interest. The purity is calculated as the (mass) fraction of a component in a particular stream. The yield is calculated as the mass of that component retrieved in a particular product stream relative to the feed. For a system with 3 products, 3 purities and 3 yields exist corresponding to their DP (Eqs. (5.4) – (5.9)). Despite the different functionalities related to the chain length, all oligosaccharides with DP higher than 3 are considered valuable. Therefore, the yield calculation of FOS for the product streams rich in DP3 and DP \geq 5 include all oligosaccharides with DP more than 3.

$$Py_1 = \frac{C_{1,s}}{\sum_{i=1}^5 C_{i,s}} \quad (5.4)$$

$$Y_1 = \frac{C_{1,s} \cdot Fl_s}{C_{1,f} \cdot Fl_f} \quad (5.5)$$

$$Py_3 = \frac{C_{3,m}}{\sum_{i=1}^5 C_{i,m}} \quad (5.6)$$

$$Y_{FOS,m} = \frac{\sum_{i=3}^5 C_{i,m} \cdot Fl_m}{\sum_{i=3}^5 C_{i,f} \cdot Fl_f} \quad (5.7)$$

$$Py_5 = \frac{C_{5,large}}{\sum_{i=1}^5 C_{i,large}} \quad (5.8)$$

$$Y_{FOS,l} = \frac{\sum_{i=3}^5 C_{i,l} \cdot Fl_l}{\sum_{i=3}^5 C_{i,f} \cdot Fl_f} \quad (5.9)$$

In addition to the purities and yields, the separation factors are commonly used to evaluate a separation process. The separation factors represent the efficiency of a process in separating 2 specific components (Eq. (5.10)), which can be calculated for any pair of components. In a non-binary mixture, only separation factors between components with adjacent size are important.

$$SF_{i,j} = \frac{C_{i,product}/C_{j,product}}{C_{i,f}/C_{j,f}}, \quad \text{product} = s, m \text{ and } l \quad (5.10)$$

5.2.3 Optimization and multi-criteria decision-making model

Each membrane stage can be operated independently, giving numerous alternatives to run the cascaded system. Each alternative contains a combination of operating parameters. The large number of possible combinations leads to the problem of selecting the optimal combination. Solving the optimization problem can only be done by applying a specific objective function related to the performance indicators. Having multiple performance indicators as criteria, the optimization faces another challenge: how to include all criteria to select the best alternative combination?

A multi-criteria decision-making (MCDM) approach is a common method to select a single alternative out of numerous options by considering all criteria. Various MCDM methods have been discussed in the literature, including the straightforward simple adjusted

weight method [109–111]. This method forms a single summed parameter, S_a , for all alternatives after applying a particular weight, w_c , to each criteria value, $v_{a,c}$. The optimized setup can be found by maximizing this parameter (Eq. (5.11)). In this equation, index c refers to the criteria and a refers to the alternatives. The total number of criteria considered within a problem is expressed as nc .

$$\text{Max} \left\{ S_a = \sum_{c=1}^{nc} w_c v_{a,c} \right\} \quad (5.11)$$

Solving Eq. (5.11) can only be done after the weights for all criteria are assigned. Determining criteria weights requires meticulous consideration depending on how the weights are interpreted. This is often performed in a separate method. Avoiding a subjective opinion in the weight determination, a mathematical model is used to assign criteria weights by minimizing the distance, D , to the ideal (Eqs. (5.12) and (5.13)). The ideal condition is defined as the maximum value of each criterion. The lower the value for a specific criterion, the longer the accumulative distance to the maximum. Therefore, this criterion will be assigned a lower weight.

$$\text{Min} \left\{ D = \sum_{c=1}^{nc} \sum_{a=1}^{na} w_c (v_c^{\max} - v_{a,c}) \right\} \quad (5.12)$$

subject to

$$\sum_{c=1}^{10} w_c = 1, \quad w_c \geq 0 \quad (5.13)$$

Before determining the weight, w_c , for each criterion, the performance indicators (Eqs. (5.4) – (5.10)) need to be normalized. Normalization is necessary to eliminate a dominance among criteria due to different scales and to accommodate different units. Jahan and Edwards [112] listed 31 normalization methods for ranking. Specific normalization methods should be chosen according to the behaviour of the raw data and the interpretation of the result. Some ranking methods are built based on specific normalization methods.

Min-max normalization is a commonly used normalization method. Min-max normalization transforms a dataset into a certain range. The most commonly used range is [0–1]. The lowest value, v_c^{\min} , is transformed to 0, the highest value, v_c^{\max} , is

transformed to 1 and the other data points are transformed to intermediate values, keeping the relative distance between them (Eq. (5.14)). Creating a new dataset with similar relative distances makes the min-max normalization method suitable for Eq. (5.12) compared with the other normalization methods.

$$v_{a,c} = \frac{\dot{v}_{a,c} - \dot{v}_c^{\min}}{\dot{v}_c^{\min} - \dot{v}_c^{\max}} \quad (5.14)$$

Unlike the purities and yields, the separation factors show a non-linear distance between values. The values that are 2-fold do not have the same distance as the value that is half a reference. This non-linear behaviour can be normalized using logarithmic normalization (Eq. (5.15)), creating transformed values around zero with linear distances. These transformed values can be further normalized using Eq. (5.14) to create comparable datasets with purities and yields.

$$v_{a,c} = \frac{\ln(\dot{v}_{a,c})}{\ln(\prod_{a=1}^n \dot{v}_{a,c})} \quad (5.15)$$

5.2.4 Backward analysis using a sensitivity coefficient

In addition to the best alternative, the criteria weights can be used to rank all alternatives. These alternative ranks, Rk_a , indicate which alternative performs better than the others. A smaller value of Rk_a indicates a better alternative with the best Rk_a equal to 1.

$$Rk_a = Rank(S_a), \quad a = \{1, \dots, na\} \quad (5.16)$$

Each alternative contains a combination of several process parameters. A backward analysis can be performed to find which process parameter is critical to the overall performance. In this analysis, the change of Rk_a in response to a change in a certain process parameter, X , is evaluated. The average rank, \overline{Rk}_a , of alternatives that use a similar process parameter needs to be calculated and compared among different settings of parameters. This response change is expressed by a sensitivity coefficient, SC. The higher the absolute value of the sensitivity coefficient, the more critical the process parameter is. A negative value of SC indicates that the low setting of a particular process parameter gives a better performance. Conversely, a positive value indicates a better performance using a high setting.

$$SC = \frac{\Delta \overline{Rk}_a / \overline{Rk}_a}{\Delta X / X} \quad (5.17)$$

5.3 Materials and methods

5.3.1 Materials

The validation experiments were performed using 5 wt% dilution of FOS syrup. The syrup with 75 wt% dry matter content (Frutalose L85®) was kindly provided by Sensus (Roosendaal, the Netherlands).

5.3.2 Analyses

The oligosaccharides in the samples at each stream were analysed using high performance liquid chromatography. The chromatography system used a Shodex KS-802 8.0 × 300 (mm) column operated at 50°C. The column was attached to a refractive index (RI) detector (Shodex RI-501). The system used milli-Q water as eluent with a flow rate of 1 mL/min.

Fructooligosaccharides contain carbohydrates with DP ranging from 2 to 10 as well as monosaccharides. All carbohydrates were quantified according to their corresponding DP up to DP4. Carbohydrates with DP5 and higher were analysed as a lumped component (DP≥5). Carbohydrate content in the feed was analysed (Table 5.1).

Table 5.1. Feed component and concentration for validation experiments using 5 wt% FOS syrup.

Annotation, <i>i</i>	Component	Concentration (mg/mL) ^a	Composition (wt%)
1a	Fructose	3.02 ± 0.18	6.9
1b	Glucose	0.88 ± 0.10	2.0
2	Sucrose	4.41 ± 0.46	10.0
3	DP3	10.37 ± 0.58	23.6
4	DP4	10.52 ± 0.53	23.9
5	≥DP5	14.76 ± 0.89	33.6

^aUncertainties were calculated based on the 95% confidence interval.

5.3.3 Simulation and process configurations

In this study, we investigated 8 different configurations of modified cascade divided into 2 clusters: the S strategies and the L strategies (Figure 5.2). The S strategies were developed by extracting the small fraction at the feed stage and the L strategies by extracting the large fraction at the feed stage. Strategies S-1 and S-2 explored the bottom region only and strategies L-1 and L-2 explored the top region only. This design was developed based on the fact that improvement of the fractionation cascade was more effective if the expansion was done towards one specific region only [60]. The other strategies had both regions in a 3-stage configuration with modification of the stream arrangements, which included the recycle stream.

The prediction of these new proposed configurations was done using a steady state model explained in Section 5.2.1 following an iteration algorithm [60]. This model was applied to every configuration with adjustment of the mass balances. Two total mass balances were developed to relate streams at (1) the mixing point and (2) the membranes at every stage. At the mixing point, the flow rate of the stream that entered the feed stage, Fl'_f , is the sum of the original feed stream, Fl_f , and the recycle stream, Fl_{rec} . At every stage, the feed stream, $Fl_{F.stage}$, split into permeate, $Fl_{P.stage}$, and retentate, $Fl_{R.stage}$. The component mass balances followed the relation for the total mass balances (Eqs. (5.18) – (5.21)).

$$Fl'_f = Fl_f + Fl_{rec} \quad (5.18)$$

$$SC'_f \cdot Fl'_f = C_f \cdot Fl_f + C_{rec} \cdot Fl_{rec} \quad (5.19)$$

$$Fl_{F.stage} = Fl_{P.stage} + Fl_{R.stage} \quad (5.20)$$

$$C_{F.stage} \cdot Fl_{F.stage} = C_{P.stage} \cdot Fl_{P.stage} + C_{R.stage} \cdot Fl_{R.stage} \quad (5.21)$$

Depending on the configurations, the feed and the product streams were unique. The feed stream for each stage and the product streams are summarized in Table 5.2. In this table, F represents the feed stream, P represents the permeate stream and R represents the retentate stream for each particular stage: F, B1, B2, T1 and T2 (Figure 5.2).

5

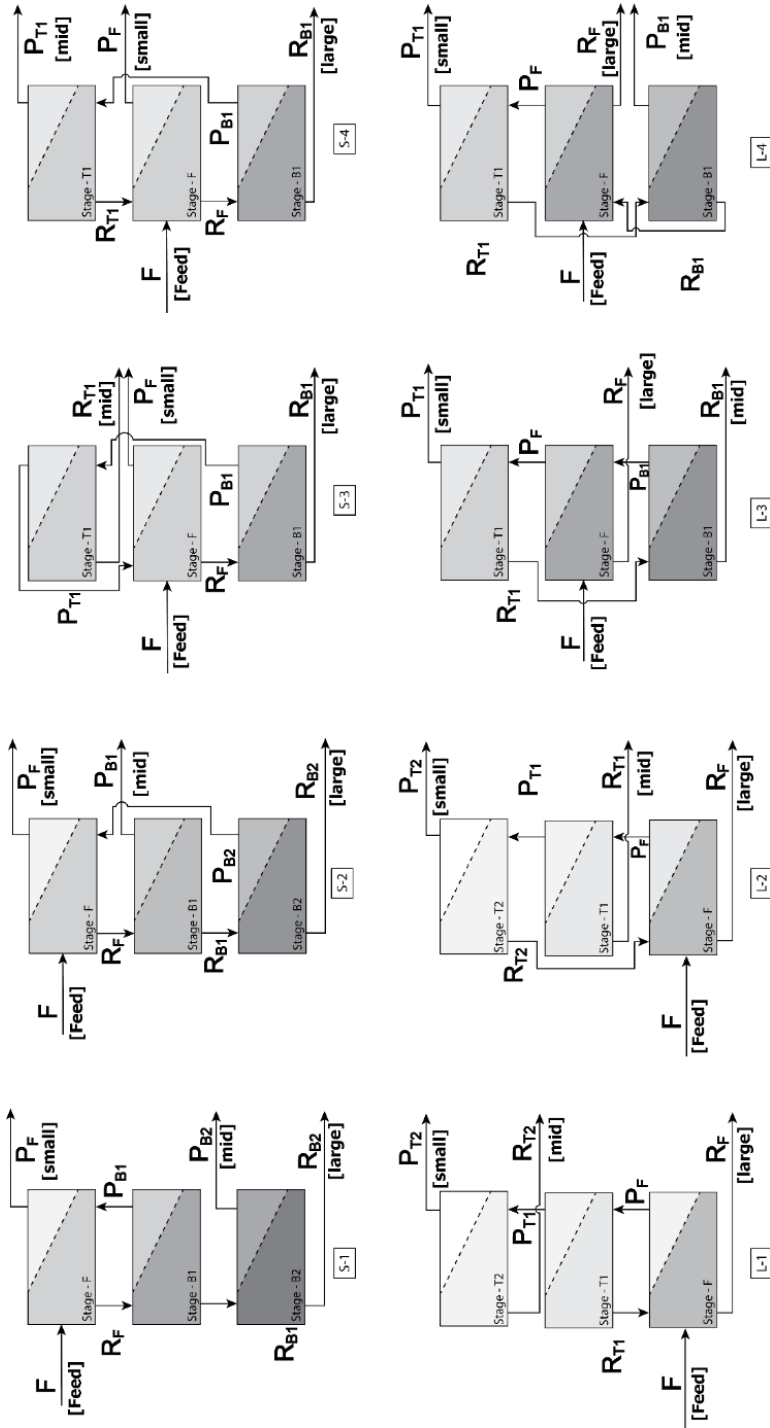


Figure 5.2 Eight new configurations of 3-stage fractionation cascades.

Table 5.2. Declaration of recycled, stage feed and product streams in all configurations.

Configuration	Recycled stream	Stage Feed Stream				Products		
		F _{B1}	F _{B2}	F _{T1}	F _{T2}	Small (s)	Mid (m)	Large (l)
S-1	P _{B1}	R _F	R _{B1}	–	–	P _F	P _{B2}	R _{B2}
S-2	P _{B2}	R _F	R _{B1}	–	–	P _F	P _{B1}	R _{B2}
S-3	P _{T1}	R _F	–	P _{B1}	–	P _F	R _{T1}	R _{B1}
S-4	R _{T1}	R _F	–	P _{B1}	–	P _F	P _{T1}	R _{B1}
L-1	R _{T1}	–	–	P _F	P _{T1}	P _{T2}	R _{T2}	R _F
L-2	R _{T2}	–	–	P _F	P _{T1}	P _{T2}	R _{T1}	R _F
L-3	P _{B1}	R _{T1}	–	P _F	–	P _{T1}	R _{B1}	R _F
L-4	R _{B1}	R _{T1}	–	P _F	–	P _{T1}	P _{B1}	R _F

A numerical simulation was performed before the validation experiments to screen some promising setups. Within these configurations, various combinations of (1) feed flow rate, (2) membrane type and (3) operating pressure at each stage were simulated. Using these variables, we generated matrices based on a 3-level fractional factorial design that included 3 levels of flow rate (50, 60 and 70 kg/h), 3 types of membrane (GE, GH and GK) and 3 levels of pressure (8, 12 and 16 bar). Each matrix consisted of 81 combinations of variables constructed using a design explained by Xu [104]. Each combination in the table was then simulated and assessed based on the performance indicators (Eqs. (5.4) – (5.10)).

The simulation could give unfeasible results due to an insufficient flow. In further analyses, we only considered the feasible combinations.

Selecting alternative combinations to improve a certain criterion affected the other criteria. A pair-wise correlation between criteria showed how much one criterion changed as another criterion changed. This correlation was quantified as a correlation coefficient between criteria, $CC_{c1,c2}$. In Eq. ((5.22)), $c1$ and $c2$ represent the 2 criteria being compared, \bar{v}_a represents the criteria value for certain alternatives and \bar{v} represents the average criteria value.

$$CC_{c1,c2} = \frac{\sum_{a=1}^n (\dot{v}_{a,c1} - \bar{v}_{c1})(\dot{v}_{a,c2} - \bar{v}_{c2})}{\sqrt{\sum_{a=1}^n (\dot{v}_{a,c1} - \bar{v}_{c1})^2} \sqrt{\sum_{a=1}^n (\dot{v}_{a,c2} - \bar{v}_{c2})^2}} \quad (5.22)$$

5.3.4 Experimental setup

The validation experiments were performed using a 3-stage cascade membrane unit on a pilot scale (Figure 5.3). Each unit had a dead volume of 2.5 L, making a total processed solution of 15 L, including 7.5 L in the feed tank. All experiments were performed at a constant temperature of $45 \pm 1^\circ\text{C}$ and cross flow velocity of 0.08 m/s following the same conditions as in the previous research [60].

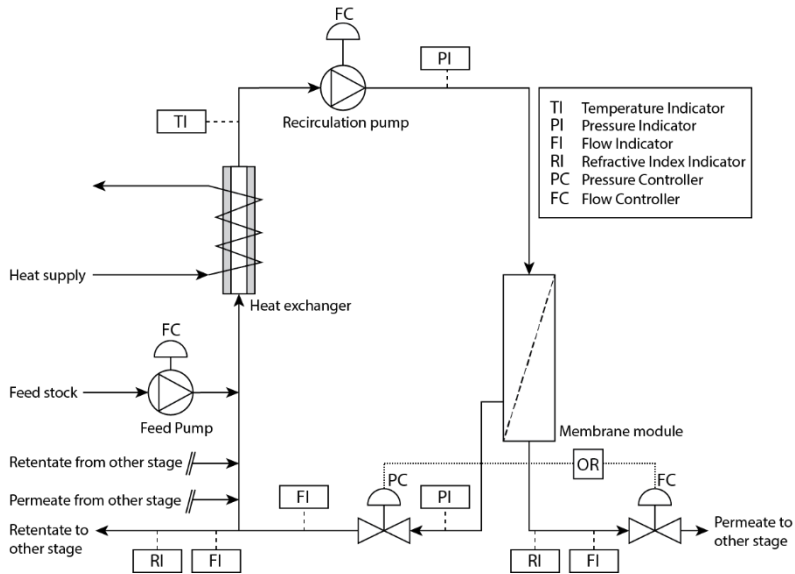


Figure 5.3 Schematic representation of a pilot scale membrane unit.

Three types of membranes varying in molecular weight cut off (MWCO) were used in this study: GE with MWCO of 1000 Da, GH with MWCO of 2500 Da and GK with MWCO of 3500 Da. All membranes were the 1812C-34D model produced by GE (GE Osmonic, Sterlitech, Kent, WA, USA).

Selected combinations based on the simulation were tested. These combinations are summarized in Table 5.3.

Table 5.3. Combinations of feed flow rate, membrane type and pressure at each stage for validation experiments.

Experiment number	Configuration	Membrane type (T2/T1/F/B1/B2)	Pressure (bar) (T2/T1/F/B1/B2)	Feed flow rate (kg/h)
1	S1	-/-/GH/GE/GE	-/-/12/8/8	50
2	S2	-/-/GH/GK/GE	-/-/12/8/8	50
3	S4	-/GE/GE/GH/-	-/8/8/8/-	50
4	S4	-/GE/GH/GH/-	-/8/12/8/-	50
5	L1	GE/GH/GE/-/-	8/8/12/-/-	50
6	L1	GE/GK/GK/-/-	12/12/8/-/-	50
7	L2	GE/GH/GH/-/-	8/8/12/-/-	50
8	L4	-/GE/GH/GE/-	-/12/8/12/-	50
9	L4	-/GK/GK/GH/-	-/8/8/8/-	50

5

5.3.5 Criteria weights determination and backward analysis using the sensitivity coefficient

The criteria weights were determined by solving Eqs. (5.12) and (5.13) using a specific dataset. The dataset was taken from the feasible alternatives of the simulation results. In our case, the criteria, represented by subscript c , correspond to the purities and yields (Eqs. (5.4) – (5.9)) and 4 separation factors of adjacent components: $SF_{1,3}$, $SF_{3,1}$, $SF_{3,5}$ and $SF_{5,3}$ (Eq. (5.10)). The alternatives, represented by subscript a , correspond to the feasible combinations from the simulation results. For purities and yields, the simulated results were normalized by Eq. (5.14) before determining the weights. For the separation factors, the data were normalized by Eqs. (5.15) and (5.14) consecutively. The calculations were performed using the optimization software FICO Xpress.

After determining the criteria weights, each alternative could be compared with respect to their alternative ranks, Rk_a . The alternative ranks were averaged to calculate the sensitivity coefficient in response to a change of process parameters. We simulated 3 levels of each process parameter. Therefore, the alternative ranks were averaged within each subset of alternatives that had a similar level of process parameters. In Eq. (5.23), X

represents the process parameters: feed flow rate, membrane type and pressure at each stage in 3 different level, lv , as explained in Section 5.3.3 .

$$\overline{Rk}_{a,lv} = \frac{\{\sum Rk_a | X = lv\}}{\{n_a | X = lv\}} \quad (5.23)$$

For each process parameter, 3 different values of average rank were obtained related to each level of process parameter. Using the middle level as a reference, 2 sensitivity coefficients (Eq. (5.17)) were calculated in response to the high (+) and low (-) level. The average of these 2 values was used to analyse the performance.

$$SC_{Rka} = \frac{1}{2} (SC_{Rka}^+ + SC_{Rka}^-) \quad (5.24)$$

Analogous to the average ranks, the sensitivity coefficient could also be calculated for the criteria weights, w_c . Unlike the alternative ranks, criteria weights are single values that represent all alternatives for each criterion and thus cannot be averaged. To obtain the criteria weight corresponding to each level of process parameter, we solved Eqs. (5.12) and (5.13) repetitively using a subset of alternatives at 3 different levels. Using these criteria weight values, sensitivity coefficients were calculated (Eq. (5.25)).

$$SC_{wc} = \frac{1}{2} \left(\frac{\Delta w_c^+}{\Delta X^+} + \frac{\Delta w_c^-}{\Delta X^-} \right) \quad (5.25)$$

The weights determination and backward analysis were first performed and assessed using configuration S-1. Later, the same procedure was expanded to all configurations.

5.4 Results and discussion

5.4.1 Validation experiments

The steady state model used in this study was validated in terms of its prediction for the flow rate and concentration at each stream in all configurations proposed. Within each configuration, a preliminary simulation was done to select the combination of setups (Table 5.3) that produced good purities and yields.

The model predicted the flow rate well with small deviations observed (Figure 5.4a). The deviation might arise from variation in the batch of membrane in addition to experimental variations. Relatively high deviations were observed at low flow rates, which might simply relate to measurement errors in low flow rate values.

The prediction of the component concentrations showed some deviations, especially at the higher concentrations (Figure 5.4b and c). Different types of deviations were observed with different strategies. The outcome for the S strategies in Figure 5.4b showed a tendency of overprediction, whereas the L strategies in Figure 5.4c showed the opposite behaviour. This overprediction showed a dependency on both molecular size and concentration. Only big molecules ($DP \geq 5$) at higher concentration showed a significant deviation. This higher concentration might relate to the bottom region of the cascades, which was explored by the S strategies.

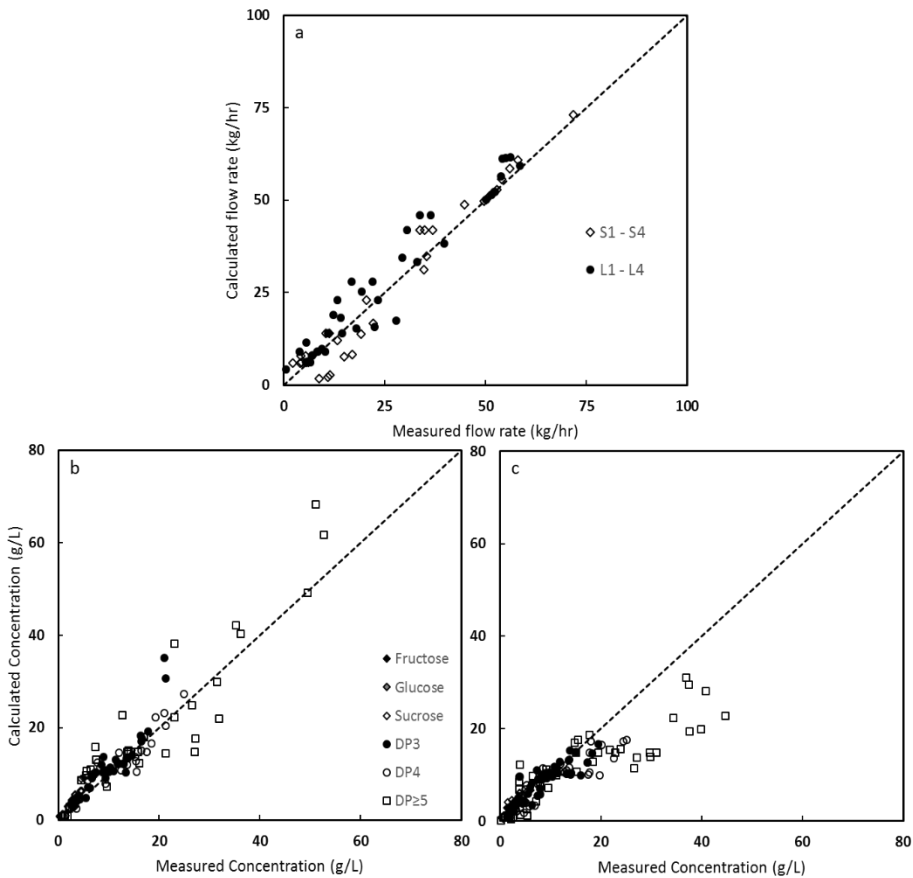


Figure 5.4 Validation results of the steady state model using various setups (Table 5.3) for (a) flow rate, (b) concentration using S strategies and (c) concentration using L strategies. The points represent the flow rate or concentration value at every stream in every configuration.

Despite the deviations that the model showed, the performance predictions simulated by the model were satisfactory. The maximum root mean squared error observed for this model was 10.27 for DP4 concentration. In general, moderate deviations only appeared for $DP \geq 4$ at the bottom stages, which refer to only a small part of the study. Therefore, the predictions of this model were acceptable for the scope of this study. A detailed quantification of errors for the model is summarized in table S.14 (supplementary material).

5.4.2 Simulated performance indicators

All configurations tested were able to fractionate the FOS well, resulting in 3 outlet products with higher purities compared with the feed stream (Table 5.4). Focusing only on the purities for each fraction of interest separately, the cascaded system could purify monosaccharides up to 47% from 9%, DP3 up to 34% from 24% and $DP \geq 5$ up to 77% from 34%. These results were achieved by selecting a combination that maximized the targeted purity. These values exceeded the maximum values achieved by 3-stage fractionation cascades using the side-stream strategy [60]. Not only via simulation, we also experimentally found purer products using the new proposed configurations. Maximum experimental purities reached 30.7% for DP1, 33.1% for DP 3 and 49.9% for DP5 within the setups mentioned in Table 5.3. Previously, the maximum experimental purities were reported as 19.5% for DP1, 26.3% for DP3 and 39.6% for DP5.

Altering the flows in 3-stage configurations could be driven towards specific products. Improving the purity of $DP \geq 5$ could be achieved by altering the streams towards the bottom region only (configuration S-1 and S-2). Furthermore, the purification of $DP \geq 5$ using these 2 configurations even exceeded the performance of 4- and 5-stage fractionation cascades. In contrast, altering the stream towards the top region only (configurations L-1 and L-2) improved the purity of monosaccharides. However, the purification of monosaccharides using these configurations was not as good as for the 4- and 5-stage systems. This was related to the fact that the monosaccharides were the most permeating component. Therefore, recovery of monosaccharides was better when more of them were being recycled using more stages.

The results also showed that extracting products from different stages gave the best performance (configuration S-2 and L-2). Using this approach, the selection of conditions in every stage became more focused towards specific components. Each stage could use a specific setup that was best for the particular separation.

Table 5.4. Maximum simulated purities and yields using various configurations.

Configuration	Max{Py ₁ }	Max{Y ₁ }	Max{Py ₃ }	Max{Y _{FOS,m} }	Max{Py ₅ }	Max{Y _{FOS,1} }
Feed	8.9		23.6		33.6	
S-1	25.6	82.3	32.8	89.9	59.0	93.5
S-2	25.6	77.0	32.7	77.8	77.1	93.5
S-3	25.6	82.3	32.0	91.4	55.9	93.8
S-4	24.1	83.6	34.1	69.3	55.9	93.5
L-1	46.6	33.2	32.4	87.9	40.9	94.1
L-2	47.0	38.1	33.0	81.0	42.1	98.7
L-3	39.7	62.7	31.7	88.3	41.2	96.2
L-4	37.5	73.1	33.9	87.8	46.5	96.7
3 stages ^a	41.3	57.9	32.2	43.9	43.3	98.0
4 stages (top) ^a	67.3	44.6	32.8	51.6	49.1	99.6
4 stages (bot) ^a	51.2	59.0	32.7	48.4	53.8	98.8
5 stages ^a	65.4	41.6	33.0	64.2	49.9	99.7

The maximum values of purities and yields may use different combinations. Numbers in bold type are the highest values among the configurations.

^aSimulated values using a side-stream strategy [60].

Table 5.4 can help with selecting a configuration towards a targeted purity or yield. However, selecting that configuration within a particular setup would decrease the other purities or yields.

We observed that further improvement of DP3 purification was problematic. As a mid-sized component, DP3 can only be purified by improving both $SF_{3,1}$ and $SF_{3,5}$ simultaneously. However, $SF_{3,1}$ and $SF_{3,5}$ had a strong negative correlation (Figure 5.5), indicating that improving $SF_{3,1}$ could only be realized at the expense of $SF_{3,5}$. This correlation was found to be configuration dependent. Within the configurations studied, the strong negative correlations were suppressed at the centred configurations (S-3, S-4, L-3 and L-4). Within these 4 configurations, the maximum $SF_{3,5}$ values were higher using configuration S-4 and L-4 where DP3 was collected as the permeating component.

In practice, it is common to have multiple criteria, maximizing both purity and yield or purities of all fractions. Therefore, a multi-criteria approach is needed for a comprehensive decision.

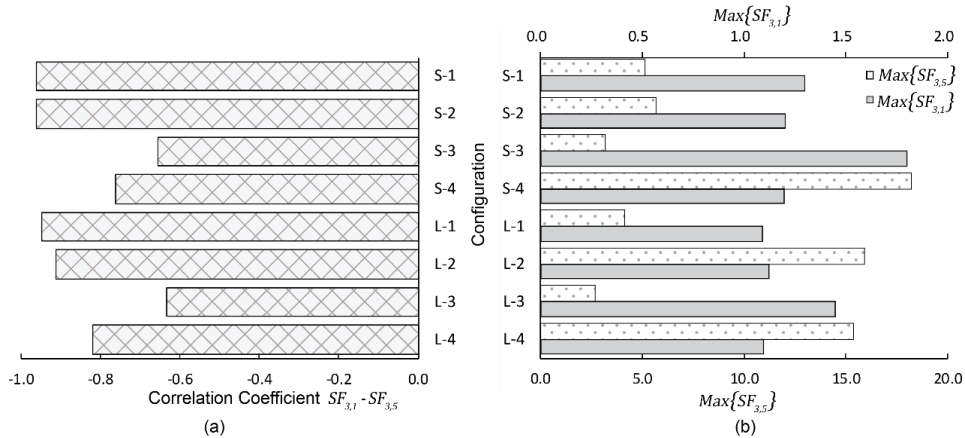


Figure 5.5. (a) Correlation coefficient (Eq. (5.22)) between $SF_{3,1}$ and $SF_{3,5}$ and (b) maximum values of separation factors simulated from each configuration. The maximum values are chosen from feasible alternatives.

5.4.3 Weights determination and optimized setup for S-1

In this and the following section, the analyses were performed and discussed for 1 arbitrarily selected configuration, S-1. The outcomes discussed in these 2 sections are then expanded to all configurations for selection purposes in Section 5.4.5.

For configuration S-1, the criteria weights (Eqs. (5.12) and (5.13)) were determined for all purities, yields and separation factors. This determination can be done in 2 ways: (1) separately between purities-yields and separation factors and (2) simultaneously for all purities, yields and separation factors. The result for configuration S-1 (Table 5.5) showed that the weights calculated using both methods had similar relative importance between criteria, indicated by the weights rank (Eq. (5.16)). For example, in Table 5.5, Py_5 had the lowest rank among other purities and yields. Using simultaneous determination, Py_5 also had the lowest rank among purities and yields. This is also visible in the separation factor group; $SF_{1,3}$ had the highest rank within separation factors when the weights were determined by considering the separation factors only or simultaneously with the purities and yields. Moreover, using simultaneous determination we can see that $SF_{1,3}$ is also more important than all purities and yields, giving a complete overview of which criterion is

more important among other types of criteria. This behaviour indicated that the weight determination was robust regardless of the number of criteria considered.

Table 5.5. Criteria weights and their ranks for purities, yields and separation factors determined separately, (1a) only Py_i and Y_i and (1b) $SF_{i,j}$, and simultaneously, (2) all Py_i , Y_i and $SF_{i,j}$, using configuration S-1.

		Weights									
		Py_1	Y_1	Py_3	$Y_{FOS,m}$	Py_5	$Y_{FOS,l}$	$SF_{1,3}$	$SF_{3,1}$	$SF_{3,5}$	$SF_{5,3}$
(1a)	Py_i and Y_i	0.24	0.13	0.20	0.13	0.12	0.20	–	–	–	–
(1b)	$SF_{i,j}$	–	–	–	–	–	–	0.36	0.23	0.25	0.17
(2)	Py_i , Y_i and $SF_{i,j}$	0.14	0.08	0.12	0.08	0.07	0.12	0.14	0.09	0.10	0.07
		Weights rank									
(1a)	Py_i and Y_i	1	4	2	5	6	3	–	–	–	–
(1b)	$SF_{i,j}$	–	–	–	–	–	–	1	3	2	4
(2)	Py_i , Y_i and $SF_{i,j}$	2	7	3	8	9	4	1	6	5	10

The weighting method we developed was assessed to confirm its robustness. The robustness was confirmed if the result from this method was in agreement with other methods. The result was reflected in the alternative rank, Rk_a , that was calculated using the criteria weights. We assessed the method by evaluating the correlation coefficient (Eq. (5.22)) of Rk_a calculated by different methods [113] and evaluating the agreement of the top 10% of the alternatives, which was adapted from the agreement of the top 3 [114] using dataset from configuration S-1.

The method in this study showed good agreement with CRITIC method [115] and Ma's method [116]. The alternative ranks generated from this study had a correlation coefficient of 0.94 with the CRITIC method and 0.98 with Ma's method. In addition, the top 10% alternatives showed 91% agreement with the CRITIC method and 82% agreement with Ma's method. Compared to both mentioned methods, the method in this study was simpler yet giving a better representative for relative importance between criteria. In the CRITIC methods, pair-wise correlation coefficients must be calculated which is creating more steps in solving the problems. On the other hand, Ma's method had a similar form with the method used in this study, however it has a quadratic

distance. A quadratic distance resulted in (1) a non-linear optimization problem, which required a more complicated solver, and (2) a bigger penalty to data points that are far from the ideal. The penalty made the criteria weight smaller when more non-ideal data points occurred, which was not desired. Since there is an excellent concordance between the method developed in this study and two other independent methods, we concluded that our method was robust and further analysis based on that would be reliable.

Using the criteria weights that were determined simultaneously (Table 5.5), we were able to design configuration S-1 by selecting the best membrane and best pressure setting for each stage at the best feed flow. This setup accommodated all criteria, therefore the individual criteria values were below the maximum values as listed in Table 5.4. Comparing with the individual optima, Y_1 and $Y_{FOS, Mid}$ were far below the maximum values whereas Py_1 and $Y_{FOS, large}$ were close to the maximum (Table 5.6). This was because their criteria weights had more importance on Py_1 than on Y_1 . A similar procedure was applied for any configuration to select the best setup within that particular configuration or even the best setup among all configurations (Table 5.A.1).

Table 5.6. The best setup and criteria values for configuration S-1

Setup									
M_F	M_{B1}	M_{B2}	$Press_F$	$Press_{B1}$	$Press_{B2}$	Fl_F			
GE	GK	GE	8 bar	16 bar	12 bar	70 kg/h			
Performance indicators									
Py_1	Y_1	Py_3	$Y_{FOS, m}$	Py_5	$Y_{FOS, l}$	$SF_{1,3}$	$SF_{3,1}$	$SF_{3,5}$	$SF_{5,3}$
25.4%	14.7%	31.5%	3.1%	36.2%	93.5%	2.18	0.52	5.14	1.12

The best setup is chosen within feasible alternatives that have the best rank.

In addition to selecting the best setup, the criteria weights can also be interpreted to describe the system behaviour. The purity Py_1 had the highest weight among the purities and yields and the Py_5 was the lowest. According to Eq. (5.12), a higher weight would be assigned to a criterion with a value close to its maximum. This implied that within configuration S-1, most alternatives arrive approximately at the same value of (normalized) Py_1 . If a single optimization were to be performed, optimizing Py_1 will not improve the system significantly, whereas an improvement could be achieved by focusing on Py_5 . This conclusion is strengthened by the difference in the performance indicators in

Table 5.4, optimized for P_{y_1} and P_{y_5} independently, and the values for the weighed optimization as given in Table 5.5. ΔP_{y_1} is 0.2 whereas P_{y_5} ranges from 59% (optimized for P_{y_5} only) to 36.2% for the weighed optimization.

5.4.4 Backward analysis using the sensitivity coefficient

The criteria weights helped us to select the best setup that accommodated all criteria. However, from a process design perspective, a single best setup might not be the most important issue. The setup that performs in second or third place might still be acceptable. Therefore, additional insight is needed on how a change in the setup affects the performance.

The backward analysis gave an indication of the sensitivity of a process parameter. The performance could be evaluated as an overall performance, which was represented by the average rank, \overline{Rk}_a (Eq. (2.24)), or individually for each performance indicator, which was represented by the criteria weight, w_c (Eq. (5.25)).

5.4.4.1 Backward analysis for overall performance via average rank, \overline{Rk}_a

The change in the average rank when a condition was changed was represented in the sensitivity coefficient, SC_{Rka} , of the individual process parameter: the membrane type at each stage, M_{stage} , the pressure at each stage, $Press_{stage}$, and the feed flow rate, Fl_F . The absolute value of the sensitivity coefficient showed how sensitive a parameter is to a change. Furthermore, a negative value indicated that using a lower value of a process variable gave a better performance. These values provided a tool to pinpoint the critical variables.

Table 5.7 shows that the membrane at the feed stage, M_F , the membrane at stage B2, M_{B2} , and the feed flow rate, Fl_F , are sensitive to change. Changing the membrane from GE to GK at the feed stage would reduce the performance as the average rank increases from 38.2 to 83.5. On the other hand, changing the membrane at stage B1 would not result in any change to the overall performance. This worked in the same way for the feed flow rate which showed increased performance with a lower value. Apart from those, setting up any pressures for each stage would hardly affect the overall performance. We conclude that using configuration S-1, tight membranes are needed at stage feed and B2 with a low feed flow rate. The other parameters can be set arbitrarily.

Table 5.7. Average rank and sensitivity coefficient (Eq. (5.24)) for variable membrane type and pressure at each stage and feed flow rate using configuration S-1.

Process variable	Average ranks, \overline{Rk}_a	SC_{Rka}
	GE (1000 Da)	38.2
M_F	GH (2500 Da)	79.2
	GK (3500 Da)	83.5
	GE (1000 Da)	48.8
M_{B1}	GH (2500 Da)	60.0
	GK (3500 Da)	49.8
	GE (1000 Da)	38.2
M_{B2}	GH (2500 Da)	61.6
	GK (3500 Da)	67.6
	8 bar	55.0
$Press_F$	12 bar	50.1
	16 bar	52.9
	8 bar	56.3
$Press_{B1}$	12 bar	51.1
	16 bar	51.3
	8 bar	56.6
$Press_{B2}$	12 bar	46.5
	16 bar	55.9
	50 kg/h	43.4
Fl_F	60 kg/h	53.1
	70 kg/h	58.7

Ranks were calculated using all criteria weights determined simultaneously.

5.4.4.2 Backward analysis via criteria weights, w_c

Evaluating the sensitivity coefficients using criteria weights gives a detailed explanation about the performance change as a response to the parameter change. It shows how each criterion contributed to the overall performance. The negative SC of the average rank in

response to the membrane type at the feed stage (Table 5.7) came as an overall result of the various sensitivity coefficients of all criteria.

Table 5.8 shows the sensitivity coefficients for each criterion using configuration S-1. The values confirm that Py_1 and $SF_{1,3}$ were negatively sensitive to the membrane at the feed side. Conversely, most of the other criteria were positively sensitive. This indicated that using a membrane with low MWCO at the feed stage improves Py_1 and $SF_{1,3}$ yet decreases the other criteria. Each criterion responded at various levels, as represented by the magnitude of the sensitivity coefficients. Moreover, each criterion had a different contribution to the overall performance, which is represented by the criteria weights. These different levels of responses and contributions from each criterion were accommodated by the alternative rank.

Different sensitivities of every criterion might negate each other, resulting in a non-sensitive overall performance. For example, a high pressure at stage B2 improved Py_1 with an SC of 0.68. At the same time, this high pressure decreased the yield with almost similar SC.

Table 5.8. Sensitivity coefficient for criteria weights (Eq.(5.25)) for variable membrane types and pressures at each stage and feed flow rate using configuration S-1.

Variable	Py_1	Y_1	Py_3	$Y_{FOS,m}$	Py_5	$Y_{FOS,l}$	$SF_{1,3}$	$SF_{3,1}$	$SF_{3,5}$	$SF_{5,3}$
M_F	-3.49	1.06	0.34	0.12	0.59	-0.19	-2.41	0.37	0.49	0.74
M_{B1}	0.11	-0.09	0.03	-0.03	-0.04	-0.01	0.02	0.02	0.01	-0.08
M_{B2}	0.91	-0.05	-2.42	1.09	0.12	-0.59	0.89	-0.76	-1.53	0.13
$Press_F$	0.17	0.09	-0.05	-0.25	-0.01	-0.07	0.20	-0.30	-0.08	0.04
$Press_{B1}$	0.13	-0.06	-0.08	0.01	0.00	-0.05	0.09	-0.03	-0.06	-0.06
$Press_{B2}$	0.68	-0.60	-0.36	0.41	-0.26	-0.31	0.61	-0.38	-0.46	-0.34
Fl_F	-1.18	0.57	0.21	0.31	0.30	0.43	-0.98	0.78	0.40	0.38

5.4.5 Selection of configuration

Selecting a configuration from several options can be done using 2 approaches: either the overall performance or more specifically directed towards certain criteria. In addition to that selection, backward analysis can be performed to give an indication about critical

parameters (analogous to Section 5.4.4). These approaches and analyses were also in order of increasing details in the design.

5.4.5.1 Overall performance via average rank, \overline{Rk}_a

Analysis of the overall performance was done using the complete dataset. This complete dataset was a combination of all feasible (simulation) results for all configurations proposed. Using this dataset, the overall criteria weights were calculated by solving Eqs. (5.12) and (5.13). These criteria weights were used to calculate the alternative ranks for all configurations. The best setup could be chosen from the best rank and was found to be within configuration L-1 (Table 5.A.1).

5 These alternative ranks were later averaged for each configuration, analogous to calculating an average rank for process parameters (Eq. (5.23)). The average ranks for each configuration are summarized in Table 5.9. The values are much higher magnitude than the values presented in Table 5.7. This is reasonable because the alternatives in Table 5.9 were ranked using a dataset that was 8-fold larger. Therefore, comparing values in these 2 tables is not relevant.

Comparing average ranks for configurations (Table 5.9), we achieved a fairer comparison between configurations. In general, S strategies had a better performance than L strategies. This contradicted the fact that the best performance was within the L strategies. This also indicated that the performance distribution in configuration L-1 was not uniform; the best performance could only be achieved using specific set up (Table 5.A.1). When other set up used within L-1 configuration, it was often found that the second and third best alternatives were far below the best alternative.

However, the average ranks could not give us sufficient information about the possible cause. Despite the clear distinction between S and L strategies, these average ranks were close within the same strategy cluster. Therefore, a detailed evaluation for each performance indicator was needed.

Table 5.9. Average ranks of proposed configurations calculated using feasible alternatives.

Strategy	Average rank
S-1	224
S-2	244
S-3	282
S-4	210
L-1	364
L-2	386
L-3	360
L-4	329

5.4.5.2 Performance indicator analysis via criteria weight, w_c

Criteria weights contain information about how important a criterion is compared with the others. A criterion becomes more important if most alternatives for that particular criterion are close to optimal. Using a similar number of criteria, the criteria weights could be used to compare one design with another. A high criterion value indicates that a particular design is more suitable towards a specific criterion.

To evaluate the performance of each configuration towards certain criteria, the criteria weights for all configurations were calculated separately (Eqs. (5.12) and (5.13)) and compared with each other (Figure 5.6). Figure 5.6 gives insight on which configuration should be chosen to correspond to specific criteria. In general, any S strategies can be chosen instead of L strategies to improve Py_1 , with configuration S-1 as the best one, with a weights value of 0.24. In contrast, any L strategies can be chosen to improve Py_5 . Apart from those, improving Py_3 could be done by choosing centred configurations (S-4 or L-4). All these results are in agreement with the first approach using only the maximum criteria value as explained in Section 4.2. However, criteria weights were calculated using the complete dataset instead of choosing 1 single best alternative. Therefore, the interpretation gives more confidence.

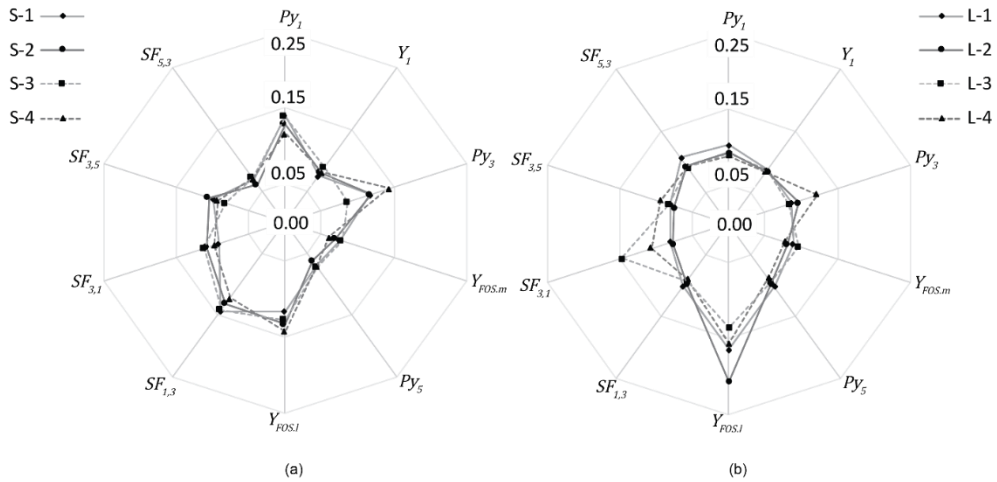


Figure 5.6. Criteria weights of (a) *S* strategies and (b) *L* strategies determined using simulated data.

Using Figure 5.6, we could distinguish which configuration had exceptional weight and was thus preferable for that particular criterion. Configuration L-2 had a good weight for $Y_{FOS,l}$ compared with the other configurations. Extracting a large fraction from the feed stage might reduce the FOS yield as a result of insufficient separation at the first stage. However, the key factor to increase this yield would be the recycle stream. The recycle stream at configuration L-1 came from stage T-1, indicating all FOS that went to stage T-2 would be extracted in either the small or mid fraction. At configuration L-2, the unrecovered FOS from stage T-2 would be recycled to the feed stage, increasing the $Y_{FOS,l}$.

We were able to select configuration S-4 to improve Py_3 and configuration L-2 to improve $Y_{FOS,l}$ using Figure 5.5. If further improvement of the performance is desired, a backward analysis using sensitivity coefficients can be performed. The backward analysis is shown in the supplementary material (Table S.13, supplementary material) and shows that we could improve Py_3 using configuration S-4 via a tight membrane in stage T-1, whereas a loose membrane is needed in the feed stage. The other parameters are less sensitive, which indicated that we had more freedom on selecting the setup.

5.5 Conclusion

Eight configurations were tested in this study to improve the fractionation of FOS resulting in 3 outlet streams. Using those configurations, improved performances could be achieved while keeping the stage number at 3.

Improving all performance indicators (purities, yields and separation factors) at once was a dilemma regarding the trade-offs between (conflicting) indicators. This problem was solved using a multi-criteria decision-making approach. An optimization model was developed to select a single best setup. This setup consisted of a combination of process variables that produced the most acceptable compromise between performance indicators.

In addition, using backward analysis with sensitivity coefficients, we were able to pinpoint critical variables. Knowing these critical variables, further targeted improvements could be reached more efficiently. However, the critical variables are configuration dependent. For configuration S-1, an improvement can be done by using low flow rates and a tight membrane at the feed stage. Finally, the set of analyses performed in this study enabled us to discriminate one design to from another. Using these analyses, we have 2 options for system design to select our system: (1) based on the overall performance or (2) specifically directed towards certain criteria. Within the chosen setup, we can retrieve information on parameters that should get more attention. Consequently, the design process becomes more focussed and efficient.

The approaches discussed in this study are useful to assess a separation process system with multi-process variables and multi-performance indicators. This is not only useful for the multi-stage cascaded fractionation of fructooligosaccharides. We believe that a similar analysis is applicable for most integrated processes with multi-process variables and multi-performance indicators. To be able to do this analysis, a model that predicts the performance indicators is needed. The outcome of this model will be a dataset for further analysis: an MCDM model and sensitivity analysis.

Each additional stage in the membrane cascade, will increase the number of decision variables in the optimization procedure; the complication to solve the problem increases. Applying the same procedure to the previously reported 4 or 5-stage cascades will give 3 or 6 additional decision variables, respectively.

Acknowledgements

The authors would like to acknowledge Lembaga Pengelola Dana Pendidikan, Kementrian Keuangan Indonesia, for financial support. The authors also acknowledge Ruurd Olde Bijvank for the validation experiments.

Nomenclature

Latin symbols

C	solute concentration (g/L)
C'	solute concentration at the mixing point (g/L)
D	distance in the minimization model (dimensionless)
Fl	flow rate (kg/h)
Fl'	flow rate at the mixing point (kg/h)
J	mass flux (kg/m ² /s ¹)
M	membrane type
MW	molecular weight (kg/mol)
Py	product purity (%)
$Press$	applied pressure (Pa)
R_g	gas constant (J/mol/K)
Rk	alternative rank (dimensionless)
R_r	real rejection (dimensionless)
Res	membrane resistance (m ² /kg)
S	summed parameter (dimensionless)
SC	sensitivity coefficient (dimensionless)
SF	separation factor (dimensionless)
T	process temperature (K)
TMP	trans-membrane pressure (Pa)
v	(normalized) alternative values

\dot{v}	alternative values
\dot{v}^{\max}	maximum alternative value
\dot{v}^{\min}	minimum values
w	criteria weight values (dimensionless)
Y	product yield (%)

Greek symbols

μ	dynamic viscosity (Pa s)
π	osmotic pressure (Pa)

Subscripts

1, 3, 5	solute, degree of polymerization
a	alternatives
c	criteria indices
i, j	solute, degree of polymerization
n	number of alternatives
p	permeate side
s, m, l	small, mid and large products
$F, B1, B2, T1, T2, s$	stage indication
P, R, rec	stream indication
w	membrane wall

Appendix

Table 5.A.1. Optimum setup and simulated criteria values at the optimum setup for 8 configurations tested.

Setup	L-1 ^a	S-1	S-2	S-3	S-4	L-1	L-2	L-3	L-4
M_{T_2}	GE	–	–	–	–	GE	GE	–	–
M_{T_1}	GE	–	–	GE	GE	GE	GE	GE	GE
M_F	GE	GE	GE	GE	GE	GE	GE	GE	GE
M_{B_1}	–	GK	GE	GE	GE	–	–	GE	GE
M_{B_2}	–	GE	GK	–	–	–	–	–	–
$Press_{T_2}$ (bar)	8	–	–	–	–	8	8	–	–
$Press_{T_1}$ (bar)	12	–	–	8	8	16	16	16	12
$Press_F$ (bar)	12	8	12	12	12	16	16	16	12
$Press_{B_1}$ (bar)	–	16	8	12	12	–	–	8	8
$Press_{B_2}$ (bar)	–	12	8	–	–	–	–	–	–
Fl_F (kg/h)	50	70	70	50	50	50	50	50	50
Criteria		S-1	S-2	S-3	S-4	L-1	L-2	L-3	L-4
Py_1 (%)	44.8	25.4	24.7	23.9	22.7	45.4	46.0	33.6	35.6
Y_1 (%)	8.8	14.7	21.1	30.7	31.3	9.3	9.3	20.0	14.0
Py_3 (%)	32.4	31.5	31.6	32.0	32.3	31.6	32.7	31.2	33.9
$Y_{FOS.Mid}$ (%)	6.8	3.1	2.0	3.2	1.9	10.7	2.1	8.5	2.4
Py_5 (%)	36.3	36.2	36.6	37.8	38.3	37.2	35.3	37.2	36.0
$Y_{FOS.large}$ (%)	92.5	93.5	92.7	88.8	89.4	88.7	97.2	88.6	95.8
$SF_{1,3}$	4.9	2.2	2.1	2.0	1.9	5.0	5.1	3.0	3.2
$SF_{3,1}$	0.7	0.5	0.5	0.9	0.4	0.7	0.4	1.0	0.5
$SF_{3,5}$	4.0	5.1	5.6	3.1	17.4	3.2	12.7	2.4	15.1
$SF_{5,3}$	1.1	1.1	1.1	1.2	1.2	1.2	1.1	1.2	1.1

^aOverall best setup.

Supplementary material is available in the online version

<https://doi.org/10.1016/j.seppur.2019.116349>



Chapter 6

Design optimization of a 3-stage membrane cascade for oligosaccharides purification using mixed integer non-linear programming

This chapter is based on

Z. Rizki, A.E.M. Janssen, E.M.T. Hendrix, A. van der Padt, R.M. Boom, G.D.H. Claassen, “Design optimization of a 3-stage membrane cascade for oligosaccharides purification using a mixed integer non-linear programming”,
submitted for publication

Abstract

Inhomogeneous membrane cascade systems have been utilized to improve the performance of a single-stage membrane separation process, more specifically for purification of fructooligosaccharides (FOS). Such a process allows a different setup at every stage of the cascade, resulting in better purity and yield compared with a homogeneous cascade with fixed setup and compared with single-stage membrane processes. Allowing a different setup at every stage implies an optimization problem related to selection of the membrane and combinations of operating conditions. A manual search of the optimum setup among all possible combinations is impractical and costly. This study solves this problem by developing an optimization model that selects the best type of membrane and optimizes the trans-membrane pressure (TMP), temperature and membrane area in a 3-stage cascade system. The optimization problem in the 3-stage membrane cascade design was formulated as a mixed integer, non-linear programming model and solved using the global optimization solver, BARON. By maximizing the yield repetitively with varying purity requirements, a frontier curve was constructed. This frontier curve was mapped showing the window of operation. From this map, one can observe the shift in operating conditions at all stages with a shift of the objective from a high yield to high purity. The map guides towards the setup that promotes higher permeation in the feed stage when we switch from high yield to high purity. On the other hand, the setup selection at the bottom stage does not show a clear switch, which indicates that the selection at this stage is less critical.

6.1 Introduction

We have studied membrane separation processes for purification of fructooligosaccharides (FOS). A cascaded membrane system performs better than a single-stage separation [18,23,101]. A single membrane is limited by its inherent permeation and separation principles. This limit can be exceeded by creating more selective membranes, either using new materials or by modifying the surface [15–17]; but it is obvious that this approach has its limits. Besides changing the membrane, the separation can be improved by adding extra loops using available membranes, which is commonly known as a multi-stage membrane system [19]. However, simply using membranes in series is inefficient, because some of the material gets lost at every stage. Recycling the streams in a cascaded configuration bypasses this issue, thus improving the product yield while allowing higher purity [23,101].

The concept for the ideal 3-stage membrane cascade design was inspired by the design of a distillation column, and proposed by Lightfoot et al. [23]. In this design, both permeate and retentate from the first stage are fed to two additional membrane stages, giving a more refined permeate and a more concentrated retentate. The streams that are not taken as products are recycled and mixed with the feed stream (Figure 6.1). According to the concept of the ideal cascade, these recycle streams should have a similar composition. This is the case only when both the separation factors and the size of the fluxes in all stages are exactly the same. This condition is hardly tenable in practice. Having dissimilar compositions of recycle streams implies that the cascade can be improved by having different operating conditions and membranes at every stage. This design is known as an inhomogeneous cascade, which can give a better performance than an ideal cascade [20,117]. Moreover, modification of the configurations of the cascade may increase the separation performance [24,63].

However, the design of an inhomogeneous cascade is complicated. Varying the configuration of every stage, plus the operating conditions (e.g. trans-membrane pressure [TMP] and temperature) for every stage implies a challenge in the optimization of the design. The use of multiple stages gives a combinatorial increase in the number of possible configurations, and selecting one particular optimal combination is not trivial. A straightforward approach would be to enumerate and simulate all possible combinations and select the best outcomes. However, this requires unrealistically large computing power, given the number of possible configurations. To alleviate this, a subset of all

possible combinations can be chosen [60,63] as representative, and a selection can be made within this subset. However, there is no guarantee that the globally best outcome is part of this subset.

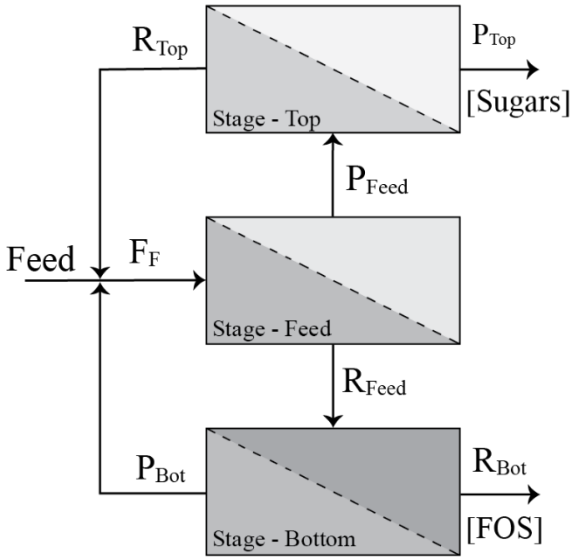


Figure 6.1. Graphical representation of a 3-stage membrane cascade.

Another approach is to develop an optimization model and determine the best combination automatically. An optimization algorithm can be used to solve the model and ensure that the solution is optimal [118,119]. This saves a lot of computation time because it avoids unnecessary evaluation of combinations that are far from optimal [120–124].

Here, we formulate the design of a 3-stage membrane cascade as a combinatorial, mixed integer, non-linear problem (MINLP). The membrane cascade is modelled to purify fructooligosaccharides (FOS) from mono- and disaccharides. FOS are commonly used as a prebiotic and rheology improver in many food products. However, their functionality is hindered due to the presence of small sugars; these add sweetness and caloric value to the oligosaccharides and are not prebiotic [31,33–35,54]. Purification of FOS using membrane processes has been done previously [41,56,125], and earlier studies showed that a modified, inhomogeneous cascade can perform better than homogeneous, ideal cascades in terms of product purity and yield [25,60], even though these systems were not yet fully optimized.

In previous work, membrane cascades were optimized by scenario simulations of a limited set of configurations and choosing the best performing setup [60]. This method is not effective, because there is no guarantee that these selected systems are optimal. An alternative route is to optimize the membrane cascade design and the process parameters at the same time, which, to the best of our knowledge, is a new approach in membrane cascade design. This numerical approach to optimize a 3-stage membrane cascade for FOS purification using an MINLP is presented in this paper.

6.2 Model formulation

A 3-stage cascade model is developed based on the performance of a single-stage model. Each stage in the cascade can be operated using a different type of membrane and a different TMP, temperature and membrane area. These variables are the independent design variables that describe the selection of options at each stage. The performance of a single-stage membrane is characterized by the permeate flow rate, Fl_p , and the observed sieving coefficient, Sv . These values determine the feed conditions of the consecutive stages and consequently the outlet streams. Numerical optimization can be performed to select the best setup with respect to the outlet stream.

6.2.1 Input data and variable declaration

The permeate flow rate, Fl_p , and the observed sieving coefficient, Sv , depend on the independent operating variables, as is specified in Table 6.1. In this table, the argument m represents the membrane type that can be used in stage s (1, 2 or 3). The arguments p and t represent the TMP and the temperature applied, and the argument a refers to the membrane area. Because in practice membranes are supplied as modules with a specific membrane surface area, the value of a can be represented by the number of identical membrane modules used in parallel, and thus in our approach, it is a discrete value. The sieving coefficient is not dependent on the surface area of the membrane and is the same for every identical module that is used in parallel. However, the value of the sieving coefficient varies for every component, i . In a mixture of FOS, component i represents carbohydrates with a differing degree of polymerization (DP).

Table 6.1. Process parameters and variables used in the optimization model.

Variables	Symbols	
Permeate flow rate with given design options (m, p, t, a)	$Fl_p = f(m, p, t, a)$	(6.1)
Sieving coefficient of component i with given design (m, p, t)	$Sv = f(m, p, t, i)$	(6.2)
Retentate flow rate at stage s with given design options (m, p, t, a)	$Fl_R = f(s, m, p, t, a)$	(6.3)
Concentration of permeate stream at stage s for component i	$c_p = f(s, m, p, t, a, i)$	(6.4)
Concentration of retentate stream at stage s for component i	$c_R = f(s, m, p, t, a, i)$	(6.5)
Binary variable selecting design options for stage s	$y = f(s, m, p, t, a)$	(6.6)

6

The values of Fl_p and Sv for a given configuration m, p, t, a and i can be obtained either via experiments or via a model. The effects of the operating variables on the flow rate and sieving coefficient are not straight-forward or linear. A recent publication explains the mechanistic relation between the input variables and the flow rate and sieving coefficient [126]. Direct incorporation of this mechanism into an optimization model is possible but will result in a complex optimization model, which may cause the model to become computationally intensive and may even become unsolvable. Alternatively, we can evaluate the mechanistic model under a wide range of conditions and apply the result as an input dataset for the optimization model. This will strongly decrease the computational effort during the optimization, while still capturing the response of the full model.

The value of the permeate flow rate does not depend on the stage. However, the retentate flow rate does. The permeate flow rate can be approached as constant values obtained in the dataset for every operating variable considered. The retentate flow is related to the permeate flow via a mass balance (Eq.(6.7)), which also depends on the feed flow. The flow enters each stage in a different condition, and therefore the retentate flow also depends on the stage position (Eq. (6.3)).

$$Fl_{F,s} = Fl_{P,s} + Fl_{R,s} \quad \text{for all stages } s \quad (6.7)$$

$$c_{F,s,i} Fl_{F,s} = c_{P,s,i} Fl_{P,s} + c_{R,s,i} Fl_{R,s} \quad \text{for all stages } s \text{ and component } i \quad (6.8)$$

These mass balances in every stage also relate the concentration of every flow that exits and enters the stage (Eq. (6.8)). The concentrations in the permeate and retentate flows of a stage are related through the *observed* sieving coefficient (Eq. (6.9)). This sieving coefficient is different from the *real* sieving coefficient, which is most commonly used [11,127] and relates the solute concentrations at the permeate side and on the membrane surface at the retentate side. The real sieving coefficient value is higher than the observed sieving coefficient because the concentration at the membrane surface is higher than that in the retentate bulk due to concentration polarization. The effect of concentration polarization differs as the concentration and flux change. The effect of the flux is taken into account by having the (apparent) Sv values vary as a function of the membrane type, the TMP and the temperature.

$$Sv_i = \frac{c_{P,i}}{c_{R,i}} \quad \text{for all components } i \quad (6.9)$$

Incorporating the stage indication, s , as an argument together with the operating variables (m , p , t and a) creates a combinatorial option at each stage.

To select the optimal combination of m, p, t, a , the binary variable $y(s, m, p, t, a)$ is introduced for each stage s . The task is to find the best combination of m, p, t, a for each stage, therefore, y should be binary ($y \in \{0, 1\}$); it is or it is not the optimal combination. Because only one single combination of m, p, t, a exists at every stage s , the sum of $y(s, m, p, t, a)$ should be 1 for each stage. This variable enables us to generalize the model and optimize the design effectively: Multiplying $y(s, m, p, t, a)$ with all options will negate all non-optimal combinations and only give 1 optimal combination for each stage.

The system is assumed to be in a steady state. In the 3-stage cascade configuration, the permeate from the feed stage, P_F , becomes the feed stream for the top stage, F_{Top} . The retentate, R_{Feed} , becomes the feed for the bottom stage, F_{Bot} . The retentate from the top stage and the permeate from the bottom are recycled and mixed with the original feed stream. The mixed stream is then fed to the feed stage. The flow rate and concentrations of that mixed feed stream can be calculated via mass balances (Eqs. (6.10) and (6.11)).

$$Fl_{FF,i} = Fl_{Feed} + Fl_{R,Top} + Fl_{P,Bot} \quad \text{for all components } i \quad (6.10)$$

$$c_{FF,i} Fl_{FF} = c_{Feed,i} Fl_{Feed} + c_{R,Top,i} Fl_{R,Top} + c_{P,Bot,i} Fl_{P,Bot} \quad \text{for all components } i \quad (6.11)$$

Solving the mass balances in the mixing point is not straight-forward. We can only calculate the recycle streams after knowing the outlet from the feed stage. However, solving the mass balance in the feed stage requires the condition of its feed, which is the unknown mixed stream. This is not an issue in the ideal cascade concept because it assumes identical concentrations from the streams entering the mixing point. The previous model for membrane cascades [60,63] solved this problem iteratively; estimating the mixed stream and repeating the calculation until the mass balance in Eq. (6.11) is met. However, in a constrained optimization model, this so-called pooling problem is a rather challenging problem, and strategies have been developed to include this pooling problem in optimization procedures [128,129]. This turns the system into an MINLP. MINLP problems are often non-convex, in which local optima can be found rather than the global optimum. Therefore, solving such problems requires a global optimization solver.

6

6.2.2 Purity and yield

The performance of a separation process is commonly assessed with the purity and yield of the product coming from the system. The purity of a product is defined as a fraction of the main component in the product, in the total amount of solutes. In a mixture of FOS, oligosaccharides with DP3 or higher are considered to be the main product and the small sugars with DP2 and lower are contaminants to be removed. Therefore, we can formulate the purity and yield of FOS product coming from a 3-stage cascade as described in Eqs. (6.12) and (6.13).

$$Purity = \frac{\sum_{(i \geq 3)} c_{r,Bot,i}}{\sum_i c_{r,Bot}(i)} \times 100\% \quad (6.12)$$

$$Yield = \frac{\sum_i c_{r,Bot}(i \geq 3) Fl_{r,B}}{\sum_i c_F(i) Fl_F} \times 100\% \quad (6.13)$$

6.2.3 Optimization problem

An optimization model is formulated to find the combination of membrane, TMP, temperature and membrane surface area for every stage of a 3-stage cascade that gives the best performance. For this, we formulate a maximization problem. The performance

indicator can be represented by either the purity or the yield. By definition, using purity as the objective function may lead to a fractional objective [130] because both the nominator and the denominator in Eq. (6.12) follow from the calculations. This is not the case with the yield as an objective. Therefore, the yield is a more appropriate objective. The purity is included as 1 of the constraints (Eq. (6.14) and (6.15)). A frontier curve can then be used to find optimal combinations for purity and yield.

The optimal configuration can be found by maximizing the yield subject to the set of constraints as described in Eqs. (6.15) – (6.29). The mass balances defined in the previous section are reformulated as constraints in Eqs. (6.17) – (6.25). In addition, some ranges are added as both lower- and upper-bounds for variables to limit the scope of the search. The lower bounds need to be defined considering the computing sensitivity, whereas the upper bounds can be chosen arbitrarily according to experimental observation or data from the literature.

$$\max \quad Yield \quad (6.14)$$

subject to (Minimum requirements)

$$Purity \geq Low_{Purity} \quad (6.15)$$

$$\sum_{m,p,t,a} y(s, m, p, t, a) = 1 \quad \text{for all } s \in \{top, feed, bottom\} \quad (6.16)$$

(Flow balances)

$$Fl_{FF} = Fl_F + \sum_{m,p,t,a} [Fl_r(Top, m, p, t, a) + y(Bottom, m, p, t, a) \cdot Fl_p(m, p, t, a)] \quad (6.17)$$

$$Fl_{FF} = \sum_{m,p,t,a} [y(Feed, m, p, t, a) \cdot Fl_p(m, p, t, a) + Fl_r(Feed, m, p, t, a)] \quad (6.18)$$

$$\sum_{m,p,t,a} [y(\text{Feed}, m, p, t, a) \cdot Fl_p(m, p, t, a)] \quad (6.19)$$

$$= \sum_{m,p,t,a} [y(\text{Top}, m, p, t, a) \cdot Fl_p(m, p, t, a) \\ + Fl_r(\text{Top}, m, p, t, a)]$$

$$\sum_{m,p,t,a} Fl_r(\text{Feed}, m, p, t, a) \quad (6.20)$$

$$= \sum_{m,p,t,a} [y(\text{Bottom}, m, p, t, a) \cdot Fl_p(m, p, t, a) \\ + Fl_r(\text{Bottom}, m, p, t, a)]$$

(Concentration equilibrium)

$$Sv(m, p, t, i) \cdot \sum_a c_r(s, m, p, t, a, i) \quad \text{for all } s, m, p, t \text{ and } i \quad (6.21)$$

$$= \sum_a c_p(s, m, p, t, a, i)$$

(Component balances)

$$c_{FF}(i) \cdot Fl_{FF} = c_F(i) \cdot Fl_F \quad (6.22)$$

$$+ \sum_{m,p,t,a} [c_p(\text{Bottom}, m, p, t, a, i) \\ \cdot y(\text{Bottom}, m, p, t, a) \cdot Fl_p(m, p, t, a) \\ + c_r(\text{Top}, m, p, t, a, i) \cdot Fl_r(\text{Top}, m, p, t, a)]$$

$$c_{FF}(i) \cdot Fl_{FF} = \sum_{m,p,t,a} [c_p(\text{Feed}, m, p, t, a, i) \cdot y(\text{Feed}, m, p, t, a) \quad (6.23)$$

$$\cdot Fl_p(m, p, t, a) \\ + c_r(\text{Feed}, m, p, t, a, i) \cdot Fl_r(\text{Feed}, m, p, t, a)]$$

$$\sum_{m,p,t,a} [c_p(\text{Feed}, m, p, t, a, i) \cdot y(\text{Feed}, m, p, t, a) \cdot Fl_p(m, p, t, a)] \quad (6.24)$$

$$= \sum_{m,p,t,a} [c_p(\text{Top}, m, p, t, a, i) \cdot y(\text{Top}, m, p, t, a) \\ \cdot Fl_p(m, p, t, a) + c_r(\text{Top}, m, p, t, a, i) \\ \cdot Fl_r(\text{Top}, m, p, t, a)]$$

$$\begin{aligned}
\sum_{m,p,t,a} [c_r(Feed, m, p, t, a, i) \cdot Fl_r(Feed, m, p, t, a)] & \quad (6.25) \\
= \sum_{m,p,t,a} [c_p(Bottom, m, p, t, a, i) & \\
\cdot y(Bottom, m, p, t, a) \cdot Fl_p(m, p, t, a) & \\
+ c_r(Bottom, m, p, t, a, i) & \\
\cdot Fl_r(Bottom, m, p, t, a)] &
\end{aligned}$$

(Bounds)

$$Low_{Fl} \leq Fl_r \leq Up_{Fl} \quad \text{for all } s, m, p, t, a \quad (6.26)$$

$$Fl_r \geq Low_{rat} \cdot y \cdot Fl_p \quad \text{for all } s, m, p, t, a \quad (6.27)$$

$$c_r \leq Up_c \quad \text{for all } s, m, p, t, a, i \quad (6.28)$$

$$c_p \leq Up_c \quad \text{for all } s, m, p, t, a, i \quad (6.29)$$

The solution of Eqs. (6.14) to (6.29) is a set of binary variables, $y(s, m, p, t, a) \in \{0,1\}$ for each stage and for all possible combinations of membrane types, TMPs and areas. Among those combinations, there are only 3 variables y with a value of 1 corresponding to the 3 stages of the cascade. These y values describe the optimal combination in every stage.

6.3 Methods

6.3.1 Feed condition

The optimization model is in line with the model that was used in a previous study [126], in which a mixture of FOS was fed into a 3-stage membrane cascade system resulting in a higher purity of the product. This previous model simulated the outcome of both single- and 3-stage systems with a given membrane, TMP, temperature and membrane area at each stage. Here, that model is referred to as the *sim* model.

The current model was developed based on mathematical programming. Further, this model is referred to as the *MP* model. Both the *MP* and the *sim* models use a pre-defined feed stream, which contains a mixture of oligosaccharides with a DP from 1 to 10. The oligosaccharides with a DP higher than 5 are clustered as 1 component, so we have 5 components in the system. The component composition of this feed stream is summarized in Table 6.2. The feed enters the system at a flow rate of 60 kg/h.

Table 6.2. Feed concentration for the optimization model

Index value, i	Component	Concentration for characterization (g/L) ^a
1	DP1	0.380 ± 0.022
2	DP2	0.396 ± 0.024
3	DP3	0.706 ± 0.049
4	DP4	0.769 ± 0.050
5	DP ≥ 5	1.329 ± 0.089

^aUncertainties are calculated based on the 95% confidence interval for all experiments.

6.3.2 Design variables

The search for the optimum configuration was done with 5 independent operating variables to be optimized: for each stage, s , we choose a membrane type, m , TMP, p , temperature, t , and membrane area, a (Table 6.3). For each of the 3 stages in the cascade design, the binary variable y represents the choices of the design variables. The constraints (Eqs. (6.15) – (6.29)) ensure that only 1 combination of the design variables will be selected for every stage.

The membrane variable represents the available choice of membranes. Three different membranes from General Electric were used: GE with molecular weight cutoff (MWCO) of 1 kDa, GH with MWCO of 2.5 kDa and GK with MWCO of 3.5 kDa. The 3 membranes were used with a TMP of 4–16 bar and at a temperature of 25°C–45°C. These variables are continuous and may assume any value within the indicated ranges. However, a continuous variable in the model requires a defined relationship between the independent variables and the dependent variables. These relations between TMP, temperature and membrane properties exist but are complex. Therefore, for the optimization model, we simplify the problem by only using a discrete set of values for these variables.

In practice, membranes are offered in modules with a specific membrane surface, therefore we assume that the membrane surface area can only be a multiple of the surface of identical modules. We consider using 1 or 2 modules per stage in the MP mode with a surface area of 0.38 m² per module. Because the surface area per module is fixed, we only show the number of modules as the input variable. The relationship between the surface area and the permeate flow rate is linear and does not affect the sieving coefficient.

Table 6.3. Values of the operating design variables used in the optimization model.

Decision variables	Indices	Levels
Stage	s	Feed, Top, Bottom
Membrane	m	GE, GH, GK
TMP	p	4, 8, 10, 12, 14, 16 bar
Temperature	t	25, 30, 35, 40, 45°C
Area	a	1 and 2

6.3.3 Dataset of single-stage membranes

The performance of a single stage is represented by its permeate flow rate plus its sieving coefficient. Both flow rate and sieving coefficient depend on the independent operating parameters (Table 6.3). The performance of a single membrane is assumed to be consistent and thus independent of the stage position. The sieving coefficient does not depend on the membrane area, but the permeate flow rate scales linearly with the surface area. Apart from this, the permeate flow rate depends on the type of membrane, the TMP and the temperature. The permeate flows and sieving coefficient were simulated using the model given the complete factorial combination of m , p and t at all levels (Table 6.3). This lookup table for single-stage separations (see Supplementary Table 1) is then used in the optimization procedure.

6.3.4 Optimization model and validation

The optimization problem was written using the general algebraic modelling system (GAMS). This system allows different solvers related to many optimization problems to be used. We used the network-enabled optimization system (NEOS) [131] using a global optimization solver, BARON. This solver follows a branch-and-bound algorithm to ensure that an optimum is global [132–134].

Before the optimization, the MP model was validated using the sim model in predicting both the purity and yield of a 3-stage FOS fractionation. The sim model itself was previously validated using experimental data under various conditions [126]. Using the

sim model to validate the new MP model allows us to test any combination, which might have not been possible experimentally.

Combinations of the operating variables were used as input variables. For validation purposes, we used a fractional factorial design to generate combinations of input variables. This design considered all 3 types of membranes, 3 levels of TMPs (8, 12 and 16 bar), 3 levels of temperatures (25°C, 35°C and 45°C) and 2 level of membrane area for every stage. There were 324 possible combinations of these input variables. The generation of these combinations was done using a fractional factorial design table from the literature [103]. Not all these combinations were feasible due to insufficient flow. Excluding the infeasible combinations, 132 combinations remained to be validated.

6.4 Results and discussion

6.4.1 Model validation

The MP model was validated using the sim model with 132 independent combinations of values for the process variables (Figure 6.2). The horizontal axis represents all 132 combinations that were considered for validation. These combinations are sorted based on the predicted yield value. We hardly see any differences between the models, especially at higher yields. However, differences become larger at smaller yields.

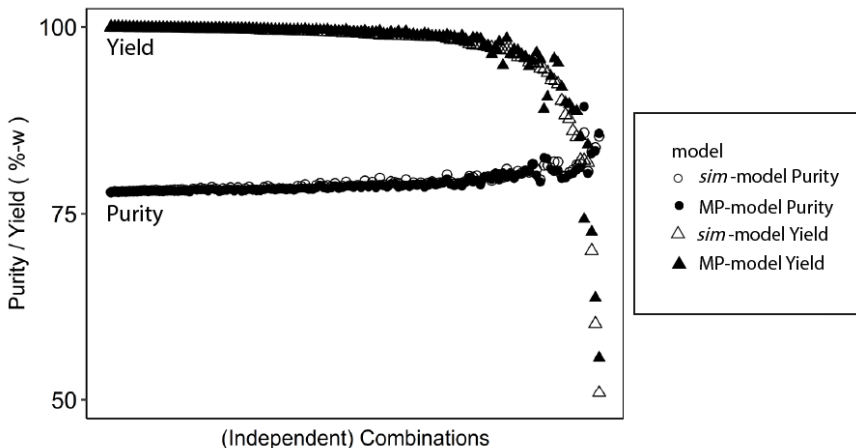


Figure 6.2. Validation of the MP model using the sim model in predicting purity and yield with various combinations of setup.

The deviations between the MP and sim model stem from the inability of the MP model in handling continuous concentration variations in streams. The MP model uses fixed

values of the permeate flow rate and observed rejection with a given membrane type, TMP and temperature, whereas the sim model calculates the exact values. Differences in concentration will change the concentration polarization, which affects the permeate flux, because the osmotic pressure over the membrane changes. Figure 6.3.a shows that there are differences in the fluxes predicted by the sim model and those predicted by the MP model. However, as concentration polarization in nanofiltration remains relatively insignificant, the effect on the sieving coefficient remains small (Figure 6.3.b).

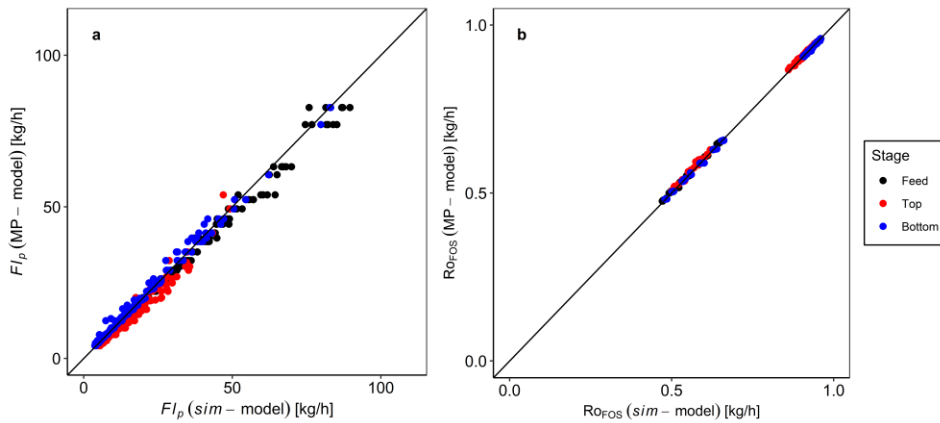


Figure 6.3. Parity plot between the sim model and the MP model in predicting (a) the flow rate and (b) FOS observed sieving coefficient for each stage of the cascade system.

Despite the differences, the MP model gives predictions of the purity and yield that agree well with the sim model. A paired t-test analysis for both models showed that there is no significant difference between these 2 models in predicting the purity and yield (within a 95% confidence interval). The differences are just 0.18% in the purity and 0.29% in the yield (Table 6.4).

Table 6.4. Paired t-test result between the MP model and the sim model in predicting purity and yield.

Predictor	Difference between models (95% confidence Interval)	p-values
Purity (%)	0.11 – 0.26	2.19 * 10 ⁻⁶
Yield (%)	0.51 – 0.73	0.009

We therefore conclude that the MP model describes the purity and yield of a 3-stage cascade system with sufficient reliability.

6.4.2 Model solution

Solving Eqs. (6.8) – (6.24) identifies a set of input variables (Table 6.1) that give the maximum yield subject to given constraints, such as the minimum purity. The binary variable y identifies the system layout that gives the maximum yield. There are exactly 3 y variables that have a value of 1, corresponding to each stage. Because this variable is a function of the operating variables, we can find which combination of operating variables is the best. As an example, Table 6.5 shows the combination of membrane type, TMPs, temperature and area that leads to the maximum yield given a minimum purity of 80%.

Table 6.5. The solution for the optimization model with minimum purity 80%.

Parameters	Value
Minimum purity [%]	80
Purity [%] (constraint)	80.01
Yield [%] (optimization result)	97.43
Membrane	GK
Stage Feed	
TMP [bar]	16
Temperature [°C]	45
Area	2
Membrane	GH
Stage Top	
TMP [bar]	10
Temperature [°C]	30
Area	2
Membrane	GE
Stage Bottom	
TMP [bar]	4
Temperature [°C]	35
Area	1

This solution gives an indication that the search for an optimum combination can be successfully done numerically. Considering all levels of the decision variables, a manual search means a search of millions of possible options, which is costly and impractical. Using the MP model, we can easily find other optimal combinations when we require different purities.

6.4.3 Trade-off of best case scenarios

We constructed a frontier curve by optimizing the system using various purity requirements. Due to the discretization, the model could not give solutions at every purity value. The model either gave a solution with a higher purity than required or the problem became non-convergent. This problem resulted in gaps between the solutions on the frontier curve. More solutions in these gaps were found by using smaller steps in the required purity. As can be observed from Figure 6.4, this resulted in smaller gaps (from black to red to blue symbols). A purity requirement lower than 77% is not meaningful because the feed mixture itself has a purity of 77% and therefore all solutions already have purities higher than 77%.

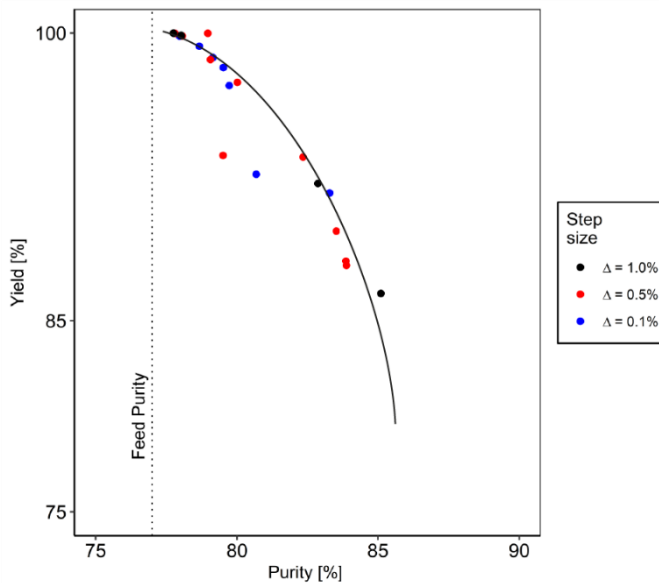


Table 6.6. Solutions for the optimization model with purity 79% using different resolutions.

Parameters	Value [different resolutions]			
	1x	10x	100x	1000x
Resolutions	1x	10x	100x	1000x
Purity	79.06	79.52	79.13	79.39
Yield	98.62	98.23	98.39	98.00
Stage Feed	Membrane	GK	GK	GK
	Pressure	16	16	14
	Temperature	40	45	35
	Area	1	2	1
Stage Top	Membrane	GE	GH	GH
	Pressure	10	10	12
	Temperature	40	25	35
	Area	2	2	1
Stage Bottom	Membrane	GH	GE	GK
	Pressure	4	4	16
	Temperature	35	30	40
	Area	1	1	2

A finer resolution may help in finding solutions within the gaps between solutions found with a coarser resolution. However, the computational capacity restricts the resolution at some point. Figure 6.5 shows that because of this, less solutions are found a 100× and 1000× resolutions. Thus, we conclude that there is an optimal resolution.

The MP model still gives some solutions below the frontier curve. These solutions are not real optima. However, somehow the solver recognized them as optimum solutions. Looking closer at those problems, these solutions have purities that are much higher than the requirement. Solving this issue can be done by finding a strategy to ensure that the purity constraint is binding. Another way is to add an extra constraint such as a minimum yield or maximum purity. However, the values of these constraints will necessarily be educated guesses, because we can only get good estimates after we have constructed the

frontier. Moreover, the addition of an extra constraint increases the model complexity, which may lead to an unsolvable problem.

In Section 6.2.3 we discussed the difference in using the purity as a constraint and the yield as the optimization objective, and the use of the purity as the objective with the yield as constraint. Figure 6.6 shows the results for both approaches. Both approaches give similar solutions and give the same frontier curve. However, there is a numerical difference. The use of a global mixed integer quadratic programming solver (ANTIGONE) did not lead to a solution when maximizing purity, whereas BARON, which uses deterministic global optimization algorithms of the branch-and-bound type was able to attain solutions. It is therefore important to formulate the objective towards the specific algorithm that is chosen.

It is also possible to optimize both criteria, purity and yield, simultaneously, by combining them in a single objective function. We expect that the solutions will follow the same frontier line, with the precise location dictated by the weights that are assigned for the two factors.

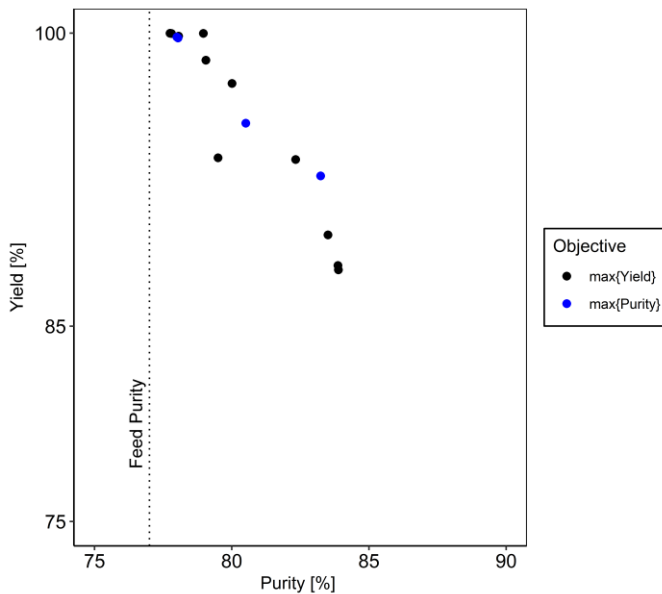


Figure 6.6. Optimal solutions with different objectives: maximizing yield and maximizing purity simultaneously using the BARON solver.

6.4.4 Maps of best operating conditions

The frontier curve that is constructed is important because it gives the best possible performance by the system. In addition, analysing the configurations that give this best performance may offer guidelines on how to design cascaded membrane systems.. Figure 6.7 shows a map of the configurations and operating conditions along the frontier. A membrane with a low MWCO, the GE membrane, in the feed stage is only recommended when a very high yield is requested. The consequence of this is low purity; other components will also be partially retained. For higher purity at the expense of the yield, the membrane with the largest MWCO is chosen for the feed stage, the GK membrane. The intermediate membrane, the GH membrane, with MWCO in between the other membranes, is never optimal in the feed stage. The feed stage therefore mostly acts as a flow divider and not as the main purification stage.

For the top stage, a tight membrane (GE) is chosen for the highest yields, but for all other conditions, the intermediate membrane (GH) is chosen. The role of this stage in those latter cases is to polish the stream by removing some lower molecular weight components to obtain the required purity. Some loss of the high molecular weight components into the permeate is accepted, because this is returned to the feed stage, which will then redirect it again to the top stage. The membrane with the largest MWCO is never optimal for the top stage, because the permeate of the top stage is considered as waste.

In the bottom stage, we see more mixed configurations. All 3 membranes are selected at different sets of yield and purities. This implies that the choice of this membrane is not crucial, and the difference between different configurations is small. It may therefore be logical to choose the GK membrane, because this membrane is most open and will allow the largest flux, or the smallest membrane surface area.

Considering the operating conditions, we also see a clear trend. Higher pressure and temperature is optimal in the feed and top stages, whereas, on average, lower pressure and temperature is optimal in the bottom stage. However, also here, we see a mixed selection of conditions for the bottom stage, indicating that the differences are not very large.

This supports previous studies in membrane cascading, which concluded that in the feed stage, a balanced flow is important, hence an open membrane can be used. Good

separation is more crucial in the top stage; hence, a tighter membrane is chosen there, using a large TMP to ensure reasonable flux.

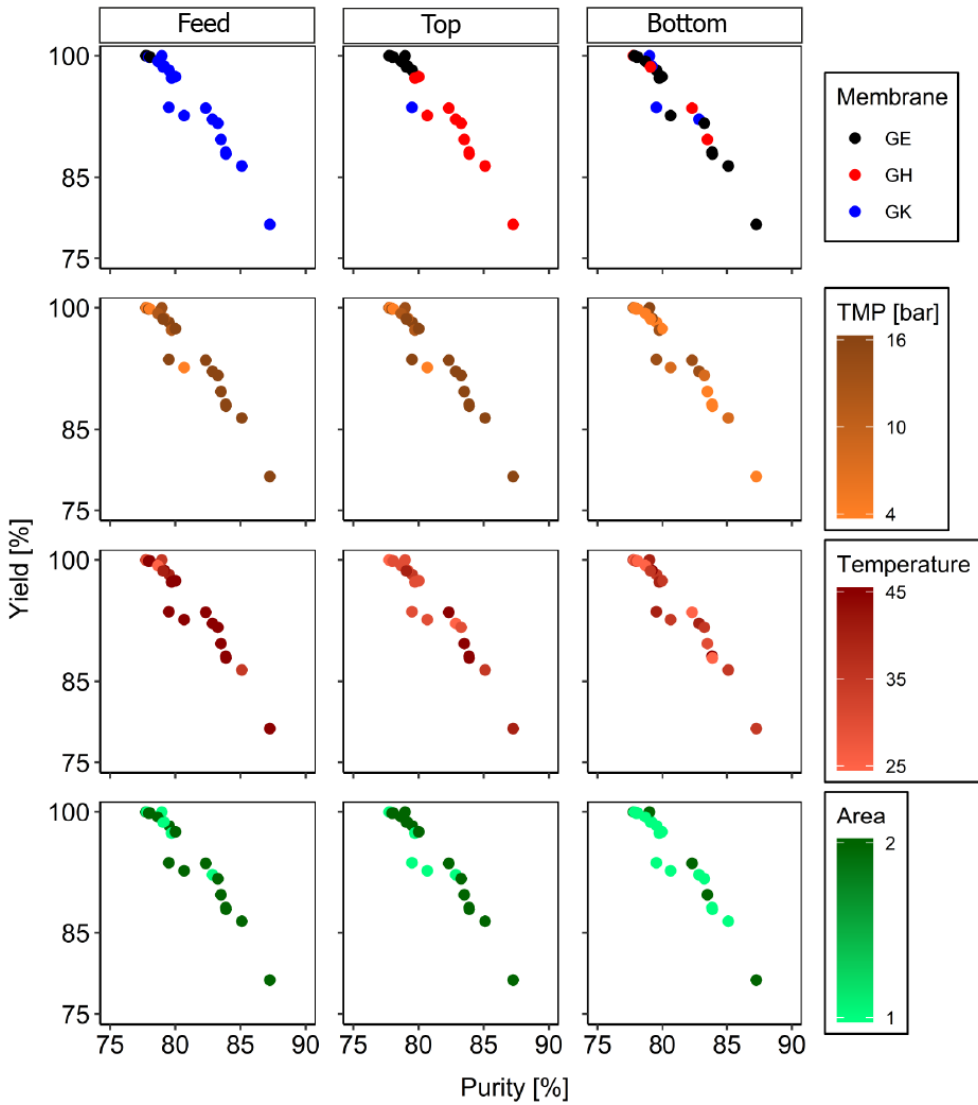


Figure 6.7. Map of the operating conditions in the optimum solutions with yield higher than 75%.

Unlike the feed and top stage, we cannot see a clear shift of the operating conditions in the bottom stage. We see that the choices are spread. This implies that the differences that are achieved by a specific choice in this stage do not greatly affect the yield and purity. We are therefore relatively free in the design for this stage; for example, based on other criteria, such as the required composition of the waste stream or on the minimization of the membrane surface area.

6.5 Conclusions

The design, configuration and choice of operating conditions in a 3-stage membrane cascade system for FOS purification were optimized numerically. This mixed integer non-linear optimization problem was solved using the BARON algorithm to select a membrane, and the TMP, operating temperature and membrane surface area for each stage of the cascade to achieve the highest yield for a given required purity. The optimization could also be done by optimizing the product purity with a given yield requirement with comparable outcome.

We constructed a frontier curve from the optimized solutions that represents the optimum achievable combination of purity and yield with the cascade design. Mapping the configurations and operating conditions on this frontier showed that to move from a high yield to a high purity, we need to increase the permeation in the feed stage by switching from a lower to a higher MWCO, and increase the TMP and temperature and membrane area. In the top stage, a membrane with a low MWCO is recommended, which minimizes the loss; for lower yields, a membrane with an intermediate MWCO is chosen. The design of the bottom stage is quite free and can be based on additional criteria, such as the composition of the waste product and minimization of the membrane surface area.

We can translate the finding into simple guidelines for designing inhomogeneous nanofiltration cascades:

1. The feed stage acts mainly as a flow divider; a membrane with relatively large MWCO should be chosen when high purity is preferred over a high yield; otherwise a membrane with a low MWCO should be chosen.
2. For the top stage, a membrane with a low MWCO is preferred when high purity is required; otherwise a membrane with an intermediate MWCO should be chosen.

3. The choice of the bottom stage membrane is not critical, and thus an open membrane with a larger flux may be chosen.

The study shows that optimization is useful to extract general design guidelines for complex process systems that go beyond idealized systems and can include non-ideal behaviour and experimental limitations (such as the size of modules that are available). Even with this, we can find design rules that can be applied in other designs without the need for a full optimization study.

Acknowledgements

The authors would like to acknowledge Lembaga Pengelola Dana Pendidikan (LPDP), and Kementerian Keuangan Indonesia for financial support. The authors would also like to acknowledge the MSc students who have contributed to the model development: Marlijn Orbons, Afke Politiek and Rimke Braakman.

6

Nomenclature

Symbols

c	solute concentration (g/L)
Fl	flow rate (kg/h)
Sv	sieving coefficient (dimensionless)
y	binary variable selecting design option (dimensionless)

Subscripts

F	feed
P	permeate
R	retentate

Indices

a	membrane area
i	component, degree of polymerization

- m membrane type
- p trans-membrane pressure
- s stage in the cascade
- t operating temperature



7

Chapter 7

Design of nanofiltration cascades for fructooligosaccharides using the McCabe-Thiele approach

This chapter is based on

Z. Rizki, A.E.M. Janssen, E.M.T. Hendrix, A. van der Padt, R.M. Boom, G.D.H. Claassen, “Design optimization of a 3-stage membrane cascade for oligosaccharides purification using a mixed integer non-linear programming”, *submitted for publication*

Abstract

We developed a design method for an inhomogeneous membrane cascade by adopting the McCabe-Thiele method, which is long established for designing distillation columns. The stage cut value is an independent design parameter in the design procedure and thus has to be set. Within each section, the operating conditions were uniform, but both sections could be operated differently using various combinations of membranes, trans-membrane pressure, temperature and stage cut. The procedure was applied to cascaded nanofiltration for the fractionation of a mixture of fructooligosaccharides of varying molecular weight. The stage and area requirements were strongly dependent on the initial design parameter, the overall stage cut. The total area was related to the overall system cut. However, the overall system cut was dependent on the stage cuts for both sections (top and bottom). The top stage cut could be chosen, whereas the bottom stage cut needed to be calculated iteratively to match the top design at the intersection.

7.1 Introduction

Nanofiltration is a common process to purify fructooligosaccharides (FOS) from a mixture, which appears in natural sources such as chicory as a mixture of oligosaccharides with various degrees of polymerization (DP). Both nutritional and functional properties of FOS are dependent on the DP. FOS with high DP have higher prebiotic activity, have a blander taste and higher viscosity [31,34,35,54]. These properties are less pronounced at lower DP, and the opposite properties are found in their monosaccharides: fructose and glucose. However, these monosaccharides also appear in the mixture so they need to be removed. Considering the molecular weights of both the mono- and disaccharides and the only somewhat larger oligosaccharide molecules, nanofiltration is deemed a suitable process to separate them [40,41,57].

Because the FOS oligosaccharides are very similar in molecular weight, a single-step FOS nanofiltration will not give good resolution between individual oligosaccharides. Improving the separation process can be done by either improving the membrane selectivity [15,106] or by a different system design. Without using an improved membrane, the separation performance can be enhanced using a multi-stage process [18,24,59]. Recycling the non-product streams (counter-current) to the previous stage makes the separation more efficient due to loss reduction [18,19,59,108]. Such a design is known as a membrane cascade.

The ideal membrane cascade concept assumes the same separation in each stage and imposes a “no-mixing” condition in the system [23]. This implies that all streams entering the mixing points anywhere in the cascade should have similar concentrations. This condition is not easily achievable in practice. Lifting this constraint gives us more freedom to have different conditions and settings at each stage (inhomogeneous cascades) [20,25,60].

Recent studies on the use of inhomogeneous cascades for FOS separation report an enhanced separation performance with only a limited number of stages [20,63]. This was achieved by modifying the stream configurations and operating conditions at each stage using a three-stage cascade. However, even at this newfound optimum, a three-stage cascade has its limits (Chapter 6). Addition of stages does improve the product purity [60], but there is still no systematic procedure to determine the required number of stages to achieve a certain purity target.

The McCabe-Thiele method to design a counter-current system was developed in 1925 for distillation [22]. This is a graphical procedure to design binary distillation systems. In this method, an equilibrium curve that represents the vapor-liquid equilibrium of the mixture is plotted, representing the composition after 1 stage of separation. Two operating lines are drawn between the equilibrium curve and the parity curve ($x = y$), which are based on the mass balances for the top and the bottom section. The number of required stages is then represented by a stair-like pattern that goes back and forth toward the equilibrium curve and the operating lines.

The similarities between distillation and a membrane cascade system are generally acknowledged [23,135]. The counter-current recycling streams in the cascade resemble the counter-current flows in the distillation column. Instead of the vapor and liquid flows, the streams in the cascade are presented by the permeate and retentate streams among stages. The equilibrium between the liquid and the vapor in every stage of a distillation column is analogous to the partitioning between permeate and retentate in every stage of the cascade.

7

Despite the similarities between distillation and the membrane cascade, only a few studies have been published about the McCabe-Thiele method for designing membrane cascades. Siew et al. [19,136] reported the adaptation of McCabe-Thiele to design an organic solvent nanofiltration cascade. They constructed the McCabe-Thiele curves based on the concentration of the solute that becomes more concentrated in every stage. However, this adaptation is not suitable for a binary mixture, which should give fractions with some degree of purity. Lejeune et al. [135,137] reported an adaptation of the McCabe-Thiele approach for a binary mixture in an ideal organic solvent nanofiltration cascade. However, the scope of that study was limited to an ideal design in which no mixing was allowed in the system. In this article, we extend the McCabe-Thiele approach to design a non-ideal, inhomogeneous cascade for FOS purification. This allows different operating conditions among the stages and yields the required membrane surface areas and pressure.

7.2 Development of the graphical method

The McCabe-Thiele graphical layout consists of 2 major components: the partitioning curve and the operating lines. Both the curve and the lines are plotted in an x-y diagram. The mass fraction of 1 component in the permeate (x_p) is on the vertical axis and the mass

Design of nanofiltration cascades using the McCabe-Thiele approach

fraction in the retentate (x_r) is on the horizontal axis. The permeate streams are analogous to the vapor up-flow and the retentate is analogous to the liquid down-flow in the distillation column. The mixture is considered as a binary mixture, neglecting the water as solvent in this case, with the most retained component used as the base concentration.

$$x_B = \frac{c_B}{c_B + c_A} \quad (7.1)$$

The feed enters the cascade with a known mass fraction, x_{feed} . The desired products exits at the top and bottom section with the desired mass fraction, $x_{p,top}$ and $x_{r,bottom}$.

7.2.1 Partitioning curve

The partitioning curve gives the mass fraction of the permeate that is obtained for a specific retentate. Both fractions are related in a parameter called the separation factor, α , as shown in Eq. (7.2) [135].

$$\alpha = \frac{\frac{x_p}{1 - x_p}}{\frac{x_r}{1 - x_r}} \quad (7.2)$$

Most membranes are characterized by their rejection coefficient (Eq. (7.3)), which relates the concentration at both the permeate and retentate.

$$R_{o,c} = 1 - \frac{c_{p,c}}{c_{r,c}} \quad (7.3)$$

Here, we use the observed rejection coefficient; its value is observed under practical conditions and deviates from the real rejection due to concentration polarization phenomena. To construct the partitioning curve using a known rejection value, a relationship between them needs to be defined. Lejeune et al. [135] expressed the separation factor, α , independently of the mass fraction, with a design parameter. We define the fraction of the feed that becomes the permeate as the stage cut, θ . (Eq. (7.4)), which is an input design parameter to be set. Rewriting the equations derived in the work of Lejeune et al., the separation factor, α , gives Eq. (7.5). In this equation, subscripts A and B represent the component, k , in a binary mixture, with B as the most retained component.

$$\theta = \frac{F_p}{F_f} \quad (7.4)$$

$$\alpha = \frac{\left(\frac{C_{f,A}}{C_{p,A}}\right) - \theta}{\left(\frac{C_{f,B}}{C_{p,B}}\right) - \theta} \quad (7.5)$$

The concentration ratio between feed and retentate was derived to be dependent on the stage cut and the rejection (Eq. (7.6)), with k equal to either A or B .

$$\frac{C_{p,k}}{C_{f,k}} = \frac{1}{\theta} [1 - (1 - \theta)^{1-R_{o,k}}] \quad (7.6)$$

Hence, the partitioning curve depends on 1 independent design parameter, the stage cut θ , and 1 system parameter, the rejection coefficient, $R_{(o,c)}$, which is specific for a certain membrane at given operating conditions, e.g., trans-membrane pressure (TMP) and temperature. For design purposes, the rejection value is assumed to be constant, which is mostly valid within reasonable TMP and temperature ranges under diluted conditions. A constant rejection implies a constant separation factor as well, and with this value we can plot the partitioning curve using Eq. (7.2).

7.2.2 Operating lines

The partitioning curve represents the composition of the permeate streams at every stage, and the operating lines represent the component fractions of the incoming streams, given by a mass balance with the incoming streams coming from the previous stage and the recycle from the consecutive stage (Figure 7.1). Therefore, the operating lines relate the component fractions at one particular stage to the adjacent stage. Figure 7.1 shows a graphical representation of a membrane cascade system.

The cascade consists of 2 sections: the top and the bottom section. In some reports [19,25,60] the feed stage is considered as a third section. To simplify the design, the feed stage can be considered to be part of the bottom section, as was proposed by Avgidou et al. [138]. In this case, the feed stage follows the design conditions of the bottom section. Figure 7.1 shows the streams in stage n at the top section and stage m in the bottom section. The stage number for both sections starts from both products and ends at the mid-point where the feed stream enters.

Each stage is operated with its own stage cut. However, in this approach, the stage cut values for the whole section are kept the same. This leaves only 2 stage cut values: the stage cut of the top section, θ_{top} , and the stage cut of the bottom section, θ_{bottom} .

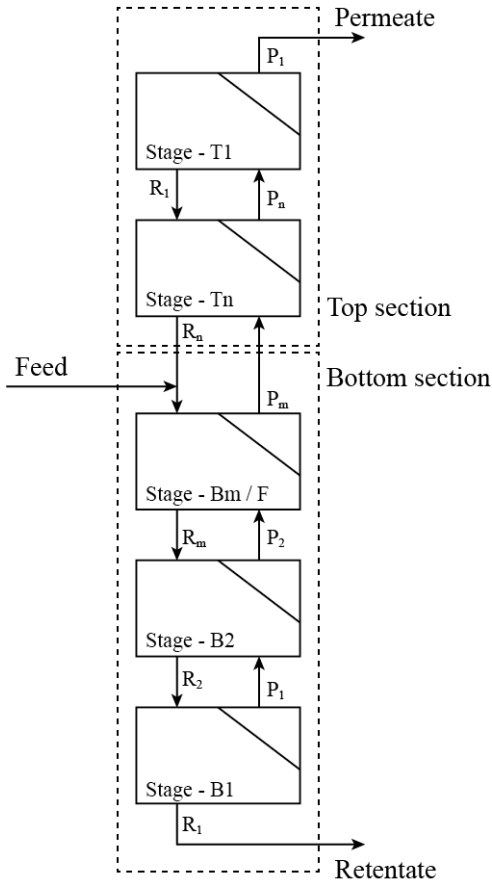


Figure 7.1. Graphical representation of a membrane cascade design with n stage at the top section and m stage at the bottom section

The equations for the operating lines can be derived via mass balances throughout the cascade, which can be evaluated separately for both the top and bottom sections. Detailed derivation for the operating lines can be found in the work of Avgidou et al. [138]. In this section, we summarize the equations that are used for the design.

Derived from the total and component mass balance, the operating line in the top section can be expressed by equation (7.7) [138]. This equation relates the permeate mass fraction at stage

$$x_{p,n+1} = \frac{\sum_{i=1}^n (\prod_{j=i}^n \gamma_{top,j})}{1 + \sum_{i=1}^n (\prod_{j=i}^n \gamma_{top,j})} x_{r,n} + \frac{1}{1 + \sum_{i=1}^n (\prod_{j=i}^n \gamma_{top,j})} x_{p,top} \quad (7.7)$$

with

$$\gamma_{top} = \frac{1 - \theta_{top}}{\theta_{top}} \text{ for all stage } n \quad (7.8)$$

In the ideal cascade design evaluated by Lejeune et al., a non-mixing condition must be obeyed. To achieve this, every stage must be operated using different stage cut values. On the other hand, a constant stage cut within stages in the top section can be achieved by allowing a mixing condition for streams that enter a particular stage (non-ideal design). Avgidou et.al., also evaluated the non-ideal cascade with the restriction of a constant stage cut within the section. In this case, Eq. (7.7) can be simplified into Eq. (7.9).

$$x_{p,n+1} = \frac{\gamma_{top} \left(\frac{\gamma_{top}^n - 1}{\gamma_{top} - 1} \right)}{1 + \gamma_{top} \left(\frac{\gamma_{top}^n - 1}{\gamma_{top} - 1} \right)} x_{r,n} + \frac{1}{1 + \gamma_{top} \left(\frac{\gamma_{top}^n - 1}{\gamma_{top} - 1} \right)} x_{p,top} \quad (7.9)$$

7

The operating line that is expressed by either Eq. (7.7) or Eq. (7.9) represents a linear equation that gives different slopes for each stage (each value of n). Nevertheless, all these lines share a pivot point, $x_{p,top}$, which is the target concentration. This indicates that the operating lines need to be evaluated for every stage despite the constant stage cut.

Similar to the top operating line, the bottom operating line can be derived from the mass balances and is expressed in Eq. (7.10) and simplified into Eq. (7.11) for a non-ideal cascade with constant stage cut. These equations also show a dynamic linear equation that pivots the target point, $x_{r,bottom}$.

$$x_{p,m} = \frac{1 + \sum_{i=1}^m \left(\prod_{j=i}^m \frac{1}{\gamma_{bottom,j}} \right)}{\sum_{i=1}^m \left(\prod_{j=i}^m \frac{1}{\gamma_{bottom,j}} \right)} x_{r,m+1} + \frac{1}{\sum_{i=1}^m \left(\prod_{j=i}^m \frac{1}{\gamma_{bottom,j}} \right)} x_{r,bottom} \quad (7.10)$$

$$x_{p,m} = \frac{\frac{1}{\gamma_{bottom}} \left(\frac{\frac{1}{\gamma_{bottom}^m} - 1}{\frac{1}{\gamma_{bottom}} - 1} \right) + 1}{\frac{1}{\gamma_{bottom}} \left(\frac{\frac{1}{\gamma_{bottom}^m} - 1}{\frac{1}{\gamma_{bottom}} - 1} \right)} x_{r,m+1} - \frac{1}{\frac{1}{\gamma_{bottom}} \left(\frac{\frac{1}{\gamma_{bottom}^m} - 1}{\frac{1}{\gamma_{bottom}} - 1} \right)} x_{r,bottom} \quad (7.11)$$

with

$$\gamma_{bottom} = \frac{1 - \theta_{bottom}}{\theta_{bottom}} \text{ for all stage } m \quad (7.12)$$

The dynamic characteristic of both top and bottom operating lines for membrane cascades distinguishes this method from the original McCabe-Thiele method for distillation. In distillation, a single line exists for every section. All stages are built up using these lines. In addition, the graphical method for membrane cascades does not use a q-line that represents the state of the feed stream. Instead, the stage cut at both sections should be chosen in such a way that the concentrations at the end of both sections match.

In the distillation column, an equimolar exchange between the liquid and vapor exists in each stage. Therefore, the inter-stage flows can be maintained constant. This condition can be represented by a single operating line for each section. To ensure that this condition occurs in every stage, the distillation column requires a reflux from the top stage and a reboiler at the bottom. These conditions do not exist in the membrane cascade, which gradually creates flow along the cascade stages. This condition explains the dynamic behavior of the operating lines as derived in the work of Avgidou et al. [138].

7.2.3 Overall system cut and total area

Referring to the work of Avgidou et al., the ratio between the permeate stream coming to the top section and the outlet permeate stream can be expressed with Eq. (7.13). To simplify the calculations, this parameter can be defined as the volume reduction at the top section, VR_{top} . The expression for the retentate leaving this section can then be expressed in Eq. (7.14).

$$VR_{top} = \frac{F_{p,n+1}}{F_{p,top}} = \left(\frac{1}{\theta_{top}} - 1 \right) \left[\frac{\left(\frac{1}{\theta_{top}} - 1 \right)^n - 1}{\frac{1}{\theta_{top}} - 2} \right] + 1 \quad (7.13)$$

$$F_{r,n} = (VR_{top} - 1) F_{p,top} \quad (7.14)$$

Similarly, the ratio of the retentate stream coming to the bottom section and the outlet retentate can be defined as the volume reduction at the bottom section, VR_{bottom} , and is expressed in equation (7.15).

$$VR_{bottom} = \frac{F_{r,m+1}}{F_{r,bottom}} = \left(\frac{\theta_{bottom}}{1 - \theta_{bottom}} \right) \left[\frac{\left(\frac{\theta_{bottom}}{1 - \theta_{bottom}} \right)^m - 1}{\left(\frac{\theta_{bottom}}{1 - \theta_{bottom}} \right) - 1} \right] + 1 \quad (7.15)$$

At the upper stage of the bottom section, where the feed stream enters, the retentate coming from the top section is mixed with the feed stream. Therefore the stream coming to the bottom section can be expressed with Eq. (7.16).

$$F_{r,m+1} = F_{r,n} + F_{feed} \quad (7.16)$$

By rearranging Eqs. (7.14), (7.15) and (7.16), we can calculate the overall system cut, which is defined as the ratio of the permeate stream coming out of the top section to the feed stream (Eq. (7.17)).

$$\theta_{all} = \frac{F_{p,top}}{F_{feed}} = \frac{VR_{bottom} - 1}{VR_{top} + VR_{bottom} - 1} \quad (7.17)$$

With a given feed stream as the basis of the design and the chosen stage cut as the design parameter, we can calculate all streams in the cascade. These include the 2 outlet streams from both the top and bottom sections and the inter-stage stream coming from and to 2 adjacent stages. With known permeate flow in each stage, we can calculate the required area, A_{stage} , by dividing it with its standard flux, J_v . The standard flux for each membrane is normally characterized under certain operating conditions (TMP and temperature). Therefore, the total area required for a design can be formulated as the sum of the total area in the top section (with n stage) and the bottom section (with m stage) (Eq. (7.19)).

$$A_{stage} = \frac{F_{p,stage}}{J_v(TMP, T)} \quad (7.18)$$

$$A_{total} = \sum_{i=1}^n A_i + \sum_{j=1}^m A_j \quad (7.19)$$

7.3 Methods and calculations

7.3.1 Filtration set up

The McCabe-Thiele method adopted here was applied to the design of an inhomogeneous nanofiltration cascade to purify a FOS mixture with a molecular weight distribution. The FOS mixture was prepared by diluting 5 wt% of Frutalose L85 (kindly provided by Sensus, Roosendaal, the Netherlands) with demineralized water. For the design, the mixture was considered as a binary mixture of sugars and FOS. The sugars comprise mono- and disaccharides and FOS comprises the oligosaccharides with DP of 3 and higher.

The feed entered the cascade with a flow rate, F_{feed} , of 50 kg/h and mass fraction, x_{feed} , of 0.78. Details on the feed conditions are summarized in Table 7.1

Table 7.1. Feed condition for designing an inhomogeneous nanofiltration cascade for FOS purification

Parameter	Notation	Unit	Values ^a
Sugar concentration	$c_{\text{feed,sugar}}$	g/L	9.04 ± 0.16
FOS concentration	$c_{\text{feed,FOS}}$	g/L	31.49 ± 0.47
Feed mass fraction (FOS)	x_{feed}		0.78 ± 0.01
Feed flow rate (design)	F_{feed}	kg/h	50

^aUncertainties were calculated based on the 95% confidence interval.

The design considers 3 different types of nanofiltration membranes, namely GE with molecular weight cutoff (MWCO) of 1 kDa, GH with MWCO of 2.5 kDa and GK membrane with MWCO of 3.5 kDa. All membranes are commercial membranes from General Electric (GE Osmonic, Sterlitech, Kent, WA, USA). Although the module size was not fixed in this design, the membrane properties are assumed to be similar. The 3 membranes have been characterized in the previous study [126] between TMP 4 – 16 bar and operating temperature between 25 – 45°C. The rejection and flux of all 3 membranes within the scope can therefore be predicted using a model.

7.3.2 Design method

We adopted a non-ideal cascade with a constant operating parameter for each section. The design and operating parameters, which included the membrane, TMP, temperature and stage cut, were chosen independently for each section. The design process started with the top section and continued with the bottom one.

In this study, a standard target (design A) was chosen arbitrarily as 0.2 at the top, $x_{p,top}$, and 0.9 at the bottom, $x_{r,bottom}$. These values are equivalent with 90% purity of FOS at the bottom and 80% purity of sugars at the top. We also discuss other target concentrations to demonstrate the effect of changing these targets in the design. The feed concentration, x_{feed} , and both targets can be indicated on the diagonal line in the McCabe-Thiele plot.

The partitioning curve was plotted using Eqs. (7.2) – (7.6). For this we need the rejection coefficients for both sugars and FOS as well as the stage cut. The rejection coefficient was calculated via a model [126] with a selected membrane type, TMP and temperature. The stage cut for the top section, θ_{top} , can be chosen arbitrarily as long as it does not exceed its maximum value. A larger stage cut implies more stages; a small stage cut implies larger volumes between each stage and therefore more membrane area. At the maximum value of the stage cut, the required number of stages at the top section becomes infinite. In the McCabe-Thiele plot, this is illustrated by the operating line that passes through the partitioning curve with the retentate concentration similar to the feed. At this point, the permeate concentration can be calculated using Eq. (7.2). The maximum stage cut theoretically gives an infinite number of stages, thus the stage number, n , in Eq. (7.8) should be infinite. Computationally, this number can be approached with an arbitrarily large number (e.g. 50). With known x_r , x_p and n , Eq. (7.8) becomes an equation with just 1 variable, θ_{top} . Solving this equation, which is a basic root finding algorithm, will give the value of maximum θ_{top} .

Using a stage cut larger than the maximum will create a design that cannot meet the bottom section. A stage cut of 0 means a minimum number of stages, but an infinitely large membrane area, because all retentates and permeates are fed back into the system (comparable to 100% reflux in distillation). Thus, we need to make a reasonable choice in between these 2 extremes. We here select a θ_{top} of 75% from its maximum.

With this value, we could plot the operating lines at the top section using Eq. (7.8). The partitioning curve, the feed and target points and the operating lines are illustrated in Figure 7.2.

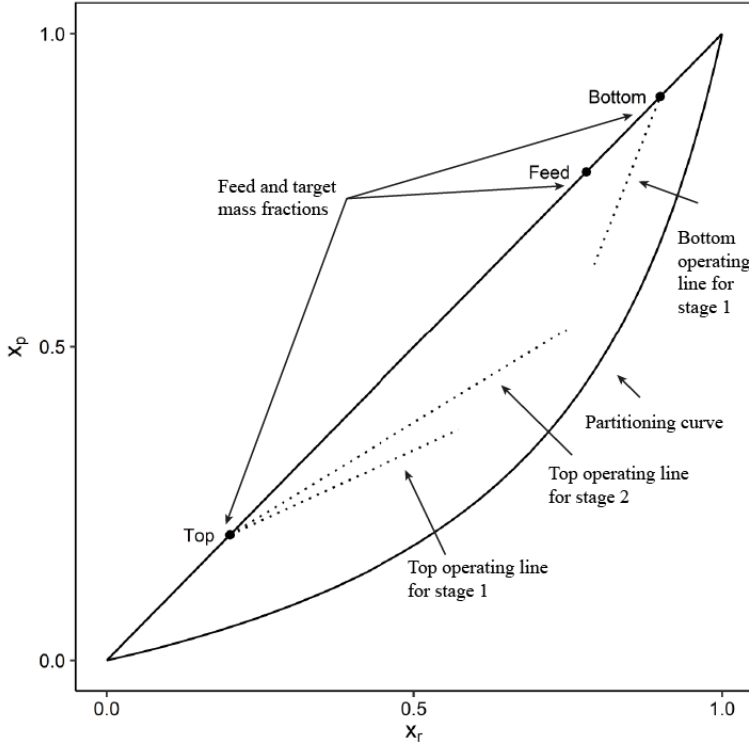


Figure 7.2. Illustration of partitioning curves, operating lines and feed and target points in the McCabe-Thiele diagram

Once the partitioning curve and the operating lines are constructed, we can start building the stages. The concentrations of the permeate streams of any stage are represented by the partitioning curve. The inlet concentration is related to the outlet concentration via the operating lines. Therefore, the stages can be built up with alternating horizontal and vertical lines going from and to both the partitioning curve and the operating lines. The target at the top section comes out of the first stage at the permeate side concentration of $x_{p,top}$. To draw the first stage in the McCabe-Thiele diagram, we draw a horizontal line from the top target point toward the partitioning curve. A line is then drawn vertically toward the operating line. This procedure is repeated until the end of the top section. The end of the top section is indicated by a retentate concentration, $x_{r,n}$, which exceeds the

feed concentration, x_{feed} . Building up the stages in the top stages is illustrated in Figure 7.3.

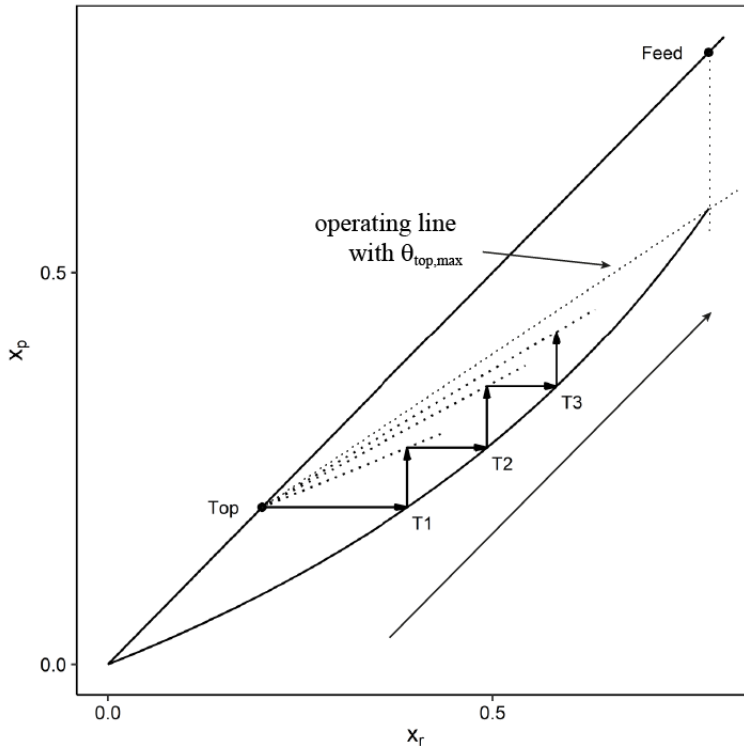


Figure 7.3. Illustration of stage build up in the top section in the McCabe – Thiele diagram for membrane cascade

Designing the bottom section is done similarly. From the bottom target, we draw the vertical line to the partitioning curve and then draw a line vertically to the operating curve. This procedure was repeated until it met the end of the top section.

A challenge in designing the bottom section is that the stage cut must be chosen such that the end point of the bottom section exactly meets the end point of the top section. This meeting point could be after any number of stages. As a consequence, an iterative procedure is required in designing the bottom section by changing the stage cut value until the end point matches the top section. To aid the calculation, the iteration was done between 2 extreme stage cuts: the minimum and maximum stage cut. The minimum stage cut would cause an infinite number of stages in the design. This condition was illustrated with the operating lines that intersect the end of top section. The maximum stage cut was

the stage cut at which the operating line caused only 1 stage at the bottom. The bottom stage must have at least 1 stage: the feed stage. The illustration of building up the bottom section is presented in Figure 7.4.

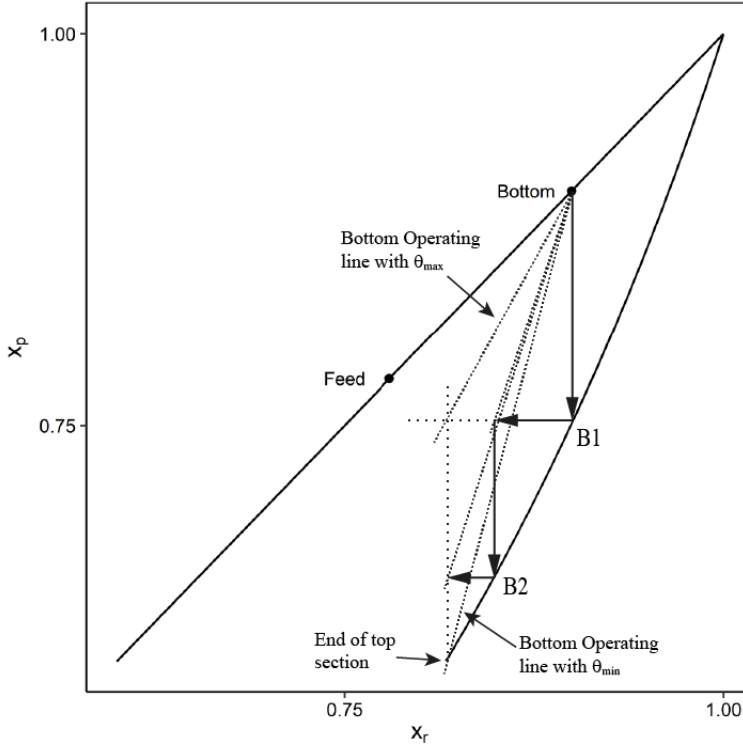


Figure 7.4. Illustration of stage build up in the bottom section in the McCabe – Thiele diagram for membrane cascade

After designing the bottom section, we calculate the overall system cut, θ_{all} . Using this parameter, we can then calculate both outlet flows and the inter-stage flows. This then lets us calculate the area for every stage and for the total system. This concludes the design procedure. A summary of the design procedure for a membrane cascade system using the McCabe – Thiele method is shown in Figure 7.5.

Here, we demonstrate the use of the design procedure by evaluating 11 designs with differing operating conditions and targets. Design A was chosen as reference, which uses only GH membranes operated at 16 bar and 45°C. This design was constructed to reach a bottom target, $x_{r,bottom}$, of 0.9 and a top target, $x_{p,top}$, of 0.2. Designs B to E use a similar configuration as design A to attain different targets. Design F uses a similar configuration

as design A, but using GE membranes; design G uses GK membranes. These 7 designs are all based on a uniform design in which the type of membrane and operating conditions are the same at all stages in the cascade. In addition, we also evaluated hybrid, inhomogeneous designs (H–K) with various combinations of membrane, TMP and temperature at the top and bottom sections. Details of all 11 designs are shown in Table 7.2.

Table 7.2. Operating conditions for the 11 designs evaluated in this study

Parameter	Design											
	Unit	A	B	C	D	E	F	G	H	I	J	K
Target (Mass Fraction)	Top	0.2	0.1	0.3	0.2	0.2	0.2	0.2	0.2	0.2	0.2	0.2
	Bottom	0.9	0.9	0.9	0.85	0.95	0.9	0.9	0.9	0.9	0.9	0.9
Operating Condition (Top)	Membrane	GH	GH	GH	GH	GH	GE	GK	GH	GE	GH	GE
	TMP	bar	16	16	16	16	16	16	16	16	6	16
	Temperature	°C	45	45	45	45	45	45	45	45	25	25
Operating Condition (Bottom)	Membrane	GH	GH	GH	GH	GH	GE	GK	GK	GH	GK	GK
	TMP	bar	16	16	16	16	16	16	16	12	10	4
	Temperature	°C	45	45	45	45	45	45	45	25	45	25

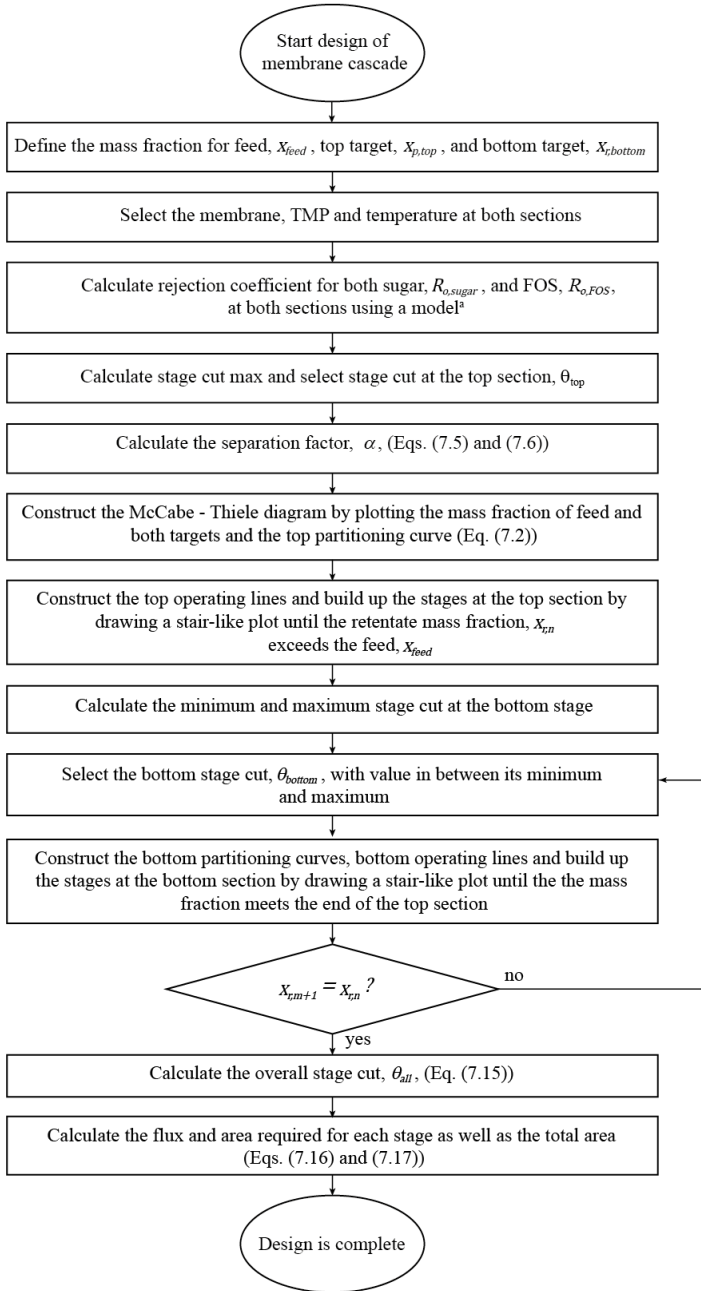


Figure 7.5. Flowchart of the design procedure for the membrane cascade using the McCabe-Thiele method.

^a The rejections were predicted using a model developed in a previous work [126]

7.4 Results and discussion

7.4.1 Effect of various operating conditions

7.4.1.1 Partitioning curves for different membranes, TMPs and temperatures

The partitioning curves were drawn for the 3 membranes considered in this study. The membranes vary in their MWCO, which affects their separation factor, α . A higher separation factor indicates better separation, implying less stages are required for a separation. In the McCabe-Thiele diagram, this is indicated by a partitioning curve that is situated farther away from the diagonal parity line. The minimum stage requirement is a theoretical number of stages needed in the cascade to achieve the separation target. This represents a system in which the product streams fully re-enter the system as reflux, and an infinite membrane area is needed. This was obtained by building up the stages as explained in Section 7.3.2. Instead of the operating lines, the diagonal line was used. The diagonal line is theoretically the operating line at stage cut 0. That means, all streams goes to the retentate and no top product is acquired; this extreme condition does not exist in practice, of course.

7

Figure 7.6 shows the partitioning curves and illustrates the minimum stage requirement for the 3 membranes. We can see that the GE membrane has the widest partitioning curve and the GK membrane has the narrowest. The partitioning curve for both GE and GH were close to each other and both membranes require the same minimum number of stages. However, the GE membrane has a lower flux than the GH membrane, which results in a larger membrane surface area requirement.

The curvature of the partitioning curve is dependent on the operating conditions, because these affect the rejection coefficient. A higher rejection can be achieved at a higher TMP and a lower temperature. However, we found the opposite effect of the TMP in the partitioning curve. In fact, a wider curve was found at lower TMP (Figure 7.7), indicating better separation at lower TMP. The temperature effect in the partitioning curve was as expected, giving a wider curve at lower temperatures.

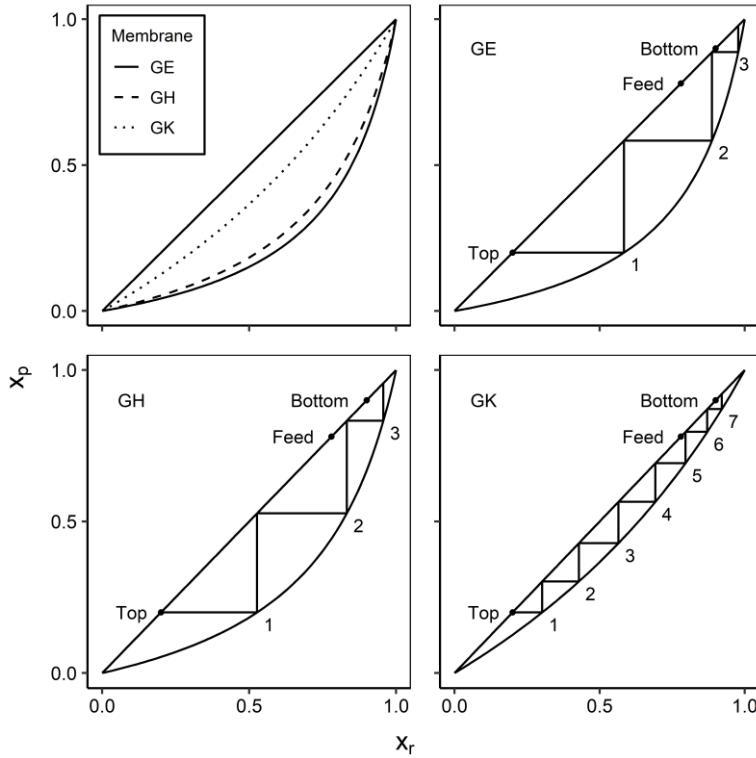


Figure 7.6. Partitioning curve and minimum stage for GE, GH and GK membranes using TMP of 16 bar, temperature of 45°C and stage cut of 0.6.

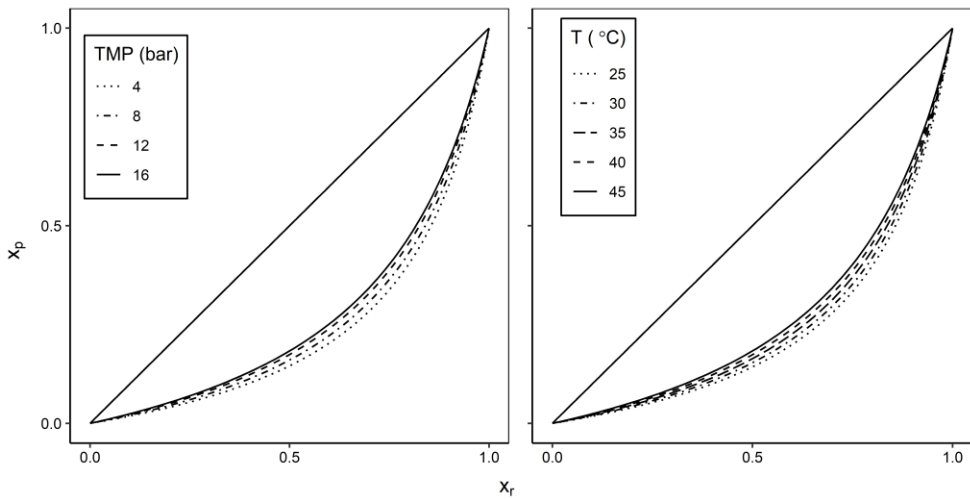


Figure 7.7. Effect of TMP and operating temperature on the partitioning curve of GH membrane using a stage cut of 0.6.

According to Eqs. (7.2) – (7.6), the partitioning curve is not solely dependent on the rejection coefficient. Instead, it is dependent on the separation factor, α , between 2 components of interest. The temperature effect in the rejection is linear [126], therefore we can expect the same effect for the separation factor. The effect of TMP in the rejection is more complex. The TMP affects the convective transport in the nanofiltration system, which is not linear. The effect is more prominent for smaller molecules [37,126]. As a result, the separation between the 2 lumped components was better at low TMP. Figure 7.8 shows contour plots for the separation factor, α , as a function of TMP and operating temperature, for all 3 membranes. A combination of a low TMP and a low temperature gives a low α , and thus a wider partitioning curve. Referring to Figure 7.8, we can select a combination of TMP, temperature and membrane that gives a certain value of α ; any system that is on the same contour line would give the same partitioning curve. This figure also shows that GE and GH membranes have an overlapping operating window with similar separation.

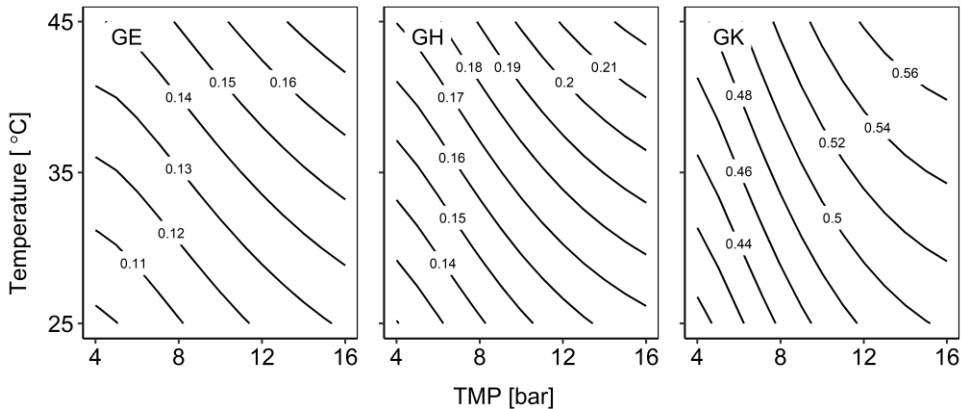


Figure 7.8. Contour plot of the separation factor, α , as function of the TMP and the operating temperature for the three membranes.

7.4.1.2 Partitioning curves and operating lines with various stage cuts

In addition to the selection of the type of membrane and the operating conditions, the value of the stage cut affects both the partitioning curve and the operating lines. However, its effect on the operating lines is stronger (Figure 7.9). The partitioning curve relates the concentrations in the permeate and retentate for each stage, calculated from the real rejection coefficient, which is independent of the flow rates. The partitioning curve is constructed with the observed rejection, which deviates from the real rejection due to

Design of nanofiltration cascades using the McCabe-Thiele approach concentration polarization. However, we found that this is not a strong deviation. The flow conditions, defined by the stage cut, affected the partitioning curve only slightly.

The slopes of the operating lines become smaller at a larger stage cut. However, this works out differently for the 2 sections. For the top section, a lower slope means the operating line is situated further from the diagonal line. As a result, the number of stages required increases. On the other hand, a lower slope for bottom operating lines brings the line closer to the diagonal line and thus requires less stages in this section. To complete the design, the values of the stage cuts at both sections need to be selected such that both intersect as closely as possible to the feed composition. This implies that very high or low values of both stage cuts are not possible, because this would construct a design of both sections that would not meet each other.

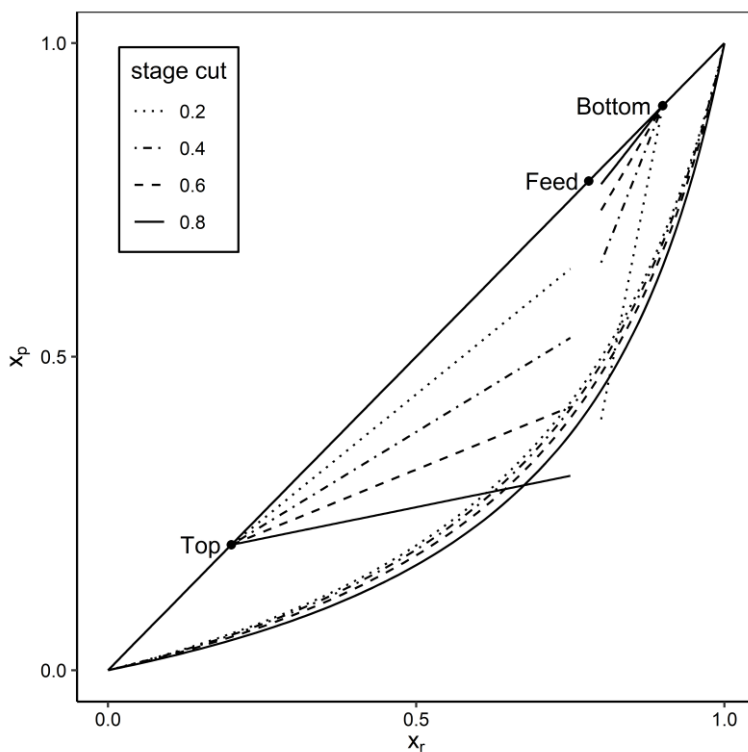


Figure 7.9. Effect of the stage cut on the partitioning curve and the operating lines for the GH membrane using TMP of 16 bar and temperature of 45°C (design A).

As expressed in Eqs. (7.7) – (7.10), the slopes of the operating lines change at every stage. The slopes increase for the top operating lines and decrease for the bottom ones; thus, the

lines for the subsequent stages are closer to the diagonal line. However, this does not change the fact that the value of the chosen stage cut affects the slope of the operating line (represented by the first stage); and it still necessitates the choice of a moderate stage cut value for both top and bottom sections.

We start from the top section downward, therefore we select the top stage cut at the start of the design. The stage cut at the bottom section will be adjusted to meet this selection. In view of the computational requirements, this method is better than adjusting both stage cuts at the same time. Here, we chose a top stage cut of 75% of its maximum. This value of 75% was chosen arbitrarily. The choice affects the number of stages and the membrane surface area required, and determines the stage cut for the bottom, which again influences the number of stages and the membrane surface area needed in that section.

Figure 7.10 shows the effect of the stage cut on the required area for both sections. The stage cut at the top is θ_{top} , and the bottom stage cut, θ_{bottom} , is adjusted to meet this. The maximum value of θ_{top} was calculated by solving the operating line equation that crosses the partitioning curve with a retentate concentration similar to the feed. The minimum value was found computationally because no values below this minimum converged into a design with an adjusted θ_{bottom} . For GH membranes with TMP of 16 bar and temperature of 45°C, the maximum top stage cut was 0.716 and the minimum was 0.35.

Figure 7.10.a shows that the required area increased with increasing stage cut. This applied for both sections. This was as expected, because a larger stage cut implies a higher permeate flow and thus a larger area was needed, given a fixed flux at certain operating conditions. The difference between both sections was that the stage cut at the top could be chosen, whereas the bottom stage cut followed from the chosen stage cut at the top. The values of θ_{bottom} varied somewhat within the selected values of θ_{top} , yet were all within a close range. Figure 7.10.c shows that the design had a short bottom section and a longer top section, because the concentration difference between the bottom target and the feed is far less than the difference between the top target and the feed.

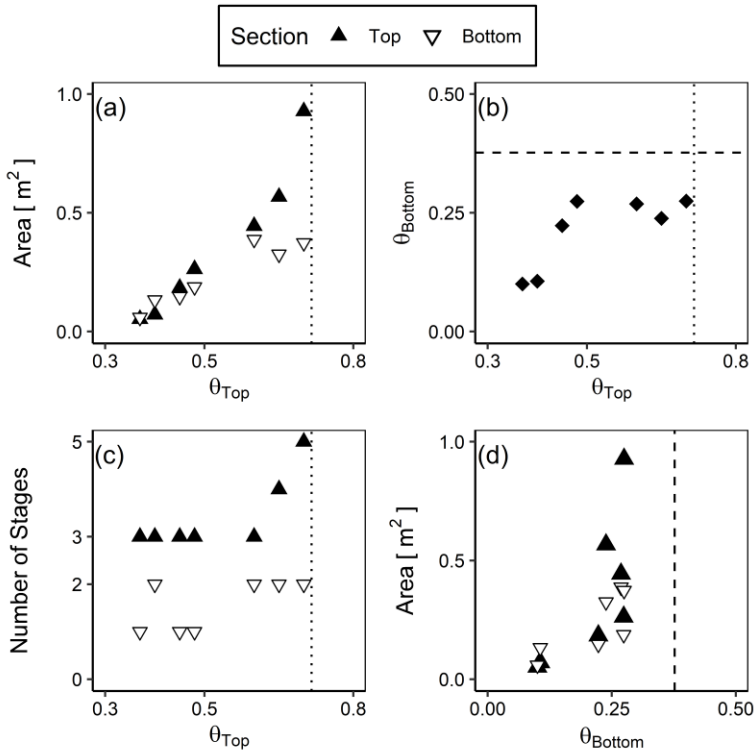


Figure 7.10. Effect of the stage cut on the required area in both sections for the GH membrane operated with TMP of 16 bar and temperature of 45°C (design A). The dotted line shows the maximum stage cut at the top section. The dashed line shows the maximum stage cut at the bottom section.

As the design delivers a discrete value of the number of stages, it is logical that there are discontinuities in the required membrane surface area, and it also allows some freedom in the design resulting in the occasional selection of one more or less stage .

7.4.2 Design of the cascades

In this section, we demonstrate the design for the cascade using a uniform setup for the whole cascade. The membrane selection, the TMP and operating temperature were the same for each stage. The stage cut was constant for each section with a different value for top and bottom, so that the design meets at the feed.

Figure 7.11 shows the McCabe-Thiele diagram for a 3+2 stage cascade for the reference design (A). The top stage cut maximum for this setup was found to be 0.71, therefore the design θ_{top} was set to 0.54. With this value, the stage cut for the bottom stage was found

to be 0.22. Figure 7.11 shows that this results in slightly different partitioning curves for the top and bottom sections (see Eqs. (7.5) and (7.6)).

The design consists of 3 stages in the top section and 2 stages in the bottom section, thus 5 stages in total. Therefore, we see 4 operating lines in the design that relate the compositions between adjacent stages. As a convention, we determine that the feed enters the last stage of the bottom section, represented here as stage B2. This stage was also operated with the stage cut of the bottom section, and thus connects with the bottom operating line.

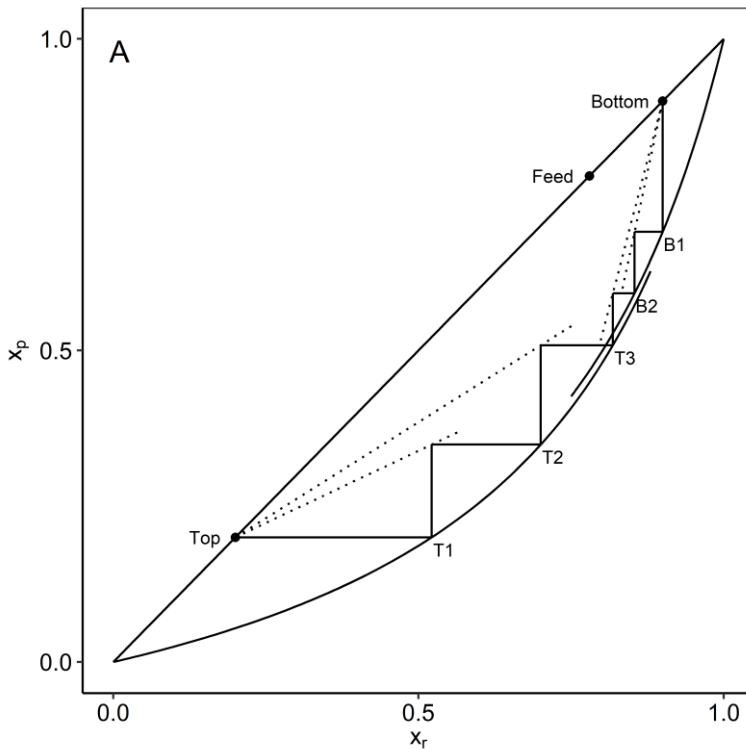


Figure 7.11. McCabe-Thiele diagram of the 5-stage design of the fractionation cascade using GH membrane with TMP of 16 bar and temperature of 45°C (design A). See Tables 2 and A.1 for further details.

Setting a different separation target requires recalculation and may result in a different design. Figure 7.12 (top side) shows the designs of the cascade with top targets of 0.1 (B) and 0.3 (C). Compared with the reference (Figure 7.11), design B was stretched toward the top section and required more stages. Design C had a similar number of required

stages yet with a more compact design. From Figure 7.12 and Figure 7.11, we can also see that the bottom design for all 3 designs was different despite the similar bottom target. The stretch and compaction of the design can also be seen for designs D and E with different bottom targets. In this case, the design for the top section did not change.

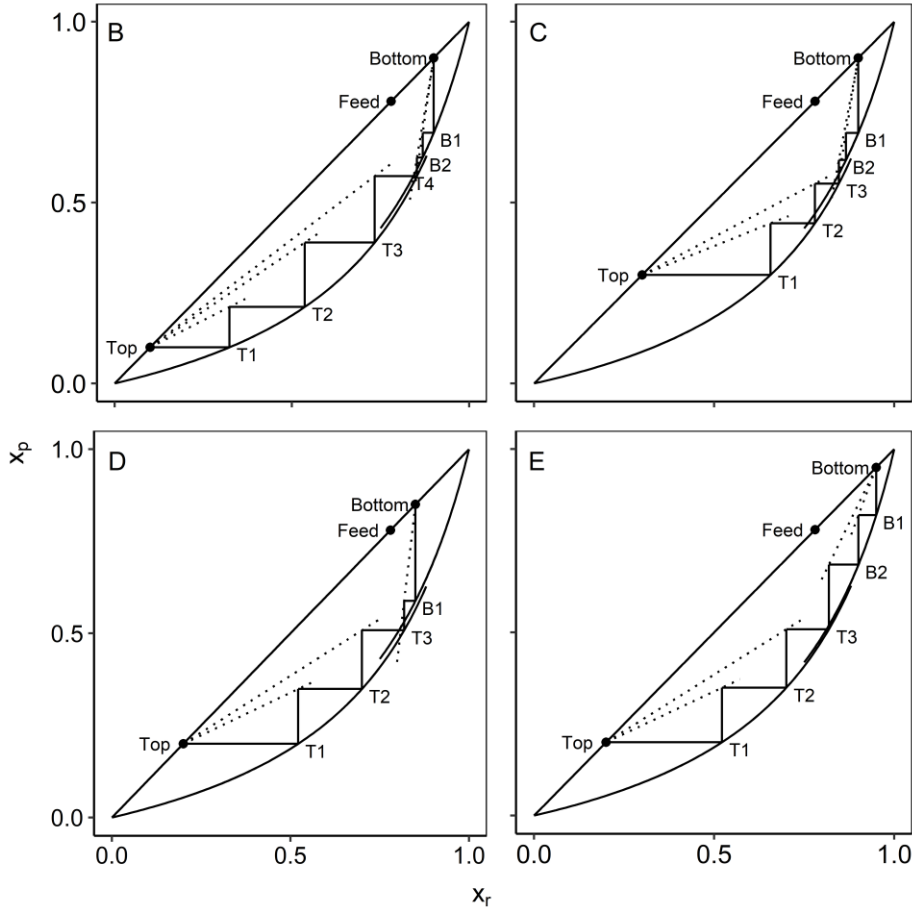


Figure 7.12. McCabe-Thiele diagram of the membrane cascade design with various targets using the GH membrane operated with TMP of 16 bar and temperature of 45°C. Top side shows a top target, $x_{p,top}$, of 0.1 (design B) and 0.3 (design C) with a bottom target, $x_{r,bottom}$, of 0.9. The bottom side shows a bottom target, $x_{r,bottom}$, of 0.85 (design D) and 0.95 (design E) with a top target, $x_{p,top}$, of 0.2.

Changing the top target to design B or C required a complete recalculation for both sections, whereas changing the bottom target to design D or E only affected the design at the bottom. The change in the top target affected the slope of the operating line that passed through the feed concentration at the partitioning curve and thus affected $\theta_{top,max}$.

As a consequence, the operating θ_{top} also changed. Setting the stage cut constant was possible in principle; the choice of using 75% $\theta_{\text{top,max}}$ was arbitrary. However, the value must still be clearly lower than its maximum. In addition, a constant stage cut will still imply different slopes for different top targets, because the operating lines pivot on the target point (Eq. (7.12)). As a consequence, the design of the bottom section would also change despite having no change in the bottom target. In the other case, changing the bottom target would only affect the design at the bottom because there is no change at the top section.

A similar design procedure could be applied with other membranes resulting in a 3+2 stage design with GE membranes and a 7+2 stage design with GK membranes (Figure 7.A.1). The designs follow our expectations considering the shape of their partitioning curves (Figure 7.6).

The required membrane area per stage for GH, GE and GK cascades (designs A, F and G) is shown in Figure 7.13. The required areas for GH and GE are in the same range, whereas the required area for the GK membrane cascade is much higher. Both GE and GH membrane cascades require the same number of stages at both sections. The GE membrane has a lower flux and as a result, the area requirement was slightly higher compared with the GH membrane cascade (Figure 7.13). The GK membrane has a higher flux than the other 2 membranes, which would suggest the requirement of less area. In fact, the design with the GK membranes required significantly more membrane area than the other 2 membranes. The reason for this is the large number of stages. The whole section was operated with a fixed stage cut, therefore, it is logical that the membrane near the feed processes a larger flow rate thus require a larger area. The more stages are required in a section, the more this flow accumulates, resulting in a much larger required area. Figure 7.13 illustrates the area distribution among stages in the cascades. This result also supports a previous study on the inhomogeneous cascades, which reported a larger area requirement at the feed stage [25].

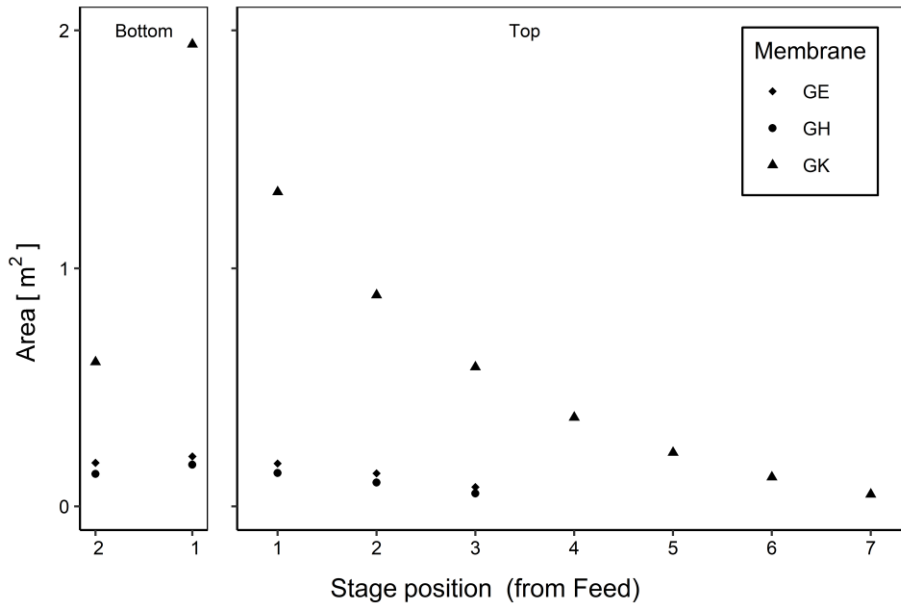


Figure 7.13. Area distribution among the stages in the design of membrane cascades using GE, GH and GK membranes operated at 16 bar and 45°C (designs F, A and G).

7.4.3 Hybrid design of the cascades

The design procedure suggests that we use different values for the stage cut for both sections such that the design meets at the feed. As a consequence, the partitioning curves for the 2 sections are not the same. However, the difference was small due to the small effect of the stage cut on the partitioning curve (section 7.4.1.2). Nevertheless, this does show that working with different partitioning curves for both sections is possible. In this case, one can also achieve that by using different membranes. This will indeed result in a larger difference in the partitioning curves for top and bottom. Apart from the choice of membrane and the stage cut, the operating TMP and temperature affect the partitioning curve and may be used to tune the curve.

In Figure 7.14, we demonstrate 4 hybrid designs (designs H–K) using arbitrarily chosen combinations of setup conditions at the top and bottom sections. All designs were constructed to reach a $x_{p,top}$ of 0.2 and a $x_{r,bottom}$ of 0.9. Constant conditions (membrane, TMP, temperature and stage cut) were applied for all stages within a particular section. The selection of the design variables for these designs is shown in Table 7.2. The details of these designs are provided in Table 7.A.1.

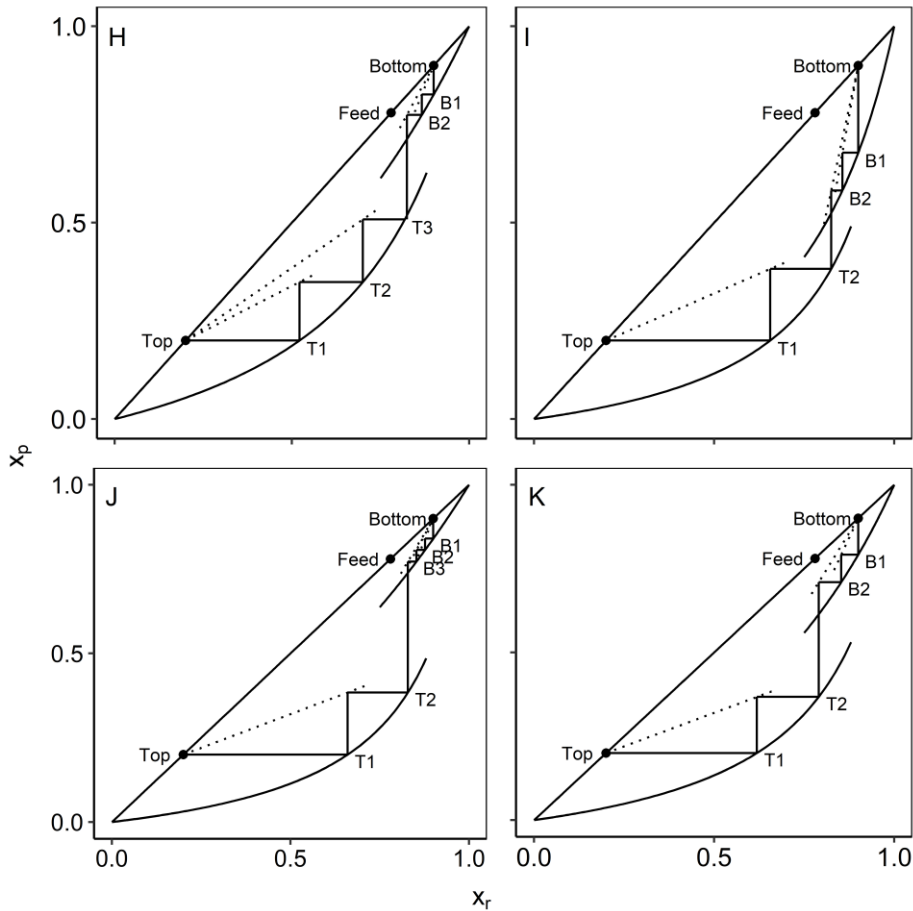


Figure 7.14. McCabe-Thiele diagram for selected hybrid membrane cascade designs. For the design decisions, refer to Table 7.2

Unlike the previous studies on membrane cascades, the target in the design using the McCabe-Thiele method is not achieving a certain purity, because this is a constraint imposed on all designs. The design procedure in fact helps to minimize the number of stages, the membrane area requirement, and to maximize the yield of a specific product (either top or bottom). Using a hybrid design may help achieve these targets, because the stage requirement at the bottom was not really affected by the choice of membranes and the top design is more compact using GE or GH membranes. On the other hand, using GK membranes at a similar number of stages may reduce the surface area requirement, because this membrane features a larger flux. However, a lower number of stages does not guarantee a lower total membrane surface area requirement.

The total area requirement is closely related to the overall system cut. This parameter is dependent on the stage cut at both sections (Eqs. (7.15) – (7.19)). We can see a clear relationship between the stage cut at the top with the membrane, the TMP and the temperature. However, the relationship of those operating conditions with the bottom stage cut was unclear, because it was determined iteratively such that the operating lines crossed at composition of the feed. One critical issue that was found during the design is that the chance of finding a converged iteration (in order to find the bottom stage cut) was less when the difference between 2 partitioning curves was large. This was the case, for example, with design J (Figure 7.14), which had small separation steps at the bottom section. At the same time, finding the minimum amount of membrane surface area may require balancing all the different parameters, for which a numerical procedure would probably be preferred. Therefore, further development is needed to make the method more robust for numerical evaluation.

7.5 Conclusions

We developed a method to design an inhomogeneous membrane cascade to purify a FOS mixture by adapting the classic McCabe-Thiele approach for distillation. The method determines the number of stages needed and the required membrane surface area in the cascade to achieve specific target compositions for both products: small mono- and disaccharides and larger oligosaccharides. As an independent design parameter, the stage cut should be defined before the design procedure.

The procedure starts from the top section followed by the bottom section. The membrane selection, TMP, temperature and stage cut in any stage within 1 section are uniform. Nevertheless, the method allows us to use different combinations of membranes and operating conditions in both sections (hybrid design).

Apart from the selection of the membranes, TMP and temperature, the stage cut value strongly determines the required number of stages and the total membrane surface area of the cascades. The lower the overall stage cut, the larger the internal recycle is and the larger the membrane surface area is for a given feed volume. The overall system cut depends on the stage cuts of the top and bottom sections, which were determined separately. The value of the bottom stage cut was calculated iteratively to match its design with the that of the top section. However, the relationship between both stage cuts is not trivial and is now found iteratively. To obtain an optimal design using possible

combinations of the available membrane, TMP and temperature, further adaptation toward a robust numerical optimization procedure is important.

Acknowledgements

The authors would like to acknowledge Lembaga Pengelola Dana Pendidikan (LPDP), and Kementerian Keuangan Indonesia for financial support.

Appendix

7.A.1 Supplementary figure and table

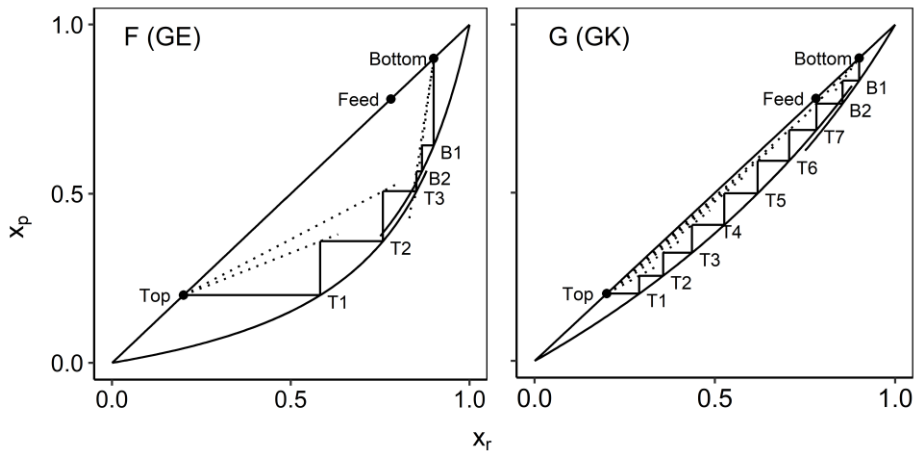


Figure 7.A.1. McCabe-Thiele diagram for membrane cascades using GE (F) and GK (G) membranes operated at 16 bar and 45 °C.

Table 7.A.1. Details of various cascade designs using the McCabe-Thiele approach.

Parameter	Unit	Design													
		A	B	C	D	E	F	G	H	I	J	K			
Target (Mass Fraction)		0.2	0.1	0.3	0.2	0.2	0.2	0.2	0.2	0.2	0.2	0.2	0.2	0.2	0.2
Operating Condition (Top)		0.9	0.9	0.9	0.85	0.95	0.9	0.9	0.9	0.9	0.9	0.9	0.9	0.9	0.9
Operating Condition (Bottom)		GH	GH	GH	GH	GH	GH	GH	GH	GH	GH	GH	GH	GH	GH
Operating Condition (Top)	bar	16	16	16	16	16	16	16	16	16	16	16	16	6	16
Operating Condition (Bottom)	°C	45	45	45	45	45	45	45	45	45	45	45	25	25	35
Operating Condition (Top)		GH	GH	GH	GH	GH	GH	GH	GH	GH	GH	GH	GH	GH	GH
Operating Condition (Bottom)	bar	16	16	16	16	16	16	16	16	16	16	16	12	10	4
Operating Condition (Bottom)	°C	45	45	45	45	45	45	45	45	45	45	25	45	45	25
stage cut		0.537	0.502	0.600	0.537	0.537	0.583	0.411	0.537	0.600	0.600	0.600	0.600	0.385	0.434
stage cut		0.219	0.150	0.164	0.121	0.379	0.128	0.688	0.453	0.199	0.199	0.385	0.128	0.374	0.391
stage cut	overall	0.100	0.040	0.089	0.041	0.233	0.061	0.155	0.318	0.128	0.128	0.374	0.128	0.374	0.391
Number of stages	Top	3	4	3	3	3	3	7	3	2	2	2	2	2	2
Number of stages	Bottom	2	2	2	1	2	2	2	2	2	2	3	2	3	2
Number of stages	Total	5	6	5	4	5	5	9	5	4	4	5	4	5	4
Area	m ²	0.29	0.22	0.23	0.12	0.69	0.40	3.57	0.94	0.43	0.43	1.55	0.43	1.55	1.29
Area	m ²	0.31	0.20	0.21	0.07	0.66	0.39	2.55	0.58	0.35	0.35	0.95	0.35	0.95	1.87
Area	m ²	0.61	0.41	0.44	0.19	1.35	0.79	6.11	1.51	0.78	0.78	2.50	0.78	2.50	3.16

7.A.2 Derivation of equations based on the work of Lejeune et. al. [135]

The design in the work of Lejeune et al. was developed based on 2 design parameters: the volume reduction ratio (VRR) and the abatement (Ab_c) as defined in Eqs. (A1) and (A2).

$$VRR = \frac{F_f}{F_r} \quad (7.A.1)$$

$$Ab_c = 1 - \frac{c_{p,c}}{c_{f,c}} \quad (7.A.2)$$

The stage cut, θ , is defined in Eq. (7.4). Therefore, the relationship between VRR and θ is expressed in Eq. (A3)

$$\theta = 1 - \frac{1}{VRR} \quad (7.A.3)$$

Lejeune et al., expressed the abatement and the separation factor, α , as functions of VRR and $R_{o,c}$.

$$Ab_c = 1 - \frac{1}{\left(1 - \frac{1}{VRR}\right)} \left[1 - \left(\frac{1}{VRR}\right)^{(1-R_{o,c})} \right] \quad (7.A.4)$$

$$\alpha = \left[\frac{(1 - Ab_B)}{(1 - Ab_A)} \right] \left[\frac{1 - \left(1 - \frac{1}{VRR}\right)(1 - Ab_A)}{1 - \left(1 - \frac{1}{VRR}\right)(1 - Ab_B)} \right] \quad (7.A.5)$$

Substituting equation 7.A.3 into equation 7.A.4 results equation 7.A.6.

$$Ab_c = 1 - \frac{1}{\theta} \left[1 - (1 - \theta)^{(1-R_{o,c})} \right] \quad (7.A.6)$$

Substituting equation 7.A.6 and 7.A.3 into equation 7.A.5 results equation (7.5)

Nomenclature

A area [m^2]

c solute concentration [g L^{-1}]

F	flow rate [kg h ⁻¹]
J_v	volumetric flux [m ³ . m ⁻² s ⁻¹]
R_o	observed rejection [dimensionless]
T	process temperature [K]
TMP	trans membrane pressure [Pa]
VR	section volume reduction [dimensionless]
x	mass fraction [dimensionless]

Greek letters

α	separation factor [dimensionless]
θ	stage cut [dimensionless]

Subscripts

A, B	component
$Top, Bottom$	section indication
m	stage number at the bottom section
n	stage number at the top section
p	permeate side
r	retentate side



8

Chapter 8

General discussion



8.1 Introduction

The study reported in this thesis aimed to develop a rational guideline to design a process system with a nanofiltration cascade as model system. This was done via modelling on 4 levels. At the first level, an understanding of the smallest unit within the system was developed. The outcome of the model in this first level was then used to develop a model at level 2, which is the nanofiltration cascade itself. Using the cascade model that was developed at level 2, an optimization procedure was then developed at level 3. Two main issues related to optimization were discussed: handling multiple objectives and computationally selecting the best set of operating conditions. At level 4, a procedure to design the whole process system was finally developed using information that was developed in the previous levels. This chapter highlights the findings of the previous chapters and uses this for a general design rationale for process systems, which is extrapolated from the nanofiltration cascades that were investigated.

8.2 Main findings

To lay the basis for the design of process systems, the whole range of the operating windows of the individual units needs to be considered. In an inhomogeneous nanofiltration cascade system, the operating window includes several types of membranes operated at a range of TMPs and temperatures. Therefore, a model is required that can predict the performance of a nanofiltration membrane based on a given set of membrane properties, the TMP and temperature. **Chapter 2** describes such a model to predict the performance of a nanofiltration membrane based on the steric pore model (SPM), putting attention on the effect of the temperature. The influence of the temperature is often neglected in membrane separation processes as independent parameter, since no clear explicit relations were available before. The model developed here describes the effect of temperature on three aspects: the molecular thermal expansion of the solute, the decrease of the solution viscosity and the thermal expansion of the membrane. Even though the mechanism is specific for a specific process, these 3 main aspects are relevant for all processes: the behavior of an individual material, the property of the mixture and the behavior of the unit or equipment.

Chapter 3 reports on an interesting experimental observation, that glucose and fructose can be separated with NF in the presence of mixtures of FOS, in spite of their equal molecular weight. It is concluded that the FOS are necessary to separate the

monosaccharides. This implies that certain useful separation phenomena may only happen if we deviate from the ideal condition: under ideal conditions, there is no interaction between the monosaccharides and FOS, and no separation occurs.

With the understanding of a single stage nanofiltration model as basis, a cascade model was developed in **Chapter 4**. This chapter focuses on utilizing the cascade design to simultaneously fractionate a stream into three products by extracting part of the recycle stream. Improvement of the design was performed by the addition of extra stages. As expected this resulted in improved separation, but the stage should be placed carefully depending on the separation target. Adding an extra stage to the top section improves the purity of the small fraction and an extra stage towards the bottom section improves the purity of the large bottom fraction.

Chapter 5 confirms the findings in chapter 4 related to the expansion of the design towards a specific section of the model. Using only 3 stages, the purity of the small fraction can be improved when the design is arranged towards only the top section. The opposite works for the large fraction, where the purity increases with addition to the bottom section. Chapter 5 also addresses the multi criteria issue that occurs in most processes, especially in processes with multiple products. A method was explained to assign the criteria weights. These weights represent a degree of importance for each criterion. With these weights, a new objective, which was a linear sum of each criterion multiplied by its weight, was formed. An evaluation can then be referred to this new objective. In this chapter, also a backward analysis with sensitivity coefficients was performed. This analysis helped to identify which process parameters are critical for the separation. The critical parameters and the criteria weights are configuration dependent. However, a general understanding from this analysis is that the most critical parameters are connected to the feed stage.

Chapter 6 describes a numerical model to select an optimum combination of operating variables within 3-stage nanofiltration cascades. The model optimized the product yield with given purity constraint. By optimizing iteratively with various purity constraints, a frontier curve was constructed to show a window of operation that gives the optimum results. It is again concluded that the feed stage is critical in achieving an optimum performance, as concluded in chapter 5 as well. We can here see that its main role is to maintain a good split towards the next two stages. The separation itself is more critical in the top stage, in which a combination that gives a high rejection is suggested.

With the findings obtained in the previous chapters, a procedure for designing inhomogeneous nanofiltration cascades was developed in **Chapter 7**. Adapting the classical McCabe Thiele method to design a distillation column, allows a non-ideal design that includes different configurations for the top and the bottom sections. Unlike the original McCabe-Thiele method, the design method for a nanofiltration cascade can have different partitioning curves and has multiple operating lines for each section. This procedure gives us new freedom in the system design with an independent set up for each stage, since the operating line is separately evaluated for every stage.

8.3 Design guidelines

Based on the findings from the previous chapters, a guideline for designing a process system is established. The guideline is constructed into seven design phases that will be described in this section. Prior to these steps, a global target should be defined as a basis for designing (Figure 8.1).

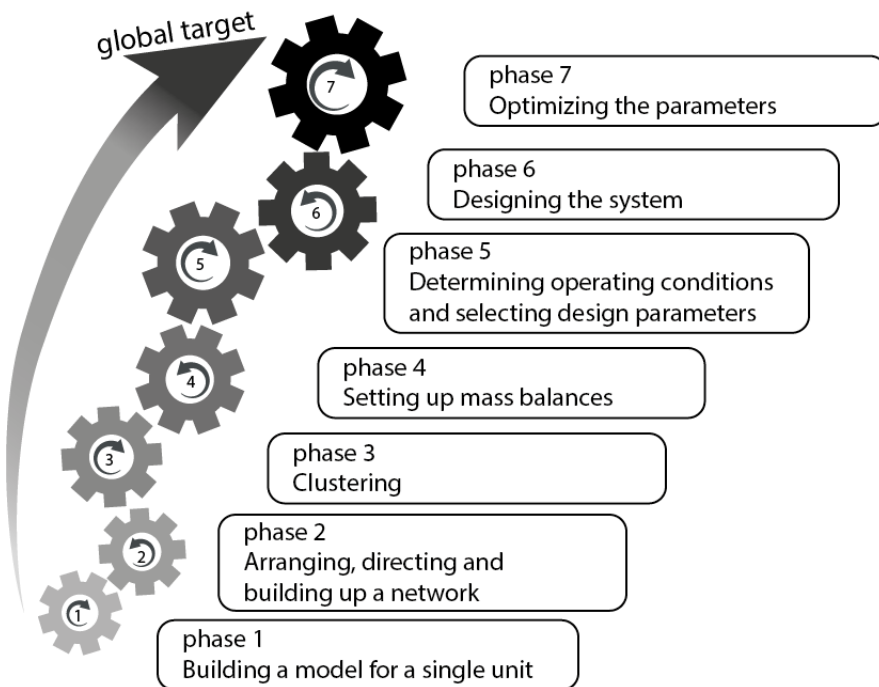


Figure 8.1. Seven design phases of process systems

8.3.1 *Building a model for a single unit*

In order to build a system, the smallest building blocks need to be defined. A model that describes these building blocks is required such that the outcomes of each block at the given conditions can be predicted. Within a block or process unit, a model is required that describes the individual material, the mixture and the equipment. Combining these aspects with a model that describes the phenomena in the process unit, an outcome of a process unit can be predicted. This outcome is necessary to build a larger system.

Development of such a model can be done in between two extreme approaches: a full mechanistic approach and a black box approach [139] In chapter 2, a mechanistic model was developed. Such a mechanistic model requires a good understanding about the phenomena happening inside the unit. It often considers many parameters either implicitly or explicitly already. Adaptation of the model is relatively easy based on understanding. However, developing a mechanistic model that fundamentally explains the phenomena needs a lot of investment in work, expertise and time. Developing an empirical model is faster. This model is usually built up by collecting experimental data at various conditions. Correlations between variables are then determined and used to build a set of correlations that connects the independent (input) parameters to the dependent (output) parameters. However, an empirical model cannot be used outside of its validated parameter space and is not flexible to include an extra parameter in the model or extend it to a wider range of operation (e.g. a lower or higher temperature). For such conditions, the model needs to be redeveloped by collecting experimental data from scratch. Considering the benefits and disadvantages of both models, a model that is at least partially mechanistic is preferable for a process that has been well defined. For a relatively new and unknown process, an empirical model would be sufficient.

While moving forward to the next step in designing a process system, the models on this level may be simplified to reduce the complexity in the model on the next level. One should keep in mind however that every simplification will have an effect at the next level, as was demonstrated in chapter 4, 5 and 6. By using a mechanistic model, we are free to choose the level of complexity of the model that will be used at the next level. An empirical model does not have this freedom.

8.3.2 *Arranging, directing and building up a network*

After defining the single unit in the system, we need to start building up the system itself. In this phase, we need to arrange the units and give the system a configuration. Arranging the units is simply putting one unit after another. Those units are then connected to each other, as demonstrated in chapter 5. Some streams may be recycled to the previous unit, which is a signature characteristic of a membrane cascade, and of any system in which recycling is used to amplify the resolution of the process.

A process system can be focused on one main product. This main product is commonly created together with a waste stream or a side product. This waste or the side product does not get priority in processing, therefore less or no units are placed towards further refining this stream.

Nowadays, having two valuable products instead of one valuable product and a low-value waste stream, is common practice in processing (e.g. distillation, extraction, membrane separation). A strategy to operate these processes is to have at least three units: first to split the stream, followed by two units to refine each product stream. Increasing the number of products requires a different strategy. Chapter 4 and 5 demonstrate a route to improve the cascade design while simultaneously obtaining three products. While the design successfully refined the small and large product, the process did not yield a desirable middle product. This is simply because there was no unit assigned to refine the middle product. This can be overcome by creating a larger system (superstructure) consisting of sequential separation units [140,141]. This superstructure then requires at least two splitting units and three refining units.

In conclusion, more products require more units in a process system. An illustration of arranging and directing individual units in a process system is shown in Figure 8.2.

8.3.3 *Clustering*

In this phase of design we need to divide the system into several clusters. A cluster contains repeating units with similar function that are operated with similar design parameters and operating variables. This cluster can then be treated as a larger unit that can be represented by a single model or mass balance.

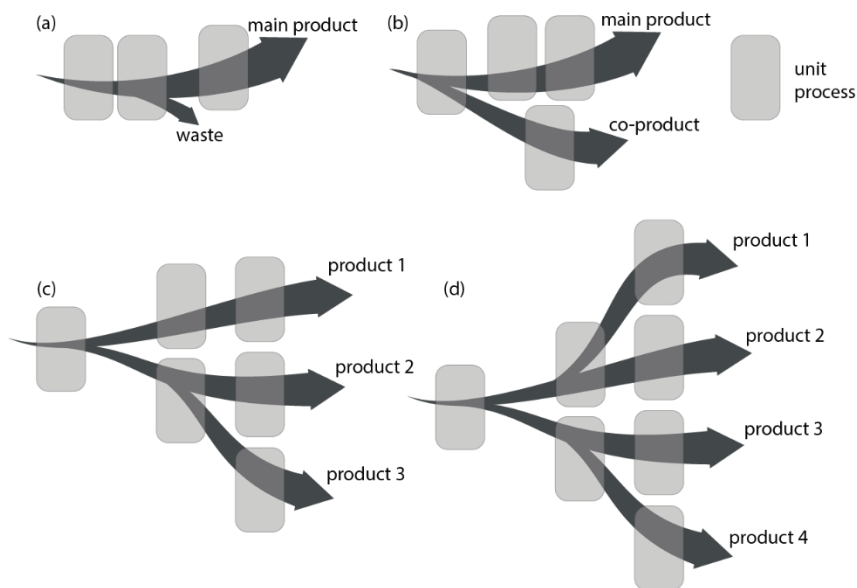


Figure 8.2. Illustration of unit arrangement in a process system with (a) a main product and waste, (b) two co-products and superstructures with (c) 3 products and (d) 4 products.

Clustering can greatly reduce the size and complexity of a design problem. Instead of designing every single unit, we only design the clusters within a process system. The repeating units in a cluster then have similar properties. Process clustering is shown in chapter 7, in which the nanofiltration cascade system was divided into two clusters: a top and bottom section. Each cluster was represented by a single model and a mass balance, in this case respectively the partitioning curves and the operating lines. Each cluster contains several units (stages of nanofiltration cascade) operated at a similar stage cut, membrane type, TMP and temperature.

8.3.4 Setting up mass balances

The mass balances relate to the streams that are involved in a system. This can be constructed as an overall balance and a detailed balance for every unit. By reducing the size of the system into several clusters, as explained in the previous phase, the mass balance for each unit within a cluster can then be generalized as one general balance. This is usually expressed as an operating line (chapter 7). It is then necessary to set up a balance at the intersection of two clusters and also an overall mass balance.

8.3.5 *Determining operating conditions and selecting design parameters*

To start the calculations for the design, the design parameters and operating conditions need to be selected. The selected parameters determine the quality of the design, which makes this phase crucial in the design process. The selection itself is a decision making process that needs to be made out of the numbers of options in relation with the number of units, operating parameters and the design parameters. Having a large number of options will raise the complexity of the decision making model. Therefore, reducing the number of options is as important as the decision making procedure itself. One method to select the operating parameters was demonstrated in chapter 5.

Reducing the number of options can be done in relation to the number of units, the operating parameters and the design parameters. The clustering step is important here, as it significantly reduces the number of options. Within each cluster, we need to decide which operating variables are considered. Each unit can be operated using a certain range of those variables. In this thesis for example, TMPs between 4 to 16 bar and temperatures between 25 to 45°C were selected. The possible options are then generated as a combinatorial problem considering the number of clusters, operating parameters and the levels within the operating parameters. At this point, the number of options can still be very large in spite of the reduction achieved with the clustering. Further reduction can be done by only considering the critical parameters in the system. The backward analysis that was discussed in chapter 5 can be used to identify the critical parameters. The non-critical parameters can then be removed as a decision variable, greatly reducing the number of options. The value for the non-critical parameters can be chosen arbitrarily.

The options that were generated based on the clusters and the operating variables are then combined with the design parameters. The freedom in choosing the design parameters depends on the design method itself. For example, the McCabe – Thiele method (chapter 7) only requires one independent design parameter, the stage cut. Changing the number of independent design parameters can affect the whole design procedure and may require a complete reformulation. The McCabe – Thiele method gives a good example of a design method in relation of the number of independent design parameters. In other cases when developing a design method is required, it is therefore important to consider keeping the independent design parameters at a minimum.

8.3.6 *Designing the system*

Once all the parameters are set, the design can be carried out. This phase is mostly about calculating the size of the system to achieve the target. The design parameter need to be chosen by considering the characteristics of the system. In chapter 7, a method for designing a nanofiltration cascade was developed based on the classical McCabe-Thiele method. Another example of a design method that is used for a process system is the pinch analysis [5,142], which is commonly used to design a heat exchanger or water utilization network.

The calculations will show how many units are needed within a section and also how big each unit is. In case of a nanofiltration unit, the unit size is represented by the membrane surface area. The exact procedure presented in chapter 7 may or may not apply to other systems; this is dependent on the characteristics of the system and the target. The McCabe-Thiele method is based on a separation of a binary mixture into 2 phases. Other systems that are based on the same principle (e.g. extraction) can potentially be designed by this method.

8.3.7 *Optimizing the parameters*

At this point we have created the configuration of a process system that contains information about the selected operating variables, design parameters and the size of the units. This design can then be assessed using performance indicators (e.g. yield, cost). The initially selected parameters may not give an optimum performance, and therefore, phase 5 and 6 are often repeated to find a global optimum. An optimization model, as explained in chapter 6, is needed to be able to find the optimum automatically.

8.4 **How to handle the optimization procedure**

In chapter 4, 5, 6 and in the design guidelines in this chapter, it was discussed that optimization is prominent in different stages of the design process. Automated optimization becomes a requirement to have the optimum in a reasonable time, and to give an objective outcome. Optimization is performed to maximize (or minimize) certain objectives. In our case the objective was represented by performance indicators. A process system often has multiple performance indicators. The choice of the indicators for optimization then are a challenge for the designing engineer.

In this thesis, several performance indicators are discussed: purity and yield (chapter 4, 5 and 6) and the separation factor (chapter 5). In chapter 7, the indicator purity was not optimized, but was a design constraint; all designs must achieve the selected purity targets. The design was then optimized based on the product yield or surface area requirement. In other processes, different indicators are used as performance indicators, such as product conversion, energy requirement or total investment. Chapter 5 shows that even optimization with multiple objectives is feasible. Despite the similar procedure in handling more than two objectives, a large number of objectives increases the computing load of the model to assign the criteria weights. Moreover, it may raise confusion for engineers related to how the design should be interpreted. It is therefore important to keep the number of objectives at a minimum without losing important qualities of the design. The weighting method, is a suitable method to reduce the number of objectives by running it iteratively. At the first evaluation, all considered objectives can be used. The result of the weighing method can then be used to see which objectives are more important and which are less important. It is often found that the weights of some objectives are much higher than the other one. The objectives with a very low value of the weight factor can then be removed as they do not have significance in the outcome. Further optimization can then be done with only the critical objectives.

8

In principle, an optimization is used to aid in a decision making process. This may appear in any stage of the design: a single unit, a cluster of units or the whole system, and it indicates that optimization can be performed on any level.

In chapter 6, the optimization model was initially developed for a single nanofiltration unit and then expanded into a 3-stage nanofiltration cascade with increased number of variables. This illustrates that a similar model can be expanded to solve different levels of a process system. This also implies that the same model can further be expanded to optimize the design result that was shown in chapter 7.

Optimizing a single unit requires the least simplification in the optimization, because it considers less operating variables. An easy assumption is that a system with these settings should also be an optimum because it is constructed by optimum units. However, the optimum design that was identified in chapter 6 did not contain an optimum individual unit. The reason for that is that when a process system is constructed, a global objective is established, which does not necessarily translate to the same objective for each unit. To achieve a global objective, each unit plays a certain function, which may be

very different from that of other units. For example, to achieve the best purity in a three-stage cascade, the feed stage is primarily a stream splitter and not a purifying unit. Therefore, the originally chosen operating variables for the feed stage will give poor purity if it is evaluated individually but will give the best purity when it is evaluated as a three-stage cascade.

8.5 How *inhomogeneous* a design can be

The design procedure discussed in this chapter is developed by considering the design of an inhomogeneous nanofiltration cascade. In this case, the inhomogeneity comes from the possible use of different membranes and operating variables at each stage. This freedom in design then has to be translated into models that describe the unit with different configurations. Earlier in this chapter, it was discussed that somehow a model, or design procedure should be simplified in order to make it executable; but it was clearly seen that including an extra variable, which makes the system more inhomogeneous, raises the model complexity. Therefore, a limit of system inhomogeneity exists in order to not let the complexity on the next level explode to unrealistic levels.

Both process inhomogeneity and model complexity are often left unquantified. This means that the decision of determining the process inhomogeneity can only be done using intuition. A quantification of both parameters is then needed to have a proper, objective assessment. In a membrane cascade system, an ideal design is defined as a design in which all streams entering a mixing point have similar composition, and in which all membranes have the same separation factor. When two streams enter a mixing point with different compositions, the difference between the compositions is then considered as a degree of non-ideality. This term was once used in a membrane cascade system [138] without utilizing it further in the design. In general terms, the concept of entropy that represents a degree of disorder can be related into a process inhomogeneity.

A complexity of a model depends the number of variables and linear or nonlinearity of the model. This complexity is then determined by the response of a computing unit (e.g. the solver). With this response one then determines whether a model is solvable or not. If both process inhomogeneity and computational response are quantified, their relation may follow a curve that is shown in Figure 8.3. We see that the calculation response increase drastically with an increase of system inhomogeneity. At some point, the

calculation is limited by the computing capacity, which is then limits the inhomogeneity of a model.

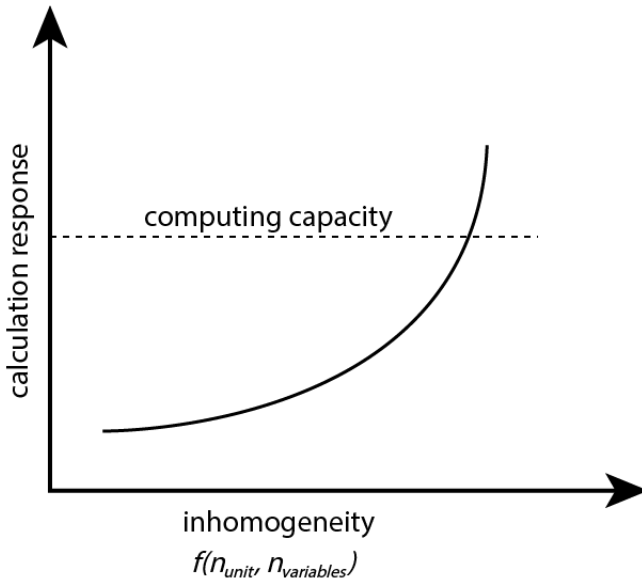


Figure 8.3. Relationship between process inhomogeneity and calculation response for models.

8

8.6 Concluding remarks

The aim of this thesis was to develop a rational design for a process system, which until now has been done mostly intuitively. A cascaded nanofiltration system for fractionation of fructooligosaccharides is used as model system, representing process systems with some level of complexity in general. Incorporating a rationale into design procedure requires a deep understanding and thorough evaluation, which is obtained by developing models in several levels. Arising from those models, a design guideline is developed as constructed in seven phases of design.

The approach that was developed in this thesis can greatly reduce the subjectivity in the design process. However, some part of the design will always require decisions based on intuitive knowledge (e.g. maximum complexity), and will therefore always remain a creative process. The translation of these creative decisions into quantified performance is the key for an objective design.



References



- [1] S. Hall, *Rules of thumb for chemical engineers*, Elsevier, 2017.
<https://doi.org/10.1016/c2016-0-00182-1>.
- [2] M.M. El-Halwagi, ed., *Introduction to process integration*, in: *Process Syst. Eng.*, 2006: pp. 1–20. [https://doi.org/10.1016/S1874-5970\(06\)80002-0](https://doi.org/10.1016/S1874-5970(06)80002-0).
- [3] M.C. Dimian, ed., *Chapter 7 Process synthesis by hierarchical approach*, in: *Comput. Aided Chem. Eng.*, 2003: pp. 229–298. [https://doi.org/10.1016/S1570-7946\(03\)80031-7](https://doi.org/10.1016/S1570-7946(03)80031-7).
- [4] S. Balakrishna, L.T. Biegler, *Chemical Reactor Network Targeting and Integration: An Optimization Approach*, *Adv. Chem. Eng.* 23 (1996) 247–300.
[https://doi.org/10.1016/S0065-2377\(08\)60204-5](https://doi.org/10.1016/S0065-2377(08)60204-5).
- [5] T. Gundersen, *Heat Integration: Targets and Heat Exchanger Network Design*, in: *Handb. Process Integr. Minimisation Energy Water Use, Waste Emiss.*, Elsevier Inc., 2013: pp. 129–167. <https://doi.org/10.1533/9780857097255.2.129>.
- [6] W. McCabe, J. Smith, P. Harriott, *Unit Operations of Chemical Engineering*, 7th editio, McGraw-Hill, 2005.
- [7] F.P. Cuperus, H.H. Nijhuis, *Applications of membrane technology to food processing*, *Trends Food Sci. Technol.* 4 (1993) 277–282.
[https://doi.org/10.1016/0924-2244\(93\)90070-Q](https://doi.org/10.1016/0924-2244(93)90070-Q).
- [8] V. Dhineshkumar, D. Ramasamy, *Review on Membrane Technology Applications in Food and Dairy Processing*, *J. Appl. Biotechnol. Bioeng.* 3 (2017) 399–407. <https://doi.org/10.15406/jabb.2017.03.00077>.
- [9] A.W. Mohammad, C.Y. Ng, Y.P. Lim, G.H. Ng, *Ultrafiltration in Food Processing Industry: Review on Application, Membrane Fouling, and Fouling Control*, *Food Bioprocess Technol.* 5 (2012) 1143–1156.
<https://doi.org/10.1007/s11947-012-0806-9>.
- [10] B. Van Der Bruggen, C. Vandecasteele, T. Van Gestel, W. Doyen, R. Leysen, *A review of pressure-driven membrane processes in wastewater treatment and drinking water production*, *Environ. Prog.* 22 (2003) 46–56.
<https://doi.org/10.1002/ep.670220116>.

- [11] W.R. Bowen, J.S. Welfoot, Modelling the performance of membrane nanofiltration-critical assessment and model development, *Chem. Eng. Sci.* 57 (2002) 1121–1137. [https://doi.org/10.1016/S0009-2509\(01\)00413-4](https://doi.org/10.1016/S0009-2509(01)00413-4).
- [12] W.J. Koros, Evolving Beyond the Thermal Age of Separation Processes: Membranes Can Lead the Way, 5 (2004) 2326–2334. <https://doi.org/10.1002/aic.10330>.
- [13] W.L. Kerr, Food Drying and Evaporation Processing Operations, in: *Handb. Farm Dairy Food Mach.*, Elsevier Inc., 2007: pp. 303–340. <https://doi.org/10.1016/B978-081551538-8.50013-3>.
- [14] J.S. Cohen, T.C.S. Yang, Progress in food dehydration, *Trends Food Sci. Technol.* 6 (1995) 20–25. [https://doi.org/10.1016/S0924-2244\(00\)88913-X](https://doi.org/10.1016/S0924-2244(00)88913-X).
- [15] B.S. Lalia, V. Kochkodan, R. Hashaikeh, N. Hilal, A review on membrane fabrication: Structure, properties and performance relationship, *Desalination.* 326 (2013) 77–95. <https://doi.org/10.1016/j.desal.2013.06.016>.
- [16] A.W. Mohammad, Y.H. Teow, W.L. Ang, Y.T. Chung, D.L. Oatley-Radcliffe, N. Hilal, Nanofiltration membranes review: Recent advances and future prospects, *Desalination.* 356 (2015) 226–254. <https://doi.org/10.1016/j.desal.2014.10.043>.
- [17] L. Upadhyaya, X. Qian, S. Ranil Wickramasinghe, Chemical modification of membrane surface — overview, *Curr. Opin. Chem. Eng.* 20 (2018) 13–18. <https://doi.org/10.1016/j.coche.2018.01.002>.
- [18] A. Caus, L. Braeken, K. Boussu, B. Van der Bruggen, The use of integrated countercurrent nanofiltration cascades for advanced separations, *J. Chem. Technol. Biotechnol.* 84 (2009) 391–398. <https://doi.org/10.1002/jctb.2052>.
- [19] W.E. Siew, A.G. Livingston, C. Ates, A. Merschaert, Continuous solute fractionation with membrane cascades - A high productivity alternative to diafiltration, *Sep. Purif. Technol.* 102 (2013) 1–14. <https://doi.org/10.1016/j.seppur.2012.09.017>.
- [20] N. V. Patil, X. Feng, J.J.W. Sewalt, R.M. Boom, A.E.M. Janssen, Separation of an inulin mixture using cascaded nanofiltration, *Sep. Purif. Technol.* 146 (2015) 261–267. <https://doi.org/10.1016/j.seppur.2015.03.061>.



- [21] S. Hartland, Introduction, in: Counter-Current Extr., Elsevier, 1970: pp. 1–27. <https://doi.org/10.1016/b978-0-08-012976-1.50007-3>.
- [22] W.L. McCabe, E.W. Thiele, Graphical Design of Fractionating Columns, 1925. <https://doi.org/10.1021/ie50186a023>.
- [23] E.N. Lightfoot, T.W. Root, J.L. O'Dell, Emergence of ideal membrane cascades for downstream processing, *Biotechnol. Prog.* 24 (2008) 599–605. <https://doi.org/10.1021/bp070335l>.
- [24] N. V. Patil, T. Schotel, C. V. Rodriguez Gomez, V. Aguirre Montesdeoca, J.J.W. Sewalt, A.E.M. Janssen, R.M. Boom, Continuous purification of galacto-oligosaccharide mixtures by using cascaded membrane filtration, *J. Chem. Technol. Biotechnol.* 91 (2016) 1478–1484. <https://doi.org/10.1002/jctb.4746>.
- [25] V. Aguirre Montesdeoca, A. Van der Padt, R.M. Boom, A.E.M. Janssen, Modelling of membrane cascades for the purification of oligosaccharides, *J. Memb. Sci.* 520 (2016) 712–722. <https://doi.org/10.1016/j.memsci.2016.08.031>.
- [26] U. Vengateson, Design of multiple shell and tube heat exchangers in series: E shell and F shell, *Chem. Eng. Res. Des.* 88 (2010) 725–736. <https://doi.org/10.1016/j.cherd.2009.10.005>.
- [27] P.L. Dhar, Case Studies in Optimum Design, in: *Therm. Syst. Des. Simul.*, Elsevier, 2017: pp. 467–513. <https://doi.org/10.1016/b978-0-12-809449-5.00009-7>.
- [28] Q. Luo, S. Li, S. Jing, The study of fluid dynamics in countercurrent multi-stage micro-extraction system, in: *Energy Procedia*, Elsevier Ltd, 2013: pp. 275–282. <https://doi.org/10.1016/j.egypro.2013.07.214>.
- [29] J. Serna, E.N. Díaz Martínez, P.C. Narváez Rincón, M. Camargo, D. Gálvez, Á. Orjuela, Multi-criteria decision analysis for the selection of sustainable chemical process routes during early design stages, *Chem. Eng. Res. Des.* 113 (2016) 28–49. <https://doi.org/10.1016/j.cherd.2016.07.001>.
- [30] G. Chiandussi, M. Codegone, S. Ferrero, F.E. Varesio, Comparison of multi-objective optimization methodologies for engineering applications, Elsevier Ltd, 2012. <https://doi.org/10.1016/j.camwa.2011.11.057>.

- [31] G. Flamm, W. Glinsmann, D. Kritchevsky, L. Prosky, M. Roberfroid, Inulin and oligofructose as dietary fiber: a review of the evidence., *Crit. Rev. Food Sci. Nutr.* 41 (2001) 353–362. <https://doi.org/10.1080/20014091091841>.
- [32] K.R. Niness, Inulin and oligofructose: What are they?, *J. Nutr.* 129 (1999) 1402S-1406S. <https://doi.org/https://doi.org/10.1093/jn/129.7.1402S>.
- [33] D. Meyer, S. Bayarri, A. Tárrega, E. Costell, Inulin as texture modifier in dairy products, *Food Hydrocoll.* 25 (2011) 1881–1890. <https://doi.org/10.1016/j.foodhyd.2011.04.012>.
- [34] A. Franck, Technological functionality of inulin and oligofructose., *Br. J. Nutr.* 87 Suppl 2 (2002) S287–S291. <https://doi.org/10.1079/BJNBJN/2002550>.
- [35] A. Tárrega, J.D. Torres, E. Costell, Influence of the chain-length distribution of inulin on the rheology and microstructure of prebiotic dairy desserts, *J. Food Eng.* 104 (2011) 356–363. <https://doi.org/10.1016/j.jfoodeng.2010.12.028>.
- [36] L. Hobbs, Sweeteners from Starch: Production, Properties and Uses, in: *Starch*, Elsevier Inc., 2009: pp. 797–832. <https://doi.org/10.1016/B978-0-12-746275-2.00021-5>.
- [37] V. Aguirre Montesdeoca, J. Bakker, R.M. Boom, A.E.M. Janssen, A. Van der Padt, Ultrafiltration of non-spherical molecules, *J. Memb. Sci.* 570–571 (2019) 322–332. <https://doi.org/10.1016/j.memsci.2018.10.053>.
- [38] A. Zydney, Protein Separations Using Membrane Filtration: New Opportunities for Whey Fractionation, *Int. Dairy J.* 8 (1998) 243.
- [39] Y.M. Feng, X.L. Chang, W.H. Wang, R.Y. Ma, Separation of galacto-oligosaccharides mixture by nanofiltration, *J. Taiwan Inst. Chem. Eng.* 40 (2009) 326–332. <https://doi.org/10.1016/j.jtice.2008.12.003>.
- [40] R.C. Kuhn, F. Maugeri Filho, V. Silva, L. Palacio, A. Hernández, P. Prádanos, Mass transfer and transport during purification of fructooligosaccharides by nanofiltration, *J. Memb. Sci.* 365 (2010) 356–365. <https://doi.org/10.1016/j.memsci.2010.09.031>.
- [41] A.K. Goulas, P.G. Kapasakalidis, H.R. Sinclair, R.A. Rastall, A.S. Grandison,

- Purification of oligosaccharides by nanofiltration, *J. Memb. Sci.* 209 (2002) 321–335. [https://doi.org/10.1016/S0376-7388\(02\)00362-9](https://doi.org/10.1016/S0376-7388(02)00362-9).
- [42] M. Minhalma, L.L. Beal, I. Catarino, M. Mateus, M.N. de Pinho, Optimization of saccharide fractionation using nanofiltration/ultrafiltration, *Desalination*. 199 (2006) 337–339. <https://doi.org/10.1016/j.desal.2006.03.079>.
- [43] J. Hiddink, R. de Boer, P.F.C. Nooy, Reverse Osmosis of Dairy Liquids, *J. Dairy Sci.* 63 (1980) 204–214. [https://doi.org/10.3168/JDS.S0022-0302\(80\)82915-8](https://doi.org/10.3168/JDS.S0022-0302(80)82915-8).
- [44] B. Van der Bruggen, M. Mänttäri, M. Nyström, Drawbacks of applying nanofiltration and how to avoid them: A review, *Sep. Purif. Technol.* 63 (2008) 251–263. <https://doi.org/10.1016/j.seppur.2008.05.010>.
- [45] J. Marriott, E. Sørensen, A general approach to modelling membrane modules, *Chem. Eng. Sci.* 58 (2003) 4975–4990. <https://doi.org/10.1016/J.CES.2003.07.005>.
- [46] J.I. Marriott, E. Sørensen, I.D.L. Bogle, Detailed mathematical modelling of membrane modules, *Comput. Chem. Eng.* 25 (2001) 693–700. [https://doi.org/10.1016/S0098-1354\(01\)00670-6](https://doi.org/10.1016/S0098-1354(01)00670-6).
- [47] W.R. Bowen, A.W. Mohammad, N. Hilal, Characterisation of nanofiltration membranes for predictive purposes — use of salts, uncharged solutes and atomic force microscopy, *J. Memb. Sci.* 126 (1997) 91–105. [https://doi.org/10.1016/S0376-7388\(96\)00276-1](https://doi.org/10.1016/S0376-7388(96)00276-1).
- [48] J.E. Almazán, E.M. Romero-Dondiz, V.B. Rajal, E.F. Castro-Vidaurre, Nanofiltration of glucose: Analysis of parameters and membrane characterization, *Chem. Eng. Res. Des.* 94 (2015) 485–493. <https://doi.org/10.1016/J.CHERD.2014.09.005>.
- [49] N.S. Kotrappanavar, A.A. Hussain, M.E.E. Abashar, I.S. Al-Mutaz, T.M. Aminabhavi, M.N. Nadagouda, Prediction of physical properties of nanofiltration membranes for neutral and charged solutes, *Desalination*. 280 (2011) 174–182. <https://doi.org/10.1016/J.DESAL.2011.07.007>.
- [50] A.W. Mohammad, A modified Donnan-steric-pore model for predicting flux and rejection of dye/NaCl mixture in nanofiltration membranes) A modified Donnan-steric-pore model for predicting flux and rejection of dye/NaCl mixture in

- nanofiltration membranes, *Sep. Sci. Technol.* 37 (2002) 1009–1029.
<https://doi.org/10.1081/SS-120002238>.
- [51] A.A. Hussain, M.E.E. Abashar, I.S. Al-Mutaz, Effect of Ion Sizes on Separation Characteristics of Nanofiltration Membrane Systems, *J. King Saud Univ. - Eng. Sci.* 19 (2006) 1–18. [https://doi.org/10.1016/S1018-3639\(18\)30844-4](https://doi.org/10.1016/S1018-3639(18)30844-4).
- [52] S. Bandini, V. Morelli, Effect of temperature, pH and composition on nanofiltration of mono/disaccharides: Experiments and modeling assessment, *J. Memb. Sci.* 533 (2017) 57–74. <https://doi.org/10.1016/j.memsci.2017.03.021>.
- [53] M.L. Stewart, D.A. Timm, J.L. Slavin, Fructooligosaccharides exhibit more rapid fermentation than long-chain inulin in an in vitro fermentation system, *Nutr. Res.* 28 (2008) 329–334. <https://doi.org/10.1016/j.nutres.2008.02.014>.
- [54] J.R. Hess, A.M. Birkett, W. Thomas, J.L. Slavin, Effects of short-chain fructooligosaccharides on satiety responses in healthy men and women, *Appetite.* 56 (2011) 128–134. <https://doi.org/10.1016/j.appet.2010.12.005>.
- [55] B. Villegas, I. Carbonell, E. Costell, Inulin milk beverages: Sensory differences in thickness and creaminess using R-index analysis of the ranking sata, *J. Sens. Stud.* 22 (2007) 377–393. <https://doi.org/10.1111/j.1745-459X.2007.00111.x>.
- [56] M.T.C. Machado, S. Trevisan, J.D.R. Pimentel-Souza, G.M. Pastore, M.D. Hubinger, Clarification and concentration of oligosaccharides from artichoke extract by a sequential process with microfiltration and nanofiltration membranes, *J. Food Eng.* 180 (2016) 120–128.
<https://doi.org/10.1016/j.jfoodeng.2016.02.018>.
- [57] W. Li, J. Li, T. Chen, C. Chen, Study on nanofiltration for purifying fructooligosaccharides I. Operation modes, *J. Memb. Sci.* 245 (2004) 123–129.
<https://doi.org/10.1016/j.memsci.2004.07.021>.
- [58] V. Aguirre Montesdeoca, A.E.M. Janssen, R.M. Boom, A. Van der Padt, Fine ultrafiltration of concentrated oligosaccharide solutions – Hydration and pore size distribution effects, *J. Memb. Sci.* 580 (2019) 161–176.
<https://doi.org/10.1016/j.memsci.2019.03.019>.
- [59] A. Córdova, C. Astudillo, L. Santibañez, A. Cassano, R. Ruby-Figueroa, A.



- Illanes, Purification of galacto-oligosaccharides (GOS) by three-stage serial nanofiltration units under critical transmembrane pressure conditions, *Chem. Eng. Res. Des.* 117 (2017) 488–499. <https://doi.org/10.1016/j.cherd.2016.11.006>.
- [60] Z. Rizki, A.E.M. Janssen, R.M. Boom, A. van der Padt, Oligosaccharides fractionation cascades with 3 outlet streams, *Sep. Purif. Technol.* 221 (2019) 183–194. <https://doi.org/10.1016/J.SEPPUR.2019.03.086>.
- [61] R. Sharma, S. Chellam, Temperature effects on the transport of water, uncharged and charged solutes across polymeric nanofiltration membranes, *Am. Water Work. Assoc. Membr. Technol. Conference.* (2007) 17–20. <https://doi.org/10.1016/j.scitotenv.2011.11.081>.
- [62] T. Tsuru, S. Izumi, T. Yoshioka, M. Asaeda, Temperature effect on transport performance by inorganic nanofiltration membranes, *AIChE J.* 46 (2000) 565–574. <https://doi.org/10.1002/aic.690460315>.
- [63] Z. Rizki, A.E.M. Janssen, G.D.H. Claassen, R.M. Boom, A. van der Padt, Multi-criteria design of membrane cascades: Selection of configurations and process parameters, *Sep. Purif. Technol.* (2019). <https://doi.org/10.1016/j.seppur.2019.116349>.
- [64] Y. Sano, S. Yamamoto, Mutual Diffusion Coefficient of Aqueous Sugar Solutions, *J. Chem. Eng. Japan.* 26 (1993) 633–636. <https://doi.org/10.1252/jcej.26.633>.
- [65] J.C. Giddings, E. Kucera, C.P. Russell, M.N. Myers, Statistical theory for the equilibrium distribution of rigid molecules in inert porous networks. Exclusion chromatography, *J. Phys. Chem.* 72 (1968) 4397–4408. <https://doi.org/10.1021/j100859a008>.
- [66] A. Gharsallaoui, B. Rogé, J. Génotelle, M. Mathlouthi, Relationships between hydration number, water activity and density of aqueous sugar solutions, *Food Chem.* 106 (2008) 1443–1453. <https://doi.org/10.1016/j.foodchem.2007.02.047>.
- [67] A.F. Fucaloro, Y. Pu, K. Cha, A. Williams, K. Conrad, Partial molar volumes and refractions of aqueous solutions of fructose, glucose, mannose, and sucrose at 15.00, 20.00, and 25.00°C, *J. Solution Chem.* 36 (2007) 61–80. <https://doi.org/10.1007/s10953-006-9100-7>.

- [68] H. Shiio, Ultrasonic Interferometer Measurements of the Amount of Bound Water. Saccharides, *J. Am. Chem. Soc.* 80 (1958) 70–73.
<https://doi.org/10.1021/ja01534a020>.
- [69] J. Chirife, M.P. Buera, A simple model for predicting the viscosity of sugar and oligosaccharide solutions, *J. Food Eng.* 33 (1997) 221–226.
[https://doi.org/10.1016/S0260-8774\(97\)00060-5](https://doi.org/10.1016/S0260-8774(97)00060-5).
- [70] J. Chirife, G. Favetto, C.F. Fontán, Microbial growth at reduced water activities: some physicochemical properties of compatible solutes, *J. Appl. Bacteriol.* 56 (1984) 259–268. <https://doi.org/10.1111/j.1365-2672.1984.tb01346.x>.
- [71] G. Schock, A. Miquel, Mass transfer and pressure loss in spiral wound modules, *Desalination.* 64 (1987) 339–352. [https://doi.org/10.1016/0011-9164\(87\)90107-X](https://doi.org/10.1016/0011-9164(87)90107-X).
- [72] R.B. Bird, W.E. Stewart, E.N. Lightfoot, *Transport Phenomena*, John Wiley & Sons, Ltd, New York, 1961.
- [73] W.R. Bowen, J.S. Welfoot, Modelling of membrane nanofiltration-pore size distribution effects, *Chem. Eng. Sci.* 57 (2002) 1393–1407.
[https://doi.org/10.1016/S0009-2509\(01\)00412-2](https://doi.org/10.1016/S0009-2509(01)00412-2).
- [74] P. Dechadilok, W.M. Deen, Hindrance factors for diffusion and convection in pores, *Ind. Eng. Chem. Res.* 45 (2006) 6953–6959.
<https://doi.org/10.1021/ie051387n>.
- [75] R.A. Serway, J.W. Jewett, *Physics for Scientists and Engineers, with Modern Physics*, Ninth, Boston, 2014.
- [76] R.C. Team, *R: A Language and Environment for Statistical Computing*, (2019).
<https://www.r-project.org/>.
- [77] B.I. Yun, M.S. Petković, A quadratically convergent iterative method for nonlinear equations, *J. Korean Math. Soc.* 48 (2011) 487–497.
<https://doi.org/10.4134/JKMS.2011.48.3.487>.
- [78] N. Riby, J. E.; Fujisawa, T.; Kretchmer, Fructose absorption, *Am. J. Clin. Nutr.* 58 (1993) 748S–753S. <https://doi.org/https://doi.org/10.1093/ajcn/58.5.748S>.
- [79] J.P. Bantle, Dietary Fructose and Metabolic Syndrome and Diabetes, *J. Nutr.*



- 139 (2009) 1263S-1268S. <https://doi.org/10.3945/jn.108.098020>.
- [80] J.M. Johnson, F.D. Conforti, Fructose, in: *Encycl. Food Sci. Nutr.*, Elsevier B.V, 2003: pp. 2748–2752.
- [81] W.W. Pigman, Occurrence, properties, synthesis and analysis of the monosaccharides, in: *Chem. Carbohydrates*, Elsevier, 1948: pp. 89–148. <https://doi.org/10.1016/b978-0-12-395539-5.50006-x>.
- [82] A.T.C.R. Silva, K.C.L. Martinez, A.B.N. Brito, M. Giuliatti, Separation of glucose and fructose by freezing crystallization, *Cryst. Res. Technol.* 45 (2010) 1032–1034. <https://doi.org/10.1002/crat.200900566>.
- [83] A. Khosravanipour Mostafazadeh, M. Sarshar, S. Javadian, M.R. Zarefard, Z. Amirifard Haghighi, Separation of fructose and glucose from date syrup using resin chromatographic method: Experimental data and mathematical modeling, *Sep. Purif. Technol.* 79 (2011) 72–78. <https://doi.org/10.1016/j.seppur.2011.03.014>.
- [84] K. Robards, M. Whitelaw, Chromatography of monosaccharides and disaccharides, *J. Chromatogr. A.* 373 (1986) 81–110. [https://doi.org/10.1016/S0021-9673\(00\)80209-5](https://doi.org/10.1016/S0021-9673(00)80209-5).
- [85] V. Viard, M.L. Lameloise, Modelling glucose-fructose separation by adsorption chromatography on ion exchange resins, *J. Food Eng.* 17 (1992) 29–48. [https://doi.org/10.1016/0260-8774\(92\)90063-C](https://doi.org/10.1016/0260-8774(92)90063-C).
- [86] M. Di Luccio, B.D. Smith, T. Kida, C.P. Borges, T.L.M. Alves, Separation of fructose from a mixture of sugars using supported liquid membranes, *J. Memb. Sci.* 174 (2000) 217–224. [https://doi.org/10.1016/S0376-7388\(00\)00385-9](https://doi.org/10.1016/S0376-7388(00)00385-9).
- [87] A. Hinkova, Z. Bubnik, P. Kadlec, J. Pridal, Potentials of separation membranes in the sugar industry, *Sep. Purif. Technol.* 26 (2002) 101–110. [https://doi.org/10.1016/S1383-5866\(01\)00121-6](https://doi.org/10.1016/S1383-5866(01)00121-6).
- [88] M.J.L. Alles, I.C. Tessaro, C.P.Z. Noreña, Julia et al. - 2015 - Concentration and Purification of Yacon (*Smallanthus sonchifolius*) Root Fructooligosaccharides Using Membrane, 53 (2015) 190–200. <https://doi.org/http://doi.org/10.17113/ftb.53.02.15.3766>.

- [89] M. Jaseja, A.S. Perlin, P. Dais, Two-dimensional NMR spectral study of the tautomeric equilibria of D-fructose and related compounds, *Magn. Reson. Chem.* 28 (1990) 283–289. <https://doi.org/10.1002/mrc.1260280402>.
- [90] S.R. Maple, A. Allerhand, Detailed Tautomeric Equilibrium of Aqueous D-Glucose. Observation of Six Tautomers by Ultrahigh Resolution Carbon-13 NMR, *J. Am. Chem. Soc.* 109 (1987) 3168–3169. <https://doi.org/10.1021/ja00244a063>.
- [91] T. Barclay, M. Ginic-Markovic, M.R. Johnston, P. Cooper, N. Petrovsky, Observation of the keto tautomer of d-fructose in D₂O using ¹H NMR spectroscopy, *Carbohydr. Res.* 347 (2012) 136–141. <https://doi.org/10.1016/j.carres.2011.11.003>.
- [92] H.A. Tajmir-Riahi, Sugar interaction with calcium ion. synthesis and vibrational spectra of crystalline β-d-fructose and its calcium halide adducts, *J. Inorg. Biochem.* 27 (1986) 123–131. [https://doi.org/10.1016/0162-0134\(86\)80013-7](https://doi.org/10.1016/0162-0134(86)80013-7).
- [93] C. Pulla Rao, K. Geetha, M.S. S Raghavan, Fe(III) complexes of D-glucose and D-fructose*, 1994. <https://doi.org/https://doi.org/10.1007/BF00205190>.
- [94] S.J. Angyal, Complex formation between sugars and metal ions, in: *Carbohydr. Chem.*, 1973: pp. 131–146. <https://doi.org/https://doi.org/10.1016/B978-0-408-70525-7.50005-7>.
- [95] S.S. Kim, H.N. Chang, Y.S. Ghim, Separation of Fructose and Glucose by Reverse Osmosis, *Ind. Eng. Chem. Fundam.* 24 (1985) 409–412. <https://doi.org/10.1021/i100020a002>.
- [96] F. Bruni, C. Di Mino, S. Imberti, S.E. McLain, N.H. Rhys, M.A. Ricci, Hydrogen Bond Length as a Key to Understanding Sweetness, *J. Phys. Chem. Lett.* 9 (2018) 3667–3672. <https://doi.org/10.1021/acs.jpcclett.8b01280>.
- [97] S. Imberti, S.E. McLain, N.H. Rhys, F. Bruni, M.A. Ricci, Role of Water in Sucrose, Lactose, and Sucralose Taste: The Sweeter, the Wetter?, *ACS Omega.* 4 (2019) 22392–22398. <https://doi.org/10.1021/acsomega.9b02794>.
- [98] C. Bhattacharjee, V.K. Saxena, S. Dutta, Fruit juice processing using membrane technology: A review, *Innov. Food Sci. Emerg. Technol.* 43 (2017) 136–153.

- <https://doi.org/10.1016/j.ifset.2017.08.002>.
- [99] K. Pan, Q. Song, L. Wang, B. Cao, A study of demineralization of whey by nanofiltration membrane, *Desalination*. 267 (2011) 217–221.
<https://doi.org/10.1016/j.desal.2010.09.029>.
- [100] G. Foley, Water usage in variable volume diafiltration: comparison with ultrafiltration and constant volume diafiltration, *Desalination*. 196 (2006) 160–163. <https://doi.org/10.1016/j.desal.2005.12.011>.
- [101] N. V. Patil, A.E.M. Janssen, R.M. Boom, The potential impact of membrane cascading on downstream processing of oligosaccharides, *Chem. Eng. Sci.* 106 (2014) 86–98. <https://doi.org/10.1016/j.ces.2013.11.007>.
- [102] B.I. Yun, Solving nonlinear equations by a new derivative free iterative method, *Appl. Math. Comput.* 217 (2011) 5768–5773.
<https://doi.org/10.1016/j.amc.2010.12.055>.
- [103] J. Chen, D.X. Sun, C.F.J. Wu, A catalogue of Two-Level and Three-Level Fractional Factorial Designs with Small Runs, *Int. Stat. Rev.* 61 (1993) 131–145.
<https://doi.org/10.2307/1403599>.
- [104] H. Xu, A catalogue of three-level regular fractional factorial designs, *Metrika*. 62 (2005) 259–281. <https://doi.org/10.1007/s00184-005-0408-x>.
- [105] W.J. Koros, C. Zhang, Materials for next-generation molecularly selective synthetic membranes, *Nat. Mater.* 16 (2017) 289–297.
<https://doi.org/10.1038/nmat4805>.
- [106] T.M. K. C. Khulbe, C. Feng, The Art of Surface Modification of Synthetic Polymeric Membranes, *Polym. Polym. Compos.* 21 (2013) 449–456.
<https://doi.org/10.1002/app>.
- [107] A.F. Ismail, K.C. Khulbe, T. Matsuura, Membrane Modules and Process Design, in: *Gas Sep. Membr. Polym. Inorg.*, 2015: pp. 1–331. <https://doi.org/10.1007/978-3-319-01095-3>.
- [108] J.C. Te Lin, A.G. Livingston, Nanofiltration membrane cascade for continuous solvent exchange, *Chem. Eng. Sci.* 62 (2007) 2728–2736.

- <https://doi.org/10.1016/j.ces.2006.08.004>.
- [109] R.T. Marler, J.S. Arora, Survey of multi-objective optimization methods for engineering, *Struct. Multidiscip. Optim.* 26 (2004) 369–395.
<https://doi.org/10.1007/s00158-003-0368-6>.
- [110] I.Y. Kim, O.L. De Weck, Adaptive weighted sum method for multiobjective optimization: A new method for Pareto front generation, *Struct. Multidiscip. Optim.* 31 (2006) 105–116. <https://doi.org/10.1007/s00158-005-0557-6>.
- [111] R.T. Marler, J.S. Arora, The weighted sum method for multi-objective optimization: New insights, *Struct. Multidiscip. Optim.* 41 (2010) 853–862.
<https://doi.org/10.1007/s00158-009-0460-7>.
- [112] A. Jahan, K.L. Edwards, A state-of-the-art survey on the influence of normalization techniques in ranking: Improving the materials selection process in engineering design, *Mater. Des.* 65 (2015) 335–342.
<https://doi.org/10.1016/j.matdes.2014.09.022>.
- [113] Y.M. Wang, Y. Luo, Integration of correlations with standard deviations for determining attribute weights in multiple attribute decision making, *Math. Comput. Model.* 51 (2010) 1–12. <https://doi.org/10.1016/j.mcm.2009.07.016>.
- [114] S. Hajkowicz, A. Higgins, A comparison of multiple criteria analysis techniques for water resource management, *Eur. J. Oper. Res.* 184 (2008) 255–265.
<https://doi.org/10.1016/j.ejor.2006.10.045>.
- [115] D. Diakoulaki, G. Mavrotas, L. Papayannakis, Determining objective weights in multiple criteria problems: The critic method, *Comput. Oper. Res.* 22 (1995) 763–770. [https://doi.org/10.1016/0305-0548\(94\)00059-H](https://doi.org/10.1016/0305-0548(94)00059-H).
- [116] J. Ma, Z.P. Fan, L.H. Huang, A subjective and objective integrated approach to determine attribute weights, 112 (1999) 397–404. [https://doi.org/10.1016/S0377-2217\(98\)00141-6](https://doi.org/10.1016/S0377-2217(98)00141-6).
- [117] N. V. Patil, A.E.M. Janssen, R.M. Boom, Separation of whey proteins using cascaded ultrafiltration, *Sep. Sci. Technol.* 49 (2014) 140620110053007.
<https://doi.org/10.1080/01496395.2014.927488>.

- [118] X.S. Yang, S. Koziel, L. Leifsson, Computational optimization, modelling and simulation: Recent trends and challenges, in: *Procedia Comput. Sci.*, Elsevier B.V., 2013: pp. 855–860. <https://doi.org/10.1016/j.procs.2013.05.250>.
- [119] M.-H. Lin, J.-F. Tsai, C.-S. Yu, A Review of Deterministic Optimization Methods in Engineering and Management, *Math. Probl. Eng.* 2012 (2012) 1–15. <https://doi.org/10.1155/2012/756023>.
- [120] J. Kronqvist, D.E. Bernal, A. Lundell, I.E. Grossmann, A review and comparison of solvers for convex MINLP, *Optim. Eng.* 20 (2019) 397–455. <https://doi.org/10.1007/s11081-018-9411-8>.
- [121] R. Anand, D. Aggarwal, V. Kumar, A comparative analysis of optimization solvers, *J. Stat. Manag. Syst.* 20 (2017) 623–635. <https://doi.org/10.1080/09720510.2017.1395182>.
- [122] F. Boukouvala, R. Misener, C.A. Floudas, Global optimization advances in Mixed-Integer Nonlinear Programming, MINLP, and Constrained Derivative-Free Optimization, *CDFO, Eur. J. Oper. Res.* 252 (2016) 701–727. <https://doi.org/10.1016/j.ejor.2015.12.018>.
- [123] R. Misener, C.A. Floudas, A Framework for Globally Optimizing Mixed-Integer Signomial Programs, *J. Optim. Theory Appl.* 161 (2014) 905–932. <https://doi.org/10.1007/s10957-013-0396-3>.
- [124] H.S. Rvoo, N. V Sahinldlst, Global optimization of nonconvex NLPs and MINLPs with applications in process design, *Comput. Chem, Engng.* 19 (1995) 551–566. [https://doi.org/10.1016/0098-1354\(94\)00097-2](https://doi.org/10.1016/0098-1354(94)00097-2).
- [125] R.C. Kuhn, F.M. Filho, V. Silva, L. Palacio, A. Hernández, P. Prádanos, Mass transfer and transport during purification of fructooligosaccharides by nanofiltration, *J. Memb. Sci.* 365 (2010) 356–365. <https://doi.org/10.1016/j.memsci.2010.09.031>.
- [126] Z. Rizki, E. Suryawirawan, A.E.M. Janssen, A. van der Padt, R.M. Boom, Modelling temperature effects in a membrane cascade system for oligosaccharides, *J. Memb. Sci.* (2020) 118292. <https://doi.org/10.1016/j.memsci.2020.118292>.

- [127] G.B. van den Berg, I.G. Rácz, C.A. Smolders, Mass transfer coefficients in cross-flow ultrafiltration, *J. Memb. Sci.* 47 (1989) 25–51. [https://doi.org/10.1016/S0376-7388\(00\)80858-3](https://doi.org/10.1016/S0376-7388(00)80858-3).
- [128] J. Wiebe, I. Cecílio, R. Misener, Robust Optimization for the Pooling Problem, *Ind. Eng. Chem. Res.* 58 (2019) 12712–12722. <https://doi.org/10.1021/acs.iecr.9b01772>.
- [129] L. Song, M. Elimelech, Theory of concentration polarization in crossflow filtration, *J. Chem. Soc. Faraday Trans.* 91 (1995) 3389–3398. <https://doi.org/10.1039/FT9959103389>.
- [130] O.A. Yemets, T.N. Barbolina, O.A. Chernenko, Solving optimization problems with linear-fractional objective functions and additional constraints on arrangements, 2006. <https://doi.org/https://doi.org/10.1007/s10559-006-0106-3>.
- [131] J. Czyzyk, M.P. Mesnier, J.J. More, NEOS server, *IEEE Comput. Sci. Eng.* 5 (1998) 68–75. <https://doi.org/10.1109/99.714603>.
- [132] M.R. Kılınc, N. V. Sahinidis, Exploiting integrality in the global optimization of mixed-integer nonlinear programming problems with BARON, *Optim. Methods Softw.* 33 (2018) 540–562. <https://doi.org/10.1080/10556788.2017.1350178>.
- [133] N. V Sahinidis, BARON: A General Purpose Global Optimization Software Package, *J. Glob. Optim.* 8 (1996) 201–205. <https://doi.org/https://doi.org/10.1007/BF00138693>.
- [134] N. V. Sahinidis, Global optimization and constraint satisfaction: The branch-and-reduce approach, *Lect. Notes Comput. Sci. (Including Subser. Lect. Notes Artif. Intell. Lect. Notes Bioinformatics)*. 2861 (2003) 1–16. https://doi.org/10.1007/978-3-540-39901-8_1.
- [135] A. Lejeune, M. Rabiller-Baudry, T. Renouard, Design of membrane cascades according to the method of McCabe-Thiele: An organic solvent nanofiltration case study for olefin hydroformylation in toluene, *Sep. Purif. Technol.* 195 (2018) 339–357. <https://doi.org/10.1016/j.seppur.2017.12.031>.
- [136] W.E. Siew, A.G. Livingston, C. Ates, A. Merschaert, Molecular separation with an organic solvent nanofiltration cascade - augmenting membrane selectivity



- with process engineering, *Chem. Eng. Sci.* 90 (2013) 299–310.
<https://doi.org/10.1016/j.ces.2012.10.028>.
- [137] T. Renouard, A. Lejeune, M. Rabiller-Baudry, Separation of solutes with an organic solvent nanofiltration cascade: Designs, simulations and systematic study of all configurations, *Sep. Purif. Technol.* 194 (2018) 111–122.
<https://doi.org/10.1016/j.seppur.2017.11.029>.
- [138] M.S. Avgidou, S.P. Kaldis, G.P. Sakellariopoulos, Membrane cascade schemes for the separation of LPG olefins and paraffins, *J. Memb. Sci.* 233 (2004) 21–37.
<https://doi.org/10.1016/j.memsci.2003.12.007>.
- [139] P. Zhang, Industrial control system simulation routines, in: *Adv. Ind. Control Technol.*, Elsevier, 2010: pp. 781–810. <https://doi.org/10.1016/b978-1-4377-7807-6.10019-1>.
- [140] C.E. Torres-Ortega, M. Errico, B.G. Rong, Design and optimization of modified non-sharp column configurations for quaternary distillations, *Comput. Chem. Eng.* 74 (2015) 15–27. <https://doi.org/10.1016/j.compchemeng.2014.12.006>.
- [141] W. Lianying, H. Yangdong, W. Ya, Design method for multi-component distillation system based on quasi-binary method, *Korean J. Chem. Eng.* 24 (2007) 556–561. <https://doi.org/10.1007/s11814-007-0002-1>.
- [142] N. Hallale, D.M. Fraser, Optimum design of mass exchange networks using pinch technology, in: *Comput. Chem. Eng.*, Elsevier Ltd, 1999: pp. S165–S168.
[https://doi.org/10.1016/S0098-1354\(99\)80041-6](https://doi.org/10.1016/S0098-1354(99)80041-6).



Summary



In industrial practice, process systems usually consist of multiple units and can be much more complex than a single process unit. The process system, therefore, needs to be designed carefully such that all operational units work synergistically to achieve an overall objective. Designing a process system is a complicated work, which until now is mostly done intuitively. The design is usually developed via a *trial-and-error* process based on heuristic knowledge. The resulting design may be sufficient and acceptable, but the design may not be the optimum design. A more rational and objective approach is needed to design a process system to end up with an objective design that is truly optimal.

This thesis aims to develop such a rational procedure for designing process systems, represented by inhomogeneous nanofiltration cascades for fractionation of fructooligosaccharides (FOS). The design process is approached by modelling within four levels of a process system: (1) single stage nanofiltration, (2) nanofiltration cascades, (3) optimization and (4) process design. This multi-level modelling is elaborated in chapter 2 – 7. Based on these findings, a guideline for designing a process system is given in chapter 8.

Chapter 2 starts off with the multi-level modelling by developing a model for a single stage nanofiltration for FOS. The model was developed based on the steric pore model (SPM), which was then extended to application for FOS by putting more attention on the effect of temperature. Temperature affects the nanofiltration process by following three mechanisms: (1) expanding the solutes, (2) reducing solution viscosity and (3) expanding the membrane pore size.

Chapter 3 discusses the experimental finding that fructose and glucose can be separated during the fractionation of FOS by nanofiltration, even though they have the same molecular weight. Models for nanofiltration do not predict this separation since it considers both sugars as one lumped component: monosaccharides. The finding of this separation enriches the fractionation spectrum in chapter 2, where separation is only based on molecular weights.

Chapter 4 discusses modelling nanofiltration cascades, more specifically systems that produce three products simultaneously. The chapter starts with 3-stage cascade designs that are further improved by addition of extra stages, towards 4- and 5-stage cascades. Addition of stages indeed increased the separation performance. The best performance, however, was found with a 4-stage cascade and not with a 5-stage cascade. This chapter concludes that in addition to adding extra stages, the direction of the expansion is also

important. Expansion towards the top section improves the purification of small products (mono- and disaccharides) while expansion towards the bottom section improves the concentration of large product (larger oligosaccharides).

Chapter 5 describes another approach to improve the nanofiltration cascades: adaptation of the stream configurations while keeping the stage number at 3. This chapter confirms the result in chapter 4 related to direction of expansion of the cascade. A model is developed to handle multiple objectives in a design. Based on this model, further analysis was performed to identify the critical parameters for a design.

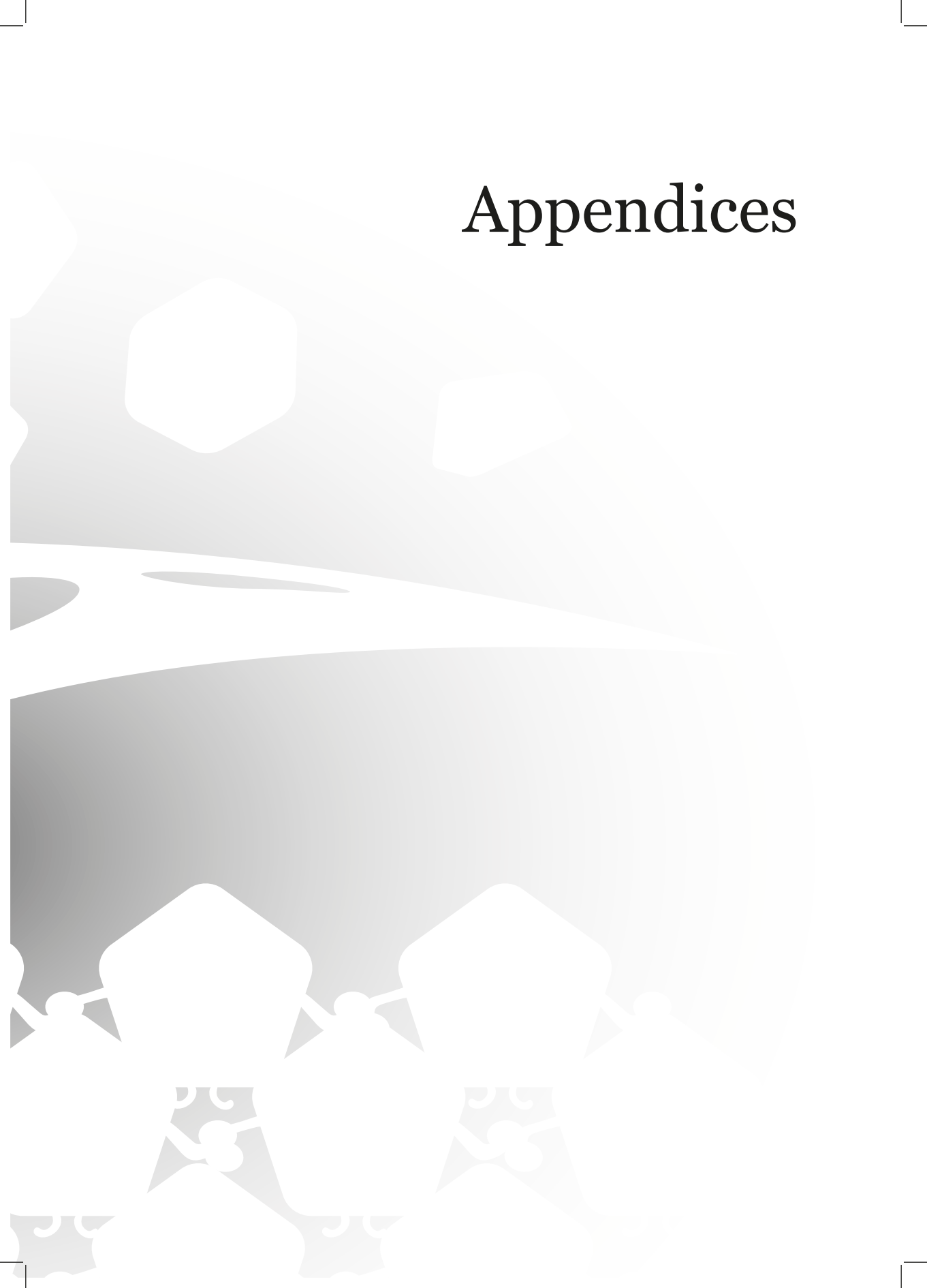
Chapter 6 describes the development of an optimization model based on mixed integer non-linear programming (MINLP). This model can automatically select the optimum combination of operating parameters in a 3-stage cascade, which could not be done in previous chapters. As the outcome of this model, a frontier curve could be drawn to map the window of operation for optimum performance.

Chapter 7 discusses a method to design inhomogeneous nanofiltration cascades based on the McCabe-Thiele approach, which is a classical design procedure for distillation processes. This method allows us to design an inhomogeneous nanofiltration cascade that can achieve a certain purity target. The models developed before this chapter were only able to predict and optimize the outcome of a given nanofiltration cascade designs, and the outcomes of these models often do not reach a satisfactory target. With the method described in chapter 7, this problem was solved.

Chapter 8 concludes this thesis by highlighting the main findings of each chapter. Extrapolating from the result in nanofiltration cascades, a general design guideline was constructed into a seven-phase design procedures. The chapter concludes with a discussion related to the intuitive choices that are still important in the design procedure, in spite of the great reduction in the subjectivity in the design that follows after the intuitive design choices have been made.



Appendices



Acknowledgement

To me, doing PhD is not only the matter of pursuing a degree. It's all about the time I spent during these four years. I am grateful that I am surrounded by amazing people whom I spent my precious time with. People that make me feels like home when I am away from home. For the goods and the bads, inside or outside academic or research activities. I cannot accomplished this without them in my life.

First of all, I would like to thank my sponsor, Indonesia Endowment Fund for Education (**LPDP**), so that I can have an opportunity to have a wonderful time in Wageningen while also doing my PhD.

I would like thank my promotors, **Remko** and **Albert** – thank you for your time supervising me, for the time we spent in interesting discussions. Your feedbacks mostly made me insecure but once I could handle them, they became valuable contributions in my research. I would also like to thank my co-promotor and my daily supervisor, **Anja** – thank you for the time you patiently spent supervising me, for weekly meetings that we had. I did not always come to you with good news, but I always came back with a good mood and motivation every time we had a discussion.

I am glad that I had an opportunity to collaborate with **Frits**, who was always energetic every time I had a discussion with him – a special thank for you. Your suggestions were always brilliant that often made me struggle to follow. I also thank **Eligius** who joined us in the latter stage of our collaboration – without your help, we could not finalize the problem.

I would like to extend my gratitude to the students I supervised. Your contribution means a lot to me. **Marlijn**, **Afke** and **Rimke** – thank you for your time in developing the optimization model. **Tim** – I never forget the creep every time you 'sneak' into my desk to start a discussion. **Ruurd** and **Ton** – I got a good insight for my research during the time you did your thesis. **Eric** – thank you for your time during your thesis and also for being a reliable colleague. **Wantong** – even though I often becomes mad every time we met, you gave me a valuable insight. **Laura** – I feel bad that I was away a lot during the time you did your thesis.

I am very grateful that I spent my time with amazing colleagues in FPE. **Anna** – thank you for your time discussing random things during random 'break time' in the office.

Thank you also for being my paranymph. My other paranymph, **Andrea** – thank you for not having a second thought while I asked you to be my paranymph. I am very grateful with the time we spent in the axis, and our collaboration preparing the FPE-cookbook.

My first officemates, **Fiona** and **Birgit** – I really miss our time together in the office, the gossips (especially with Fiona) and the dinners we have had. I also thank my other officemates **Murat** and **Ivanna** – you made my time in the office more colorful.

I give my sincere gratitude to our amazing technicians: **Maurice**, **Jos**, **Jarno**, **Martin** and **Wouter** – I could not expect a better lab-time without you guys.

Special thank you to **Victor**, whom I often spend time to discuss membrane related problem. **Juliana**, whom I could eavesdrop without any effort. Strange, but true, I miss your disturbance every time you looted my office. **Lu**, **Qinhui** and **Bijoy** – thank you for your persistence in joining the punctual 3 p.m. ‘hou chou’ time. My other PhD fellows and FPE colleagues – I am very grateful for nice times that we spent during the breaks and meetings.

I could never felt closer to home during my PhD time without my Indonesian fellows. Especially my *housemates masa gitu*, **Gendis** and **Gumilang** – thank you for your time being reliable housemates, games buddies, cooking buddies and actor and actress in all the drama happened in Lombardi. **Titis**, **Nila**, **Anto** and the kids: **Tsara**, **Farah** and **Ammar** – thank you for all the good times we had for playing Pokemon Go, eating, travelling, board gaming, making music or even just having simple chats. **Indra**, **Nuning**, **Belinda**, **Alim**, **Emilius**, **Dikky**, **Yuda**, **Linda**, **Sahri**, **Amik**, (another) **Titis**, thank you for the nice times we had in any occasions, which never exclude eating nice meals.

I would like to also thank **Susan** and **the army**, especially **Lex** – thank you for all the time we have spent for spins, turns and jumps on- and off-ice. You have successfully made a tropical guy like me misses an ice time.

My last gratitude will be given to my family: **Mayong**, my sister **Indah**, my brothers: **Mas**, **Nda** and **Nci**, all the in-laws, and all the little squads: my lovely nephews and nieces. It is unfortunate that they have never had a time visiting me here. But there is no time they lose their support for me.

Author Biography



Zulhaj Rizki was born in Jakarta on 30th July 1987. He has a dream to be a great researcher in the future. In 2005, Zulhaj started his bachelor education in the chemical engineering department in Bandung Institute of Technology (ITB), Indonesia, because it was the toughest major to get into with a very high passing grade. Later, he chose food technology as his specialization because it overlaps with his cooking hobby. In 2009, he successfully obtained his bachelor degree from ITB.

After graduation, he worked as a production supervisor in a company that produces personal body care products for three years. In 2013, he was granted the “Anne van den Ban” scholarship for an MSc in food technology in Wageningen University. After his master study, he went back to Indonesia to become a teaching assistant in his previous department in ITB.

To achieve his dream to become a great researcher, he thought that pursuing a PhD is the way to achieve it. He applied for an Indonesian Endowment Fund for Scholarship (LPDP) and successfully received a full scholarship from LPDP for his PhD. In 2016, he started his PhD journey in food process engineering group to pursue his dream to become

a great food technology researcher. During his master and PhD journey, Zulhaj had been very active in Indonesian students association and joined many clubs in the campus.

Zulhaj is a very organized person. His wonderful housemates for 3.5 years even know his routines or schedule from morning to evening. Zulhaj usually cooks, watches films until he falls asleep on the couch, sings, plays guitar, catches Pokémon, and does some sports like: running, swimming, squash, roller- and ice skating, cycling, yoga, or ‘*just dance*’-ing on Wii in his leisure time.

Zulhaj can be reached via his personal email (zulhaj.rizki@outlook.com). You can also find him in LinkedIn (http://tiny.cc/in_Zulhaj).

written by

G. A. S. (Gendis) Irawan

M. G. (Gumilang) Pramuwidyatama

housemates masa gitu

List of Publications

This thesis

1. **Z. Rizki**, A.E.M. Janssen, R.M. Boom, A. van der Padt, “Oligosaccharides fractionation cascades with 3 outlet streams”, *Sep. Purif. Technol.* 221 (2019) 183–194. <https://doi.org/10.1016/J.SEPPUR.2019.03.086>.
2. **Z. Rizki**, A.E.M. Janssen, G.D.H. Claassen, R.M. Boom, A. van der Padt, “Multi-criteria design of membrane cascades: Selection of configurations and process parameters”, *Sep. Purif. Technol.* (2019).
<https://doi.org/10.1016/j.seppur.2019.116349>.
3. **Z. Rizki**, E. Suryawirawan, A.E.M. Janssen, A. van der Padt, R.M. Boom, “Modelling temperature effects in a membrane cascade system for oligosaccharides”, *J. Memb. Sci.* (2020) 118292. <https://doi.org/10.1016/j.memsci.2020.118292>.
4. **Z. Rizki**, A.E.M. Janssen, A. van der Padt, R.M. Boom, “Separation of fructose and glucose via nanofiltration in presence of fructooligosaccharides”, (2020) *submitted for publication*
5. **Z. Rizki**, A.E.M. Janssen, E.M.T. Hendrix, A. van der Padt, R.M. Boom, G.D.H. Claassen, “Design optimization of a 3-stage membrane cascade for oligosaccharides purification using a mixed integer non-linear programming”, *submitted for publication*.
6. **Z. Rizki**, A.E.M. Janssen, A. van der Padt, R.M. Boom, “Design of nanofiltration cascades for fructooligosaccharides using the Mc-Cabe Thiele approach”, *submitted for publication*.

Overview of completed training activities

Discipline specific activities

1. Advance course bioprocess design (Biotech Delft and VLAG, Delft, The Netherlands, 2017).
2. International school of modelling and simulation (Virprofood, Seiano, Italy, 2017)
3. Wageningen Indonesia scientific expose 2017^b (Indonesian PhD and WASS, Wageningen, The Netherlands, 2017).
4. The 35th European Membrane Society (EMS) summer school (EMS, Enschede, The Netherlands, 2018).
5. Advance course in food analysis (VLAG, Wageningen, The Netherlands, 2019).
6. Blended summer school on engineering process systems and materials (University of Bologna, Bologna, Italy, 2019).
7. The 12th European congress on chemical engineering^a (AIDIC, Florence, Italy, 2019).
8. The 4th International congress on desalination using membrane technology^a (Elsevier, Perth, Australia, 2019).

General Courses

1. VLAG PHD week (VLAG, Baarlo, The Netherlands, 2017).
2. Philosophy and ethics in food science and technology (VLAG, Wageningen, The Netherlands, 2017).
3. PhD workshop carousel (WGS, Wageningen, The Netherlands, 2017).
4. The essential of scientific writing and presenting (WGS, Wageningen, The Netherlands, 2017).
5. Scientific publishing (WGS, Wageningen, The Netherlands, 2017).
6. Reviewing scientific paper (WGS, Wageningen, The Netherlands, 2017).

7. Scientific artwork (WUR library, Wageningen, The Netherlands, 2017).
8. Brain training (WGS, Wageningen, The Netherlands, 2017).
9. Project and time management (WGS, Wageningen, The Netherlands, 2018).
10. Teaching and Supervising thesis students (WGS, Wageningen, The Netherlands, 2018).
11. Poster and pitching (WGS, Wageningen, The Netherlands, 2018).
12. Scientific writing (WGS, Wageningen, The Netherlands, 2018).
13. Introduction to R (VLAG, Wageningen, The Netherlands, 2019).
14. Applied statistics (VLAG, Wageningen, The Netherlands, 2019).
15. Chemometrics (VLAG, Wageningen, The Netherlands, 2019).

Optional activities

1. Research proposal (Wageningen, The Netherlands, 2019).
2. FPE PhD trip to Canada^b (FPE, Eastern Canada, Canada, 2019).
3. FPE weekly group meetings^a (FPE, Wageningen, The Netherlands, 2016 – 2020).
4. Teaching : Food Fermentation (2017 – 2019).

^a oral presentation

^b poster presentation

A

About the cover

General: a graphical representation of membrane separation, fructooligosaccharides, configurations and modelling.

(Distorted) pentagonal and hexagonal shapes represent the monosaccharides (glucose and fructose) passing through a membrane

A porous sheet represents a sheet of membrane in a stretched perspective.

Chains of hexagonal and pentagonal shapes represent the FOS molecule that are retained by the membrane.

Curved arrows represent the configurations of membrane cascades that are extensively discussed in this thesis.

The curve in the middle arrow represent a maximum point, which is the objective of an optimization procedure that are discussed in this thesis.

The doodle of equations represent modelling, which is the core of this thesis. The equations and graphs in this cover can also be found within the chapters in this thesis.

Symbols in every chapter represent the content of each chapter :

the fire in chapter 2 represents the heat effect.

the half pentagonal and hexagonal shapes in chapter 3 represent the separation of fructose and glucose.

the trident in chapter 4 represents the 3 outlet streams.

the branches of a root in chapter 5 represent the multicriteria.

the optimum curve in chapter 6 represent an optimization.

the bowllike figure in chapter 7 represent the partitioning curve in a McCabe-Thiele diagram.

a call out shape with multiple spikes in chapter 8 represent people discuss about one thing.

the book in the references represents literatures.

the knot circle in the summary represent a conclusion or a compressed idea.

the plus sign in the appendices represent additional (informations).

The research described in this thesis was financially supported by Indonesia Endowment Fund for Education (LPDP) granted for Zulhaj Rizki.

Cover design by Zulhaj Rizki

Printed by ProeftschriftMaken